DYNAMIC RELATIONSHIP BETWEEN CARDIAC IMAGING AND PHYSIOLOGICAL MEASUREMENTS

By

Wenfeng Duan

Thesis submitted for the degree of Doctor of Philosophy

Supervisors: Dr Dingchang Zheng, Dr Philip Langley, Professor Alan Murray

Institute of Cellular Medicine
Newcastle University

April 3, 2014

Declaration

I declare that this thesis has been written by me and has not previously been submitted or accepted for any other degree. Except where specifically acknowledged, the data were collected, analysed and interpreted by myself.

Wenfeng Duan

Contents

List of figures

List of tables

List of abbreviations

Symbols	Meaning	Unit
AF	Aortic flow	N/A
Ao	Aorta	N/A
AV	Aortic valve	N/A
BMI	Body mass index	kg/m^2
DBP	Diastolic blood pressure	mmHg
ECG	Electrocardiography	N/A
EMD	Electromechanical delay	ms
HR	Heart rate	beat/min
ICG	Impedance cardiography	N/A
LED	Light emitting diode	N/A
LVET	Left ventricular ejection time	ms
MF	Mitral flow	N/A
MV	Mitral valve	N/A
PEP	Pre-ejection period	ms
PPG	Photoplethysmography	N/A
PTT_f	Pulse foot transit time	ms
PTT_p	Pulse peak transit time	ms
SBP	Systolic blood pressure	mmHg
SI	Stiffness index	m/s
TFM	TaskForce Monitor system	N/A

Acknowledgement

I would like to take this opportunity to thank the kind people around me, without their support and help this thesis would not have been possible.

First and foremost I must thank my supervisors, Dr Dingchang Zheng, Dr Philip Langley and Professor Alan Murray. They patiently provided the vision, encouragement and advise necessary in the past three years on my daily research work and on how to write and present scientific research. All of these have been invaluable on both academic and personal levels, for which I am extremely grateful.

Special thanks to my PhD project committee, Dr Guy MacGowan and Dr Michael Drinnan at Freeman Hospital, for their support, guidance and helpful suggestions through all these years. Also thank you to Dr Christ Eggett at Freeman Hospital for his vital support of echocardiography measurement.

I would also like to acknowledge the financial, academic and technical support of the Institute of Cellular Medicine of Newcastle University and its staff, particularly for the Research Studentship which provided necessary financial support for this project. I also thank to the Department of Medical Physics of Freeman Hospital for the office and facilities for scientific research.

Dozens of people have helped and taught me immensely at Medical Physics Department. Thank you to Dr John Allen shared me the measurement room and devices. Also thank you to Miss Susan King provided me the essential training of physiological measurement devices and invaluable helps for the Ethics application of my PhD study. And thank you to Mr John Riddle built me the PPG measurement device. A special acknowledgement goes to my office mate: Dr Luigi Di Marco. He was a true friend and served as a role model to me

ever since we began to share an office in 2012. And I also thank to former PhD students in the department, Dr Kun Wang and Dr Marjan Bojarnejad, for sharing experiences and ideas on PhD study.

Thanks also to the many volunteers from the Newcastle upon Tyne NHS Hospitals Trust and Newcastle University.

Finally, I would also like to express my deepest thanks to my wife Shuang Su for her love, support and infinite patience as always. My parents have sacrificed their lives for my brother and myself and provided everlasting love and care, for which my mere expression of thanks likewise does not suffice.

Abstract

Impedance cardiography (ICG) is a non-invasive technique to measure the dynamic changes in electrical impedance of the thorax. Photoplethymgraphy (PPG) is an optical-based non-invasive physiological measurement technique used to detect the blood volume pulses in the microvascular bed of tissue. These two physiological measurements have potential clinical importance to enable simple and cost-efficient ways to examine cardiovascular function and provide surrogate or additional clinical information to the measures from cardiac imaging. However, because the origins of the characteristic waveforms of the impedance and pulse are still not well understood, the clinical applications of these two techniques are limited.

There were two main aims in this study: 1) to obtain a better understanding of the origins of the pulsatile impedance changes and peripheral pulse by linking their characteristic features beat-by-beat to those from simultaneous echocardiograms; 2) to validate the clinical indices from ICG and PPG with those well-established echocardiographic indices.

Physiological signals, including ECGs, impedance, the first derivative impedance and finger and ear pulses, were simultaneously recorded with echocardiograms from 30 male healthy subjects at rest. The timing sequence of cardiovascular events in a single cardiac cycle was reconstructed with the feature times obtained from the physiological measurements and images. The relations of the time features from the impedance with corresponding features from images and pulses were investigated. The relations of the time features from peripheral pulses with corresponding features from images were also investigated. Furthermore, clinical time indices measured from the impedance and pulse were validated with the reference to the echocardiograms. Finally, the effects of age, heart rate and blood pressure on the image and physiological measurements were examined.

According to the reconstructed timing sequence, it was evident that the systolic waves of the thoracic impedance and peripheral pulse occurred following left ventricular ejection. The impedance started to fall 26 ms and the pulse arrived at the fingertip 162 ms after the aortic valve opened. A diastolic wave was observed during the ventricular passive filling

phase on the impedance and pulse. The impedance started to recover during the late ventricular ejection phase when the peripheral pulse was rising up. While the pulsatile impedance changes were mainly correlated with valve movement, the derivative impedance (velocity of impedance change) was more correlated with aortic flow (velocity of blood flow). The foot of the finger pulse was significantly correlated with aortic valve open (R^2 = 0.361, $P < 0.05$), while its systolic peak was strongly correlated with the aortic valve closing (R^2 = 0.579, $P < 0.001$). Although the pulse had similar waveform shapes to the inverted impedance waveform, the associations between the time features of these two signals were weak.

During the validation of potential clinical indices from ICG, significant correlation was found between the overall duration of the derivative impedance systolic wave (359 ms) and the left ventricular ejection time (LVET) measured by aortic valve open duration from M-mode images (329 ms) (R^2 = 0.324, $P < 0.001$). The overall duration from the finger pulse foot to notch (348 ms) was also significantly correlated with the LVET from M-mode images (R^2 = 0.461, $P < 0.001$). Therefore, both ICG and PPG had the potential to provide surrogates to the LVET measurement.

Age influenced the cardiovascular diastolic function more than systolic function on normal subjects. With age increasing, the reduction of the left ventricular passive filling was compensated by active filling. The ratio of the passive filling duration to the active filling duration decreased with age (R^2 = 0.143, $P < 0.05$). The influence of age on the diastolic wave of the impedance signals was striking. The impedance diastolic wave disappeared gradually with age. The effects of age on the peripheral pulse were mainly on the shortened pulse foot transit time (PPT_f) and prolonged pulse rise time. The large artery stiffness index (SI) increased with age. Most time intervals were prolonged with heart rate slowing down. The effects of systolic blood pressure were evident on pulse transit time and pulse diastolic rising time. Driven by higher systolic blood pressure, both PPT_f and rising time decreased significantly ($P < 0.001$).

In conclusion, from the analysis based on simultaneous physiological measurements and echocardiograms, both the pulsatile impedance changes and peripheral volume pulse were initiated by left ventricular ejection. The thoracic impedance changes reflected volume changes in the central great vessels, while the first derivative impedance was associated

with the velocity of blood flow. Both ICG and PPG had the potential to provide surrogates for the measures of cardiac mechanical functions from images. The PPG technique also enabled the assessment of changes in vascular function caused by age.

Chapter 1 Introduction

This introductory chapter gives an overview of the cardiovascular system and commonly used non-invasive cardiac imaging and physiological measurement techniques. The rational of this study and the organization of thesis are also introduced.

1.1 An overview of the cardiovascular system

1.1.1 Anatomy of the cardiovascular system

The function of the human cardiovascular system is to transport oxygenated blood into organs in the body and take oxygen-depleted blood back to the heart. The cardiovascular system is comprised of the heart and two circulation systems (Figure 1-1): the pulmonary circulation and the systemic circulation. The heart is physiologically separated into the right side and left side by the two circulations. In the pulmonary circulation, oxygen-depleted blood is pumped from the right ventricle to the lungs via the pulmonary artery, where carbon dioxide in the blood is exchanged with oxygen in the lung alveoli. Refreshed blood is then transported into the left atria via the pulmonary veins, thereby pulmonary circulation completes. The systemic circulation begins from the left ventricle, which ejects oxygenated blood into the aorta during systole. The blood is then distributed to all the organs via arterial system. After nutrient and gas exchange, oxygen-depleted blood is carried by the veins back to the right atrium.

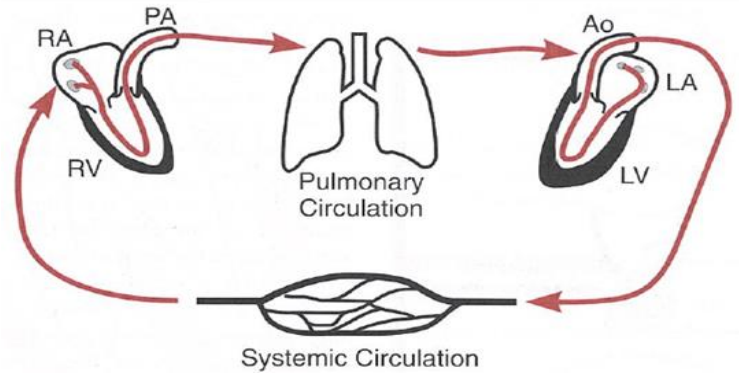

Figure 1-1. Anatomy of the cardiovascular system. RV/LV = right/left ventricles; RA/LA: right/left atrium; Ao = Aorta; PA = pulmonary artery. (Klabunde 2005).

1.1.2 Cardiac anatomy

Figure 1-2 shows the anatomy of the heart, which is comprised of four chambers, two atria and two ventricles, with a thick muscular wall separating them into left and right sides. These chambers act as temporary containers of blood carried by the vessels connecting them. The aorta and pulmonary artery connect with the left ventricle and right ventricle respectively to take blood away from the heart, while the venae cavae and pulmonary veins connect with the right atrium and left atrium respectively to bring blood back to the heart. The return blood from the systemic circulation for the upper body is carried by the superior vena cava and that for the lower body is carried by the inferior vena cava.

There are two valves between the atria and ventricles: the tricuspid valve between the right atrium and ventricle and mitral valve between the left atrium and ventricle. There are two other valves between ventricles and arteries: aortic valve between left ventricle and the aorta and pulmonary valve between the right ventricle and the pulmonary artery. The main function of these valves is to ensure that blood flows only in one direction.

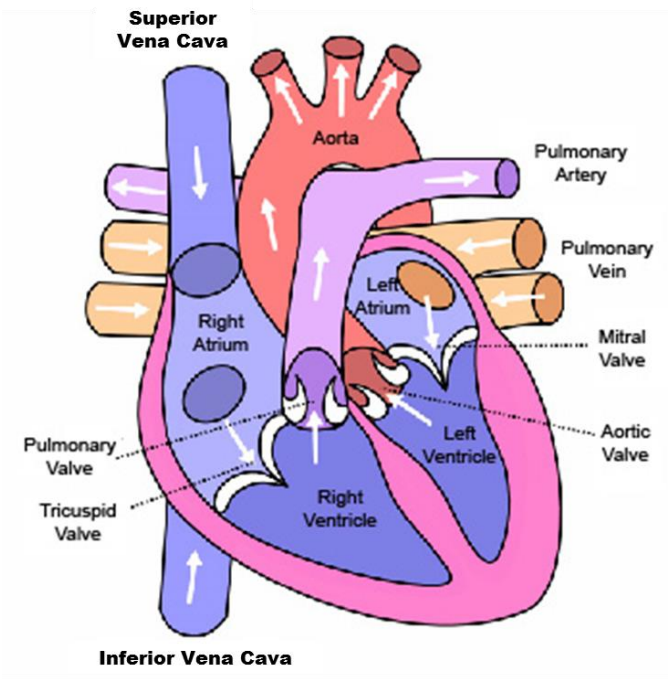

Figure 1-2. Anatomy of the heart.

1.1.3 Cardiac electrical activity

Action potentials originate from the pace-making cells, known as the sinoatrial (SA) node, which is located in the posterior wall of the right atrium near the base of the superior vena cava. It travels downwards and leftwards throughout the heart along a specific conduction system and leads to the depolarization of myocardial cells. The cardiac electrical conduction system is shown in Figure 1-3. In the right atrium, the action potentials conduct cell by cell through internodal tracts and into the left atrium through Bachmann's bundle. Because separated by non-conducting tissue, the potentials from the atria can only enter into ventricles via a specialised cluster of cells, known as atrioventricular (AV) node. The conduction velocity of the action potential is slowed down in the AV node, which makes sure that there is enough time for the myocytes in the atria to depolarise and contract. Action potentials leave the AV node and enter into the ventricles via the bundle of His, which sequentially branches into left and right pathways along the interventricular septum. There are numerous Purkinje fibres on the bundle branches connecting with ventricular myocytes, where the action potentials spread out from cell-to-cell. The conduction velocity in the His-Purkinje system is high compared with that in the ventricular myocytes.

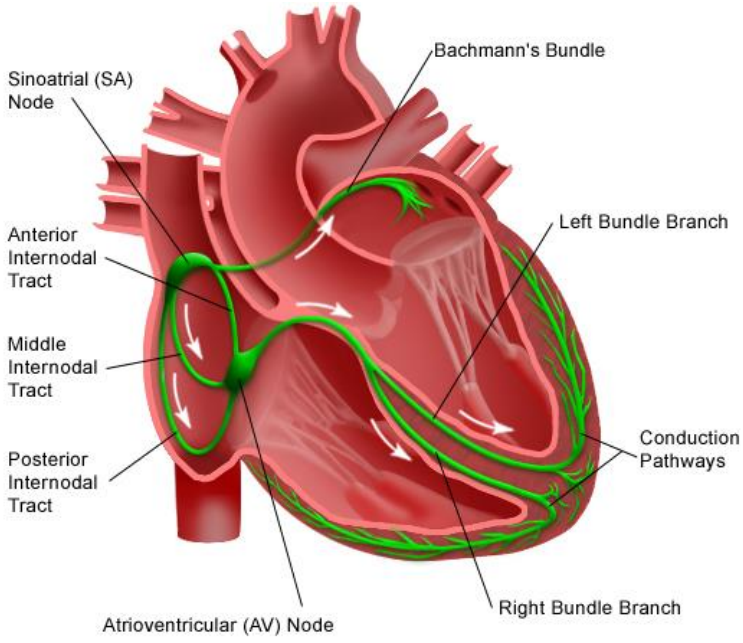

Figure 1-3. Illustration of cardiac electrical conduction system.

Both the electrical conduction pathways and velocity are important as they initiate and regularise the cardiac mechanical functional sequence. The action potential conduction velocity in each section of the conduction systems is summarized in Table 1-1.

Table 1-1. Action potential conduction velocity in different paths on the human beings (Klabunde 2005).

Paths	**Velocity (m/s)**
Atrial myocytes	0.5
Bachmann's bundle	0.5
AV node	0.05
His fibres	2
Purkinje fibres	4
Ventricular myocytes	0.5

1.1.4 Cardiac cycle

Initiated by the cardiac electrical activity, the heart contracts and relaxes rhythmically. A cardiac cycle is comprised of three main phases in sequence: atrial systole, ventricular systole and ventricular diastole. Figure 1-4 shows the changes in the pressure, volume and blood flow velocity in the aorta, left atrium and left ventricle in each phase. Those changes in the right side of the heart are similar to those in the left side in normal hearts.

Traditionally, a cardiac cycle is considered to start from the atrial systole phase. The depolarization of the atria initiates the atrial myocardial contraction, which in turn causes an increase in the pressure in the atria (the A wave on the left atrial pressure trace). Driven by the pressure gradient, the mitral valve is reopened from an incomplete closing status and the left ventricle is filled with the blood from the left atrium. The pressure in the left ventricle continuously rises with the filling. When the left ventricular pressure exceeds the left atrial pressure, the mitral valve is closed and the filling ends. The ventricular filling

phase during atrial systole is also known as the active filling phase because it results from atrial contraction. The active filling is the second ventricular filling phase in each cardiac cycle, which contributes only 10 – 20% blood volume of the resting young heart. This proportion increases significantly with advancing age and exercise (Levick 2010).

When the action potential arrives at the ventricles through the AV node, cardiac electrical depolarization initiates ventricular systole. Because of the myocardial contraction, the ventricular pressure rises rapidly and quickly exceeds the pressure in the aorta. The aortic valve is opened allowing the left ventricle to eject blood into the aorta. The period from the mitral valve closing to aortic valve opening is known as the isovolumic contraction phase, because the blood volume in the left ventricle does not change. Driven by the pressure gradient, the velocity of left ventricular ejection increases rapidly during the early stage (rapid ejection). However, when the ventricular pressure decreases below the aortic pressure, the blood velocity slows down (slow ejection). The aortic pressure also decreases during the slow ejection when the blood volume draining away from the aorta to the peripheral circulation overwhelms that of blood ejected into the aorta from the left ventricle. With the reversed pressure gradient between the left ventricle and the aorta increasing further, the aortic valve closes, and thus the left ventricular ejection is completed. The valve closing produces a characteristic notch (incisura) on the aortic pressure curve, which is followed by a long-tail decay period.

The ventricular pressure keeps falling with myocardial relaxation during the early stage of ventricular diastole. The atria receive blood returned from the veins during the ventricular ejection phase which results in pressure elevation in the atria. The left atrial pressure overwhelms the left ventricular pressure during the early ventricular diastole and the mitral valve opens. The period from the aortic valve closing to the mitral valve opening is known as left ventricular isovolumic relaxation, following which the left ventricle is filled by the blood from the left atrium. In this phase, because the blood flows passively from the veins through the atrium into the ventricle, it is usually known as passive filling phase. In addition, because the filling velocity during this phase is faster than that during the active filling phase, it is also known as the rapid ventricular filling phase. The major ventricular filling is completed in the passive rapid filling phase.

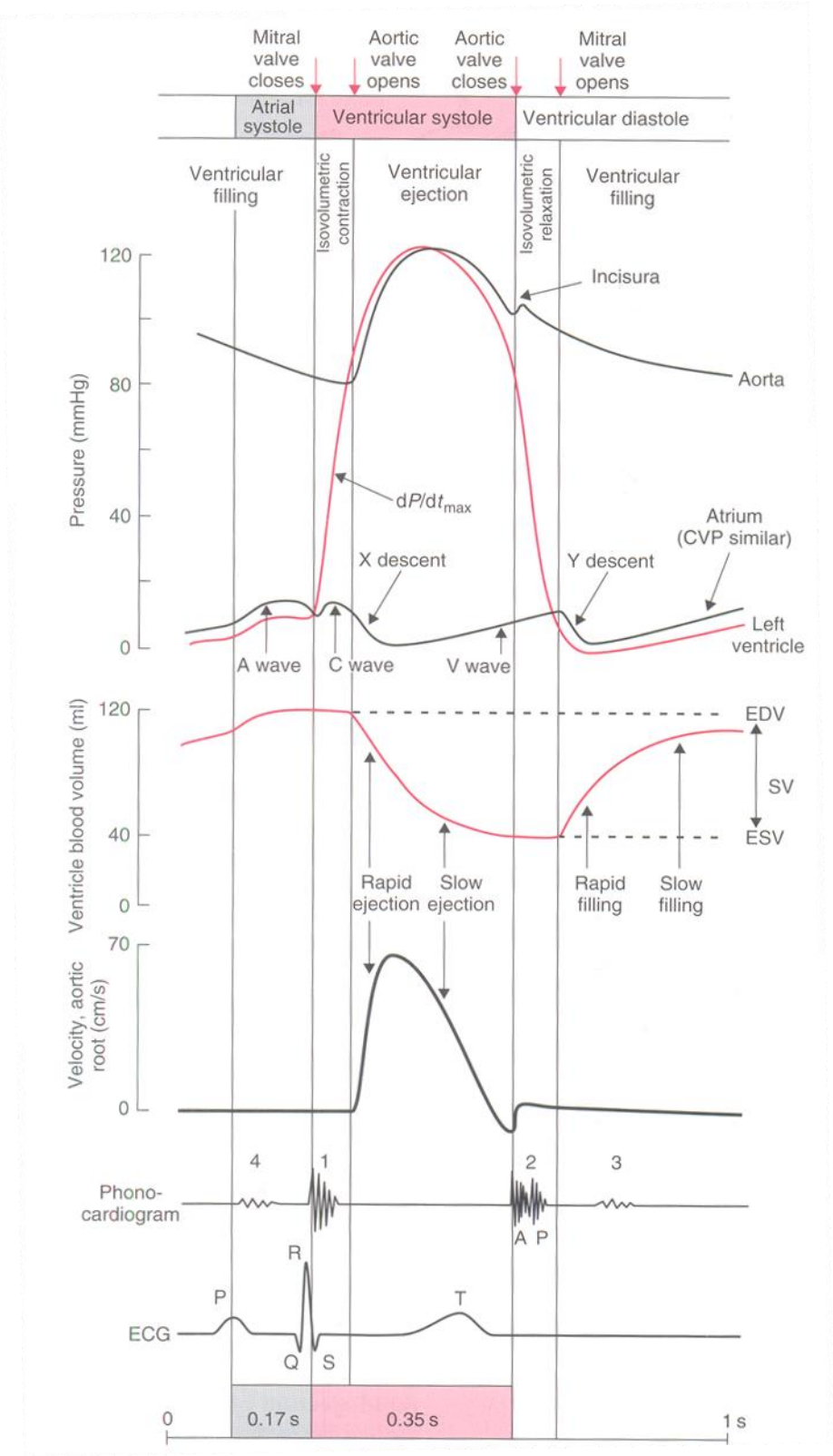

Figure 1-4. Pressure, volume and flow velocity changes in aorta, atrium, and left ventricle in a cardiac cycle (Levick 2010).

The reference values of the time durations of each cardiac cycle phase and valve movement and volume changes in the left atrium and ventricle are summarized in Table 1-2.

Table 1-2. Time intervals, valve movement, and volume changes in the left atrium and left ventricle during each cardiac cycle phase on normal subjects (Levick 2010).

Phases		Time durations (s)	Valve movement		Volume changes	
			Mitral	Aortic	Atrium	Ventricle
Atrial systole	Active ventricular filling	0.17	Open	Close	Decrease	Increase
Ventricular systole	Isovolumetric contracion	0.05	Close	Close	No change	No change
	Ventricular ejection	0.3	Close	Open	Increase	Decrease
Ventricular diastole	Isovolumetric relaxation	0.08	Close	Close	Increase	No change
	Passive ventricular filling	0.33	Open	Close	Decrease	Increase

1.1.5 The arterial system and pulse wave

The arterial system

Blood is carried by the arterial system away from the heart to the rest of the body. The arterial system of the human body is shown in Figure 1-5. The arterial system starts from an ascending portion (ascending aorta) that connects with the left ventricular outflow track. At the following arch (arch of the aorta), the aorta braches into several parts including carotid arteries which provide blood supply to the brain, subclavian arteries which provide blood supply to the arms, and a continuous descending aorta which runs down through the chest and abdomen. The descending aorta is the largest arterial vessels in the body with the inner

diameter around 25 mm. It is divided into thoracic aorta and abdominal aorta according to the cavities where it is situated. The extension of the abdominal aorta forms the common iliac artery, which in turn branches into the iliac artery to carry blood into the legs. The aorta and large arteries are also known as distribution vessels because they are the main vessels to distribute blood flow to specific organs. Arteries within organs further branch into small arteries and then arterioles. As the diameters of small artery and arteriole are so small (< 0.2 mm), they produce resistance to blood flow. The small arteries and arterioles together are recognized as resistance vessels which regulate blood pressure and flow within organs. Capillaries are the last part of the arterial tree, which joins with veins. Although even smaller than resistance vessels, they are arranged in parallel, and thus own a huge cross-sectional area. This structure allows blood flow through them with little resistance. Capillaries are where there are nutrient and gas exchange. After that the blood flows back to the right atrium via the venous system.

The aorta and large arteries are elastic vessels with thick muscular wall, which means that they are distensible. When the left ventricle ejects, the aorta and large arteries expand passively to accommodate more blood. When the left ventricle relaxes, the aorta constricts to reduce its volume. This distensability of vessels to increase and decrease volume passively due to changes in pressure is termed compliance, which is significant to minimise workload of the heart. Compliance is quantified by the ratio of volume change to pressure change in the vessels. The reciprocal of the compliance, defined as stiffness, is also used as another way to quantify distensability. The vascular compliance is determined by the ratio of elastin to collagen in the muscular wall of a vessel. The higher the ratio is, the more compliant a vessel is. As the ratio continues to decrease, the compliance keeps falling in the arterial vessels proceeding towards the periphery of the body. At the resistance vessels, the compliance almost disappears as they have only few layers of smooth muscle.

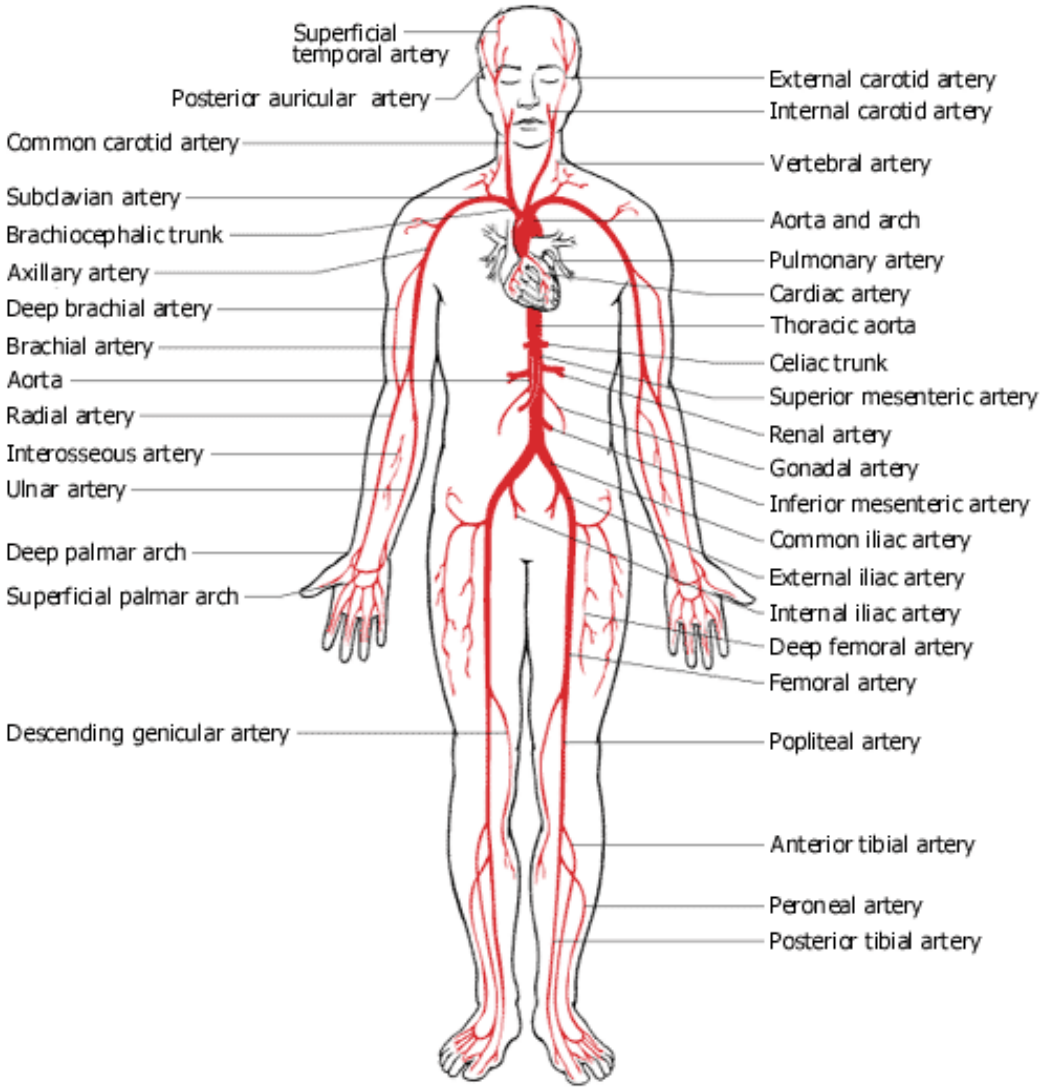

Figure 1-5. Anatomy of human arterial system.

Pulse wave propagation in arteries

The blood ejection of the left ventricle during systole causes pulsatile changes in flow, pressure and blood volume in the ascending aorta, which then propagate along the arterial system throughout the body. As the stroke volume of the left ventricle is pumped into the aorta, the pressure in the ascending aorta experiences a rapid rise. In the meanwhile, the volume in the aorta is draining to the periphery, which leads to the pressure starting to decrease since in late systole ejection slows down. As in the previous description, the aortic valve closing causes an incisura on both the aortic pressure pulse and flow curves. As the pressure pulse travels forward (incident), a reflected wave is produced from the periphery

and travels backward in the arterial system. The exact reflecting sites are still not clear, but it is assumed to be at the junction between highly conducting large arteries and highly resistant arterioles (O'Rourke et al. 1992). The reflection generates a second wave following the incisura, which is clearer on young people.

Both the amplitude and contour of the pulses change gradually during the propagation from the ascending aorta to the peripheral arteries. As shown in Figure 1-6, from the central to distant arteries, the amplitude of the flow pulse decreases, but the overall shape becomes more rounded. By contrast, the amplitude of the pressure pulse increases, but the forward wave is abbreviated. The incisura on both the pressure pulse and flow contours becomes less apparent on the peripheral arteries, and the second wave caused by the reflection becomes more significant. Age also changes the pulse contour. With increasing age, the effects of the reflected wave are less significant. The augmentation of the forward wave is less and the fluctuation of the second wave is reduced (O'Rourke et al. 1992).

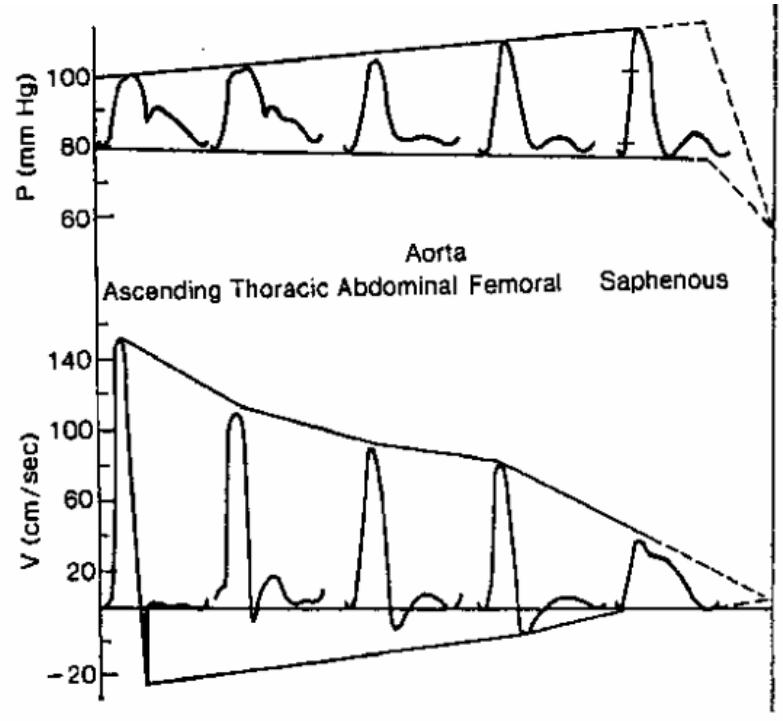

Figure 1-6. Illustration of pressure and flow pulse propagation along the arterial system (McDonalds 1974).

The velocity of the pressure pulse transiting in the arterial system is affected by the characteristics of arterial vessels and blood, which was described by the Moens-Korteweg formula below (Callaghan et al. 1986):

$$\mathrm{PWV} = \sqrt{(\mathrm{d} \times \mathrm{E})/(2 \times \mathrm{D} \times \rho)}$$

Where PWV = pulse wave velocity, d = vessel wall thickness, E = Young's modulus of elasticity, D = arterial inner diameter, ρ = density of blood.

It can be seen from the above formula that the pulse wave velocity is inversely dependent on the arterial inner diameter. In the ascending aorta the pulse wave velocity is slowest at around 5 m/s, while in the normal peripheral arteries this velocity can increase to 10 m/s (Nichols and O'Rourke 1990). In addition, the pulse wave travels faster in arteries with stiffer walls. The arteries become stiffer with advancing age due to the loss of elastin fibers in the wall. Cardiovascular diseases, such as hypertension, also make significant contributions to the stiffening of the arterial vessels. Therefore, the pulse wave velocity usually increases in older people and hypertensive patients. Another important age-related change in the arterial system is the calcification which thickens the vessel wall, and consequently speeds the pulse wave velocity.

1.1.6 The venous system and blood flow

The venous system

The function of the venous system is to carry the de-oxygenated blood from the body to the heart. As arteries and veins travel and branch out through the body side-by-side in the most part, they usually share similar names. Two large veins, the superior vena cava and the inferior vena cava, connect with the heart and discharge the return blood into the right atrium. All venous vessels from the head, chest and upper extremities lead into the superior vena cava, while those vessels from the parts below the diaphragm lead into the inferior vena cava. Veins are different from arteries in structure and function; because they lack muscular power, the veins do not function primarily in a contractile manner, but have a prominent capacity for vasodilation; veins are collapsible, and collapse when they are not filled with blood; veins are also more compliant than arteries, which enable them to

maintain about two-thirds of the blood pool; most veins contain one-way valves to keep blood flowing toward the heart.

Venous blood flow

Blood flow in the great veins is pulsatile. As shown in Figure 1-7, the changes in the flow velocity in the vena cava are inversely related to the changes in the right atrial pressure. An increase in the pressure corresponds to a decrease in the flow velocity and vice versa. In each cardiac cycle there are three characteristic components on the velocity tracing of the vena cava. During the atrial systole phase, resulting from a rapid rise in the right atrial pressure, the flow velocity in the vena cava is sharply reduced and the flow is halted or even reversed. With the relaxation of the atrium, the flow recovers and the velocity goes back to the normal level. The flow is accelerated when the right ventricular ejection starts, and the major peak flow occurs during the ventricular systole phase. The reinforcement of the ventricular ejection to the flow in the great veins is explained by the 'sucking effect' (Levick 2010): the ejection of the ventricles causes the ventricular annulus fibrous to descend, which leads to the atria being stretched as the pressure decreases, and consequently blood in the great veins is sucked into the atria. The velocity of venous blood declines during the slow ejection phase. A second increase in the blood flow is seen during the earlier diastole. The pressure in the right atrium falls when the tricuspid valve opens. The blood in the great veins is sucked into the right atrium driven by the pressure gradient. This diastolic component is vulnerable to heart rate variation. At rapid heart rates, this component is much reduced in size or even disappears (Wexler et al. 1968).

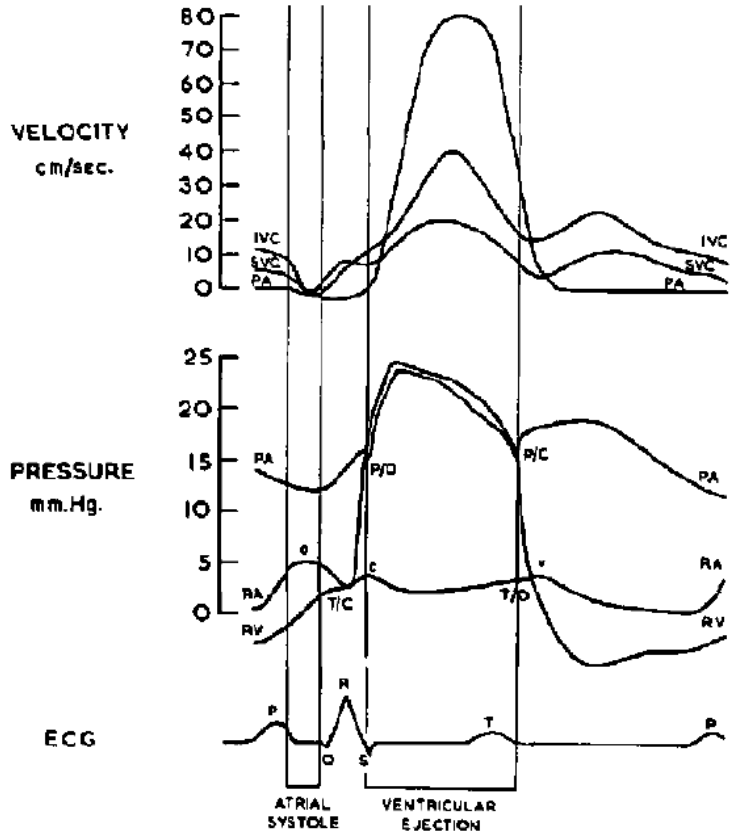

Figure 1-7. Diagram of pressure and velocity of blood flow into and out of the right heart on normal human subjects. Top: velocity of blood in the superior vena cava (SVC), inferior vena cava (IVC) and pulmonary artery (PA); Middle: pressure waveform in pulmonary artery (PA), right atrium (RA) and right ventricle (RV); Bottom: simultaneous ECG tracing. (Wexler et al. 1968).

1.2 Non-invasive techniques for cardiac function assessment

1.2.1 Echocardiography

Echocardiography is currently one of the most commonly used cardiac imaging techniques. It employs very high-frequency ultrasound wave (frequency > 1.5 MHz) to scan the heart. Cardiac structure and function are examined based on the images reconstructed from reflected waves (echo). A piezoelectric transducer is contained in a scanning probe to transform the electrical signal into mechanical vibrations of the crystal with the desired ultrasound frequency. The range of ultrasound frequency is normally between 2 and 18 MHz. The choice of frequency depends on the specific application.

Higher frequencies provide higher resolution but suffer from poorer penetration than lower frequencies. Like any other mechanical wave, when the ultrasound encounters an interface formed by two adjoining tissues with different impedance, it will be reflected, refracted and scattered. The reflected ratio r is determined by the formula as following:

$$r = \frac{(Z_1 - Z_2)^2}{(Z_1 + Z_2)^2}$$

Where Z_1 and Z_2 denote the impedance of the two tissues respectively. The echo will be recorded by a detector and then transformed back to an electrical signal. As the transmitting speed of ultrasound in soft tissues is usually considered as constant (around 1540 m/s), the depth of the reflection point can be estimated by the product of half the delay of echo and the wave traveling speed. Additionally, as different tissues possess different impedances, it is possible to distinguish them according to the intensity of the echo.

Because of the obstruction of bones and gas zones in the body, there are only a few specific points on the chest available for the ultrasound probe to scan the heart. These points are often referred to as echocardiography windows. Three main windows are commonly used, including: 1) the left parasternal window, at the left sternal edge between the 2nd and 4th intercostal spaces; 2) the apical window, near the apex of the left ventricle; 3) the subcostal window, under the xiphisternum. Different views to the heart are provided by placing the probe on different windows or rotating it on the same window. Figure 1-8 illustrates the recording of 2D echocardiography in the long-axis parasternal view, where a number of cardiac structures can be seen.

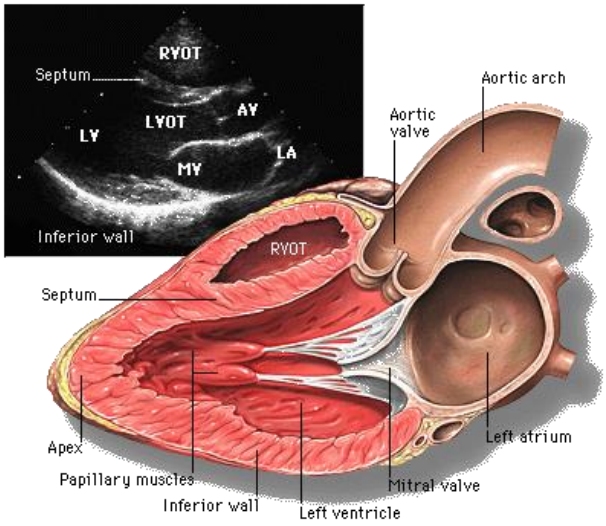

Figure 1-8. Illustration of 2D echocardiography in long-axis parasternal view. Cardiac structures seen in this view include: right ventricular outflow tract (RVOT), interventricular septum, left ventricular outflow tract (LVOT), aortic valve (AV), left ventricle (LV), mitral valve (MV), left atrium (LA).

A series of echocardiography techniques have been delivered in the last decades. The earliest diagnostic application is A-mode (amplitude-based) ultrasonography, which presents the echo as a spike with the amplitude denoting the intensity. The following B-mode (brightness-based) technique converts the spike into dots and replaces amplitude with brightness. Positions of the dots represent the depth of tissues under the body surface and the brightness represents the intensity of the echo. The movement of tissues with time can be examined by continuous B-mode recording and this technique is called M-mode (motion-based) echocardiography. The temporal resolution of the M-mode echocardiography can be high as 2000 samples per second. However, as M-mode images are difficult to interpret and the measurement of dimensions is heavily influenced by the location of the acoustic window, it is gradually replaced by more anatomically correct 2D (two-dimensional) echocardiography (Feigenbaum 2010). Although still based on B-mode, the 2D mode technique employs a probe with a linear array of crystals inside, which produces multiple ultrasound lines at the same time. A cross-sectional area of the heart can be reconstructed by the echoes along these lines. 2D echocardiography provides a temporal resolution of around 100 frames per second, which is lower than that provided by the M-mode. However, the 2D technique, based on some simple geographic models, is able to provide much more accurate dimension measurement. Subsequently, 3D (three-dimensional)

method has become available for clinical applications. Because no anatomical assumption of the heart is required, it provides excellent performance on volume related parameter measurement (Nosir et al. 1996).

Doppler imaging is another important echocardiographic technique, which is able to provide cardiovascular hemodynamic information non-invasively. The underlying principle of the Doppler technique is that the frequency of echo is altered by a moving target, such as red blood cells; the magnitude of the frequency shift is proportional to the velocity of the target, and the polarity of the shift reflects the movement direction of the target toward (positive) or away (negative) from the probe (Quiñones et al. 2002). There are two Doppler echocardiography modalities that are in common use: continuous wave (CW) Doppler and pulsed wave (PW) Doppler imaging. The CW Doppler technique employs two separate transducers to transmit the ultrasound beam (transmitter) and receive echoes (receiver) continuously. The CW technique is able to measure high velocities accurately. However, its main disadvantage is that the velocities measured reflects the mean velocity along the sound beam and thus lack selectivity and depth discrimination. The PW Doppler employs a single transducer that transmits and receives ultrasound alternately. During the examination, an ultrasound pulse is transmitted into the body, and the echo reflected from only a specific depth is picked up. This process is repeated for continuous monitoring. The main advantage of the PW Doppler technique is that the movement velocity at specific sites (or sample volumes) can be selectively examined by the operator. However, it is vulnerable to the aliasing phenomenon when the frequency shift is over the Nyquist limit resulting from high movement velocity.

Because of the high temporal resolution, M-mode echocardiography is still considered an effective and efficient way to record fast moving cardiac tissues, including valves and interventricular septum (Feigenbaum 2010). Mitral valve is a fast moving tissue. It initially opens during the left ventricular rapid filling phase and reopens during the active filling phase in each cycle. The movement of its anterior and posterior leaflets during these two phases generates the characteristic E wave (passive filling) and A wave (active filling) on the M-mode images for the mitral valve. The amplitude of the E wave and A wave represent the excursion of the leaflets and consequently reflect the blood volume passing through the mitral orifice. The distance between the interventricular septum and the anterior leaflet at the maximum excursion was reported as an important indicator of left ventricular

performance (Massie et al. 1977, Ahmadpour et al. 1983). In addition, timing features of the A wave were considered as an indicator of the left ventricular end-diastolic pressure. With an elevated left ventricular end-diastolic pressure, the closing motion of the mitral valve during the active filling phase starts earlier and thus the whole duration is longer, and occasionally interrupted (Konecke et al. 1973, Lewis et al. 1978, Ambrose et al. 1979). The M-mode recording for the aortic valve movement is also able to provide useful clinical information. In a normal heart, 2 of the 3 leaflets produce a parallelogram on the M-mode tracing throughout the left ventricular ejection phase. An irregular pattern may indicate an abnormal cardiac function. The abrupt closure during early or mid-systole would indicate a dynamic obstruction of aortic flow, while reduced separation of the leaflets would result from left ventricular outflow obstruction (Feigenbaum 2010). M-mode imaging can also be employed to record the pulmonary valve and tricuspid valve movement, but it is less common in clinical practice (Feigenbaum 2010). Other important applications of the M-mode technique include the measurement of left ventricular internal dimension, septal wall thickness, left ventricular posterior wall thickness. These parameters are measured at both end-systole and end-diastole, based on which important diagnostic indices reflecting the left ventricular performance are derived, including left ventricular mass, fractional shortening and midwall fraction and shortening (Lang et al. 2005, Gottdiener et al. 2004, Devereux et al. 2004).

2D echocardiography is employed to obtain volumetric measurement. Several methods have been developed for the volume measurements based on 2D images. The biplane Simpson method is the most commonly used method, which calculates the volume based on the summation of a stack of equidistant disks from two orthometric views. The left ventricular volume is measured from apical 4 chamber and 2 chamber views by the biplane Simpson method. The volume is obtained at end diastole (end-diastolic volume), which is defined as the frame with the largest cardiac dimension in the cardiac cycle, and obtained at end systole (end-systolic volume), which is defined as the frame with the smallest cardiac dimension in the cardiac cycle (Lang et al. 2005). Based on the calculated volumes, two important indices representing left ventricular systolic function can be derived, including stroke volume (SV = end-diastolic volume – end-systolic volume) and ejection fraction (EF = SV / end-diastolic volume).

One of the most important applications of Doppler echocardiography is to evaluate the left ventricular diastolic function, which is characterized by the left ventricular filling flow and pressures. For this purpose, transmitral inflow is examined by pulsed wave Doppler imaging. The mitral flow in a Doppler image is similar to that in an M-mode image; an E wave during rapid filling phase and an A wave during active filling phase. However, the Doppler image represents the velocity information, while the M-mode image represents the volumetric information. They are physiologically complementary (Feigenbaum 2010). The Doppler E wave primarily reflects the pressure gradient between the left atrium and left ventricle during ventricular early diastole, while the A wave reflects the pressure gradient during atrial systole. Therefore, the E wave is affected by left ventricular preload, relaxation, early diastolic pressure and compliance (Appleton et al. 1988a). The peak velocities, time intervals and velocity-time integral from the E wave and A wave can provide significant information for the assessment of the left ventricular diastolic function. The age-associated alteration in the transmitral inflow measured from the Doppler imaging is well appreciated; the ratio of the E wave peak velocity to the A wave velocity (E/A) decreases with age, the velocity decelerating time (DT) of the E wave is prolonged because of a slowing of myocardial relaxation in elder people (Klein et al. 1994). The pulsed wave Doppler is also used to record the velocity of aortic flow during left ventricular ejection. In combination with the 2D images, the left ventricular stroke volume in each cardiac cycle can be calculated by the product of the velocity-time integral of the aortic flow and the cross-sectional area at the left ventricular outflow tract (Quinones et al. 2002). Another promising application of Doppler echocardiography techniques is to record the longitudinal velocities within the myocardium. The myocardium movement velocity is usually recorded with the pulsed wave Doppler modality by placing a sample volume at the junction of the left ventricle wall with the mitral annulus. The velocity tracing of myocardium is typically comprised of two diastolic waves, one corresponding to the left ventricular early diastole and the other to the atrial systole, and a systolic wave. It has been reported that the early diastolic wave on the myocardial velocity tracing is mainly associated with left ventricular relaxation but relatively independent of left atrial pressure. Therefore, the ratio of transmitral flow E wave and the myocardial early diastolic wave is a reliable index of the left atrial pressure (Sohn et al. 1999, Nagueh et al. 1997, Ommen et al. 2000). Additionally, the myocardium deformations during the isovolumic phases are better indices representing

left ventricular systolic function in ischaemic myocardium than the peak flow of the ejection (Alam et al. 2000, Edvardsen et al. 2002).

Systolic time intervals (STI) are able to provide simple evaluation of left ventricular function. The most commonly used STIs in clinical applications included pre-ejection period (PEP) which represents the time period from the onset of ventricular depolarization to the onset of ventricular ejection, electromechanical delay (EMD) which represents the time delay from the onset of ventricular depolarization to the end of ventricular ejection and left ventricular ejection (LVET) which represents the overall duration of left ventricular ejection. The STIs were originally obtained from the combination of electrocardiogram, phonocardiogram and carotid arterial pulse tracing (Weissler et al. 1968). However, these indices can also be easily obtained from echocardiograms (Hirschfeld et al. 1975, Schieken et al. 1978, Appleton et al. 1988b). From echocardiograms, the PEP was defined as the period from ECG Q wave to the aortic valve initial opening; the EMD was defined as the time interval from ECG Q wave to the aortic valve closing; the LVET was defined as the duration from the aortic valve opening to closing. Some published reference values of the systolic time intervals and the mitral flow deceleration time (DT) during the ventricular passive filling phase are summarized in Table 1-3.

Numerous guidelines and standards, on applying the echocardiography to the examination and diagnosis of cardiac function and disease, have been established by the American Society of Echocardiography (ASE) since its foundation in 1975; recommendations for quantification of Doppler echocardiography (Quiñones et al. 2002), chamber quantification (Lang et al. 2005), the evaluation of left ventricular diastolic function (Nagueh et al. 2009), assessment of valve stenosis (Baumgartner et al. 2009), echocardiographic imaging in clinical trials (Douglas et al. 2009), and the quantitative evaluation of cardiac mechanics (Mor-Avi et al. 2011).

Table 1-3. Summary of literatures on the reference values of systolic time intervals measured from echocardiograms.

References	***Subject No.***	***Mean (SD) (ms)***				***Imaging modality***
		PEP (Q -> aortic valve open)	EMD (Q -> aortic valve close)	LVET (aortic valve open -> close)	DT (peak passive filling -> the end of filling)	
Hirschfeld et al. 1975	15	89 (10)	315 (44)	277 (40)	--	M-mode
Schieken et al. 1978	10	--	360 (80)	--	--	M-mode
Appleton et al. 1988b	30	--	--	--	193 (23)	Doppler
Tseng et al. 1989	34	101 (13)	--	295 (24)	--	M-mode
Giannuzzi et al. 1996	508	--	--	--	144 (43)	Doppler
Yeo et al. 1998	26	--	--	332 (21)	--	Doppler
Ommen et al. 2000	100	--	--	--	195 (20)	Doppler

PEP = pre-ejection period; EMD = electromechanical delay; LVET = left ventricular ejection time; DT = deceleration time.

1.2.2 Electrocardiography

Electrocardiography is a non-invasive way to record electrical voltages on the human body surface, which represents the propagation of the electrical depolarization and repolarization in the heart. Voltages are recorded by an array of electrodes placed on the chest or limbs. A standard 12-lead ECG system employs 10 electrodes to record the voltages, with 4 attached on limbs and 6 on the chest. The 12 lead ECGs, generated by different combinations of the electrodes, can be categorized into three basic types: standard limb leads (lead I, II, III), augmented limb leads (lead aVF, aVL, aVR) and chest (or precordial) leads (lead V1 ~ V6). The standard limb leads are also known as bipolar leads as each of them uses a pair of positive and negative electrodes. On the other hand, augmented limb leads and chest leads only have one positive electrode, and a virtually negative electrode provided by the electrical combination of other electrodes, so they are also known as unipolar leads.

The ECG leads examine the propagation of the electrical wave in different orientations, which are illustrated in Figure 1-9. While the standard limb leads, together with the augmented limb leads, record the electrical wave propagation in the frontal plane, the precordial leads record the wave in the horizontal plane. According to the anatomical areas of the heart to which the leads correlate, the 12 ECG leads can also be divided into four groups:

- inferior leads, including lead II, III and aVF, which examine the electrical wave propagation towards the inferior end;
- lateral leads, including lead I, aVL, V5 and V6, which examine the electrical wave propagation towards the lateral wall of the left ventricle;
- septal leads, including lead V1 and V2, examine the electrical wave propagation from the ventricular septum;
- anterior leads, examine the wave propagation from the anterior wall of the ventricles.

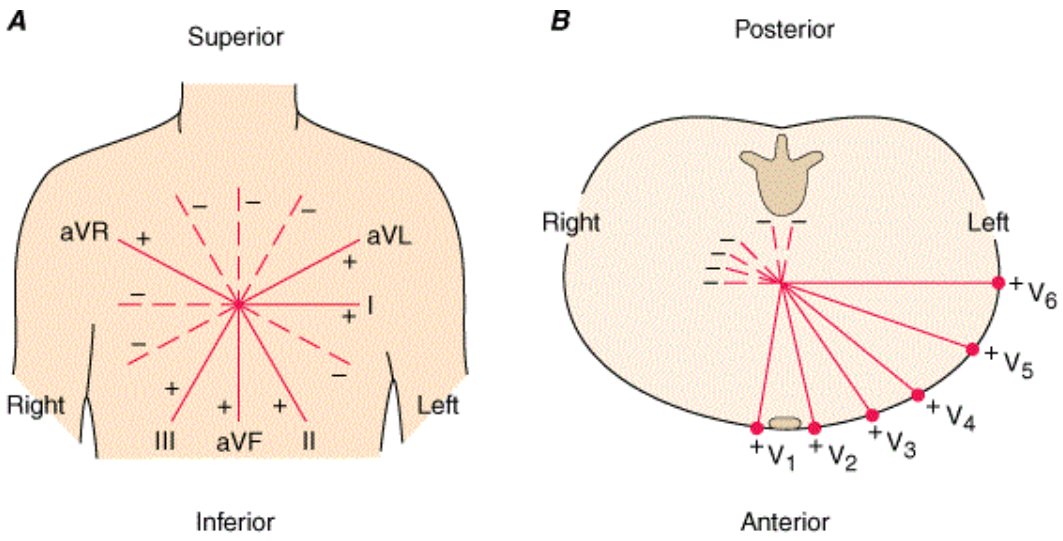

Figure 1-9. Orientations of standard ECG leads. (Fauci et al. 2008).

The ECG tracing represents the voltage change from a baseline (isoelectric) voltage. The isoelectric voltage is generated during the period when there is no electrical wave transferring in the heart or the transferring direction is precisely perpendicular to the lead orientation. Otherwise, a positive voltage is recorded in normal hearts when the depolarization wave is transferring towards or the repolarization wave is transferring away from the positive electrode of the lead, while negative voltage is recorded when the depolarization wave is transferring away or the repolarization wave is transferring towards the negative electrode.

A typical ECG tracing with timing feature definition is shown in Figure 1-10. The ECG waveform in each cardiac cycle is composed of several characteristic components: the P wave, the first positive deflection on the standard limb leads, representing atrial depolarization; the QRS complex, the largest deflection on ECG tracing, representing ventricular depolarization; the T wave: the positive deflection after the QRS complex, representing ventricular repolarization. On some precordial leads, especially Leads V2 ~ V5, a positive U wave is often seen following the T wave. Although the U wave was first designated as early in 1903 by Einthoven (1903), its generation is still in debate. The three main hypotheses for the generation of the U wave include: 1) repolarisation of the Purkinje fibres, 2) repolarisation of some portions of the ventricular myocardium, 3) stretch-induced delayed after-potentials caused by mechano-electric coupling (Surawicz 1998). However, none of them has been universally accepted.

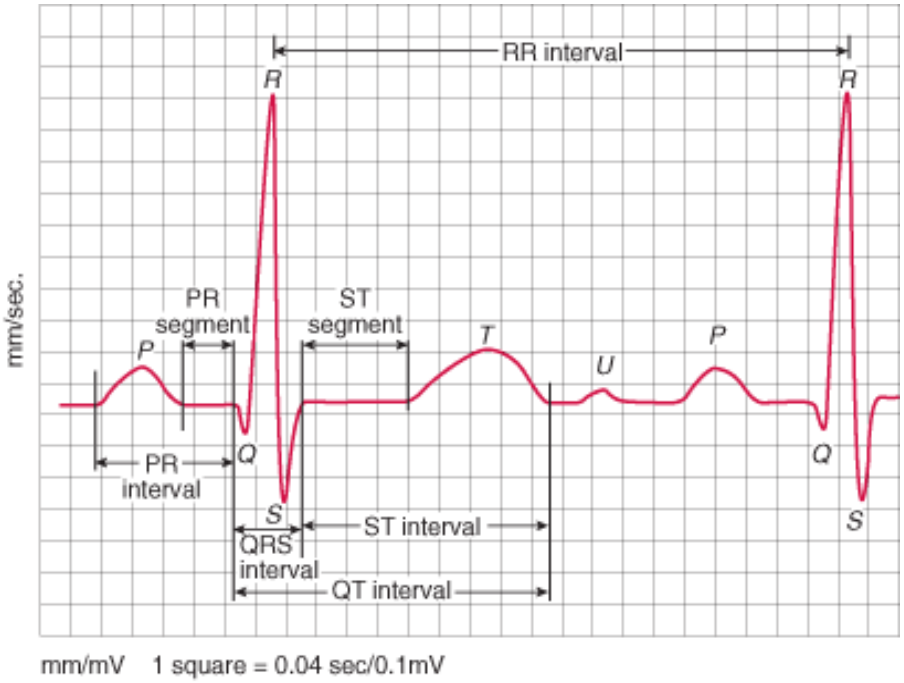

Figure 1-10. Illustration of normal ECG tracing and time feature definition.

The ECG timing intervals have significant clinical applications. The commonly used time intervals include P wave interval (the duration of atrial depolarisation), QRS interval (the duration of ventricular depolarisation), PR interval (the duration for the action potential transferred from the SA node to the ventricles), QT interval (the overall duration of ventricular depolarization and repolarization) and ST segment (the isoelectric duration between ventricular depolarization and repolarization). The definitions and reference values of the ECG timing intervals are summarized in Table 1-4.

Table 1-4. Definitions of ECG timing intervals and their reference values on normal adults.

Intervals	Measurement	Normal range (ms)
P wave interval	from P wave onset to offset	80 – 100
QRS interval	from Q wave to S wave	60 – 100
PR interval	from P wave start to Q wave	120 – 210
QT interval	from Q wave to T wave end	200 – 400
ST segment	from S wave to T wave start	80 – 120

1.2.3 Impedance cardiography

Impedance cardiography is a non-invasive technique to assess the cardiac function based on the measurements of the electrical impedance of the thorax. The study on the measurement of cardiovascular function through electrical impedance methods started from the 1930s and 1940s, while the first device which was able to obtain the impedance signals reliably on the human body was developed in the 1960s for NASA (Kubicek et al. 1967). This device was commercialized in 1968, known as the Minnesota Impedance Cardiography (MIC), which was widely employed in earlier studies (Miller and Horvath 1978). The underlying principle of impedance cardiography techniques is that when a high frequency sinusoidal current is applied across the chest, the changes in the thoracic impedance associated with cardiac mechanical activity can be recorded. Four electrodes were usually used to capture the thoracic impedance changes, with two on the neck and the other two around the upper abdomen. The outer two electrodes were paired to supply high-frequency and low-amplitude alternating current, while the inner pair was used for voltage pick up. The block diagram of the MIC system is shown in Figure 1-11 and the signals recorded by the system are shown in Figure 1-12.

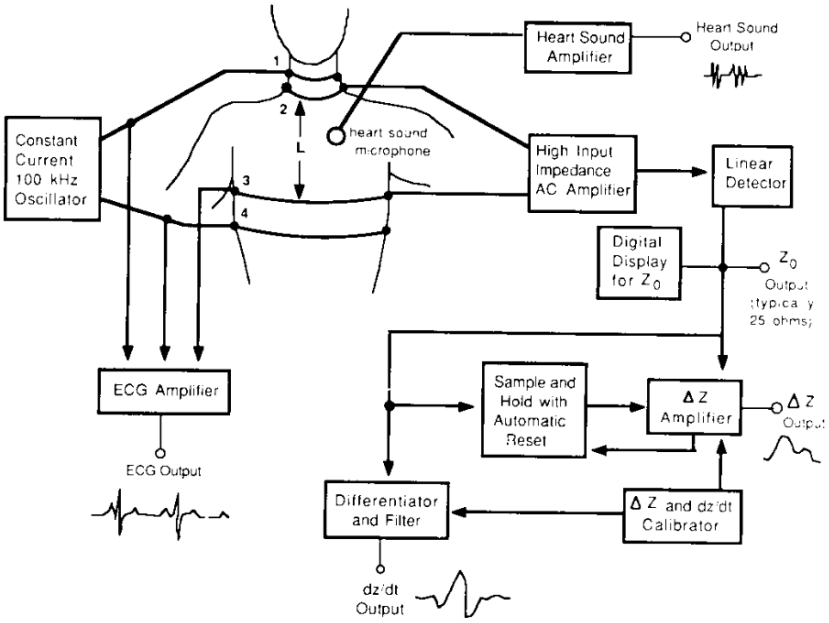

Figure 1-11. Block diagram of Minnesota Impedance Caridography (MIC) system. Four band electrodes were placed on the neck and upper abdomen. Impedance was measured at 100 kHz using constant current. With integrated phonocardiography and ECG units, the impedance waveforms were able to be measured with heart sound and ECG. (Adapted from Patterson 1989).

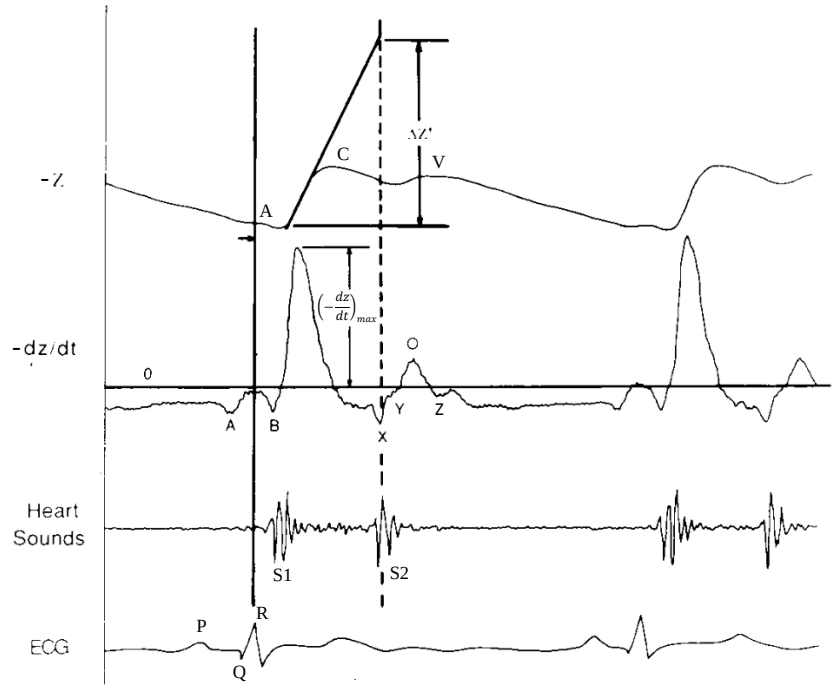

Figure 1-12. Signals recoded by the MIC system, from top to bottom is the impedance, the first derivative of impedance waveform, heart sounds and ECG. The impedance waveforms were inverted. (Adapted from Patterson 1989).

A typical normal thoracic impedance waveform is comprised of a pulsatile component for each heartbeat superimposed on a slow varying component. The pulsatile component is believed to be associated with blood volumetric changes in the heart and great vessels in the thorax (Miller and Horvath 1978, Patterson 1989, Sherwood et al. 1990). Karnegis and Kubicek (1970) defined three characteristic deflections on the pulsatile impedance waveform recorded on the human beings: a large impedance decreasing deflection marked as a C wave, which was preceded by an increasing deflection marked as an A wave and followed by a second smaller decreasing wave marked as a V wave. The three characteristic waves were related to the ECG and heart sounds. The C wave was found to be synchronous with the ECG QRS complex. It was attenuated in a beat with premature ventricular contraction and enhanced in the following compensatory beat. The A wave was found to be associated with the ECG P wave. Together with the ECG P wave, the impedance A wave shifted away from the QRS complex in heart block and disappeared in atrial fibrillation. The V wave was superimposed on the decay of the C wave, and occurred in protodiastole following the second heart sound (Karnegis and Kubicek 1970). Pickett and Buell (1993) investigated the relations of impedance A wave and V wave with transmitral flow from Doppler echocardiograms on normal subjects and patients. The amplitude of the impedance V wave was found to be significantly correlated with mitral peak flow during the ventricular passive filling phase, while the amplitude of the impedance A wave did not show significant correlation with the mitral flow during the active filling phase (Pickett and Buell 1993).

Extensive investigations on the origins of the major pulsatile impedance C waveform were performed using dogs under different controlled conditions by Patterson and his colleagues since 1960s (Patterson et al. 1964, 1978, Patterson 1965, Kubicek et al. 1966, 1970). It was found that during complete left mechanical alternans, where the left ventricle ejects only once for every two ejections of the right ventricle with unaffected ECG, the pulsatile impedance only occurred during the beats with left ventricular ejection. This observation was explained as the major decreasing impedance in each beat was mainly caused by the blood volume ejected into the aorta (Patterson 1989). However, contrary results were reported in Mohapatra (1981), who recorded thoracic impedance on patients receiving intra-aortic balloon assist pumping. The impedance did no change significantly when blood volume was pumped into the aorta during systole, which suggests that the

volume change in the aorta was not a significant contributor to the impedance change. Patterson (1989) also reported that a significant reduction occurred on the impedance change during atrial fibrillation even though the arterial flow and stroke volume kept at the similar level, which suggest that the atrial, pulmonary venous system, or lung could also be a significant contributor to the impedance change. In Patterson et al.'s study (Patterson et al. 1978), the effects of blood volume change in the lungs, atria, ventricle and aorta on the thoracic impedance change were compared. The results showed that the ventricular volume change made the least contribution to the impedance change, while the volume changes in other chambers made similar contributions.

As compared to the major impedance C wave, the origins of the A wave and V wave are less studied. By altering the preload on the subjects with tilt, Pickett and Buell (1993) found that the both the A wave and V wave were preload-dependent thus suggesting that the A wave and V wave were diastolic waveforms which may reflected the blood volume changes in the vena cava or pulmonary veins, or both.

Some investigators attributed the thoracic impedance change to blood flow rather than volumetric changes. Karnegis and Kubicek (1970) assumed that the impedance changes would probably be related to the blood flow through the venae cava or pulmonary veins according to the observation that the similarity between the pulsatile impedance waveform and the pulsatile blood flow waveform in the venae cavae and pulmonary veins. However, Miller and Horvath (1978) pointed out that this assumption could not explain the changes of the impedance waveform with the change of electrode positions, and thus the similarity would be more likely to be coincidental. Sakamoto and Kanai (1979) reported the blood electrical impedance can be affected by the flowing blood because of the orientation of erythrocytes. However, because the contribution of the orientation of erythrocytes on the impedance change was less than 15%, it was not considered as a significant contributor for the formation of pulsatile impedance waveform (Patterson 1989).

The first derivative of the pulsatile impedance waveform represents the velocity of change in the impedance, which is also associated with the cardiac cycle. Kubicek et al. (1967) pointed out that while the pulsatile impedance represented the blood volumetric changes in the aorta, the derivative impedance represented the velocity of blood flow. The first derivative impedance waveform was described and related to cardiac mechanical

events measured from simultaneous ECG and phonocardiograms by Lababidi et al. (1970). Six characteristic points were defined on the derivative impedance: an A point related with the beginning of the fourth heart sound; a B point related with the maximum vibration of the first heart sound; a X point synchronized with the aortic second sound; a Y point synchronized with the pulmonic second sound; an O point synchronized with the mitral opening snap of the phonocardiogram; a Z point synchronized with maximum vibration in the third heart sound (Lababidi et al. 1970). Kubicek (1989) studied the source of the peak velocity of changes in the impedance, which is another important characteristic point on the first derivative impedance waveform. On human volunteers and anesthetized dogs, the peak impedance change velocity occurred simultaneously with the peak velocity of aortic flow, which suggests that the peak velocity of the derivative impedance waveform is able to reflect the speed and force of ventricular contraction (Kubicek 1989). Some more recent studies which recorded the impedance signals simultaneously with echocardiograms indicated that the B point was an event corresponding to the aortic valve opening rather than the mitral valve closing (Petrovick et al. 1980, Stern et al. 1985, Cybulski et al. 2004). Therefore, the researchers in the related fields usually considered the impedance B point as the approximation of the aortic valve opening (Sherwood et al. 1990).

One of the most important applications for the impedance cardiography technique is to provide an easily and cost-efficiently non-invasive method to estimate dynamic stroke volume. The main assumption underlying this application is that a decrease in impedance is caused by a corresponding increase in blood volume in the thorax. This relationship was described by Kinnen et al. (1964) with following formula:

$$\frac{\Delta V}{V} = \frac{\Delta \mathrm{Z}}{\mathrm{Z}_0}$$

Where ΔV = stroke volume, V = total thoracic volume, ΔZ = impedance change, Z_0 = total thoracic impedance.

By modelling the blood volume path in the thorax as a column with a uniform cross-sectional area, a subsequent formula was proposed by Kubicek et al. (1967):

$$\Delta V = \frac{(-dZ/dt)_{max} \times LVET}{Z_0} \times \rho \times \frac{L^2}{Z_0}$$

Where ρ = resistivity of blood, L = length of the column. This is the widely used formula for stroke volume estimation based on the first derivative of impedance waveform.

Another important application of impedance cardiography is to provide a convenient estimation method for cardiac systolic time intervals, which were considered as important indices reflecting myocardial performance (Balasubramanian et al. 1978, Lewis et al. 1977). In Sherwood et al.'s report to provide the guideline for the impedance cardiography techniques, pre-ejection period (PEP) was recommended to be estimated by the duration from ECG Q wave to the B point of the derivative impedance waveform; the electromechanical delay (EMD) was suggested to be estimated by the duration from ECG Q wave to the X point of the derivative impedance waveform. In addition, the left ventricular ejection time (LVET) can be easily obtained from the impedance waveform by the interval between the B point and X point (Sherwood et al. 1990). The relevant publications which validated the systolic time intervals measured from the impedance with those measured from the reference techniques, including phonocardiography and echocardiography are summarized in Table 1-5.

There are a number of limitations for clinical applications of impedance cardiography techniques. The first major limitation is that the origins of the pulsatile impedance waveform are still not well understood. Secondly, the impedance changes are influenced by a number of factors, which leads to poor reproducibility. Finally, unlike other traditional methods for cardiac function assessment which are based on better understood theoretical principles, the estimation of stroke volume and cardiac output with impedance cardiography is not a direct measurement, and needs extensively cross-validation studies (Sherwood et al. 1990).

Table 1-5. Summary of literatures on comparison between systolic time intervals measured from impedance and reference techniques.

References	*Subject No.*	*Mean (SD) and Mean difference (SD) between techniques (ms)*									*Reference techniques*
		PEP (Q -> aortic valve open)			EMD (Q -> aortic valve close)			LVET (aortic valve open -> close)			
		-dZ/dt (Q ->foot)	Ref.	(-dZ/dt) - Ref.	-dZ/dt (Q ->end)	Ref.	(-dZ/dt) - Ref.	-dZ/dt (foot ->end)	Ref.	(-dZ/dt) - Ref.	
Lababidi et al. 1970	37	--	--	--	--	--	0 (2)	--	--	--	PCG
Hirschfeld et al. 1975	15	--	89 (10)	--	--	315 (44)	--	--	277 (40)	--	M-mode
Schieken et al. 1978	10	--	--	--	340 (6)	360 (8)	-20	--	--	--	M-mode
Kizakevich et al. 1993	17	--	--	-20	--	--	21	--	--	--	Doppler
Cybulski et al. 2004	13	104 (21)	97 (13)	7 (19)	--	--	--	294 (27)	311 (27)	-16 (20)	Doppler
Fellahi et al. 2009	25	--	--	--	--	--	--	317 (36)	286 (23)	32 (37)	Doppler
Carvalho et al. 2011	17	--	--	12 (9)	--	--	32 (25)	--	--	35 (38)	Doppler
Ulbrich et al. 2013	6	--	--	--	--	--	--	307	--	--	None

PCG = phonocardiography; PEP = pre-ejection period; EMD = electromechanical delay; LVET = left ventricular ejection time.

1.2.4 Photoplethymgraphy

Photoplethysmography (PPG) is an optical-based non-invasive technique that can be used to detect the blood volume change in the microvascular bed of tissue (Challoner 1979). The theoretical basis of the PPG technique is that blood has the capability to absorb or scatter light passing through it, thus the blood volume change could be assessed by light changes. PPG devices employ a transducer to convert the electrical signal into a light source to illuminate the tissue (transmitter). The reflected or scattered light from the tissue is detected and converted back to an electrical signal by a photo-electric transducer (detector). The dynamic changes in perfusion in the catchment volume are obtained from the intensity variations in the detected light. According to the placement of transmitter and detector, PPG is classified into two modes: reflection mode and transmission mode. In reflection mode PPG, both transducers are placed at the same side of the tissue; thus the detector records the light reflected by the tissue. On the other hand, in transmission mode, tissues are placed between the transducers so that the detector records the light passing through the tissue. Clearly, the transmission mode PPG system is restricted by the tissue size. The most common sites on the human body for PPG signal recording include fingertips, earlobes and toes. Red and near infrared light are often used as the PPG light source because the light in this wavelength range is not interrupted by other materials in the tissue so that it facilitates the measurement of blood volume change (Jones 1987).

The first use of the reflection PPG systems for the monitoring of blood volume changes in the rabbit ear were proposed in 1936 by two research groups independently (Molitor and Kniazuk 1936, Hanzlik et al. 1936). The preliminary application of the PPG system for the recording of blood volume changes on at the human fingertip was also reported by Molitor and Kniazuk (1936). A series of important pioneer studies were done by Hertzman and his colleagues for the establishment of PPG technique since 1937. In their first publication, the work on measuring blood volume changes with a reflection PPG system in human fingers following the Valsava manoeuvre, exercise and exposure to cold was reported (Hertzman et al. 1937). This study demonstrated the potential clinical utility of the PPG technique. In 1938, Hertzman published the work for the validation of the PPG technique by comparing the signals simultaneously recorded by a PPG system and by a mechanical plethysmography system. In this study, the main factors influencing the quality of PPG recording were investigated, which included the contact of the probes with skin, probe

movement against skin, illumination and power supply (Hertman 1938). With the advances in semiconductor technique and clinical instrumentation, PPG-based techniques have been improved rapidly in the recent decades. In 1972, Aoyagi and Kishi developed a pulse oximeter which was used to monitor patients' arterial oxygen saturation (Aoyagi et al 1974). The pulse oximeter was commercialized in 1981 and was considered as a major advance of the PPG technique in clinical use (Allen 2007).

PPG signal is composed of two components: a pulsatile 'AC' component associated with cardiac synchronous changes in the blood volume in each heartbeat, and a slow varying but large 'DC' component associated with respiration, sympathetic nervous system activity and thermoregulation. A high pass filter is often used to attenuate the dominant 'DC' component and enhance the 'AC' component before the analysis of the pulse waveform (Allen 2007). An example of the pulsatile component and simultaneous ECG signal is shown in Figure 1-13.

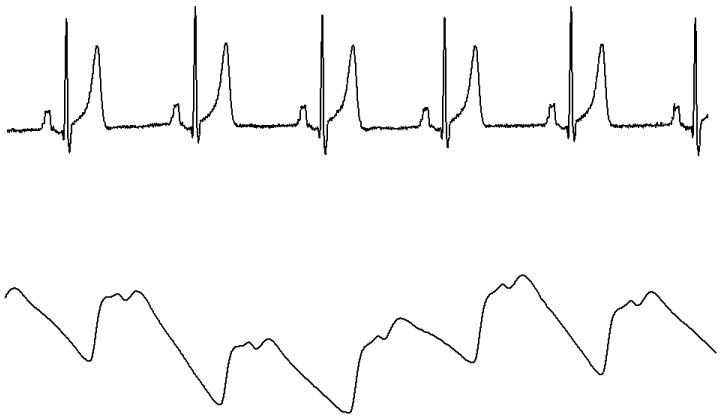

Figure 1-13. Pulsatile PPG signal recorded at fingertip with simultaneous ECG.

The major characteristics of the PPG pulse waveform on normal subjects have been described in the literature (Hertzman and Speakman 1937, Allen 2007). The pulse in a cardiac cycle is comprised of two characteristic components: a systolic component with fast rising edge and slow downward edge, and a component, associated with diastole and arterial reflection waves, superimposed on the downward edge of the systolic component. A dicrotic notch is usually seen between the two components in subjects with healthy compliant arteries. The effects of cardiovascular disease and aging on the shape of the pulse waveform have been studied. By the investigation on the finger blood volume pulse from

1778 individuals, Dawber et al. (1973) classified the pulses into four categories according to the visibility of the dicrotic notch on the downward edge of the pulse: class 1, with distinct notch; class 2, no notch but a horizontal line; class 3, no notch but a evident change in the angle of descent; class 4, neither notch nor change in angle of descent seen. The class 1 pulses were prevalent on healthy and younger individuals, while the class 4 pulses usually present in older individuals with coronary artery disease (Dawber et al. 1973). Allen and Murray (2003) used a multiple channel PPG system to record the simultaneous volume pulses at bilateral earlobes, fingertips and toes on 116 normal healthy subjects with a wide range of age. By comparing the normalized pulses in height and width between different age groups (Figure 1-14), they found that the rising edge of the pulses from all sites were subtly prolonged and the dicrotic notch gradually diminished with the advance in age. The similar findings were also reported by Brumfield and Andrew (2005) from the finger pulse recorded on 44 healthy subjects. The overall elongation of the pulse rising edge was explained by the effects of age on the resistance and compliance properties of arteries (Allen and Murray 2003), while the dicrotic notch diminishing was attributed to the stiffness of the conduit arteries, within which the reflected pulse wave transits faster and thus leads to the diastolic component moved towards the systolic component (Allen and Murray 2003, Millasseau et al. 2006).

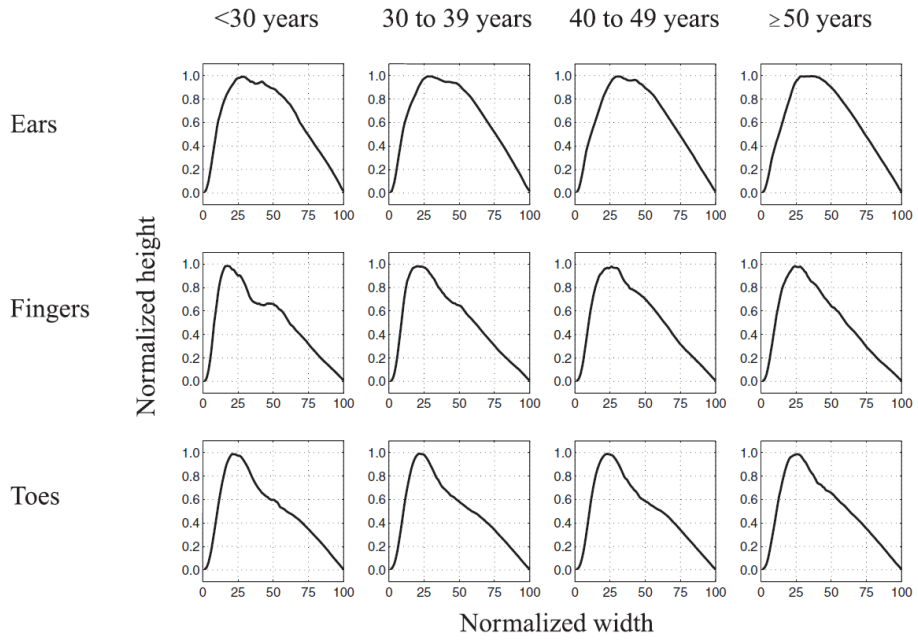

Figure 1-14. Illustration of the effects of age on PPG pulse at different body sites. (Allen and Murray 2003)

The quantitative analysis of the blood volume pulse recorded by the PPG technique was initiated by Dillon and Hertzman (1941). Two preliminary indices were defined in their study: the duration of the pulse increasing edge, named as 'crest time' and the height of the notch on the pulse downward edge. There were several important observations reported on these two indices: 1) the height of the notch rose up when immersing the hand in cold water which led to systemic vasoconstriction and decreased after inhalation of amyl nitrite which led to systemic vasodilation; 2) the crest time increased and the notch was lost in individuals with hypertension and arteriosclerosis (Dillon and Herzman 1941). Morikawa et al. (1967, 1968) subsequently founded that a depression of the dicrotic notch was caused by the vasodilator effects of organic nitrate and alcohol. The height of the notch was used as an index of general arterial vasodilatation in Klemsdal et al.'s study, which was found reduced by acetylcholine in a dose dependent manner (Klemsdal et al. 1994). The time difference between the peak of the systolic component and the peak of the diastolic component was considered as an estimation for the pulse transiting from the aorta to the major apparent reflecting site (Chowienczyk et al. 1999). In Millasseau et al.'s study (Millasseau et al. 2002) an index of large artery stiffness (SI) was defined from the finger volume pulse as the ratio of subject height to time difference between the systolic and diastolic peaks. The large artery stiffness index was significantly correlated with carotid-to-femoral pulse wave velocity (PWV), and changed in the same way as PWV with age, mean arterial blood pressure and administration of glyceryl trinitrate (Millasseau et al. 2002). A reflection index (RI) was proposed in Millasseau et al.'s following study (Millasseau et al. 2003a) to provide an index of pulse wave reflection, which was defined as the height of the reflected wave relative to the systolic wave. It was reported that the reflection index showed no significant correlation with age but was strongly correlated with angiotensin II and glyceryl trinitrate in a dose manner, which suggested that the reflection index was able to indicate the tone of small arteries (Millasseau et al. 2003, 2006).

The 2nd derivative of the finger pulse, known as acceleration plethysmogram, was described and analyzed by Takazawa et al. (1998) and Bortolotto et al. (2000). Five characteristic waves, a, b, c and d waves in systole and e wave in diastole, were defined on the acceleration plethysmogram. The relative heights of these waves, including b/a, c/a, d/a and e/a, and an aging index (b – c – d – e)/a as measures of vascular aging and effects of vasoactive drugs on normal subjects and hypertensive patients were investigated (Takazawa

et al. 1998, Bortolotto et al. 2000, Hashimoto et al. 2002, Millasseau et al. 2003a). It was reported that b/a showed a negative relationship with age, while other second derivative indices were positively related with age thus the significance of the positive correlation of the aging index with age was augmented. The d/a was also found increased after administration of nitroglycerin and decreased after administration of angiotensin, which suggested that it would be a useful measure of the effects of vasoactive agents. The major advantages of the second derivative indices include the capability of capturing subtle changes in the volume pulse and easy to be calculated. However, their physical meanings were not clear (Millasseau et al. 2003a).

In order to allow the inter-comparisons of pulse shape recorded from the left and right body sides in the same subject or those from different subjects, an amplitude normalization and temporal normalization procedure was proposed by Allen and Murray (1993, 1995). In their following study (Allen and Murray 2003), pulse templates were calculated for different age groups based on the normalized ear, finger and toe pulses from normal healthy subjects, then the effects of age on the shape of pulses from different sites were described and quantified. A shape index was defined based on the normalized pulses to detect the lower limb peripheral arterial occlusive disease, which gave substantial agreement with the well-established ankle-brachial pressure index (ABPI) measurement (Allen et al. 2005). The pulse timings, including the pulse transit time measured from the ECG R wave to pulse foot (PTT_f) and the time measured from the ECG R wave to pulse systolic peak (PTT_p), were also reported to rise on the patient with arterial occlusive disease due to a blood pressure drop (Allen et al. 2005). The pulse transit time from the PPG signal was also applied to paediatric critical care.

The definition of the commonly used timing indices from the peripheral volume pulse and its 2^{nd} derivative waveform are illustrated in Figure 1-15. The reference values of these indices from literature are summarized in the Table 1-6.

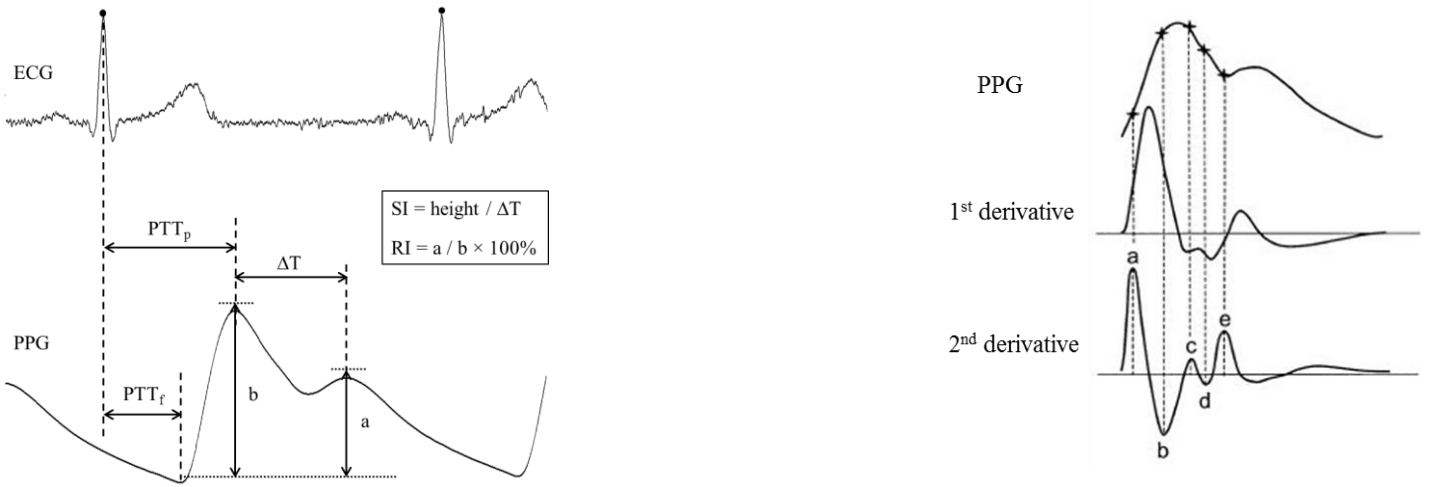

Figure 1-15. Illustration of index definition on PPG signal (left) and the 2nd derivative waveform (right).

Table 1-6. Summary of commonly used indices from PPG signal with their reference values from literatures.

References	***Subject No.***	***Reference values***								
		PTT_f (R -> foot) (ms)	PTT_p (R -> peak) (ms)	Rise time (foot -> peak) (ms)	SI (height / ΔT) (m/s)	RI (diastolic height / systolic height) (%)	2nd derivative b/a (ratio)	2nd derivative c/a (ratio)	2nd derivative d/a (ratio)	2nd derivative e/a (ratio)
Takazawa et al. 1998	39	--	--	--	--	--	Mean (SD): -0.6 (0.2)	Mean (SD): -0.1 (0.2)	Mean (SD): 0.4 (0.1)	Mean (SD): 0.3 (0.1)
Millasseau et al. 2002	87	--	--	--	Mean: 8.4	Mean (SD): 64 (3)	--	--	--	--
Millasseau et al. 2003	124	--	--	--	Mean: 6.3	Mean: 63	Mean: -0.8	Mean: 0.1	Mean: -0.1	Mean: 0.2
Brumfield and Andrew 2005	44	--	--	--	Mean: 12.3	--	--	--	--	--
Allen et al. 2008	52	Median (Range): 288 (269 – 334)	Median (Range): 611 (551 – 715)	Median (Range): 325 (280 – 372)	--	--	--	--	--	--

SI = stiffness index; RI = reflection index.

In spite of a wide range of potential clinical applications, there are two major limitations for the PPG technique which restrict its current application. The first limitation is that the origins of the component of PPG signal are not fully understood. The PPG signal is determined by the complex interactions of cardiovascular properties, which makes it difficult to interpret clearly the pulse contour indices in terms of biomechanical properties of arteries (Millasseau et al. 2006). The second limitation is from the reproducibility of the PPG signal measurement. According to Hertzman's study (Hertzman 1938) and more recent studies (Teng and Zhang 2006, Zhang and Zhang 2006), many factors, including the method to attach the probe to tissue, interface pressure between probe and tissue, signal-acquiring amplifier bandwidth, movement artefact, subject conditions and measurement environment, were believed to affect the reproducibility. Furthermore, there is no commonly recognized standard to date for PPG measurement protocol, which limited the general use of the PPG technique (Allen 2007). To improve the repeatability, bilateral measurement was proposed by Jago and Murray (1988) and an averaging of at least 60 heartbeats has been suggested by Allen (2002).

1.3 Rationale for the study

The cardiovascular system has been briefly introduced in the previous sections with emphasis placed on the non-invasive assessment methods of cardiovascular functions. Physiological measurements have promising potential to provide simple and quick ways to assess cardiovascular function at low cost. However, from the literature review it can be argued that there are still many limitations which restrict their further application in clinical services.

Cardiac imaging is currently the most important tool to provide useful information about cardiovascular function. M-mode echocardiography is one of the most effective ways to examine the motion of valves, while Doppler echocardiography is an important technique to record blood flow velocity. These techniques, however, are expensive and require skilled staff to perform the measurements.

Impedance cardiography is a simple and quick physiological measurement based on the electrical impedance technique. Changes in thoracic impedance can be easily measured and analysed, which reflect the blood volumetric changes in the heart and great vessels in the

thorax. Information about cardiovascular function can thus be extracted from the pulsatile impedance and its first derivative waveforms. The impedance cardiography technique, however, has largely failed to be accepted because of poor understanding of the origins of the characteristic waveforms and consequently its normal physiological variability, limited attempts at cross-validating impedance features with other well-established techniques, and lack of widely acknowledged standards.

Photoplethysmography (PPG) is a simple and cheap technique to capture the peripheral pulse. The PPG signal has a characteristic pulsatile waveform associated with the cardiac cycle, which changes with normal physiological changes and disease. Therefore, from the pulse waveform, quantitative assessment of normal cardiovascular function and diagnostic information about disease can be extracted. Similar factors to these encountered by impedance cardiography limit the prevalence of PPG technique. In addition, the PPG technique is traditionally considered as a potential tool for vascular function assessment, and limited attempts have been made to apply the technique to cardiac function assessment.

During left ventricular ejection, blood is ejected into the aorta through the aortic valve, and then distributed into peripheral sites, which causes blood volume changes in the heart and great vessels in the thorax, and the pulse propagating along the arterial system. Impedance cardiography and photoplethysmography techniques are able to capture these dynamic changes in different sites, which mean these two physiological measurements have the potential to provide the additional clinical information to cardiac imaging. However, because the formation of the impedance and pulse waveforms is still not fully understood, their feasibility needs to be validated by well-established cardiac imaging technique.

1.4 Aims of the study

There are seven main aims to this study:

1. To establish a measurement protocol allowing the simultaneous recording of echocardiograms with ECG, impedance and peripheral pulse on normal subjects.

2. To employ reliable signal analysis techniques to extract characteristic timing features from the echocardiograms and physiological measurement.

3. To quantify the dynamic relations between cardiac valve movement and blood flow through the valves.

4. To obtain a better understanding of the origins of the pulsatile impedance changes and its first derivative by linking their characteristic timing features to those from echocardiograms and peripheral pulses.

5. To obtain a better understanding of the origins of the peripheral pulses by linking their characteristic timing features to those from echocardiograms and thoracic impedance changes.

6. To cross validate the features for cardiovascular function assessment from impedance cardiogram and peripheral pulses with those from echocardiograms.

7. To investigate the effects of age, heart rate and blood pressure on the echocardiograms and physiological measurements.

1.5 Organisation of the thesis

The material in this thesis is divided into 10 chapters, a set of appendices, and a bibliography with cited references. This introductory chapter (1) gives a brief overview of the cardiovascular system, and literature reviews on the history, principles, characteristic features, clinical applications and limitations of the echocardiography technique, ECG,

impedance cardiography and photoplethysmography. There are three methods chapters describing measurement systems (chapter 2), measurement protocol and data collection (chapter 3), signal and statistical analysis techniques (chapter 4). There are five results chapters summarizing the repeatability of the study (chapter 5), the dynamic relations between valve movement and blood flow conditions (chapter 6), the relationships between thoracic impedance changes and cardiac mechanical function measured by echocardiography (chapter 7), the relations of peripheral pulses with cardiac mechanical function measured by echocardiography and thoracic impedance changes (chapter 8), the effects of age, heart rate and blood pressures on the echocardiograms and physiological signals (chapter 9). Chapter 10 discusses the methods and results, presents the conclusions and suggests potential directions of further work.

Chapter 2 Cardiac imaging and physiological measurement system

The echocardiography and physiological measurement systems for obtaining cardiac image and physiological signals are described in this chapter.

2.1 Introduction

In this study, 4 separate measurement devices were connected together to enable cardiac imaging and physiological data to be collected simultaneously. A schematic representation of the measurement system is shown in Figure 2-1. The system comprises an echocardiographic device, a multi-channel ECG device, an impedance cardiography (ICG) device and a dual-channel photoplethymography (PPG) device.

The echocardiographic device allowed the examination of cardiac dynamic function, including cardiac valve movement and the velocity of blood flow, by using multiple ultrasound techniques. The 12-lead ECG device was used to record cardiac electrical activities on the body surface. The ICG provided a non-invasive way to obtain haemodynamic data by monitoring thoracic impedance changes. Additionally, the blood peripheral volume pulse was recorded by a PPG device at either the ear or finger site.

Each measurement device is briefly described in this chapter sequentially. The following chapter describes how they were used in this research.

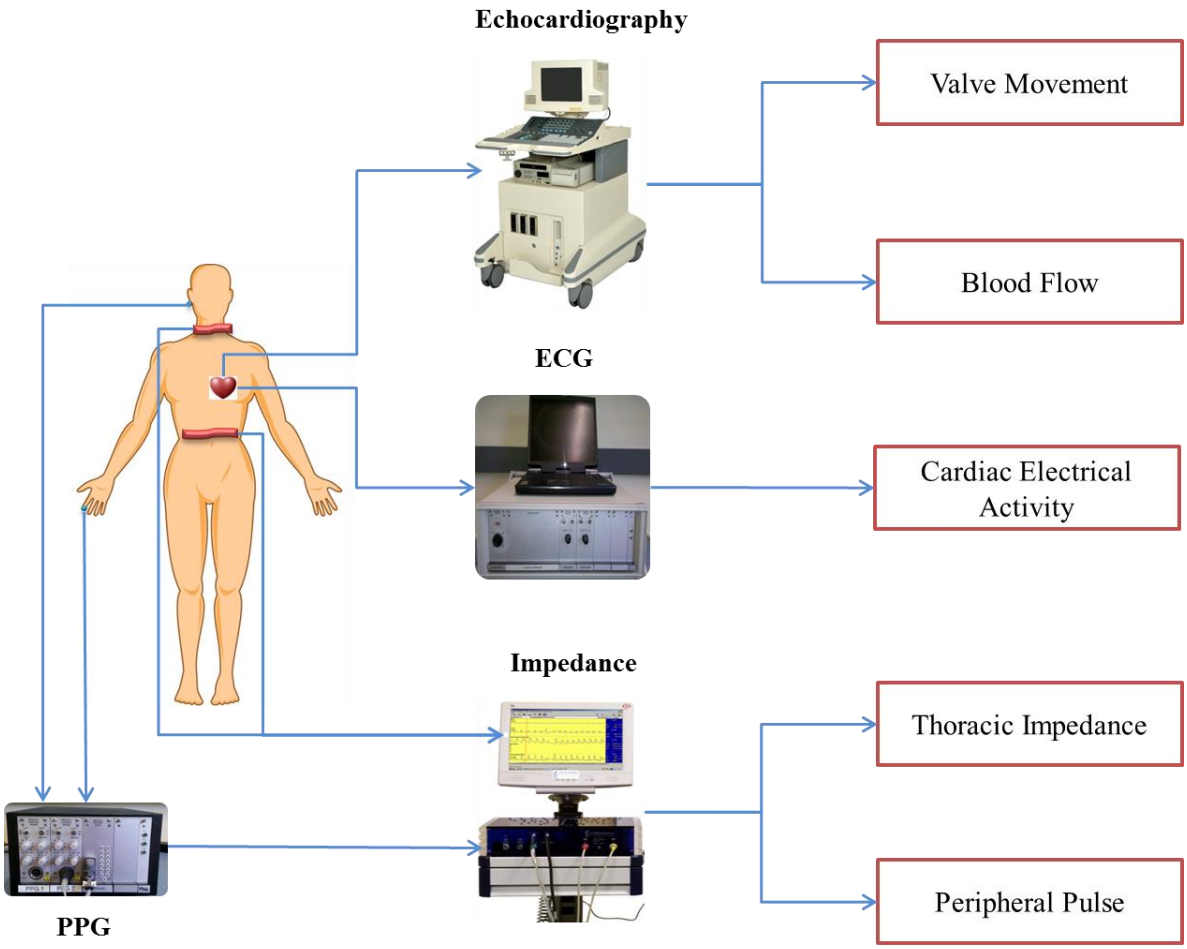

Figure 2-1: Overview of the measurement system which comprised an echocardiographic device, a 12-lead ECG device, an impedance cardiography device and a 2-channel PPG device. The cardiac dynamic mechanics (valves movement and blood flow) were measured by the echocardiographic device. Cardiac electrical activity, thoracic impedance and peripheral pulses were obtained by the ECG device, impedance cardiography device and PPG device respectively.

2.2 Echocardiographic device

2.2.1 Overview of the ultrasound platform

The HDI 5000 Ultrasound system (Philips/ATL, USA) is a general-purpose diagnostic ultrasound system, with the functions of acquiring, processing and displaying ultrasound images. As shown in Figure 2-2, the HDI 5000 system includes mainly a monitor, a control panel, peripherals and a card cage. There are eight card slots provided in the card cage. Three of them are designed for the ultrasound transducers and the others are left for connecting external physiological measurement systems. The whole system is mounted on four casters with a brake lock on each. Together with the handle at the front, it increases the mobility and safety of the system.

Figure 2-2: Philips/ATL HDI 5000 Ultrasound platform.

2.2.2 Ultrasound transducer

Three types of transducer are provided with the HDI 5000 system: linear, convex and phased array. Different transducers have different shapes or footprints, and generate ultrasound waves within different frequency ranges. The main frequency of the ultrasound wave determines the resolution of the imaging. The wave with higher frequency gives a better resolution. However, on the other hand, the frequency of the ultrasound wave is inversely related to the penetration capability. The higher the frequency, the more attenuation occurs on the ultrasound wave for traveling a given distance. Therefore, as it is

equipped with different types of ultrasound transducers, the HDI 5000 system can be used for different clinical applications. An ATL P4-2 phased array transducer, which is shown in Figure 2-3, is usually used for the examination of adult cardiac function. It has a small footprint and forms an electronic beam by using a compact array of sensors to steer to the area of interest. As the direction of the beam steering is adjustable electronically, it is good for cardiac imaging applications, where the ultrasound wave needs to get between the ribs (Markowitz 2011). The frequency range of the ultrasound emitted by the P4-2 transducer is between 2 to 4 MHz, which provides a trade-off between imaging resolution and penetration, covering the standard frequency demanded for adult cardiac applications 2.5 – 3 MHz (Solomon 2007).

Figure 2-3: ATL P4-2 ultrasound transducer.

2.2.3 User control panel

The control panel is shown in Figure 2-4. As can be seen, the control panel consists of a full-size keyboard, a trackball, a set of pushbuttons, toggle switches, slidepots and rotary controls. The keyboard is used for accessing the setting menu and typing in text whenever it is wanted, while the trackball controls the pointer displayed on the monitor. The commands are allowed by the pushbuttons, such as switching between imaging modes, starting and terminating image capture, and freezing the current screen for preliminary investigations. A variety of imaging modes are allowed by the HDI 5000 system, including 2D mode, M-mode, Doppler imaging and 3D mode. Most modes could be implemented in either grayscale or colour. The gain, frame rate (for 2D and 3D mode), sweep speed (for M-mode and Doppler imaging), focus zone and zoom region are adjustable to optimize the recording quality by using the toggle switches, slidepots and rotary controls on the control panel.

Figure 2-4: User control panel of the HDI 5000 Ultrasound platform.

In addition to the image acquiring stage, the user control panel is also useful for image retrieval, analysis and transfer. Images recorded by the system are stored into its hard disk. Retrieval and measurement tools are provided for primary image analysis, by which anatomical structures, such as the distance between two points, border of a region of interest and time/slope can be measured. Cardiac parameters, such as volume, cardiac output, area/diameter reduction, can be calculated by using the analysis package. The stored images can also be transfer to another computer for further analysis.

2.2.4 External physiological signal inputs

Five physiological external connection channels are dedicated to normal ECG, high-level ECG, pulse, phonography signal and an auxiliary channel. The normal ECG channel provides a bandwidth between 0.65 and >30 Hz, and the high-level ECG has wider bandwidth (0.05 – 32 Hz). The sampling rates of the external signals are determined by the imaging frame rate or sweep speed. The triggering mode provided by the system allows the image capture to be triggered by a predefined reference time on the physiological signal, such as the ECG R wave.

2.3 ECG device

A 12-lead ECG device developed in the Medical Physics Department, Freeman Hospital, UK, records the cardiac electrical waveforms on the body surface. The device, shown in Figure 2-5, has a rack system with two FM169 Bioelectric Amplifiers (Medical Physics Department, Freeman Hospital, UK) and an electrical power supply module mounted into it. An ECG signal input port connecting to the electrodes via a cable is provided on the front panel, and signal output ports are available at the rear panel of the device to allow analogue ECG signals to be exported to other data acquiring systems.

Figure 2-5: Twelve-lead ECG measurement device.

2.3.1 ECG amplifiers

One of the two groups of amplifiers is for the limb lead ECG acquisition and the other for the chest leads. Each amplifier comprises a filtering stage, an amplification stage and each group has a user control panel to adjust the gain and mode settings. The filtering stage allows a diagnostic bandwidth between 0.05 and 100 Hz for ECG recording. The gain is adjustable so that the amplitude of recordings can be fitted into the expected range. Four pre-defined gains are available from the user control panel, including 500, 1000, 2000 and 5000, which allows very low ECGs to be boosted and recorded. The following two working modes are provided by the amplifier:

- ‘Zero’ mode: the output signal is set to zero when this mode is selected;
- ‘Use’ mode: normal output signal is enabled;

The ‘Zero’ mode is useful when time markers are wanted at the beginning of ECG recording.

2.3.2 Data collecting software

Software is provided with the device for ECG signal acquisition, displaying and storing. The subject’s information, sampling rate, channel selection and recording length can be set with the software. The interface of the software is shown in Figure 2-6.

Figure 2-6: Screenshot of the ECG acquisition software.

2.4 Thoracic impedance device

2.4.1 Principle of impedance cardiography

The 4-terminal sensing method is a traditional method to measure electricity impedance. The schematic representation of this method is illustrated in Figure 2-7. Two separate pairs of electrodes are used for the measurement. A pair of electrodes is placed at the outer ends of the network to carry constant current (current-carrying electrodes), and the other pair placed at the inner ends to sense the voltage (voltage-sensing electrodes). The impedance between the voltage-sensing electrodes is calculated by dividing the measured voltage by

the source current. The advantage of this method is that any impedance of the electrode contacts does not affect the measurement.

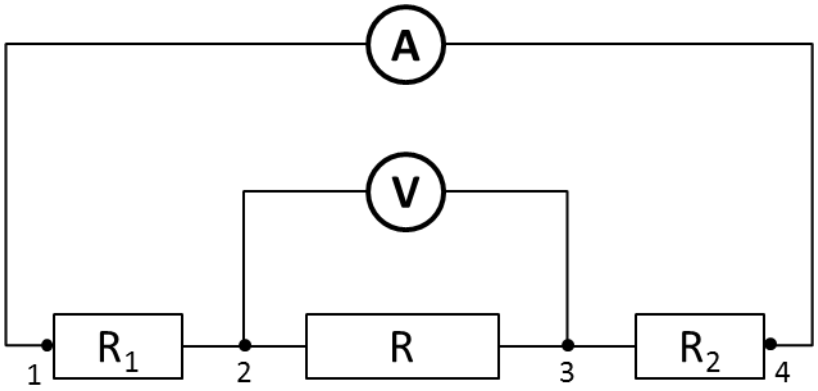

Figure 2-7: Illustration of 4-terminal sensing method for impedance measurement. In order to measure the impedance of R, constant current is carried by the current-carrying electrodes 1 and 4, while the voltage is measured at the voltage-sensing electrodes 2 and 3. The impedance is calculated by dividing the measured voltage by the input current. R1 and R2 are system impedance of the circuit.

This method is used to measure the thoracic impedance. As illustrated in Figure 2-8, two pairs of electrodes are attached outside the region of interest on the human body. The current-carrying electrodes at the outer ends are connected to the current source so that excitation current can be conducted through the region. The thoracic impedance (Z) is defined as the ratio of the voltage measured between the voltage-sensing electrodes at the inner ends to the current, with the unit of 'Ω'. However, this could measure impedance in the volume between the voltage electrodes only if the current was uniformly distributed throughout the volume, which is never the case with the device. Nevertheless, the device does measure impedance that reflects that of the volume, and is used in this thesis for that purpose. The impedance reflects the conductivity of the region between the voltage sensing electrodes. An increase in the conductivity will cause a decrease of the impedance. In addition, the impedance cardiography device is usually used to monitor thoracic impedance changes, since it is more important than the actual impedance.

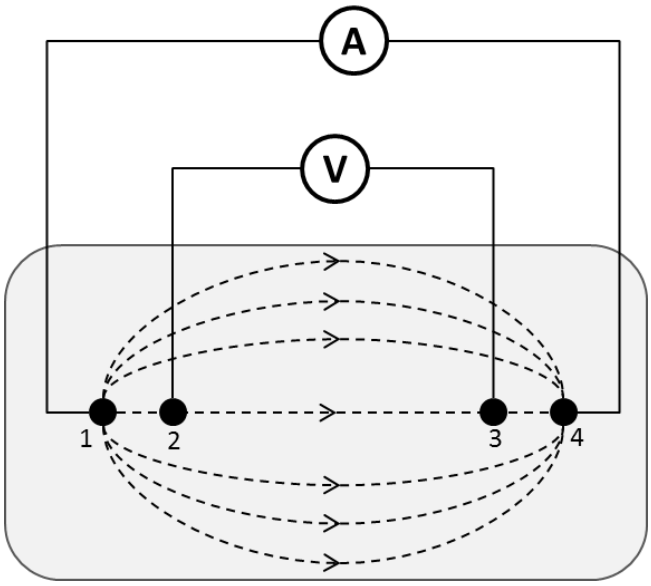

Figure 2-8: Illustration of thoracic impedance measurement. The constant excitation current is conducted through the region between the current-carrying electrodes at the outer ends (1 and 4). Voltage is measured between the inner voltage-sensing electrodes (2 and 3). The impedance (Z) within the range between electrodes 2 and 3 is defined as the ratio of measured voltage and the source current.

2.4.2 Impedance cardiography device

The TaskForce Monitor 3040i system (CNSystems Company, Graz) is a multi-functional non-invasive haemodynamic monitoring system. The system, which is shown in Figure 2-9, comprises a monitor, a keyboard, a physiological signal recording box, a PC and a printer. There is an impedance cardiography (ICG) module, a 6-limb lead ECG module and two external signal input ports embedded into the signal recording box. The ICG module of the TaskForce Monitor system is used to obtain the thoracic impedance signals, including the impedance (Z) and its negative first derivative (-dZ/dt). Data collection software is also provided with the system to support collection and display of multiple physiological signals simultaneously.

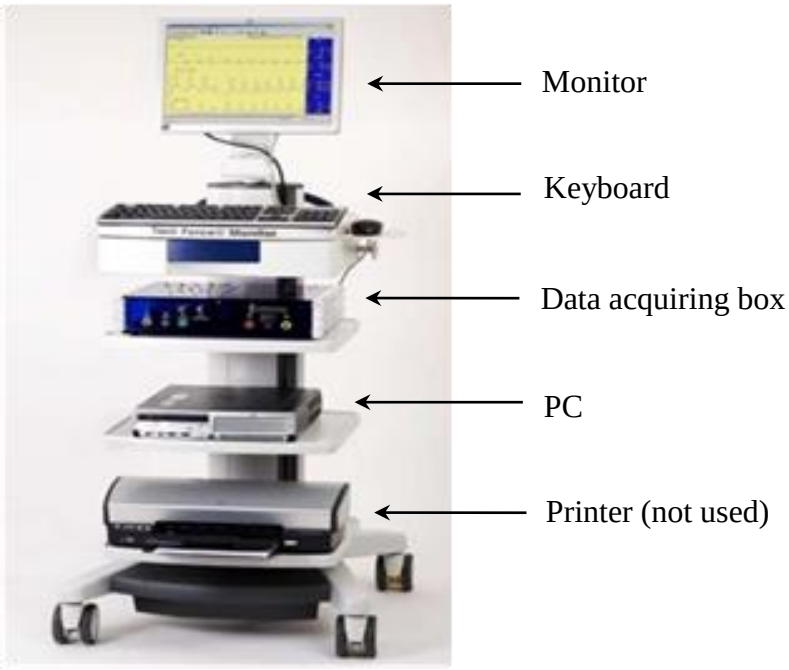

Figure 2-9: TaskForce Monitor 3040i system.

In order to measure the thoracic impedance, alternating constant excitation current with amplitude lower than 4 mA in the frequency range between 20 and 100 kHz is recommended because of the two following reasons (Sherwood et al 1990):

1) Human tissue has resistivity that can be measured at this frequency range;
2) The frequencies prevent direct current damage and are far away from 50 Hz which can induce ventricular fibrillation.

For the ICG module of the TaskForce Monitor system, the alternating current source with the amplitude of 400 μA at 40 kHz is used.

The impedance (Z) is sampled at the lower rate of 50 Hz, and its first derivative impedance (-dZ/dt) is sampled at the rate of 1 kHz. The allowed range of the derivative impedance is ± 10 ohm/s.

2.4.3 Impedance cardiography electrodes

There are two basic types of electrodes for ICG signal measurement; band electrodes and spot electrodes. A band electrode usually consists of a long strip of adhesive tape with a current-carrying or voltage-sensing electrode along the centre. Four band electrodes are normally attached circumferentially around the neck and abdomen. The band electrodes

may cause inconveniences because of this large contact area with the body (Sherwood et al 1990): first of all, it is impractical to apply band electrodes to those patients with chest injury or following thoracic surgery; secondly, they can make the subject feel distressed or anxious if they are applied too tightly; thirdly, the signal recorded by the band electrodes is prone to motion artefact. Compared with the band electrodes, spot electrodes are more cost effective (even standard spot ECG electrodes can be used) and easier to implement (with much smaller contact areas). However, the spot electrodes suffer from a variable signal and consequently poor reproducibility (Patterson 1989). It has been reported that when the device is used to estimate absolute stroke volume, the ICG signal measured by the spot electrode has less accuracy than that from the signal measured by the band electrodes (Penney et al 1985).

In order to obtain a balance between the advantages and disadvantages of the traditional long band electrodes and spot electrodes, special short band electrodes are provided for the ICG module of the TaskForce Monitor system. As shown in Figure 2-10, a short strip of adhesive tape is used to maintain a short current-carrying electrode and a short voltage-sensing band electrode. The main body of the strip is 21 cm long and 5 cm wide, with a narrow joint head connecting to the clip of the cable. The pair of electrodes is placed in parallel on the strip with a distance between the centres of 3.3 cm.

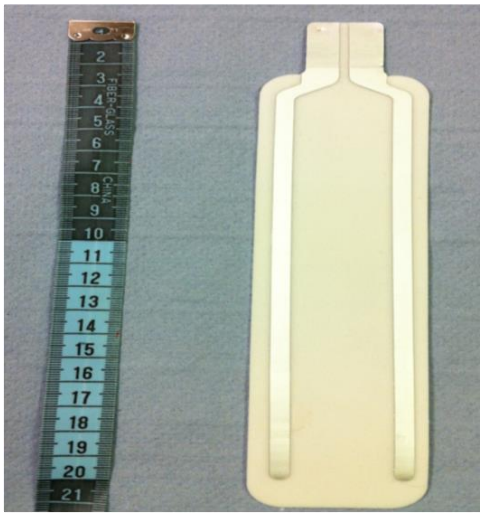

Figure 2-10: Short band electrode for the impedance cardiography device.

There are three short strips used for the ICG module. The placement of these strips for the thoracic impedance measurement is described in a later chapter.

2.4.4 External signal inputs

The TaskForce Monitor system allows other physiological measurements to be recorded with ICG signals. It has a 6-lead ECG module, allowing 6 limb ECGs to be recorded within the bandwidth between 0.08 and 150 Hz. The default sampling rate for the ECGs is 1 kHz. Furthermore, the system also provides two channels for external inputs. Each channel allows an analogue input within the range of ± 5 V and samples them at a rate of 1 kHz.

2.4.5 Data collecting software

Software is provided by the TaskForce Monitor system for data acquisition. As shown in Figure 2-11, the simultaneously recorded physiological signals are displayed in real time on the screen. They are then stored into the hard drive of the system after recording is finished.

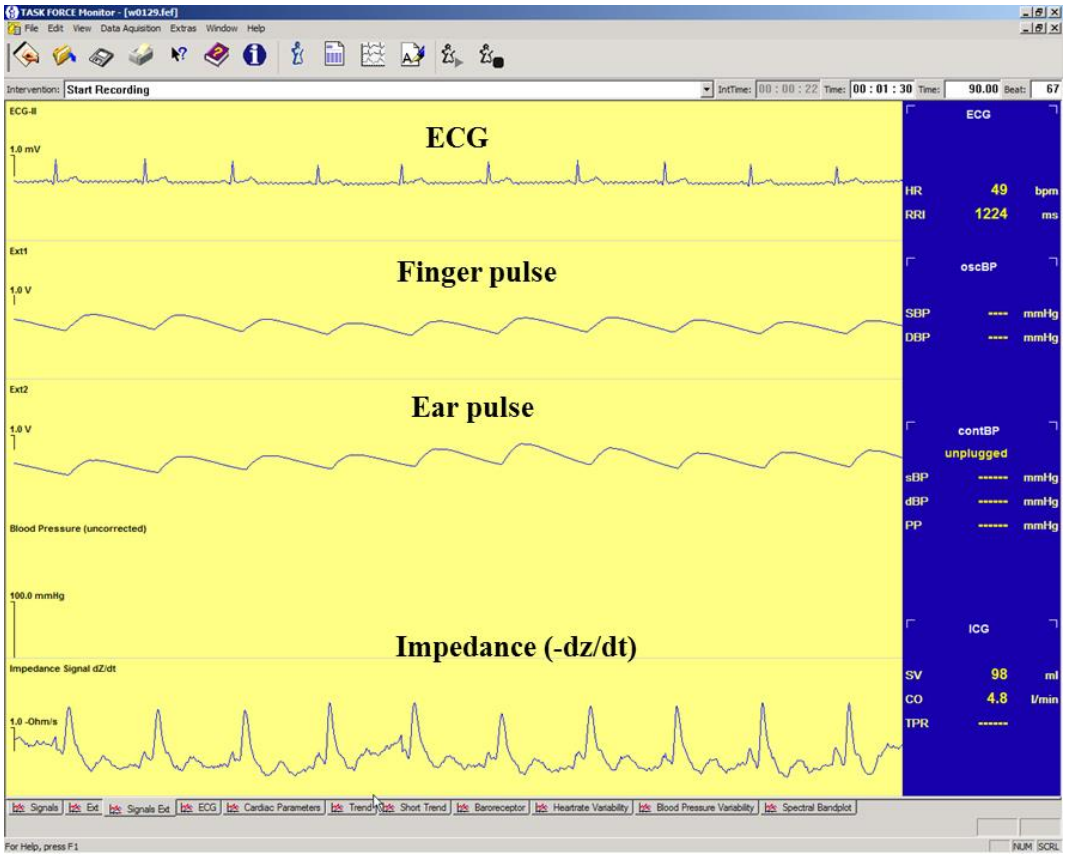

Figure 2-11: Screenshot of the TaskForce Monitor signal acquiring software. The waveforms of simultaneously recorded ECG, pulses and impedance are displayed from the top to the bottom. The finger and ear pulses are two external input signals in this example.

2.5 Peripheral pulse measurement device

A dual-channel reflectance mode PPG device developed in the Medical Physics Department records the peripheral blood volume pulse. The measurement device, shown in Figure 2-12, contains two pulse amplifiers embedded into a rack system with a power supply module and a signal output port which allow the analogue signals to be exported to other devices with data recording software.

Figure 2-12: Dual-channel PPG measurement device.

2.5.1 PPG amplifiers

Each amplifier module includes a LED driving circuit, a current (from the detector photodiode) to voltage convertor circuit, a filtering stage and an amplification stage.

With filtering the main frequency components of the PPG signals within 0.5 to 20 Hz (Allen 2007) are kept, while noise and interference are reduced. A 4th-order low pass Butterworth filter with cut-off frequency at 42 Hz is used to remove higher frequency components and a single order high pass filter with adjustable cut-off frequency between 0.005 and 1 Hz to remove DC and lower frequency components. A 50 Hz notch filter attenuates power line interference (Clayton 1979). Finally, two cascaded low pass filters with cut-off frequencies at 30 Hz are used to smooth the pulse waveform and consequently, giving an overall high cut-off frequency at around 20 Hz.

The amplification stage provides variable gains which can be adjusted manually. This helps to fit the amplitude of the PPG signals into a normal display range.

2.5.2 PPG probe

A reflectance mode PPG probe is connected to each amplifier by a cable. There is an emitting diode (SME 2470-001, Honeywell, USA) and a sensing photodiode (SMD 2420-001, Honeywell, USA) equipped into the probe. The peak wavelength of the emitting diode is 880 nm, matching with the maximum sensitivity of the photodiode. In order to reduce artefacts caused by movement or losing contact, a strap and a plastic clip are used to help attach the probes on the fingertip and earlobe respectively.

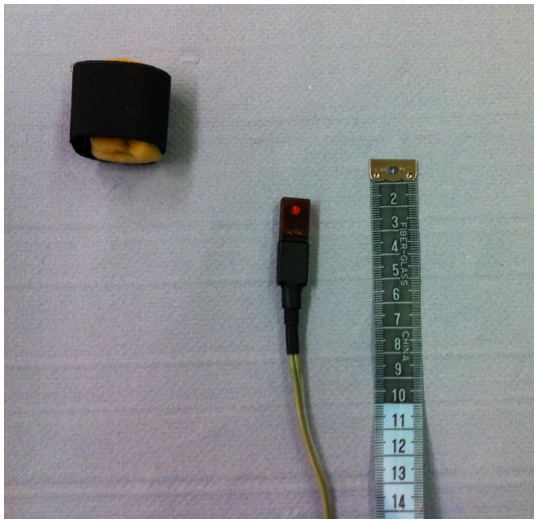

Figure 2-13: PPG probe and the strap.

Chapter 3 Measurement protocol

The measurement protocol for collecting simultaneous imaging and physiological data simultaneously is described in this chapter.

3.1 Introduction

The echocardiographic and physiological measurement devices have been described in the Chapter 2. The main aim of the work in this chapter is to describe the protocol for the collection of echocardiograms, ECGs, thoracic impedance and peripheral pulses, and the development of a recording system to enable data to be collected simultaneously, and then to be synchronized ready for analysis is also introduced.

Ideally, all the signals should be recorded from the 4 devices (echocardiographic device, ECG device, impedance device and pulse device) simultaneously. However, in the experimental setting this was not practical. For echocardiography there were four areas of interest: mitral valve and aortic valve movement in M-mode, and blood flow through these two valves in Doppler mode. It was possible to collect data from only one at a time, so these four areas were examined sequentially. Additionally, because the electrode placement for the chest leads (V1 ~ V6) of the standard 12-lead ECG and the ultrasound probe need the same chest position, these chest ECGs could not be recorded with the images.

In this study, the following recordings were obtained in three sessions in sequence from different combinations of the 4 devices on each subject:

- standard 12-lead ECG data from the ECG device only (session 1);
- impedance and 6 limb lead ECG from the TaskForce Monitor system, and ear and finger pulses from the PPG device (session 2);
- M-mode and Doppler images from the echocardiographic device, with simultaneous ECGs from the ECG device, impedance from the TaskForce Monitor system, and finger pulse from the pulse device (session 3).

The recordings were repeated in the same session. The first and the repeated recordings were coded as 1a, 1b, 2a, 2b, 3a and 3b. The details of these data recording and the corresponding device combinations are summarized in Table 3-1.

Table 3-1. Summary of data recorded in the three sequential sessions from different device combination: 1) standard 12-lead ECG signals recorded by using the multi-channel ECG device; 2) 6 limb lead ECG, thoracic impedance and 2 channels of pulses (finger and ear) recorded by using the TaskForce Monitor (TFM) system; 3) images, including mitral valve movement, aortic valve movement, mitral flow and aortic flow sequentially, recorded with ECG, impedance and finger pulse. Each recording was repeated in the same session. The first and the repeated recordings were coded as 1a, 1b, 2a, 2b, 3a and 3b.

Recording sessions		Images				ECG		TaskForce Monitor		Pulse		Device used
		M-mode		Doppler								
		MV	AV	MF	AF	Limb	Chest	Z	-dZ/dt	Finger	Ear	
1	a (first)					✓	✓†					ECG
	b (repeated)					✓	✓†					
2	a (first)					✓		✓	✓	✓	✓	TFM & Pulse
	b (repeated)					✓		✓	✓	✓	✓	
3	a (first)	✓				✓	✓‡	✓	✓	✓		Echo & ECG & TFM & Pulse
			✓			✓	✓‡	✓	✓	✓		
				✓		✓	✓‡	✓	✓	✓		
					✓	✓	✓‡	✓	✓	✓		
	b (repeated)	✓				✓	✓‡	✓	✓	✓		
			✓			✓	✓‡	✓	✓	✓		
				✓		✓	✓‡	✓	✓	✓		
					✓	✓	✓‡	✓	✓	✓		

†: all the 6 chest leads (V1 ~ V6) were recorded; ‡: only V1 was recorded.

MV: mitral valve; AV: aortic valve; MF: mitral flow; AF: aortic flow.

In this chapter, the subject recruitment is first described. Suitable electrodes/probes placement and gain/filtering setting were determined for the echocardiography and physiological data measurement techniques, followed by the technique used to synchronize the devices. Finally, the method used to pre-process the data from the separate devices is described.

3.2 Subjects

3.2.1 Ethics approval

The study design required the recruitment of 30 normal subjects within a wide range of age. Ethical approval was sought for this study and granted in July 2012 by the National Research Ethics (NRES) Committee North East – Newcastle & North Tyneside 2.

3.2.2 Recruitment

Subjects were recruited from the Newcastle upon Tyne NHS Hospitals Trust and the Newcastle University. Advertisements were sent out through internal group mail lists and also placed on the electrical noticeboards throughout the Trust. A copy of the information sheet (Appendix 1), which described the aim of this study, recruitment criteria, measurement instruments and procedures, was sent to each responder expressing an interest in volunteering. The majority of the responders were staff or colleagues from the Regional Medical Physics Department of Freeman Hospital. Additionally, a number of students from the university participated in this study.

3.2.3 Study inclusion criteria

Only male healthy subjects were studied. Volunteers were informed that they would be studied only if they met all of the following criteria:

- Male adult with age above 18 years old;
- Without any diagnoses or symptom of cardiovascular disease, such as hypertension, diabetes or atrial fibrillation;
- Without any physical abnormality or any observable skin problem.

Five age bands were used to group the volunteers: 20 – 29 years, 30 – 39 years, 40 – 49 years, 50 – 59 years, over 60 years group. Each volunteer was put into one of the five

groups according to their age. Matched numbers of subjects were entered into each group to participate in the study.

3.3 Measurement environment

All measurements were undertaken in the measurement room at the Medical Physics Department, Freeman Hospital. A quiet and comfortable experimental environment was maintained in the room. To minimize external distraction, access to the room was limited during the whole measurement. The layout of the measurement room is illustrated in Figure 3-1. While the furniture was placed at the left side, most space in the room was left for the subject and measurement devices. The echocardiographic device, TaskForce Monitor system, ECG and PPG devices were arranged to form a half circle with a couch positioned at the other end. A disposable paper sheet was placed over the couch and changed after the measurements finished on each subject.

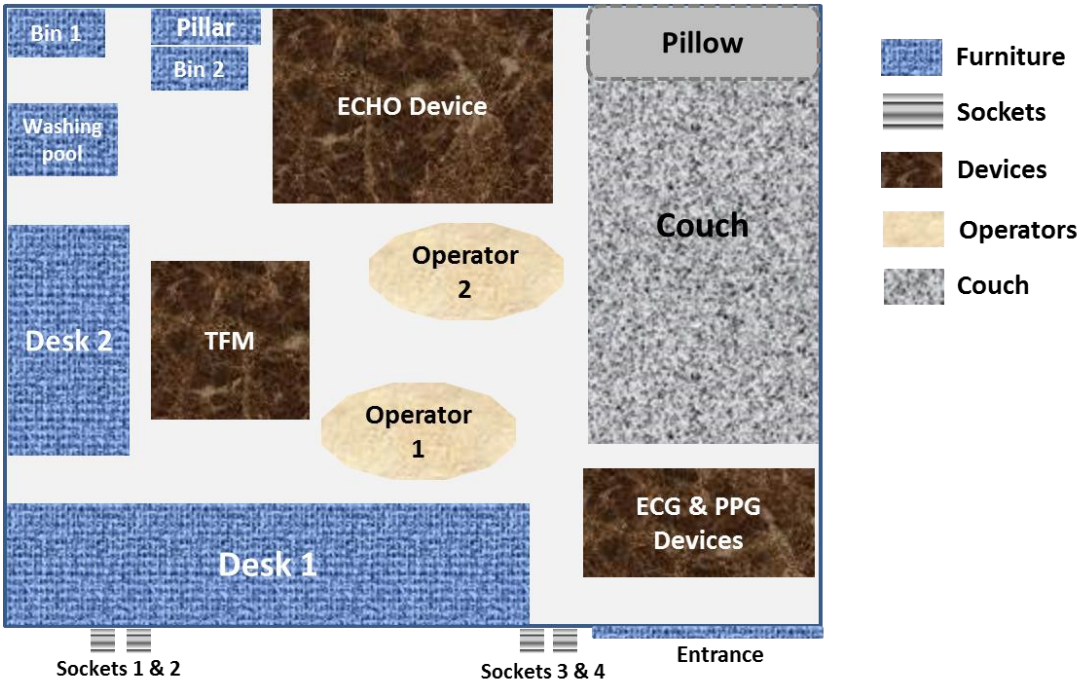

Figure 3-1: Illustration of the measurement room layout. Devices were arranged to make a comfortable experimental environment for the operators and the subjects. The mains sockets 1, 2, 3, 4 were used to provide electrical power for the echo device, TaskForce Monitor system (TFM), ECG and PPG devices respectively.

The measurement devices and their connections to the subject were placed so as to avoid one device and its mains cable interfering with another device. The couch where the subjects lay down was positioned at the right corner of the room. In order to reduce the interference from mains power supplies, those mains sockets which were far away from the couch and the subject were used. I recorded all data (operator 1), with assistance from a second operator who was an ultrasound specialist (operator 2) for help in obtaining echocardiograms. Both operators were located at the central area surrounded by the devices and the couch. The aim of this arrangement was to ensure that the two operators could operate the devices easily and the subjects could feel comfortable and relaxed.

3.4 Measurement techniques

3.4.1 Echocardiographic techniques

M-mode and Doppler imaging techniques were employed to assess cardiac dynamic mechanics. They were obtained with guidance from 2D echocardiography; the M-mode image recorded the movement of the tissues along the M-mode cursor in a 2D view, and the Doppler imaging recorded the velocity of the blood within a sample volume, which was placed on an M-mode cursor guided by a 2D view.

Two-dimensional echocardiography

The parasternal long axis (PLAX) view was used as it was the most common view to guide M-mode echocardiography for mitral valve and aortic valve movement. Right ventricle, left ventricle, left ventricular outflow track (LVOT), left atrium and the two valves were seen in this view. To obtain the images, the ultrasound transducer was positioned at the parasternal window, which is at the right side of the sternum between the 3rd and 5th intercostal spaces. The acquisition of 2D images in the PLAX view and an example is shown in Figure 3-2 (A).

The apical views were used to guide the Doppler echocardiography for mitral flow and aortic flow measurement. To obtain the 4-chamber view images, the transducer was positioned at the apex of the heart and oriented toward the right shoulder. As shown in Figure 3-2 (B), the left and right atria, ventricles, atria-ventricular valves can be seen in this

view. By tilting the ultrasound transducer upwards at the same position the aorta can also be included, which is known as the apical 5-chamber view.

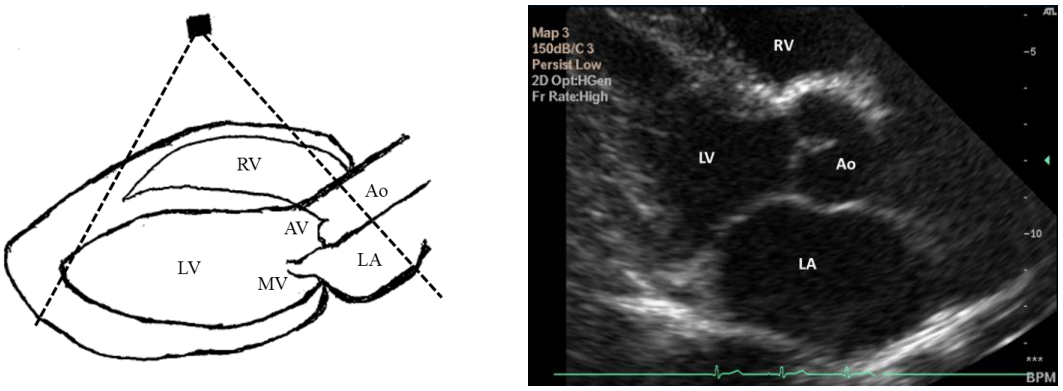

(A)

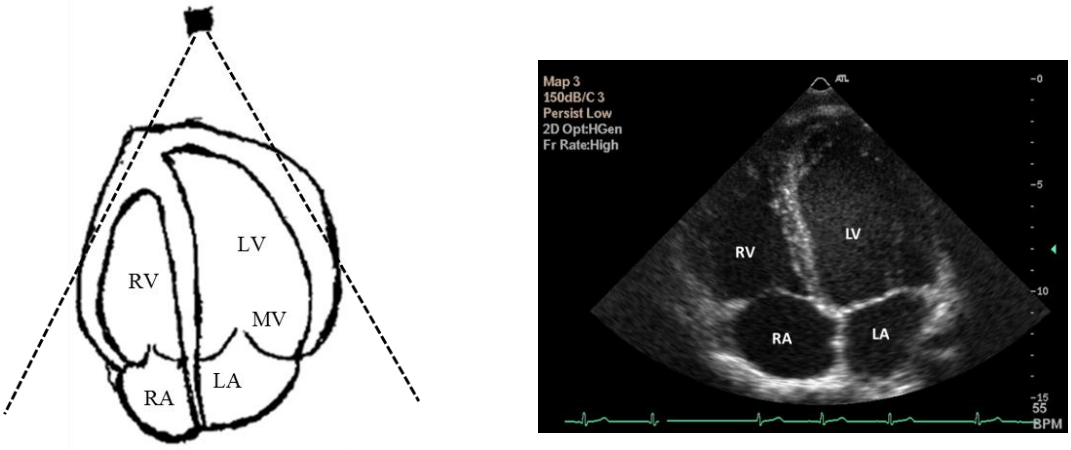

(B)

Figure 3-2: 2D echocardiography in: (A) parasternal long axis (PLAX) view; (B) apical 4-chamber view. The triggering ECG tracing was displayed at the bottom of the images. RV: right ventricle; LV: left ventricle; RA: right atrium; LA: left atrium; Ao: the aorta; MV: mitral valve; AV: aortic valve.

M-mode echocardiography

The mitral valve is a fast moving structure in the heart. The movement of its anterior leaflet and posterior leaflet was recorded by placing the M-mode cursor through the tips of the leaflets in the PLAX view, which is shown in Figure 3-3 (A). As can be seen, when open during early diastole and atrial contraction phases, the two leaflets separated and

moved in opposite directions, which caused two characteristic waves on each heartbeat. Once the valve closed during systole, the two leaflets touched and moved as one.

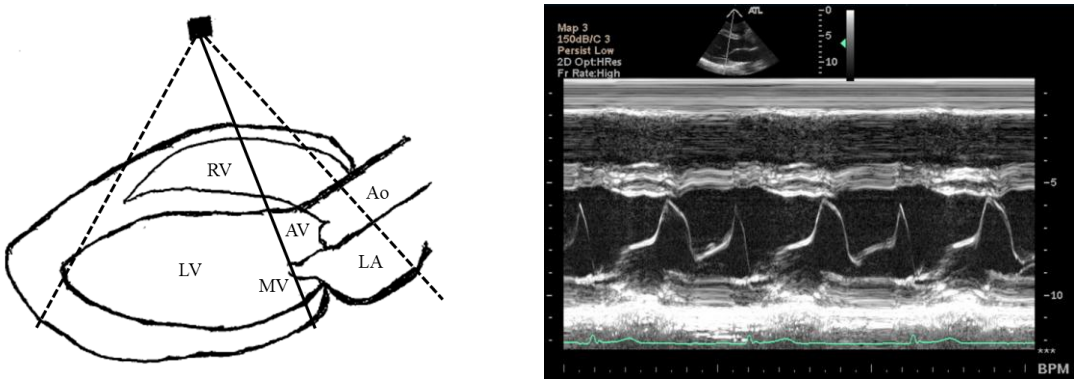

(A)

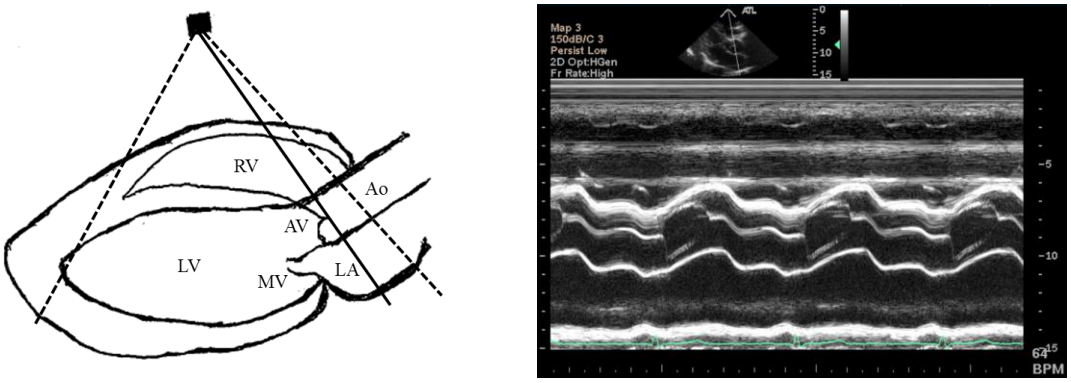

(B)

Figure 3-3: M-mode echocardiograms for: (A) mitral valve movement; (B) aortic valve movement. On the left, the M-mode cursor is illustrated in solid lines. The 2D guiding image and triggering ECG are displayed with each M-mode image. RV: right ventricle; LV: left ventricle; RA: right atrium; LA: left atrium; Ao: the aorta; MV: mitral valve; AV: aortic valve.

Aortic valve movement was recorded in the same view by adjusting the M-mode cursor through the aortic root at the valve level. The motion of the aortic valve is not as complex as the mitral valve. There are three leaflets, left-coronary, right-coronary and non-coronary leaflets, for a normal aortic valve. Only the right-coronary and non-coronary leaflets were visible in the PLAX view, which separated during systole and moved synchronously in

parallel. The acquisition of the aortic valve movement in the M-mode echocardiography is shown in Figure 3-3 (B).

Doppler echocardiography

Pulsed-wave Doppler echocardiography was performed to obtain the velocities of blood flow through the mitral valve and aortic valve. A small sample volume was positioned on an M-mode cursor to assess the mean blood flow velocity in the volume. Both the depth and the size of the sample volume were adjustable. To measure accurate velocity of movement with the Doppler technique, the sound wave was oriented as parallel as possible to the movement direction. For the Doppler modality in the HDI 5000 echocardiographic device, orientation of the ultrasound wave was mainly determined by the placement of the M-mode cursor. A minor angle correction was allowed for the sample volume. When the object within the sample volume moved towards the transducer, a positive velocity was recorded. In contrast, if the movement was away from the transducer, a negative velocity was recorded. A velocity filter was provided by the device to set a velocity threshold; the recording value was set to 0 when the detected velocity was below the threshold.

Mitral flow velocity was measured in the apical 4-chamber view. As shown in Figure 3-4 (A), a sample volume was positioned near the tip of the mitral valve leaflets inside the left ventricle. Because the blood moved towards the transducer when it came through from the atria to the ventricle, positive waves were recorded. The Doppler image for the mitral flow showed a similar shape to the M-mode image for mitral valve movement. There were also two components within a single beat with the major one corresponding to the ventricular passive filling and the other to left atrial contraction. The Doppler recording represented the blood flow velocity rather than cardiac dimension information represented by the M-mode.

The acquisition of the aortic flow velocity measurement is shown in Figure 3-4 (B). The apical 5-chamber view was used for this application. A sample volume was placed proximal to the aortic valve within the left ventricular outflow track (LVOT) on the M-mode cursor. Because the blood moved away from the transducer during systole, a negative wave was recorded for each beat.

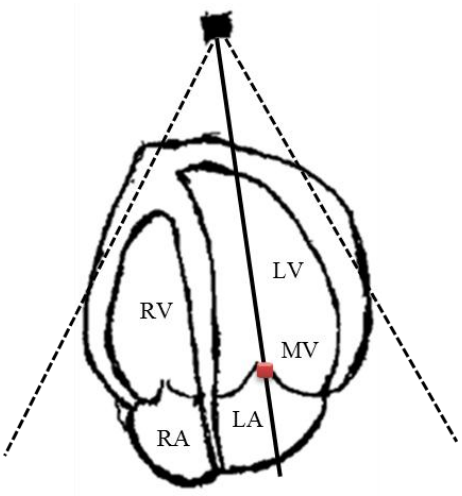

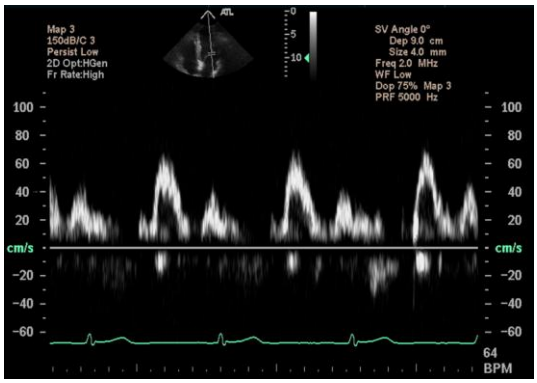

(A)

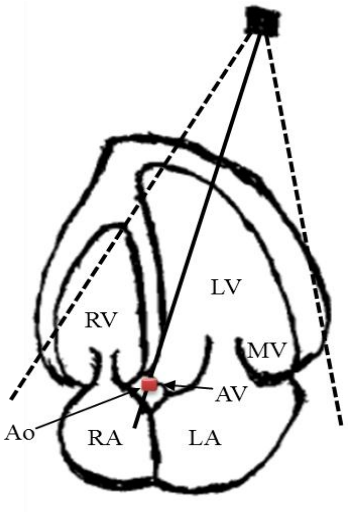

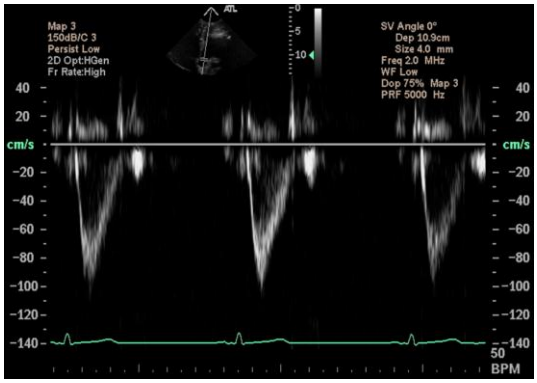

(B)

Figure 3-4: Pulsed-wave Doppler echocardiograms for: (A) mitral flow; (B) aortic flow. The Doppler sample volumes are illustrated by filled cylinders on the solid M-mode cursor lines on the left of the plots. The 2D guiding image and triggering ECG are displayed with each velocity trace. RV: right ventricle; LV: left ventricle; RA: right atrium; LA: left atrium; Ao: the aorta; MV: mitral valve; AV: aortic valve.

3.4.1.4 Parameter setting for echocardiography

Parameters were set via the user interface of the software and the user control panel on the devices. For the echocardiography image recording, the ECG triggering mode was

configured so that the device started to capture images automatically immediately after the 1st detected ECG QRS complex once the 'Capture' button on the control panel was pressed. The recording length was set to 15 s for each measurement. Therefore, the image acquisition stopped 15 s automatically after the starting point.

The frame rate was set to 25 frames per second for the guiding 2D echocardiography measurement. A total of 375 frames over the 15 s were obtained for each measurement. The sweep speed for the M-mode and Doppler imaging was set to 200 pixels per second, which gave a temporal resolution of 5 ms for each pixel. The gains, contrast and focus region were adjusted via the user control panel for each recording till a good quality image was available. Because of the anatomic difference of subjects, these settings varied case by case.

The axis length of the sample volume for the Doppler echocardiography was set to 4 mm and the velocity filter was set to 'Low'. Lower filter allowed a lower threshold for the velocity recording, which was helpful to retain the boundaries of flows.

3.4.2 ECG measurement techniques

Ten electrodes were used for the acquisition of standard 12-lead ECGs; 3 of them for limb leads (Lead I, II, III, aVR, aVL, aVF), 6 for the chest leads (V1 to V6) and one neutral electrode. The limb lead electrodes were positioned at the wrists or ankles as shown in Figure 3-5 (A). The standard positions of the chest lead electrodes are shown in Figure 3-5 (B). Lead V1 and V2 are between the 4th intercostal spaces at each side of the sternum respectively. V4 is at the intersection site of the 5th intercostal space and the midclavicular line, which is around the apex of the heart. V3 is at the midway between V2 and V4. The positions for V5 and V6 are located on the anterior axillary line and midaxillary line at the same level as V4 respectively. However, as the standard positions for V2 to V6 overlapped echocardiographic parasternal window and apical window, these 5 electrodes on the left chest were not used when images were wanted.

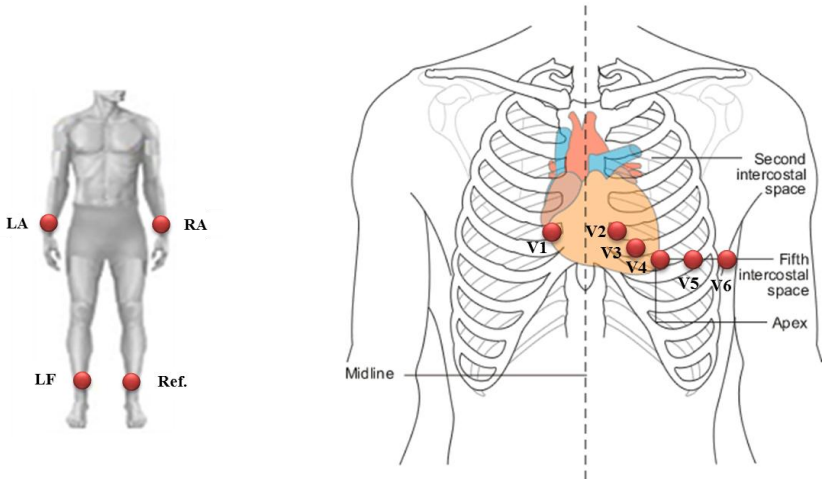

(A) (B)

Figure 3-5: Electrode placement for recording standard 12-lead ECG: (A) limb leads (I, II, III, aVR, aVL, aVF); (B) chest leads (V1 ~ V6). LA: left arm; RA: right arm; LF: left foot; Ref.: neutral device reference electrode.

To make sure of a good contact, skin below the electrodes was cleaned carefully using alcohol. Then the electrodes were attached to the body when the skin was dry. Although hair can affect the contact, it was not a problem as subjects remained still during the measurements.

The sampling rate of the ECG recording was pre-set to 1 kHz by the device. The bandwidth and the gains were adjustable from the control panel of the amplifiers. In this study, the bandwidth was set to 0.05 Hz to 100 Hz, while the gains were set to 500 for both of the limb leads and the chest leads.

3.4.3 Impedance measurement techniques

The placement of 4 traditional long band electrodes for thoracic impedance measurement has been reported in the literature (Kubicek et al 1966, Mohapatra 1981, Lamberts et al 1984, Sherwood et al 1990). The typical configuration was placing a pair of current-carrying and voltage-sensing electrodes on the neck and the other pair on the chest at the xiphoid process level, with the two voltage-sensing electrodes at the inner side. Lamberts et al. (1984) observed that the impedance measurement was affected by the distance between the voltage-sensing electrodes and suggested a standard average distance

of 22 cm. According to Mohapatra's study (Mohapatra 1981), the current electrodes had to be placed with at least a 3 cm separation from their corresponding voltage electrodes to help the excitation current density distribute more uniformly in the body between the voltage electrodes. Furthermore, Sherwood et al. (1990) emphasized that consistent placement of the electrodes was important for the repeatability of measurements.

Three short adhesive strips with a pair of current-carrying and voltage-sensing electrodes on each are provided with the TaskForce Monitor system for thoracic impedance measurement. The placement of the strips is shown in Figure 3-6. One strip was attached to the area between the neck and the hairline on the back, and the other two were positioned parallel to the neck electrode on the thorax at the xiphoid level. These two strips were connected together to form a common pair of current and voltage electrodes. A neutral electrode was placed on the right lower leg. Constant alternating current was supplied via the outer current electrodes, and conducted through the body. The voltage was measured by the inner electrodes and consequently, the thoracic impedance was calculated. The limitations of this impedance measurement have been described in Chapter 2. On a normal adult body, the distance between the upper and lower voltage electrodes was more than 22 cm, and the separation distance between the current and voltage electrodes was ensured by the adhesive strips. In addition, because the chosen positions were easily identifiable anatomical landmarks, it was possible to make consistent placement on all subjects.

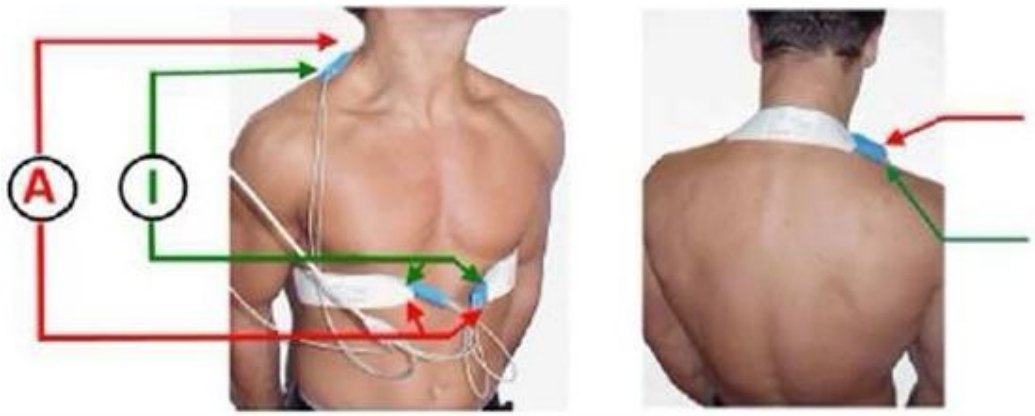

Figure 3-6: Illustration of impedance electrodes placement. Three pairs of short band electrodes were used: one on the back neck, and the other two on both lateral sides of torso. The two pairs on the torso were connected together to form a common pair. Constant current was supplied through the outer electrodes, and voltage was measured between the inner electrodes.

As described in the section 2.4.2, both the impedance (Z) and its first derivative waveform (-dZ/dt) were measured. The sampling rates for these two signals were pre-set to 50 Hz and 1 kHz by the TaskForce Monitor system.

3.4.4 Pulse measurement techniques

The left index finger and earlobe were chosen in this study as the sites for peripheral pulse measurement. This was because the arterioles at these sites are close to skin surface enabling pulse waveforms to be easily detected.

Pulse waveform measurement was sensitive to movement artifacts. To reduce the movement artifacts, the surface of PPG probe was placed flat on the centre of the fingertip or earlobe pulp, and then a finger cuff or earlobe clip was used to fix the probe on the skin. The pulse waveform was also affected by contact pressure. When the contact pressure was too high, arterioles under the skin were compressed and blood volume pulses were reduced. Ideally, an optimum pressure is required and kept consistent on all subjects. However, this was difficult to meet in practice. A good solution was to adjust the pressure manually by the operator before formal recording till a stable waveform with high amplitude pulse was displayed on the screen. The pulse device was always connected to the TaskForce Monitor system via the external input ports to enable pulse data to be recorded. The gains for pulse recording were set to 500 from the amplifiers of the pulse device. Additionally, the low cut-off frequency was set to 0.05 Hz and the high cut-off frequency was set to 30 Hz from the user control panel. The sampling rate was set to 1 kHz by the TaskForce Monitor system.

3.4.5 Summary of parameter setting on each device

The setting of sampling rates, gains and frequency bandwidth on each device for data acquisition is summarized in Table 3-2. Except the gains for the image acquiring varied case-by-case, the other parameters were kept consistent across all the subjects. For the M-mode and Doppler echocardiography, the temporal resolution of a pixel (5 ms) was converted to the corresponding sampling rates of 200 Hz. The settings of the TaskForce Monitor system were fixed by the system and not adjustable.

Table 3-2. Summary parameter setting on each device for data acquisition.

Devices	Signals	Sampling Rates (Hz)	Gains	Filter (Hz)
Echo	MV & AV (M-mode)	200	___	___
	MF & AF (Doppler)	200	___	___
ECG	Limb & chest ECGs	1,000	500	Low cut: 0.05 High cut: 100
TFM	Limb lead ECGs	1,000	___	Low cut: 0.08 High cut: 150
	Z	50	___	___
	-dZ/dt	1,000	___	___
PPG	Pulses (Ear & Finger)	1,000	500	Low cut: 0.05 High cut: 30

MV: mitral valve; AV: aortic valve; MF: mitral flow; AF: aortic flow.

3.5 Measurement system connection and operation

3.5.1 Device connections

As described above, an echocardiographic device and three physiological measurement devices were employed for data collection in this study. These four devices were connected together to record 4 sets of data (Table 3-1).

First of all, the ECG device was used alone to record standard 12-lead ECG signals. The use of the device to record this data is shown in Figure 3-7 (A). Next, both channels of the PPG device were then connected to the TaskForce Monitor system via its external input ports so that pulse data were recorded synchronously with limb lead ECGs and impedance from the TaskForce Monitor system. The connection of the PPG device and the TaskForce Monitor system for the acquisition of this data is illustrated in Figure 3-7 (B), which

allowed the simultaneous recording of 6 limb lead ECGs, impedance (Z), the first derivative (-dZ/dt), ear and finger pulses.

The connection of the 4 devices to record images and simultaneous physiological signals is shown in Figure 3-7 (C). The cardiac electrical activity was recorded by the ECG device. Because of the overlap between the ECG electrode positions and the echocardiography windows, the V2 ~ V6 leads were not recorded, but the 6 limb leads and the V1 lead were retained. ECG lead I was connected to the echocardiographic device to trigger the image acquisition, and connected to the TaskForce Monitor system for synchronisation rather than triggering. Therefore, the three devices recorded a common ECG signal to provide a time synchronisation reference. Only the finger pulse channel of the PPG device was used during imaging, and connected to the TaskForce Monitor system. This connection was used for the sequence 3 and 4 in the Table 3-1, which allowed a single recording to include: an echocardiogram (with the triggering ECG) using the software of the echocardiographic device; 6 limb lead and V1 ECGs using the software of the ECG device; synchronous ECG, impedance (Z), impedance (-dZ/dt) and finger pulse using the software of the TaskForce Monitor system.

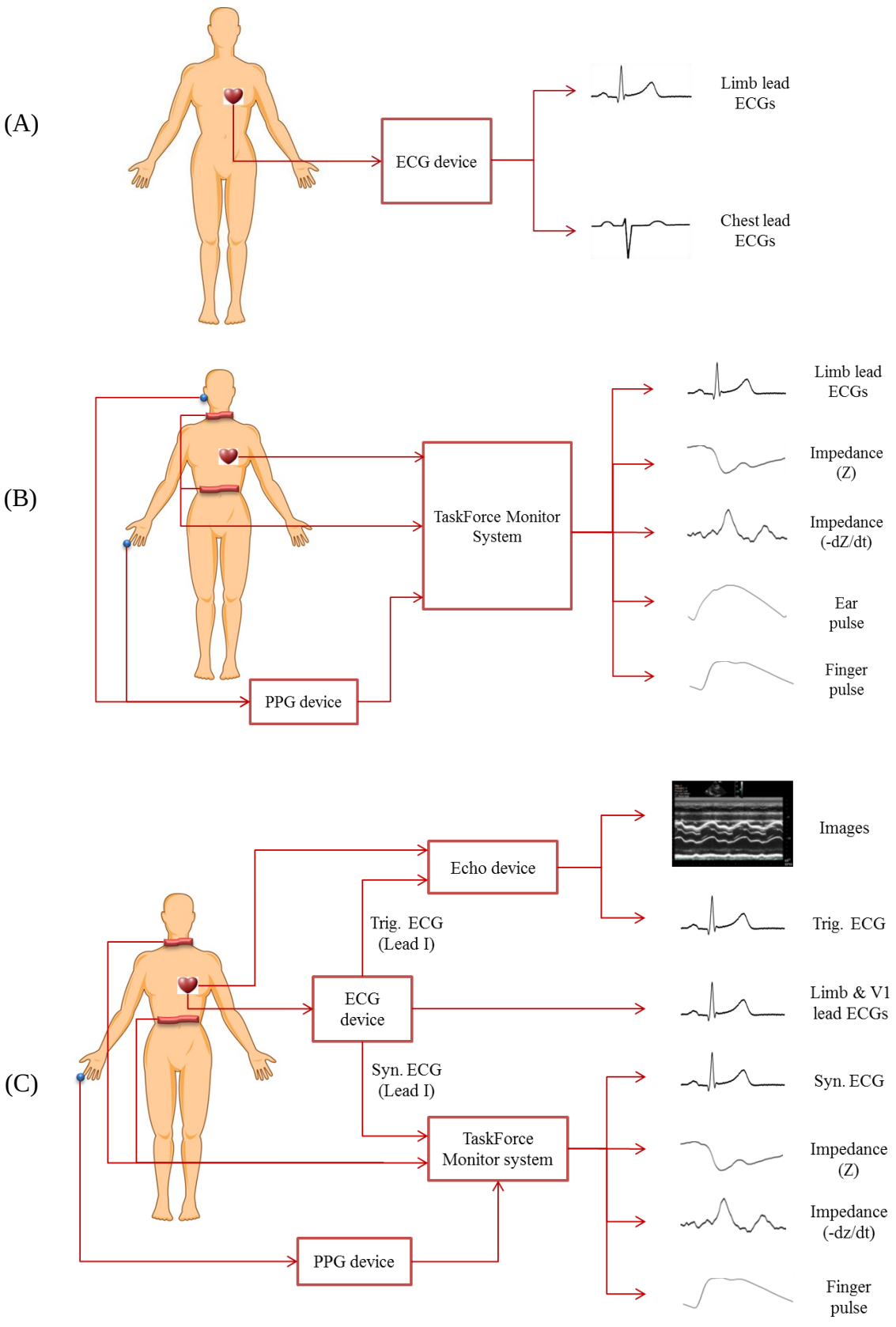

Figure 3-7: Device connections for recording of: standard 12-lead ECG (A); limb lead ECG, impedance and pulses (B); echocardiograms with ECG, impedance and pulse (C).

3.5.2 Recording length

The images and physiological signals were not stable from beat to beat because of natural variability. To enable the effect of changes to be studied, data were recorded over several respiratory cycles. In this study, measurements were taken over 60 s for recordings if only physiological signals were needed and 15 s for those with echocardiography. The image data length was chosen as it was difficult to keep a consistent probe position for longer. The length of this duration covered at least 3 respiratory cycles with subjects breathing normally. The file size of a single recording with images and physiological signals was around 500 Megabytes, and that of a recording without image was less than 10 Megabytes.

3.5.3 Operation

Using the ECG device alone or the connected TaskForce Monitor system and PPG device for data acquisition was easy as there was only one software control involved at once. It was more complex to measure images with physiological signals by using the 4 connected devices. As in the previous description, a common limb lead ECG (Lead I) was recorded by the echocardiographic device, the ECG device and the TaskForce Monitor system for this connection. However, because it was not practical to make all the devices start recording at the exactly same time, a further time marker was required to indicate the common period, during which all the devices worked simultaneously. A time marker was provided by controlling the mode switch on the ECG device. More specifically, the limb lead ECG output was kept to zero by setting the mode switch to ‘Zero’ till the imaging was ready so that a zero flat line was seen at the beginning of the common ECG. After normal ECG output was enabled, the image recording was automatically triggered by the ECG QRS complex and stopped once the pre-set length time was up. Therefore, the duration from the 1st triggering ECG QRS complex to the ending of imaging measurement was the common recording period. In summary, the following procedure was taken to operate on the combined measurement system for images and physiological signals recording:

- Step 1. Start the TaskForce Monitor system to record;
- Step 2. Start the ECG system to record, with limb leads set to ‘Zero’;

- Step 3. Press the ‘Capture’ button on the control panel of the echocardiographic device when image recording is ready;
- Step 4. Switch the limb leads to ‘Use’ mode so that the image recording can be triggered by the ECG;
- Step 5. The image recording automatically starts once an ECG complex is detected and stops automatically 15 s later;
- Step 6. Switch the limb leads back to ‘Zero’ mode again immediately after an alert sound is heard from the echocardiographic device when image recording finished;
- Step 7. Repeat Step 1 to 6 if more than one image measurements were wanted;
- Step 8. Stop the ECG device;
- Step 9. Stop the TaskForce Monitor system.

The diagram of the timing sequence for a set of recordings using the above procedure is shown Figure 3-8. The TaskForce Monitor system was kept recording during the whole period from t_1 to t_8. The ECG device was recording from t_2 to t_7. The M-mode echocardiography for the mitral valve and aortic valve, Doppler echocardiography for the mitral flow and aortic flow were taken in sequence during the period. While normal chest lead ECG (only V1) output was always allowed, limb leads were set to 0 to generate a flat line at the beginning of each image recording. The first image recording was triggered by the ECG QRS complex at t_4 after normal limb lead ECGs were turned on at t_3. This recording stopped automatically 15 s later at t_5, immediately after which the limb lead ECGs were set back to 0 at t_6 to prepare for the next image recording. After the last image was taken, the ECG device was stopped at t_7, and the TaskForce Monitor system was stopped at t_8.

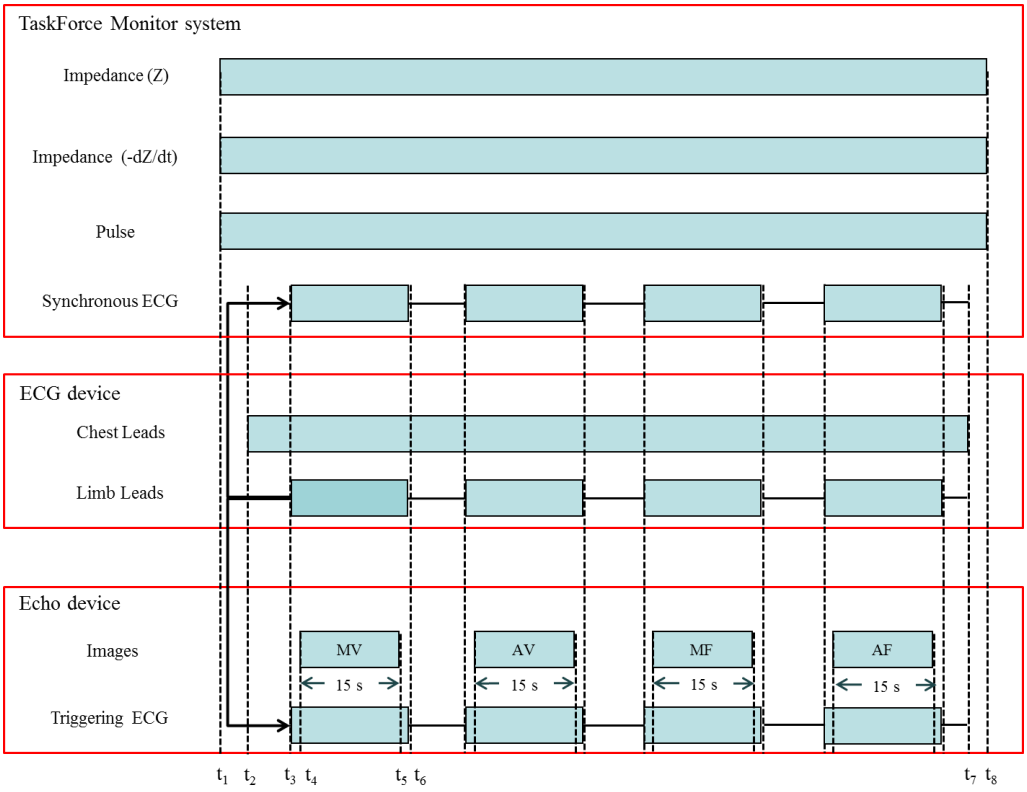

Figure 3-8: Diagram of timing sequence to use the combined system for the recording of images with simultaneous physiological signals. The TaskForce Monitor system started to record first (t_1) and stopped last (t_8). During the period from t_2 to t_7, while the chest ECGs (only V1) was always kept on, the limb lead outputs were switched between 0 and normal to generate time markers at the beginning of imaging for the mitral valve (MV), aortic valve (AV), mitral flow (MF) and aortic flow (AF).

3.6 Data acquire procedure

3.6.1 Subject preparation

Informed consent was obtained from each subject before the measurement could commence. The overall study and data collection procedure was introduced to the subjects briefly after arrival. They were then asked to confirm if they met the study inclusion criteria. An opportunity was given for the subjects to ask any question about the study. They were also told that they were free to withdraw from the measurement at any time without any reason.

3.6.2 Prior clinical information recording

Height and weight were obtained for calculating body mass index (BMI). The subject was then asked to lie down on the prepared couch with shirt and shoes off. To facilitate the image recording, the couch was adjusted to make the subject recline around 45 degrees. Five minutes was given to the subject for relaxation, and they were asked to breathe calmly. Electrodes and probes were attached to the subject during this period. Afterwards, blood pressures were measured using an A&D UA-767PCHV automatic blood pressure monitor (A&D Co., Japan).

3.6.3 Echocardiography and physiological measurement recording

After the prior clinical information was obtained, the 4 sets of data listed in the Table 3-1 were recorded in sequence. The 1st sequence was a 60 s recording of standard 12-lead ECGs, which was taken from the ECG device.

The 2nd sequence, consisting of a 60 s simultaneous recording of 6 limb ECGs, impedance (Z and –dZ/dt), ear and finger pulses, was taken from the combined PPG device and TaskForce Monitor system. This data set was used to investigate the relationship between the thoracic impedance and the peripheral pulses.

The 3rd sequence comprised a set of echocardiograms simultaneously recorded with ECGs (limb & V1 leads), impedance (Z and –dZ/dt) and the finger pulse from the combined 4 devices. Two recordings with M-mode images for the mitral valve movement and aortic valve movement were taken first, and then another two with Doppler images for the mitral flow and aortic flow were taken. Each recording lasted 15 s. These 4 recordings were used to investigate the relationships between the cardiac dynamic imaging and physiological measurements.

Finally, to assess the repeatability of the image data, a 4th sequence of data was acquired, which repeated the measurements in the 3rd sequence.

In summary, a total of 10 recordings were taken in sequence from each subject. The sequence 3 and 4, which included simultaneously recorded images and physiological measurements, were the key parts of the data set studied in this project.

3.6.4 Data transfer and storage

Data recorded by the measurement system were downloaded to a common computer for storage and further analysis. A DICOM server was set up on the computer by using the open source program Conquest DICOM so that the DICOM echocardiography images could be transferred via the internet. A K-Pacs viewer was provided by the program to give a quick view of images. Signals recorded by the TaskForce Monitor were saved in files with their own format. A file format conversion tool was provided in its integrated software, which was used to convert these files into MATLAB readable '.mat' format. ECG signals recorded by the ECG device were stored in binary files, which were converted to ASCII format by using a format conversion tool. The converted files on these two devices were then transferred to the common computer.

All data were stored on NHS and Newcastle University password protected computers and backed up over the NHS network. The data on each subject were anonymised and identified by a unique sequential code. Those non-identifiable data were stored into password protected computer systems for further analysis.

3.7 Signal pre-processing

3.7.1 Imaging reconstruction

Echocardiographic images were stored frame by frame in DICOM (Digital Imaging and Communications in Medicine) format, which is a standard format proposed by the National Electrical Manufacturers Association for storing and handling medical images. MATLAB R2010b (MathWorks, USA) provided a toolbox for DICOM image loading. An example of Doppler echocardiography for aortic flow read by MATLAB is shown in Figure 3-9. Each new frame was updated from the position of the black raster, which moved from the left to the right on the screen with a fixed sweep speed. The newest frame entered at the left side of the raster. When reaching the farthest right side on the screen, the raster was swept to the left side. The oldest frames were then flushed by the new ones.

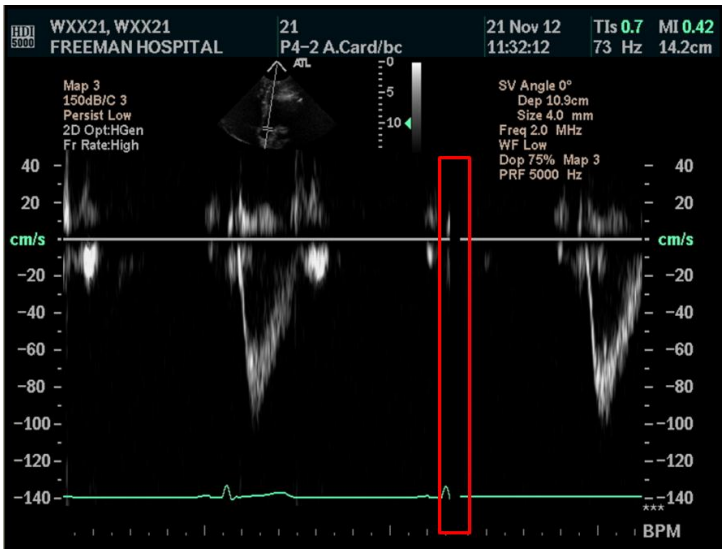

Figure 3-9. An example of a Doppler DICOM image loaded by MATLAB. Approximately 80 frames are shown on this screen. The entry of new frames was located at the left side of a raster moving from left to the right (indicated by the red box). When the farthest right side was reached, the raster was swept to the left side.

There were some disadvantages for the M-mode and Doppler echocardiograms stored in this frame-based mode. Firstly, there were many frames displayed on each screen. In the original, in addition to the current frame, all other frames which displayed on the screen were also stored. It resulted in huge redundant information being kept, and made the file size large at around 500 Megabytes for a 15 s recording. Secondly, the wrapping of the raster made it impossible to see the images over the whole recording period at once. In order to reduce the file size and display all frames on one screen, frame-based M-mode and Doppler echocardiograms were reconstructed into a pixel series. After the reconstruction, an image was represented by a series of pixel columns arranged in parallel. During the image capture, the frame rate was set to 25 frames per second. Therefore, there were 375 frames included for a 15 s recording. Eight pixel columns of image were updated in each frame by the raster. The width of the raster was 11 pixels. With this prior information, the pixel series of each frame were reconstructed by the 8 pixel columns preceding the left edge of the raster. The wrapping of the raster was about to occur when the distance between its left edge and the right end of the screen was less than 11 pixels. If the distance was less than 8 pixels, the beginning of the current frame would be left at the right side of the screen, while the rest entered at the left side. These two parts were obtained and put together to construct the pixel series of a current frame.

An example of image reconstruction is shown in Figure 3-10. As the redundant frames were removed after the reconstruction, the final file size was only around 2 Megabytes, which was 250 times less than the original size. Additionally, the frame based image was converted into the pixel series, which allow visualizing all the frames on a single screen and was easier to display with the physiological signals.

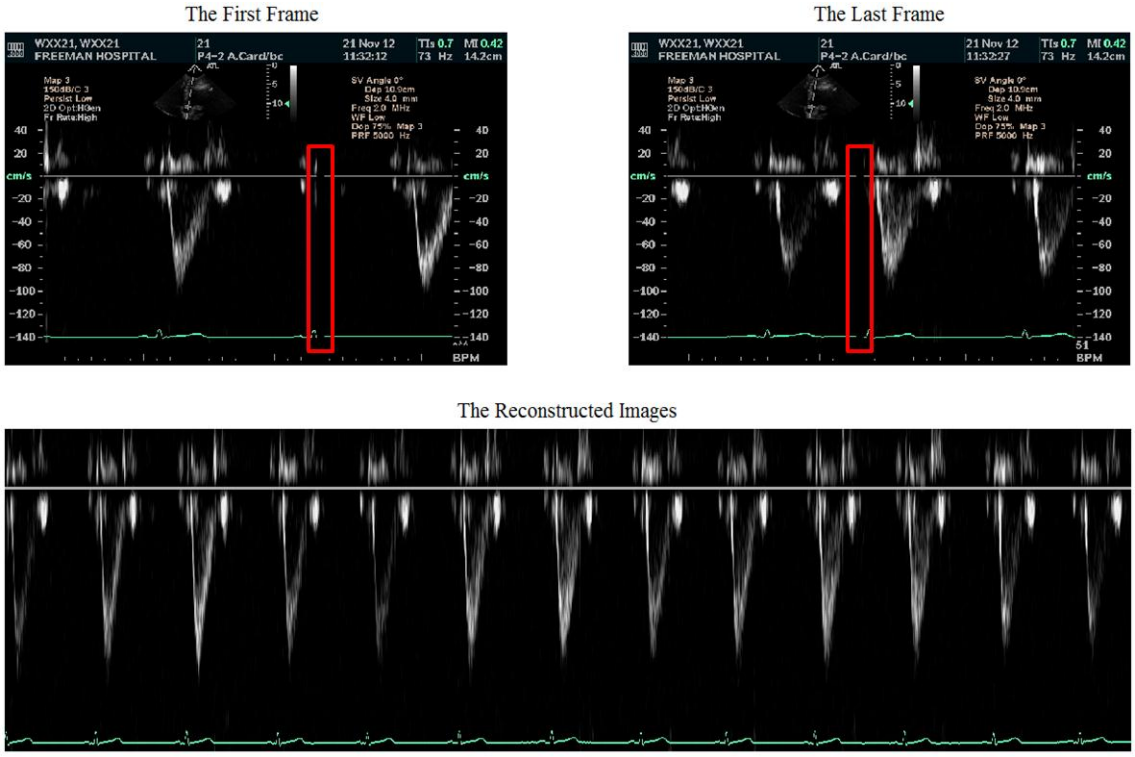

Figure 3-10. An example of reconstructing a pixel series of a Doppler image. The first frame and the last frame are shown in different screens in the original image. However, all frames were displayed on a single screen in the reconstructed image. During reconstruction, the annotation part in the original images was removed.

3.7.2 Resampling processing

In this study, physiological signals were recorded by the ECG device and the TaskForce Monitor system with their own analogue-to-digital data acquisition cards and software. Loss of synchronization existed between the signals from these two devices, although the sampling rates were set to the same 1 kHz on the both. An experiment was commenced to assess and quantify any loss of synchronization. The scheme of the experiment is shown in Figure 3-11. A TG 1304 Programmable Function Generator (Thurlby-Thandar Ltd, UK)

was employed to produce a testing 50 Hz sinusoid signal, which was fed into the ECG device. The TaskForce Monitor system was connected to the ECG system via the external input port so that it also received the same test signal. The mode switcher on the ECG system was used to generate zero lines at the beginning and end of the sinusoid signal. The number of samples of the sinusoid waveforms between the zero flat lines recorded by the two devices were counted and compared.

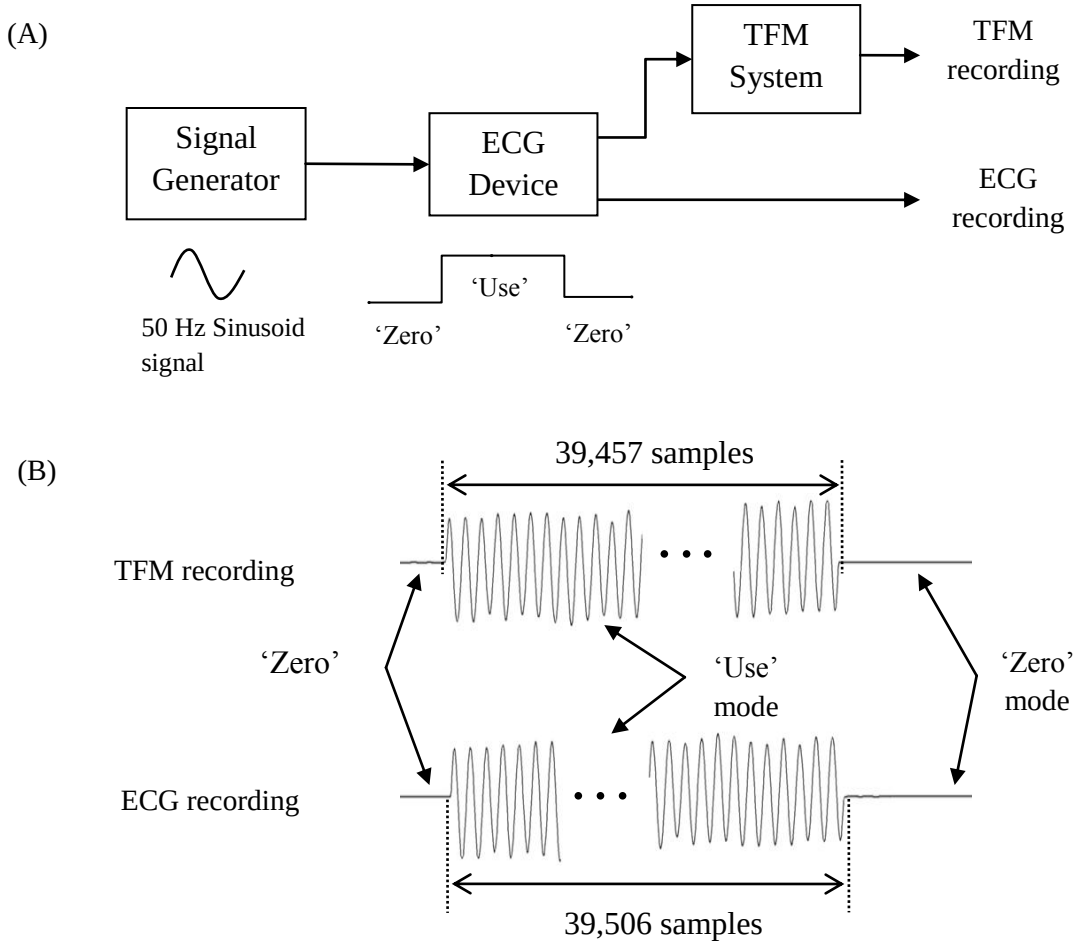

Figure 3-11. Assessing the loss of synchronization between signals captured by the TaskForce Monitor (TFM) system and the ECG device: (A) system connection; (B) an example of recorded signals taken from the measurement 5 of the Table 3-3. The ECG device recorded 49 samples more than the TFM system (39,506 vs. 39,475 samples) over the approximately 40 s recording of a 50 Hz sinusoid waveform.

Seven repeat measurements were implemented with the length of the sinusoid signals varying from 13 s to 80 s. The number of samples from the two devices and their ratio are given in Table 3-3. The ECG device recorded more samples than the TaskForce Monitor

system in the all 7 measurements. In measurement 1, the sample number difference was 16 over around 13 s. The difference was 99 samples for the long measurement 7, when the recording was around 80 s long. The ratios between the samples number were more consistent, with mean and SD of 1.00123 ± 0.00002. Therefore, the recordings from the TaskForce Monitor system were resampled by 1.00123 times using a linear interpolation method before synchronizing them with the ECGs. In addition, as explained already, the impedance waveform (Z) was captured with a sampling rate of 50 Hz. Therefore, a dual-step resampling processing was implemented for the Z waveform; it was firstly resampled by 20 times to make it similar to the other TaskForce Monitor signals and then resampled by 1.00123 times.

Table 3-3. Comparison of sample numbers of testing 50 Hz sinusoid signals recorded by the ECG device and TaskForce Monitor system.

	Measurements (number of samples)						
Devices	**1**	**2**	**3**	**4**	**5**	**6**	**7**
ECG	13288	14444	20364	29725	39506	59794	79754
TFM	13272	14426	20339	29689	39457	59720	79655
Ratio	1.00121	1.00125	1.00123	1.00121	1.00124	1.00124	1.00124

3.7.3 Synchronization

Synchronization of signals from separate devices was implemented referring to the commonly recorded ECG and the time markers on it. The scheme of the synchronization procedure is shown in Figure 3-12. A pixel series of image was reconstructed using the method introduced in the section 3.7.1. Ideally, the image recording would be triggered by the 1st ECG QRS complex following the flat line at the beginning. In reality, the recording was triggered by either the 1st or 2nd QRS complex (see Figure 3-13 for examples). Therefore, the closest QRS complex preceding the raster in the 1st frame, which was not necessarily the 1st one following the beginning zero line, was considered as the common starting for all recordings. The signals from the TaskForce Monitor system were resampled first to make them have the same sample numbers as ECGs. A fixed window of 15 s was then applied to the recordings from the TaskForce Monitor and the ECG devices to obtain the part which was simultaneously recorded with the images. The synchronized signals were then saved into a single file for further analysis.

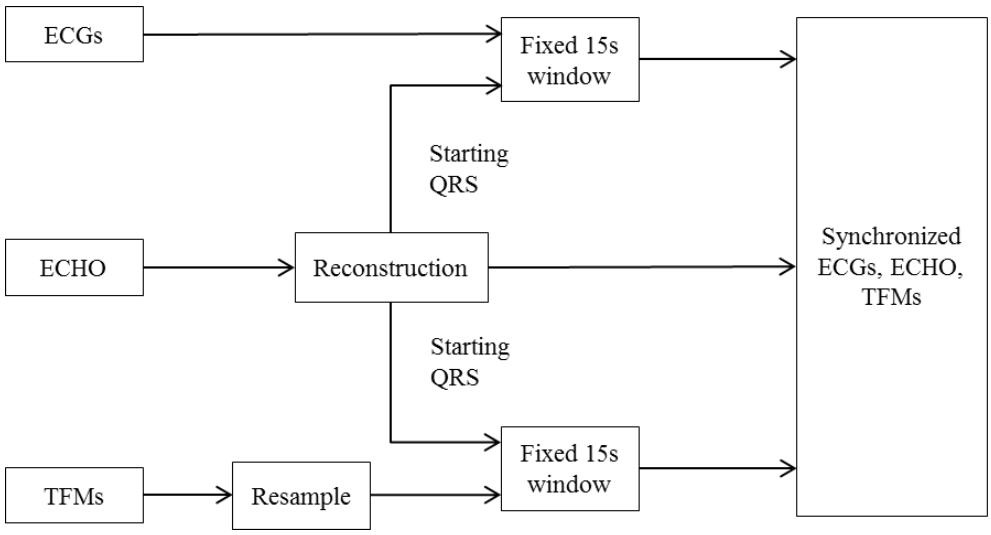

Figure 3-12. Scheme of synchronization procedure for the signals recorded from the ECG device, echo device and TaskForce Monitor system. The common starting point was the 1st R wave from the ECG triggering image capture.

(A)

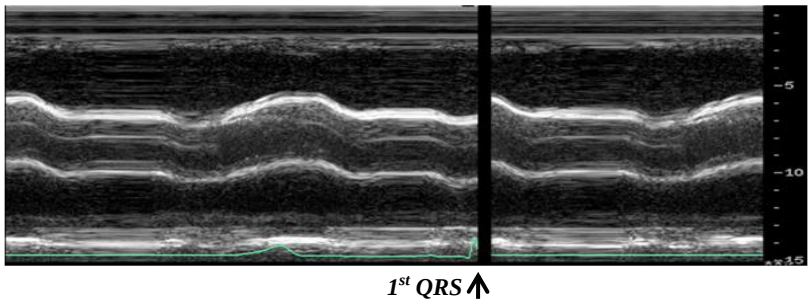

(B)

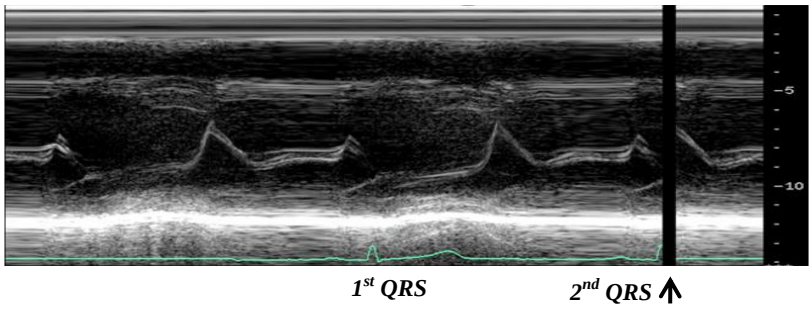

Figure 3-13. Examples of the image recording triggered by: (A) the 1st QRS complex following the beginning flat line; (B) the 2nd QRS complex after the flat line. The 1st triggering QRS complexes are denoted by black arrows.

An example of a synchronized Doppler echocardiogram for aortic flow and physiological measurements is shown in Figure 3-14, and the time aligned image and the TaskForce Monitor signals are displayed in Figure 3-15.

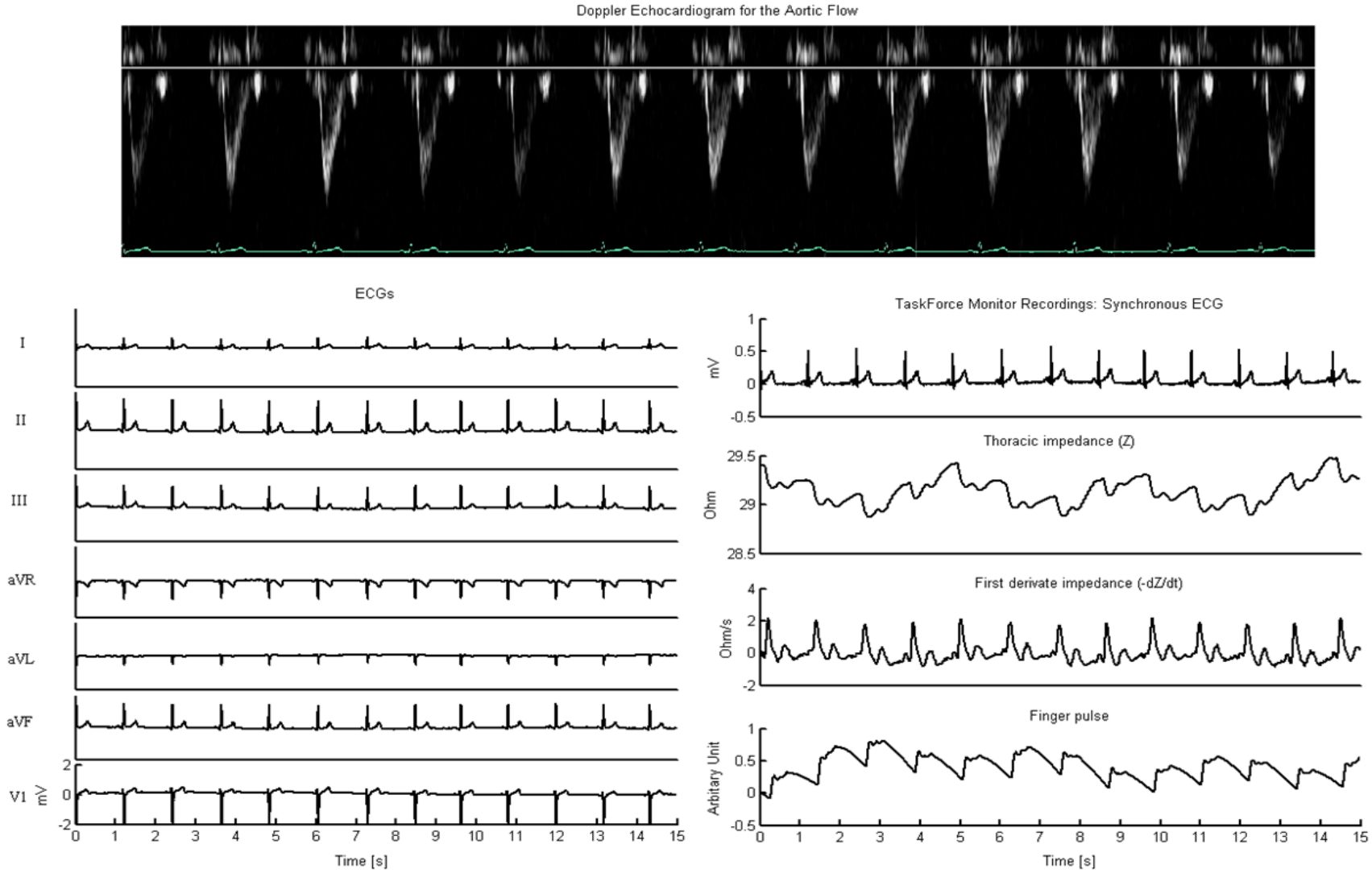

Figure 3-14. Example of synchronized Doppler image for aortic flow, ECGs and signals from the TaskForce Monitor system.

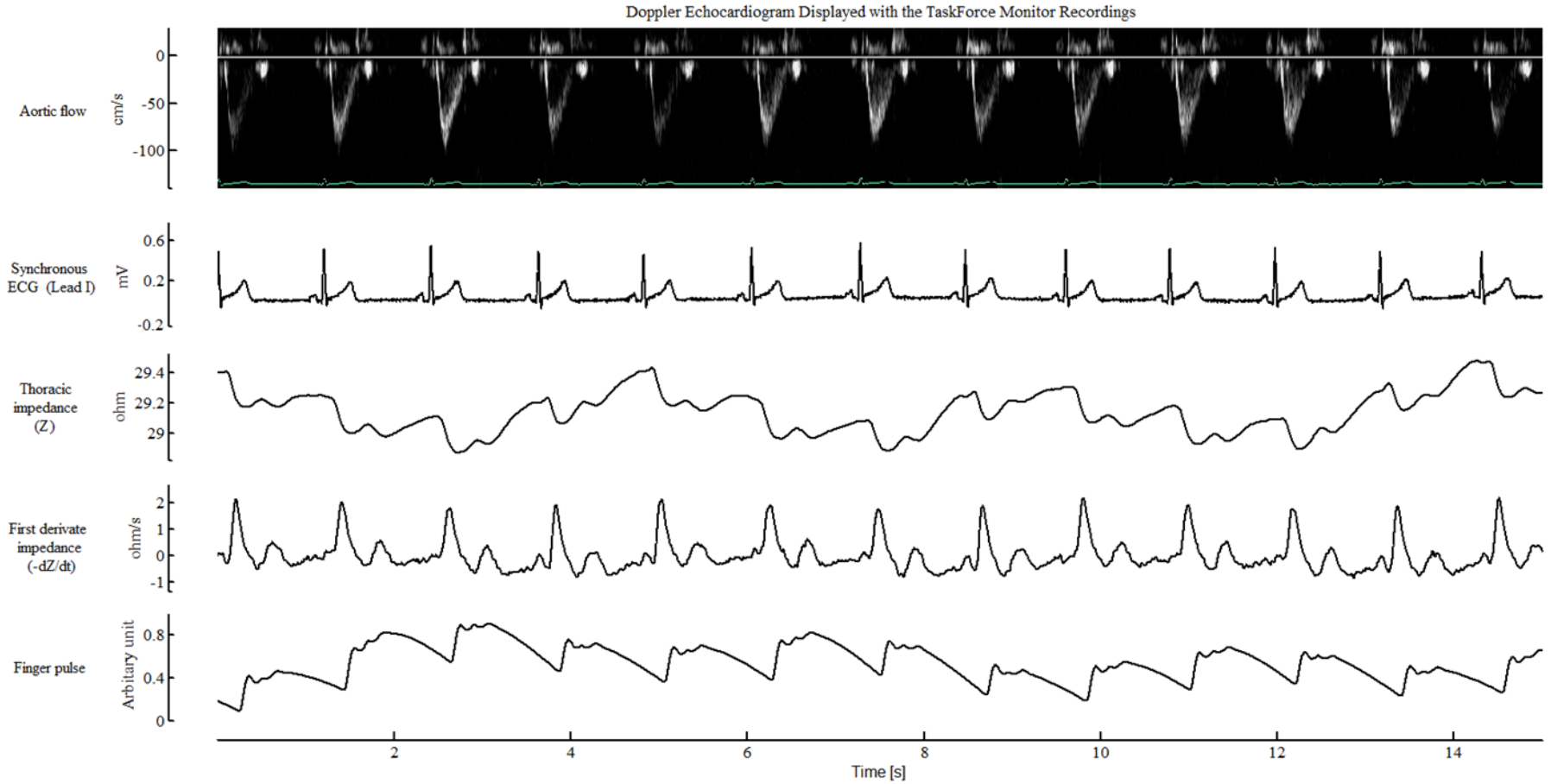

Figure 3-15. Example of synchronized Doppler echocardiogram for aortic flow displayed with synchronized physiological signals from the TaskForce Monitor system.

Table 3-1. Summary of data recorded in the three sequential sessions from different device combination: 1) standard 12-lead ECG signals recorded by using the multi-channel ECG device; 2) 6 limb lead ECG, thoracic impedance and 2 channels of pulses (finger and ear) recorded by using the TaskForce Monitor (TFM) system; 3) images, including mitral valve movement, aortic valve movement, mitral flow and aortic flow sequentially, recorded with ECG, impedance and finger pulse. Each recording was repeated in the same session. The first and the repeated recordings were coded as 1a, 1b, 2a, 2b, 3a and 3b.

Recording sessions		Images				ECG		TaskForce Monitor		Pulse		Device used
		M-mode		Doppler								
		MV	AV	MF	AF	Limb	Chest	Z	-dZ/dt	Finger	Ear	
1	a (first)					✓	✓†					ECG
	b (repeated)					✓	✓†					
2	a (first)					✓		✓	✓	✓	✓	TFM & Pulse
	b (repeated)					✓		✓	✓	✓	✓	
3	a (first)	✓				✓	✓‡	✓	✓	✓		Echo & ECG & TFM & Pulse
			✓			✓	✓‡	✓	✓	✓		
				✓		✓	✓‡	✓	✓	✓		
					✓	✓	✓‡	✓	✓	✓		
	b (repeated)	✓				✓	✓‡	✓	✓	✓		
			✓			✓	✓‡	✓	✓	✓		
				✓		✓	✓‡	✓	✓	✓		
					✓	✓	✓‡	✓	✓	✓		

†: all the 6 chest leads (V1 ~ V6) were recorded; ‡: only V1 was recorded.

MV: mitral valve; AV: aortic valve; MF: mitral flow; AF: aortic flow.

In this chapter, the subject recruitment is first described. Suitable electrodes/probes placement and gain/filtering setting were determined for the echocardiography and physiological data measurement techniques, followed by the technique used to synchronize the devices. Finally, the method used to pre-process the data from the separate devices is described.

3.2 Subjects

3.2.1 Ethics approval

The study design required the recruitment of 30 normal subjects within a wide range of age. Ethical approval was sought for this study and granted in July 2012 by the National Research Ethics (NRES) Committee North East – Newcastle & North Tyneside 2.

3.2.2 Recruitment

Subjects were recruited from the Newcastle upon Tyne NHS Hospitals Trust and the Newcastle University. Advertisements were sent out through internal group mail lists and also placed on the electrical noticeboards throughout the Trust. A copy of the information sheet (Appendix 1), which described the aim of this study, recruitment criteria, measurement instruments and procedures, was sent to each responder expressing an interest in volunteering. The majority of the responders were staff or colleagues from the Regional Medical Physics Department of Freeman Hospital. Additionally, a number of students from the university participated in this study.

3.2.3 Study inclusion criteria

Only male healthy subjects were studied. Volunteers were informed that they would be studied only if they met all of the following criteria:

- Male adult with age above 18 years old;
- Without any diagnoses or symptom of cardiovascular disease, such as hypertension, diabetes or atrial fibrillation;
- Without any physical abnormality or any observable skin problem.

Five age bands were used to group the volunteers: 20 – 29 years, 30 – 39 years, 40 – 49 years, 50 – 59 years, over 60 years group. Each volunteer was put into one of the five

groups according to their age. Matched numbers of subjects were entered into each group to participate in the study.

3.3 Measurement environment

All measurements were undertaken in the measurement room at the Medical Physics Department, Freeman Hospital. A quiet and comfortable experimental environment was maintained in the room. To minimize external distraction, access to the room was limited during the whole measurement. The layout of the measurement room is illustrated in Figure 3-1. While the furniture was placed at the left side, most space in the room was left for the subject and measurement devices. The echocardiographic device, TaskForce Monitor system, ECG and PPG devices were arranged to form a half circle with a couch positioned at the other end. A disposable paper sheet was placed over the couch and changed after the measurements finished on each subject.

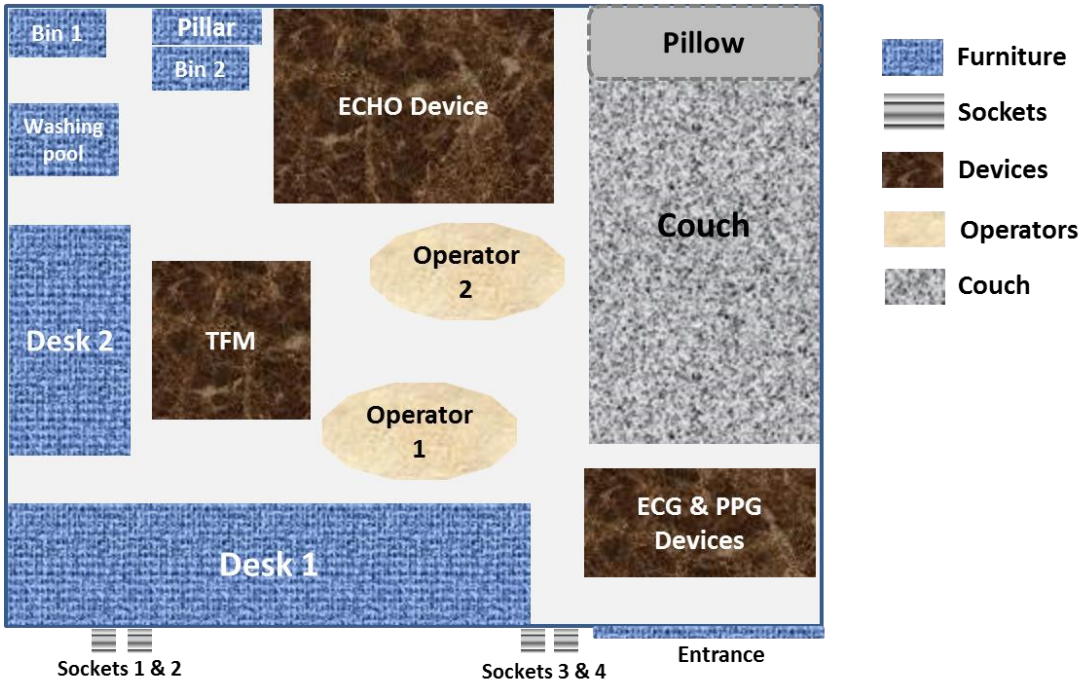

Figure 3-1: Illustration of the measurement room layout. Devices were arranged to make a comfortable experimental environment for the operators and the subjects. The mains sockets 1, 2, 3, 4 were used to provide electrical power for the echo device, TaskForce Monitor system (TFM), ECG and PPG devices respectively.

The measurement devices and their connections to the subject were placed so as to avoid one device and its mains cable interfering with another device. The couch where the subjects lay down was positioned at the right corner of the room. In order to reduce the interference from mains power supplies, those mains sockets which were far away from the couch and the subject were used. I recorded all data (operator 1), with assistance from a second operator who was an ultrasound specialist (operator 2) for help in obtaining echocardiograms. Both operators were located at the central area surrounded by the devices and the couch. The aim of this arrangement was to ensure that the two operators could operate the devices easily and the subjects could feel comfortable and relaxed.

3.4 Measurement techniques

3.4.1 Echocardiographic techniques

M-mode and Doppler imaging techniques were employed to assess cardiac dynamic mechanics. They were obtained with guidance from 2D echocardiography; the M-mode image recorded the movement of the tissues along the M-mode cursor in a 2D view, and the Doppler imaging recorded the velocity of the blood within a sample volume, which was placed on an M-mode cursor guided by a 2D view.

Two-dimensional echocardiography

The parasternal long axis (PLAX) view was used as it was the most common view to guide M-mode echocardiography for mitral valve and aortic valve movement. Right ventricle, left ventricle, left ventricular outflow track (LVOT), left atrium and the two valves were seen in this view. To obtain the images, the ultrasound transducer was positioned at the parasternal window, which is at the right side of the sternum between the 3rd and 5th intercostal spaces. The acquisition of 2D images in the PLAX view and an example is shown in Figure 3-2 (A).

The apical views were used to guide the Doppler echocardiography for mitral flow and aortic flow measurement. To obtain the 4-chamber view images, the transducer was positioned at the apex of the heart and oriented toward the right shoulder. As shown in Figure 3-2 (B), the left and right atria, ventricles, atria-ventricular valves can be seen in this

view. By tilting the ultrasound transducer upwards at the same position the aorta can also be included, which is known as the apical 5-chamber view.

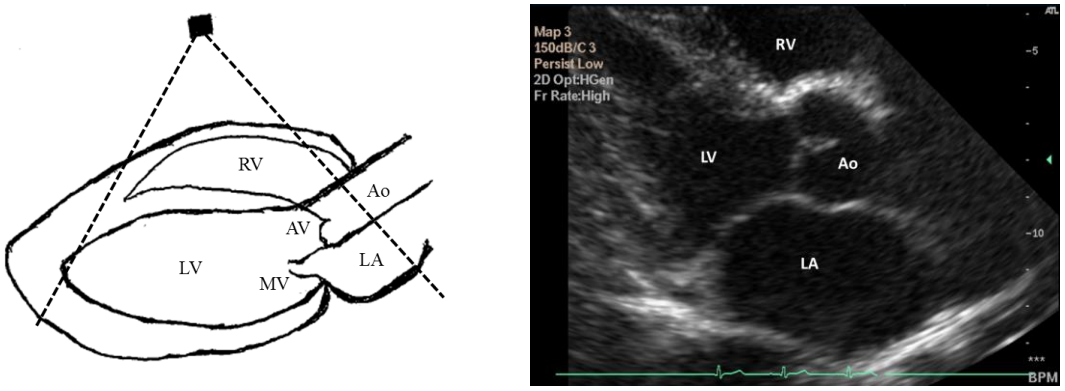

(A)

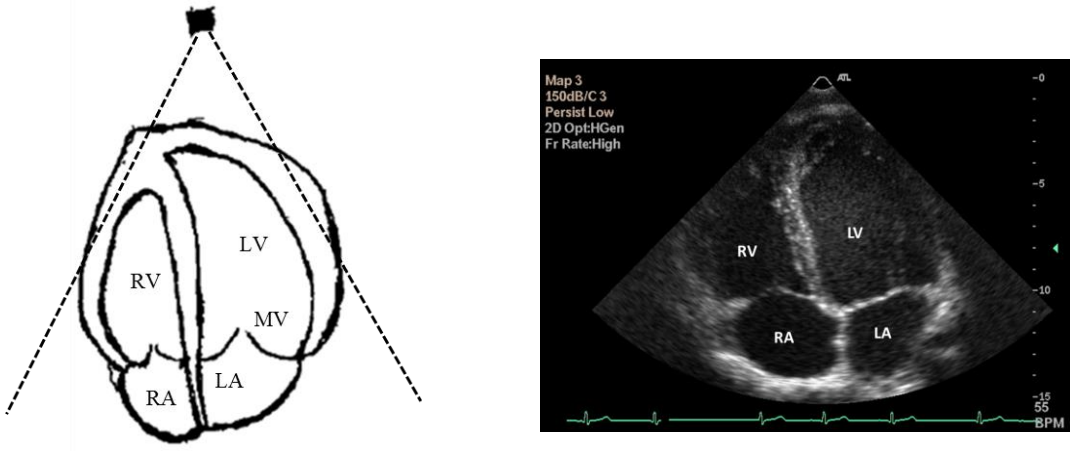

(B)

Figure 3-2: 2D echocardiography in: (A) parasternal long axis (PLAX) view; (B) apical 4-chamber view. The triggering ECG tracing was displayed at the bottom of the images. RV: right ventricle; LV: left ventricle; RA: right atrium; LA: left atrium; Ao: the aorta; MV: mitral valve; AV: aortic valve.

M-mode echocardiography

The mitral valve is a fast moving structure in the heart. The movement of its anterior leaflet and posterior leaflet was recorded by placing the M-mode cursor through the tips of the leaflets in the PLAX view, which is shown in Figure 3-3 (A). As can be seen, when open during early diastole and atrial contraction phases, the two leaflets separated and

moved in opposite directions, which caused two characteristic waves on each heartbeat. Once the valve closed during systole, the two leaflets touched and moved as one.

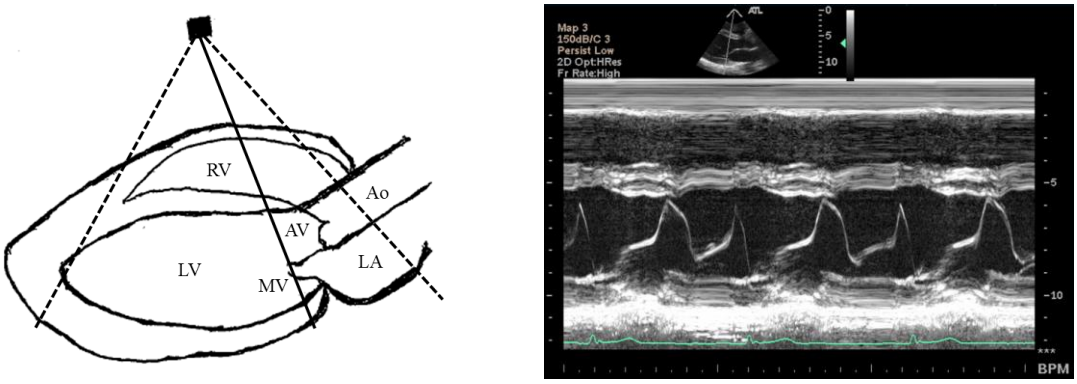

(A)

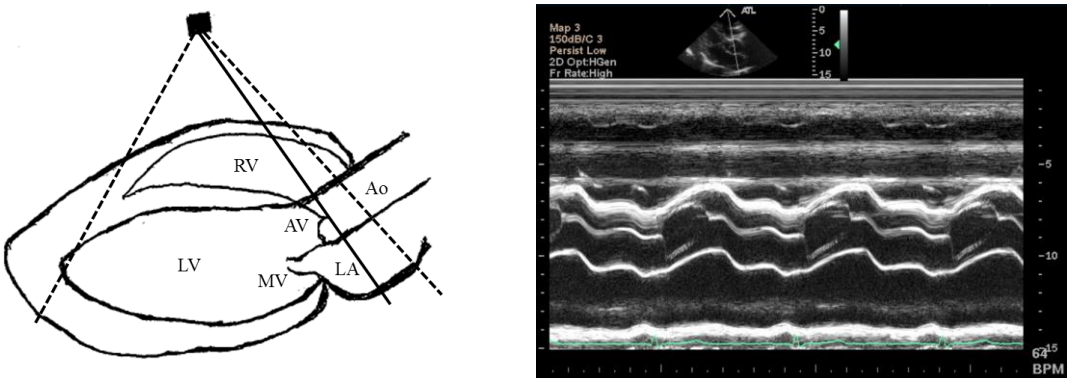

(B)

Figure 3-3: M-mode echocardiograms for: (A) mitral valve movement; (B) aortic valve movement. On the left, the M-mode cursor is illustrated in solid lines. The 2D guiding image and triggering ECG are displayed with each M-mode image. RV: right ventricle; LV: left ventricle; RA: right atrium; LA: left atrium; Ao: the aorta; MV: mitral valve; AV: aortic valve.

Aortic valve movement was recorded in the same view by adjusting the M-mode cursor through the aortic root at the valve level. The motion of the aortic valve is not as complex as the mitral valve. There are three leaflets, left-coronary, right-coronary and non-coronary leaflets, for a normal aortic valve. Only the right-coronary and non-coronary leaflets were visible in the PLAX view, which separated during systole and moved synchronously in

parallel. The acquisition of the aortic valve movement in the M-mode echocardiography is shown in Figure 3-3 (B).

Doppler echocardiography

Pulsed-wave Doppler echocardiography was performed to obtain the velocities of blood flow through the mitral valve and aortic valve. A small sample volume was positioned on an M-mode cursor to assess the mean blood flow velocity in the volume. Both the depth and the size of the sample volume were adjustable. To measure accurate velocity of movement with the Doppler technique, the sound wave was oriented as parallel as possible to the movement direction. For the Doppler modality in the HDI 5000 echocardiographic device, orientation of the ultrasound wave was mainly determined by the placement of the M-mode cursor. A minor angle correction was allowed for the sample volume. When the object within the sample volume moved towards the transducer, a positive velocity was recorded. In contrast, if the movement was away from the transducer, a negative velocity was recorded. A velocity filter was provided by the device to set a velocity threshold; the recording value was set to 0 when the detected velocity was below the threshold.

Mitral flow velocity was measured in the apical 4-chamber view. As shown in Figure 3-4 (A), a sample volume was positioned near the tip of the mitral valve leaflets inside the left ventricle. Because the blood moved towards the transducer when it came through from the atria to the ventricle, positive waves were recorded. The Doppler image for the mitral flow showed a similar shape to the M-mode image for mitral valve movement. There were also two components within a single beat with the major one corresponding to the ventricular passive filling and the other to left atrial contraction. The Doppler recording represented the blood flow velocity rather than cardiac dimension information represented by the M-mode.

The acquisition of the aortic flow velocity measurement is shown in Figure 3-4 (B). The apical 5-chamber view was used for this application. A sample volume was placed proximal to the aortic valve within the left ventricular outflow track (LVOT) on the M-mode cursor. Because the blood moved away from the transducer during systole, a negative wave was recorded for each beat.

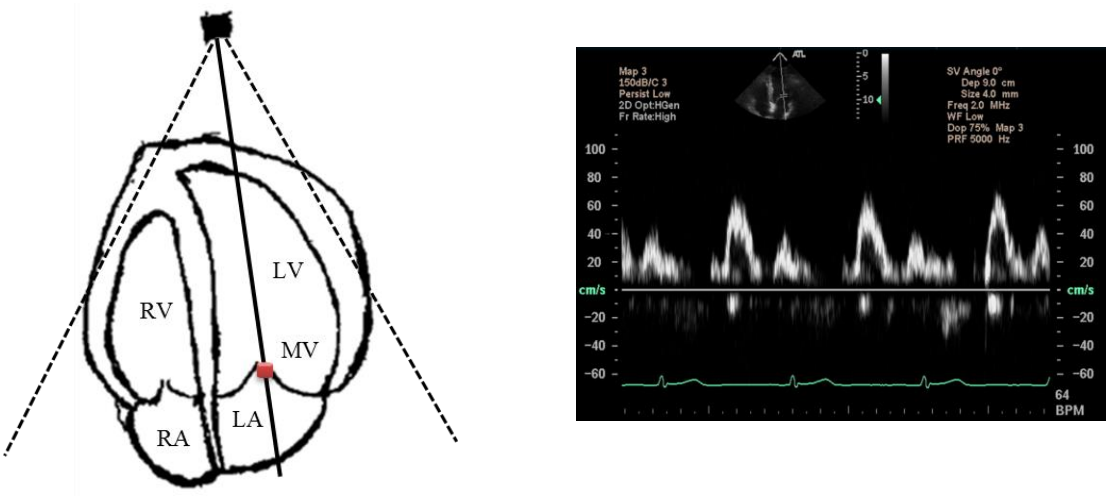

(A)

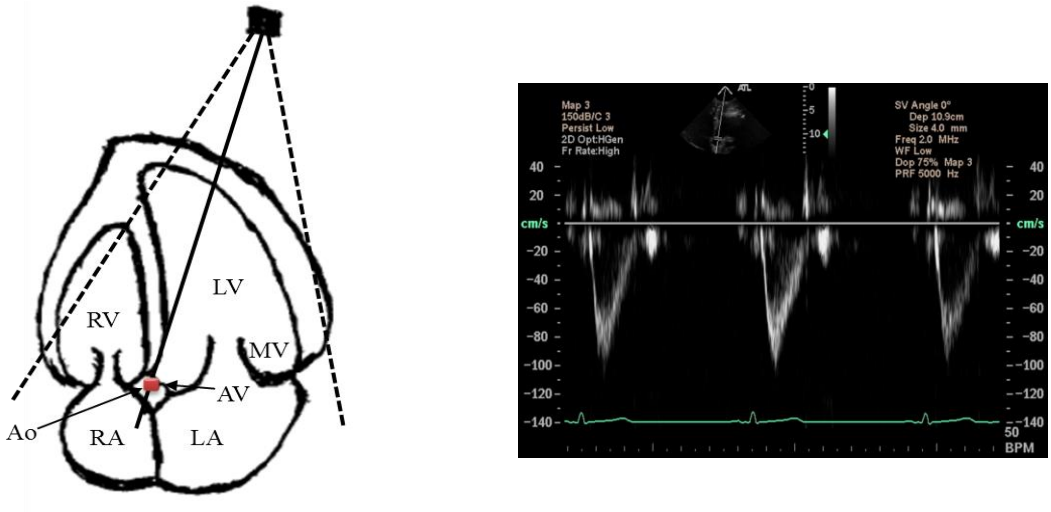

(B)

Figure 3-4: Pulsed-wave Doppler echocardiograms for: (A) mitral flow; (B) aortic flow. The Doppler sample volumes are illustrated by filled cylinders on the solid M-mode cursor lines on the left of the plots. The 2D guiding image and triggering ECG are displayed with each velocity trace. RV: right ventricle; LV: left ventricle; RA: right atrium; LA: left atrium; Ao: the aorta; MV: mitral valve; AV: aortic valve.

3.4.1.4 Parameter setting for echocardiography

Parameters were set via the user interface of the software and the user control panel on the devices. For the echocardiography image recording, the ECG triggering mode was

configured so that the device started to capture images automatically immediately after the 1st detected ECG QRS complex once the 'Capture' button on the control panel was pressed. The recording length was set to 15 s for each measurement. Therefore, the image acquisition stopped 15 s automatically after the starting point.

The frame rate was set to 25 frames per second for the guiding 2D echocardiography measurement. A total of 375 frames over the 15 s were obtained for each measurement. The sweep speed for the M-mode and Doppler imaging was set to 200 pixels per second, which gave a temporal resolution of 5 ms for each pixel. The gains, contrast and focus region were adjusted via the user control panel for each recording till a good quality image was available. Because of the anatomic difference of subjects, these settings varied case by case.

The axis length of the sample volume for the Doppler echocardiography was set to 4 mm and the velocity filter was set to 'Low'. Lower filter allowed a lower threshold for the velocity recording, which was helpful to retain the boundaries of flows.

3.4.2 ECG measurement techniques

Ten electrodes were used for the acquisition of standard 12-lead ECGs; 3 of them for limb leads (Lead I, II, III, aVR, aVL, aVF), 6 for the chest leads (V1 to V6) and one neutral electrode. The limb lead electrodes were positioned at the wrists or ankles as shown in Figure 3-5 (A). The standard positions of the chest lead electrodes are shown in Figure 3-5 (B). Lead V1 and V2 are between the 4th intercostal spaces at each side of the sternum respectively. V4 is at the intersection site of the 5th intercostal space and the midclavicular line, which is around the apex of the heart. V3 is at the midway between V2 and V4. The positions for V5 and V6 are located on the anterior axillary line and midaxillary line at the same level as V4 respectively. However, as the standard positions for V2 to V6 overlapped echocardiographic parasternal window and apical window, these 5 electrodes on the left chest were not used when images were wanted.

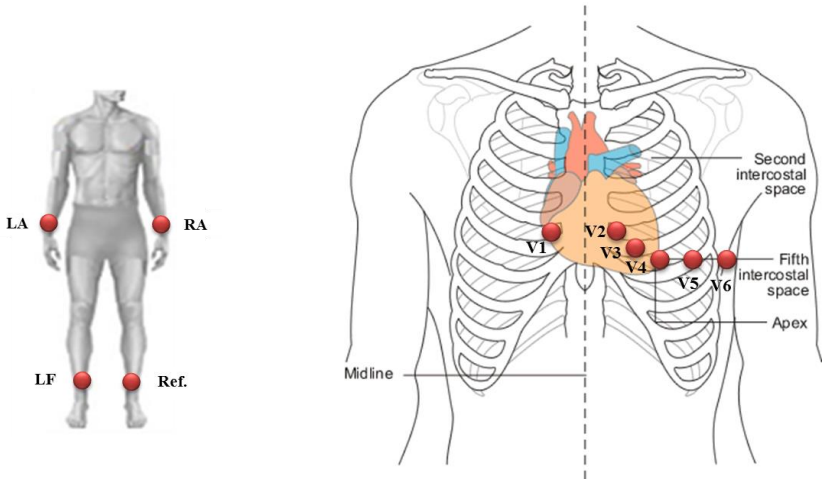

(A) (B)

Figure 3-5: Electrode placement for recording standard 12-lead ECG: (A) limb leads (I, II, III, aVR, aVL, aVF); (B) chest leads (V1 ~ V6). LA: left arm; RA: right arm; LF: left foot; Ref.: neutral device reference electrode.

To make sure of a good contact, skin below the electrodes was cleaned carefully using alcohol. Then the electrodes were attached to the body when the skin was dry. Although hair can affect the contact, it was not a problem as subjects remained still during the measurements.

The sampling rate of the ECG recording was pre-set to 1 kHz by the device. The bandwidth and the gains were adjustable from the control panel of the amplifiers. In this study, the bandwidth was set to 0.05 Hz to 100 Hz, while the gains were set to 500 for both of the limb leads and the chest leads.

3.4.3 Impedance measurement techniques

The placement of 4 traditional long band electrodes for thoracic impedance measurement has been reported in the literature (Kubicek et al 1966, Mohapatra 1981, Lamberts et al 1984, Sherwood et al 1990). The typical configuration was placing a pair of current-carrying and voltage-sensing electrodes on the neck and the other pair on the chest at the xiphoid process level, with the two voltage-sensing electrodes at the inner side. Lamberts et al. (1984) observed that the impedance measurement was affected by the distance between the voltage-sensing electrodes and suggested a standard average distance

of 22 cm. According to Mohapatra's study (Mohapatra 1981), the current electrodes had to be placed with at least a 3 cm separation from their corresponding voltage electrodes to help the excitation current density distribute more uniformly in the body between the voltage electrodes. Furthermore, Sherwood et al. (1990) emphasized that consistent placement of the electrodes was important for the repeatability of measurements.

Three short adhesive strips with a pair of current-carrying and voltage-sensing electrodes on each are provided with the TaskForce Monitor system for thoracic impedance measurement. The placement of the strips is shown in Figure 3-6. One strip was attached to the area between the neck and the hairline on the back, and the other two were positioned parallel to the neck electrode on the thorax at the xiphoid level. These two strips were connected together to form a common pair of current and voltage electrodes. A neutral electrode was placed on the right lower leg. Constant alternating current was supplied via the outer current electrodes, and conducted through the body. The voltage was measured by the inner electrodes and consequently, the thoracic impedance was calculated. The limitations of this impedance measurement have been described in Chapter 2. On a normal adult body, the distance between the upper and lower voltage electrodes was more than 22 cm, and the separation distance between the current and voltage electrodes was ensured by the adhesive strips. In addition, because the chosen positions were easily identifiable anatomical landmarks, it was possible to make consistent placement on all subjects.

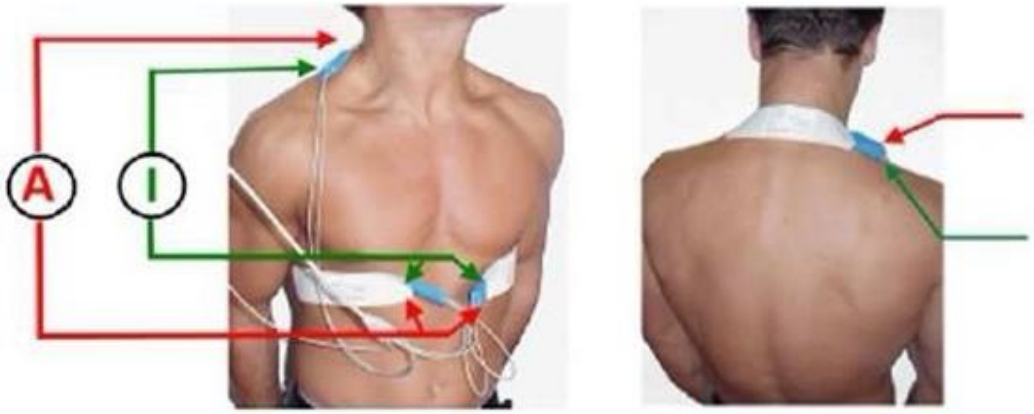

Figure 3-6: Illustration of impedance electrodes placement. Three pairs of short band electrodes were used: one on the back neck, and the other two on both lateral sides of torso. The two pairs on the torso were connected together to form a common pair. Constant current was supplied through the outer electrodes, and voltage was measured between the inner electrodes.

As described in the section 2.4.2, both the impedance (Z) and its first derivative waveform (-dZ/dt) were measured. The sampling rates for these two signals were pre-set to 50 Hz and 1 kHz by the TaskForce Monitor system.

3.4.4 Pulse measurement techniques

The left index finger and earlobe were chosen in this study as the sites for peripheral pulse measurement. This was because the arterioles at these sites are close to skin surface enabling pulse waveforms to be easily detected.

Pulse waveform measurement was sensitive to movement artifacts. To reduce the movement artifacts, the surface of PPG probe was placed flat on the centre of the fingertip or earlobe pulp, and then a finger cuff or earlobe clip was used to fix the probe on the skin. The pulse waveform was also affected by contact pressure. When the contact pressure was too high, arterioles under the skin were compressed and blood volume pulses were reduced. Ideally, an optimum pressure is required and kept consistent on all subjects. However, this was difficult to meet in practice. A good solution was to adjust the pressure manually by the operator before formal recording till a stable waveform with high amplitude pulse was displayed on the screen. The pulse device was always connected to the TaskForce Monitor system via the external input ports to enable pulse data to be recorded. The gains for pulse recording were set to 500 from the amplifiers of the pulse device. Additionally, the low cut-off frequency was set to 0.05 Hz and the high cut-off frequency was set to 30 Hz from the user control panel. The sampling rate was set to 1 kHz by the TaskForce Monitor system.

3.4.5 Summary of parameter setting on each device

The setting of sampling rates, gains and frequency bandwidth on each device for data acquisition is summarized in Table 3-2. Except the gains for the image acquiring varied case-by-case, the other parameters were kept consistent across all the subjects. For the M-mode and Doppler echocardiography, the temporal resolution of a pixel (5 ms) was converted to the corresponding sampling rates of 200 Hz. The settings of the TaskForce Monitor system were fixed by the system and not adjustable.

Table 3-2. Summary parameter setting on each device for data acquisition.

Devices	Signals	Sampling Rates (Hz)	Gains	Filter (Hz)
Echo	MV & AV (M-mode)	200	___	___
	MF & AF (Doppler)	200	___	___
ECG	Limb & chest ECGs	1,000	500	Low cut: 0.05 High cut: 100
TFM	Limb lead ECGs	1,000	___	Low cut: 0.08 High cut: 150
	Z	50	___	___
	-dZ/dt	1,000	___	___
PPG	Pulses (Ear & Finger)	1,000	500	Low cut: 0.05 High cut: 30

MV: mitral valve; AV: aortic valve; MF: mitral flow; AF: aortic flow.

3.5 Measurement system connection and operation

3.5.1 Device connections

As described above, an echocardiographic device and three physiological measurement devices were employed for data collection in this study. These four devices were connected together to record 4 sets of data (Table 3-1).

First of all, the ECG device was used alone to record standard 12-lead ECG signals. The use of the device to record this data is shown in Figure 3-7 (A). Next, both channels of the PPG device were then connected to the TaskForce Monitor system via its external input ports so that pulse data were recorded synchronously with limb lead ECGs and impedance from the TaskForce Monitor system. The connection of the PPG device and the TaskForce Monitor system for the acquisition of this data is illustrated in Figure 3-7 (B), which

allowed the simultaneous recording of 6 limb lead ECGs, impedance (Z), the first derivative (-dZ/dt), ear and finger pulses.

The connection of the 4 devices to record images and simultaneous physiological signals is shown in Figure 3-7 (C). The cardiac electrical activity was recorded by the ECG device. Because of the overlap between the ECG electrode positions and the echocardiography windows, the V2 ~ V6 leads were not recorded, but the 6 limb leads and the V1 lead were retained. ECG lead I was connected to the echocardiographic device to trigger the image acquisition, and connected to the TaskForce Monitor system for synchronisation rather than triggering. Therefore, the three devices recorded a common ECG signal to provide a time synchronisation reference. Only the finger pulse channel of the PPG device was used during imaging, and connected to the TaskForce Monitor system. This connection was used for the sequence 3 and 4 in the Table 3-1, which allowed a single recording to include: an echocardiogram (with the triggering ECG) using the software of the echocardiographic device; 6 limb lead and V1 ECGs using the software of the ECG device; synchronous ECG, impedance (Z), impedance (-dZ/dt) and finger pulse using the software of the TaskForce Monitor system.

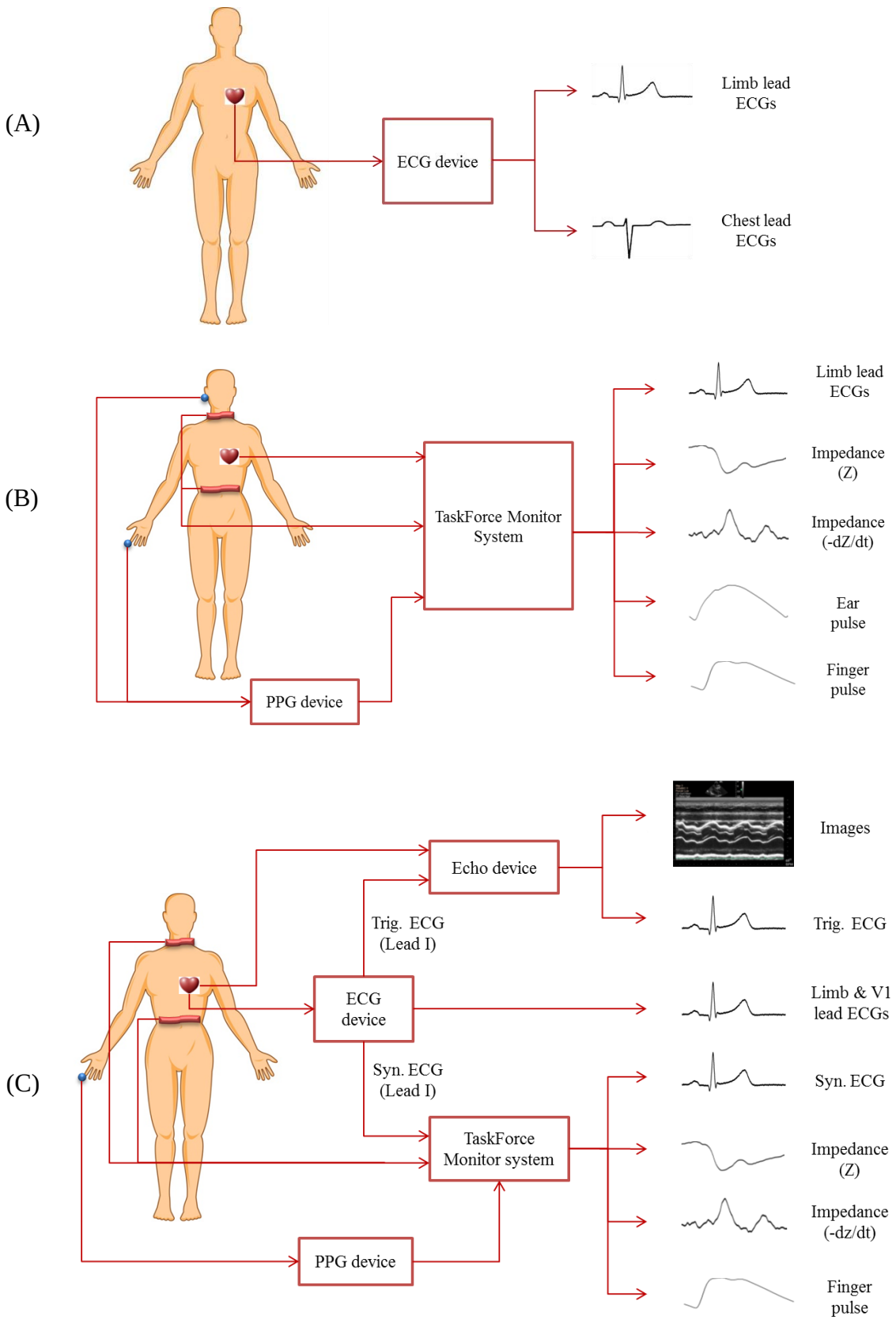

Figure 3-7: Device connections for recording of: standard 12-lead ECG (A); limb lead ECG, impedance and pulses (B); echocardiograms with ECG, impedance and pulse (C).

3.5.2 Recording length

The images and physiological signals were not stable from beat to beat because of natural variability. To enable the effect of changes to be studied, data were recorded over several respiratory cycles. In this study, measurements were taken over 60 s for recordings if only physiological signals were needed and 15 s for those with echocardiography. The image data length was chosen as it was difficult to keep a consistent probe position for longer. The length of this duration covered at least 3 respiratory cycles with subjects breathing normally. The file size of a single recording with images and physiological signals was around 500 Megabytes, and that of a recording without image was less than 10 Megabytes.

3.5.3 Operation

Using the ECG device alone or the connected TaskForce Monitor system and PPG device for data acquisition was easy as there was only one software control involved at once. It was more complex to measure images with physiological signals by using the 4 connected devices. As in the previous description, a common limb lead ECG (Lead I) was recorded by the echocardiographic device, the ECG device and the TaskForce Monitor system for this connection. However, because it was not practical to make all the devices start recording at the exactly same time, a further time marker was required to indicate the common period, during which all the devices worked simultaneously. A time marker was provided by controlling the mode switch on the ECG device. More specifically, the limb lead ECG output was kept to zero by setting the mode switch to ‘Zero’ till the imaging was ready so that a zero flat line was seen at the beginning of the common ECG. After normal ECG output was enabled, the image recording was automatically triggered by the ECG QRS complex and stopped once the pre-set length time was up. Therefore, the duration from the 1st triggering ECG QRS complex to the ending of imaging measurement was the common recording period. In summary, the following procedure was taken to operate on the combined measurement system for images and physiological signals recording:

- Step 1. Start the TaskForce Monitor system to record;
- Step 2. Start the ECG system to record, with limb leads set to ‘Zero’;

- Step 3. Press the ‘Capture’ button on the control panel of the echocardiographic device when image recording is ready;
- Step 4. Switch the limb leads to ‘Use’ mode so that the image recording can be triggered by the ECG;
- Step 5. The image recording automatically starts once an ECG complex is detected and stops automatically 15 s later;
- Step 6. Switch the limb leads back to ‘Zero’ mode again immediately after an alert sound is heard from the echocardiographic device when image recording finished;
- Step 7. Repeat Step 1 to 6 if more than one image measurements were wanted;
- Step 8. Stop the ECG device;
- Step 9. Stop the TaskForce Monitor system.

The diagram of the timing sequence for a set of recordings using the above procedure is shown Figure 3-8. The TaskForce Monitor system was kept recording during the whole period from t_1 to t_8. The ECG device was recording from t_2 to t_7. The M-mode echocardiography for the mitral valve and aortic valve, Doppler echocardiography for the mitral flow and aortic flow were taken in sequence during the period. While normal chest lead ECG (only V1) output was always allowed, limb leads were set to 0 to generate a flat line at the beginning of each image recording. The first image recording was triggered by the ECG QRS complex at t_4 after normal limb lead ECGs were turned on at t_3. This recording stopped automatically 15 s later at t_5, immediately after which the limb lead ECGs were set back to 0 at t_6 to prepare for the next image recording. After the last image was taken, the ECG device was stopped at t_7, and the TaskForce Monitor system was stopped at t_8.

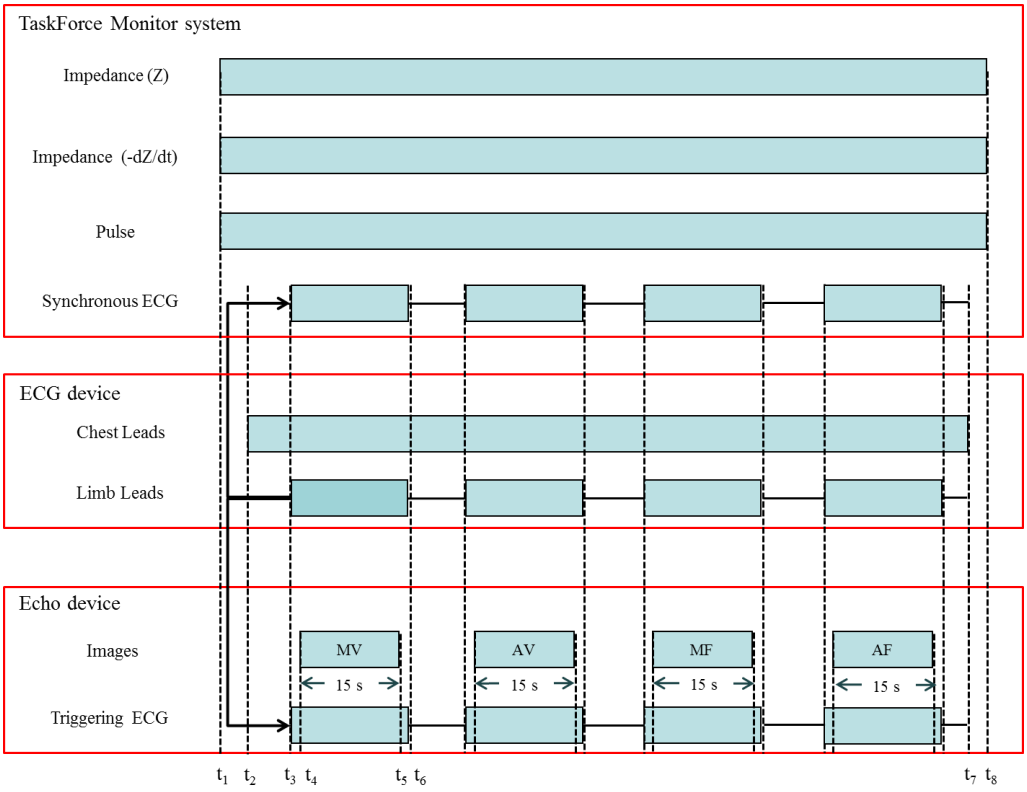

Figure 3-8: Diagram of timing sequence to use the combined system for the recording of images with simultaneous physiological signals. The TaskForce Monitor system started to record first (t_1) and stopped last (t_8). During the period from t_2 to t_7, while the chest ECGs (only V1) was always kept on, the limb lead outputs were switched between 0 and normal to generate time markers at the beginning of imaging for the mitral valve (MV), aortic valve (AV), mitral flow (MF) and aortic flow (AF).

3.6 Data acquire procedure

3.6.1 Subject preparation

Informed consent was obtained from each subject before the measurement could commence. The overall study and data collection procedure was introduced to the subjects briefly after arrival. They were then asked to confirm if they met the study inclusion criteria. An opportunity was given for the subjects to ask any question about the study. They were also told that they were free to withdraw from the measurement at any time without any reason.

3.6.2 Prior clinical information recording

Height and weight were obtained for calculating body mass index (BMI). The subject was then asked to lie down on the prepared couch with shirt and shoes off. To facilitate the image recording, the couch was adjusted to make the subject recline around 45 degrees. Five minutes was given to the subject for relaxation, and they were asked to breathe calmly. Electrodes and probes were attached to the subject during this period. Afterwards, blood pressures were measured using an A&D UA-767PCHV automatic blood pressure monitor (A&D Co., Japan).

3.6.3 Echocardiography and physiological measurement recording

After the prior clinical information was obtained, the 4 sets of data listed in the Table 3-1 were recorded in sequence. The 1st sequence was a 60 s recording of standard 12-lead ECGs, which was taken from the ECG device.

The 2nd sequence, consisting of a 60 s simultaneous recording of 6 limb ECGs, impedance (Z and –dZ/dt), ear and finger pulses, was taken from the combined PPG device and TaskForce Monitor system. This data set was used to investigate the relationship between the thoracic impedance and the peripheral pulses.

The 3rd sequence comprised a set of echocardiograms simultaneously recorded with ECGs (limb & V1 leads), impedance (Z and –dZ/dt) and the finger pulse from the combined 4 devices. Two recordings with M-mode images for the mitral valve movement and aortic valve movement were taken first, and then another two with Doppler images for the mitral flow and aortic flow were taken. Each recording lasted 15 s. These 4 recordings were used to investigate the relationships between the cardiac dynamic imaging and physiological measurements.

Finally, to assess the repeatability of the image data, a 4th sequence of data was acquired, which repeated the measurements in the 3rd sequence.

In summary, a total of 10 recordings were taken in sequence from each subject. The sequence 3 and 4, which included simultaneously recorded images and physiological measurements, were the key parts of the data set studied in this project.

3.6.4 Data transfer and storage

Data recorded by the measurement system were downloaded to a common computer for storage and further analysis. A DICOM server was set up on the computer by using the open source program Conquest DICOM so that the DICOM echocardiography images could be transferred via the internet. A K-Pacs viewer was provided by the program to give a quick view of images. Signals recorded by the TaskForce Monitor were saved in files with their own format. A file format conversion tool was provided in its integrated software, which was used to convert these files into MATLAB readable '.mat' format. ECG signals recorded by the ECG device were stored in binary files, which were converted to ASCII format by using a format conversion tool. The converted files on these two devices were then transferred to the common computer.

All data were stored on NHS and Newcastle University password protected computers and backed up over the NHS network. The data on each subject were anonymised and identified by a unique sequential code. Those non-identifiable data were stored into password protected computer systems for further analysis.

3.7 Signal pre-processing

3.7.1 Imaging reconstruction

Echocardiographic images were stored frame by frame in DICOM (Digital Imaging and Communications in Medicine) format, which is a standard format proposed by the National Electrical Manufacturers Association for storing and handling medical images. MATLAB R2010b (MathWorks, USA) provided a toolbox for DICOM image loading. An example of Doppler echocardiography for aortic flow read by MATLAB is shown in Figure 3-9. Each new frame was updated from the position of the black raster, which moved from the left to the right on the screen with a fixed sweep speed. The newest frame entered at the left side of the raster. When reaching the farthest right side on the screen, the raster was swept to the left side. The oldest frames were then flushed by the new ones.

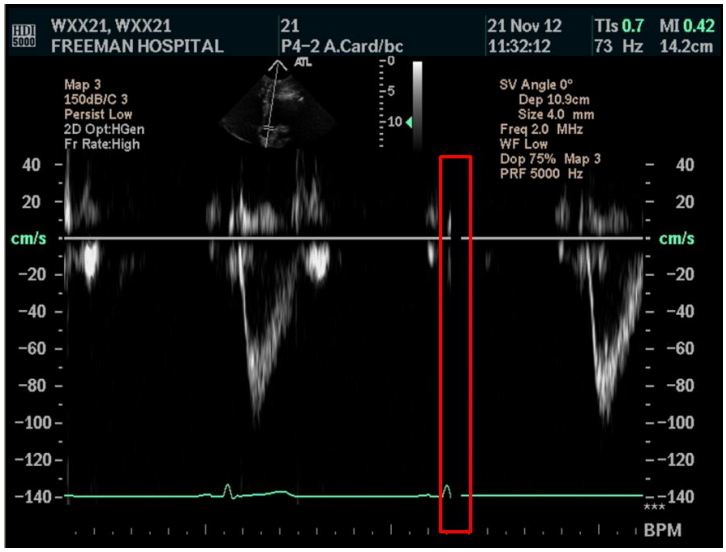

Figure 3-9. An example of a Doppler DICOM image loaded by MATLAB. Approximately 80 frames are shown on this screen. The entry of new frames was located at the left side of a raster moving from left to the right (indicated by the red box). When the farthest right side was reached, the raster was swept to the left side.

There were some disadvantages for the M-mode and Doppler echocardiograms stored in this frame-based mode. Firstly, there were many frames displayed on each screen. In the original, in addition to the current frame, all other frames which displayed on the screen were also stored. It resulted in huge redundant information being kept, and made the file size large at around 500 Megabytes for a 15 s recording. Secondly, the wrapping of the raster made it impossible to see the images over the whole recording period at once. In order to reduce the file size and display all frames on one screen, frame-based M-mode and Doppler echocardiograms were reconstructed into a pixel series. After the reconstruction, an image was represented by a series of pixel columns arranged in parallel. During the image capture, the frame rate was set to 25 frames per second. Therefore, there were 375 frames included for a 15 s recording. Eight pixel columns of image were updated in each frame by the raster. The width of the raster was 11 pixels. With this prior information, the pixel series of each frame were reconstructed by the 8 pixel columns preceding the left edge of the raster. The wrapping of the raster was about to occur when the distance between its left edge and the right end of the screen was less than 11 pixels. If the distance was less than 8 pixels, the beginning of the current frame would be left at the right side of the screen, while the rest entered at the left side. These two parts were obtained and put together to construct the pixel series of a current frame.

An example of image reconstruction is shown in Figure 3-10. As the redundant frames were removed after the reconstruction, the final file size was only around 2 Megabytes, which was 250 times less than the original size. Additionally, the frame based image was converted into the pixel series, which allow visualizing all the frames on a single screen and was easier to display with the physiological signals.

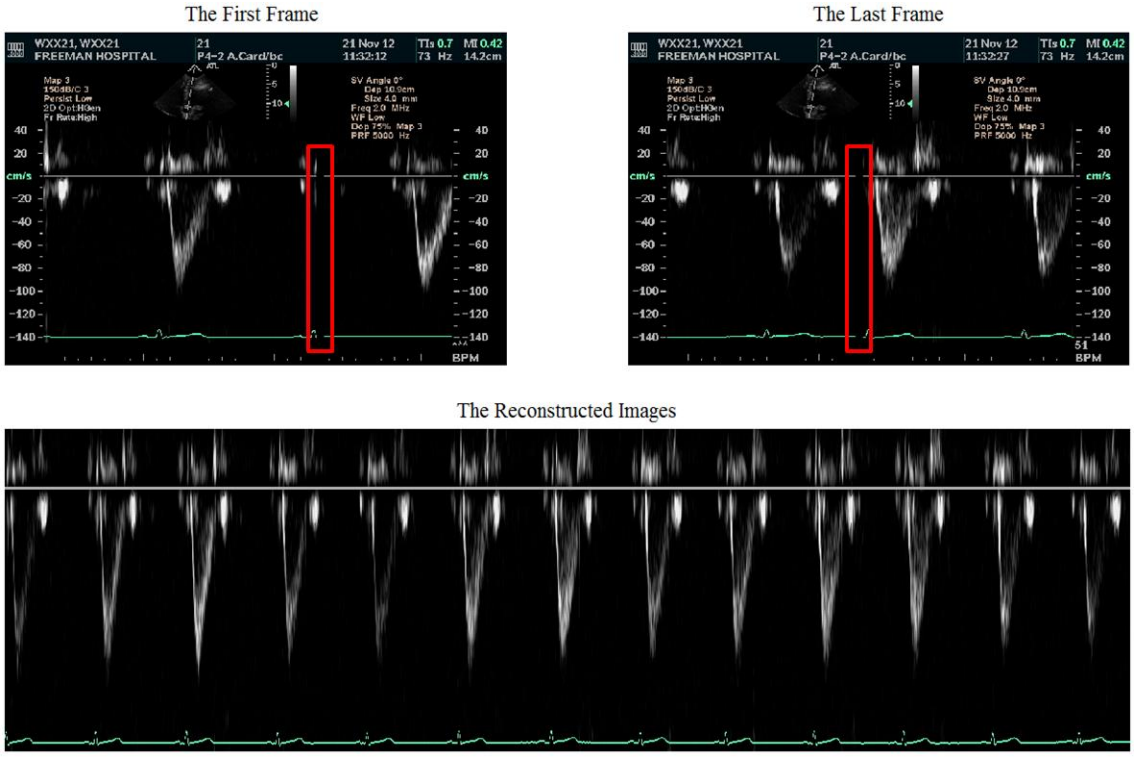

Figure 3-10. An example of reconstructing a pixel series of a Doppler image. The first frame and the last frame are shown in different screens in the original image. However, all frames were displayed on a single screen in the reconstructed image. During reconstruction, the annotation part in the original images was removed.

3.7.2 Resampling processing

In this study, physiological signals were recorded by the ECG device and the TaskForce Monitor system with their own analogue-to-digital data acquisition cards and software. Loss of synchronization existed between the signals from these two devices, although the sampling rates were set to the same 1 kHz on the both. An experiment was commenced to assess and quantify any loss of synchronization. The scheme of the experiment is shown in Figure 3-11. A TG 1304 Programmable Function Generator (Thurlby-Thandar Ltd, UK)

was employed to produce a testing 50 Hz sinusoid signal, which was fed into the ECG device. The TaskForce Monitor system was connected to the ECG system via the external input port so that it also received the same test signal. The mode switcher on the ECG system was used to generate zero lines at the beginning and end of the sinusoid signal. The number of samples of the sinusoid waveforms between the zero flat lines recorded by the two devices were counted and compared.

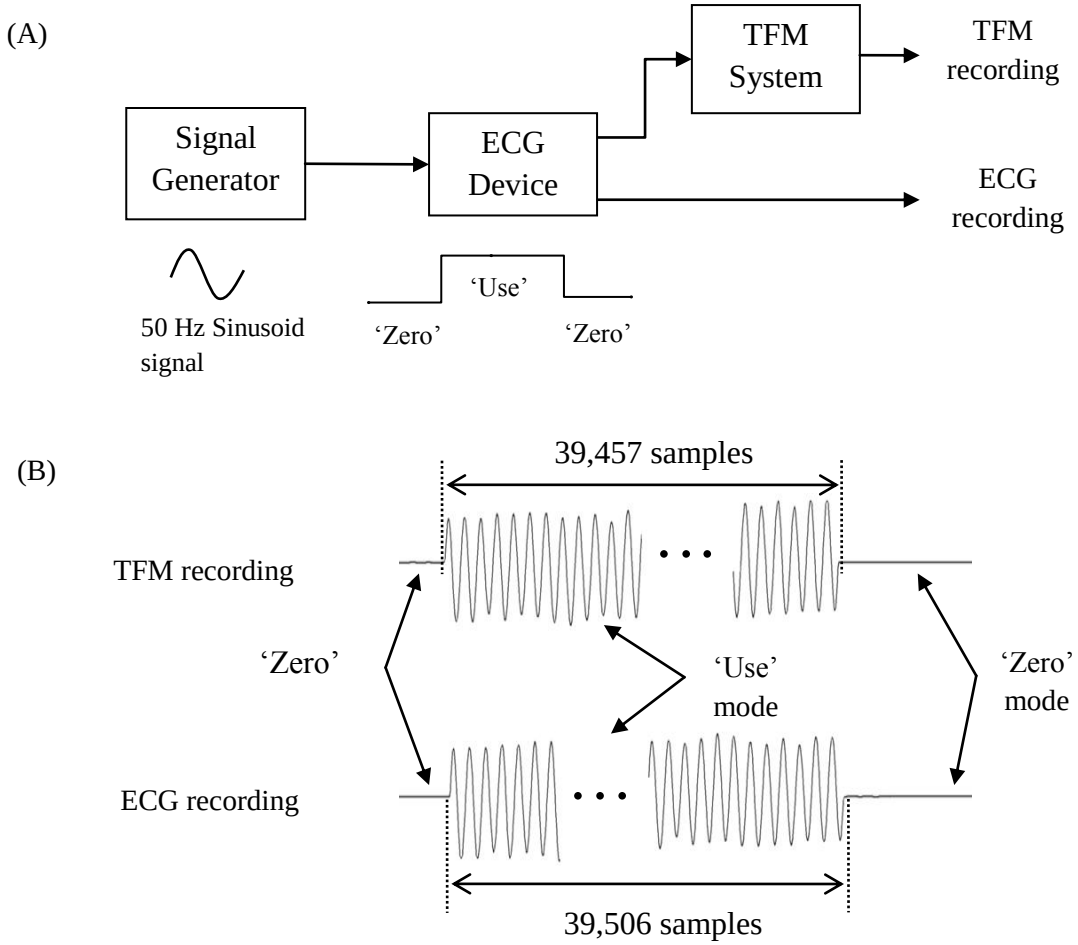

Figure 3-11. Assessing the loss of synchronization between signals captured by the TaskForce Monitor (TFM) system and the ECG device: (A) system connection; (B) an example of recorded signals taken from the measurement 5 of the Table 3-3. The ECG device recorded 49 samples more than the TFM system (39,506 vs. 39,475 samples) over the approximately 40 s recording of a 50 Hz sinusoid waveform.

Seven repeat measurements were implemented with the length of the sinusoid signals varying from 13 s to 80 s. The number of samples from the two devices and their ratio are given in Table 3-3. The ECG device recorded more samples than the TaskForce Monitor

system in the all 7 measurements. In measurement 1, the sample number difference was 16 over around 13 s. The difference was 99 samples for the long measurement 7, when the recording was around 80 s long. The ratios between the samples number were more consistent, with mean and SD of 1.00123 ± 0.00002. Therefore, the recordings from the TaskForce Monitor system were resampled by 1.00123 times using a linear interpolation method before synchronizing them with the ECGs. In addition, as explained already, the impedance waveform (Z) was captured with a sampling rate of 50 Hz. Therefore, a dual-step resampling processing was implemented for the Z waveform; it was firstly resampled by 20 times to make it similar to the other TaskForce Monitor signals and then resampled by 1.00123 times.

Table 3-3. Comparison of sample numbers of testing 50 Hz sinusoid signals recorded by the ECG device and TaskForce Monitor system.

	Measurements (number of samples)						
Devices	**1**	**2**	**3**	**4**	**5**	**6**	**7**
ECG	13288	14444	20364	29725	39506	59794	79754
TFM	13272	14426	20339	29689	39457	59720	79655
Ratio	1.00121	1.00125	1.00123	1.00121	1.00124	1.00124	1.00124

3.7.3 Synchronization

Synchronization of signals from separate devices was implemented referring to the commonly recorded ECG and the time markers on it. The scheme of the synchronization procedure is shown in Figure 3-12. A pixel series of image was reconstructed using the method introduced in the section 3.7.1. Ideally, the image recording would be triggered by the 1st ECG QRS complex following the flat line at the beginning. In reality, the recording was triggered by either the 1st or 2nd QRS complex (see Figure 3-13 for examples). Therefore, the closest QRS complex preceding the raster in the 1st frame, which was not necessarily the 1st one following the beginning zero line, was considered as the common starting for all recordings. The signals from the TaskForce Monitor system were resampled first to make them have the same sample numbers as ECGs. A fixed window of 15 s was then applied to the recordings from the TaskForce Monitor and the ECG devices to obtain the part which was simultaneously recorded with the images. The synchronized signals were then saved into a single file for further analysis.

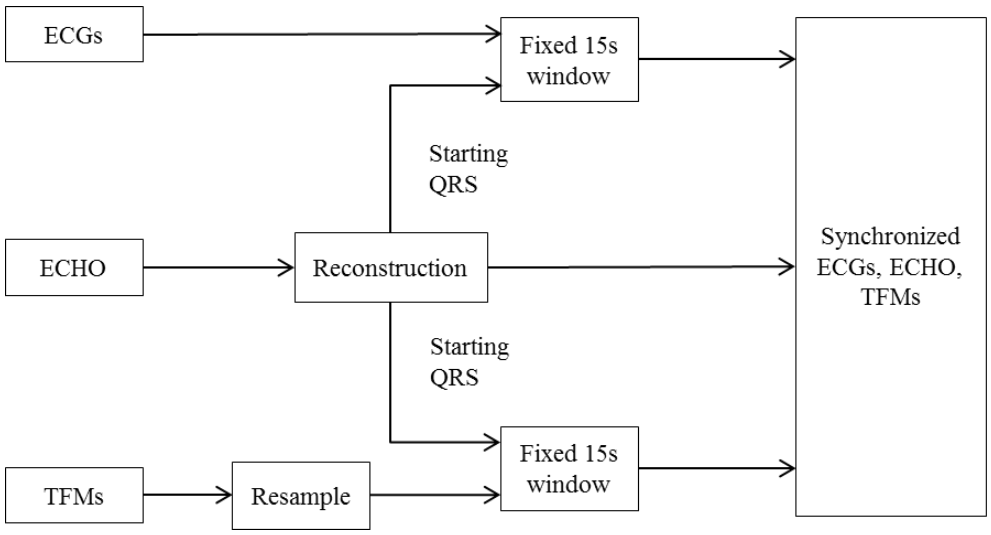

Figure 3-12. Scheme of synchronization procedure for the signals recorded from the ECG device, echo device and TaskForce Monitor system. The common starting point was the 1st R wave from the ECG triggering image capture.

(A)

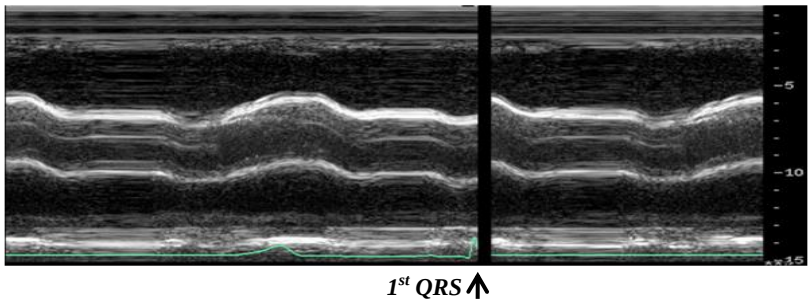

(B)

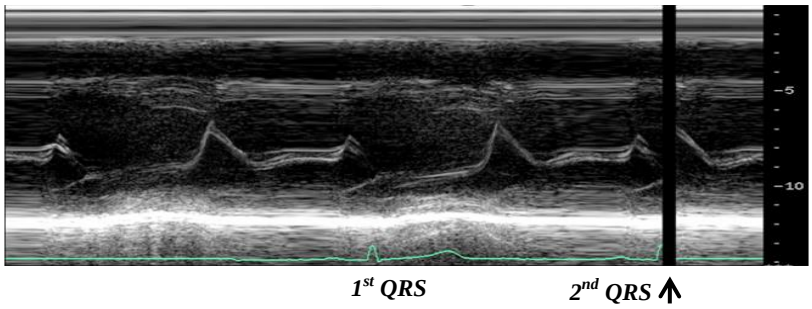

Figure 3-13. Examples of the image recording triggered by: (A) the 1st QRS complex following the beginning flat line; (B) the 2nd QRS complex after the flat line. The 1st triggering QRS complexes are denoted by black arrows.

An example of a synchronized Doppler echocardiogram for aortic flow and physiological measurements is shown in Figure 3-14, and the time aligned image and the TaskForce Monitor signals are displayed in Figure 3-15.

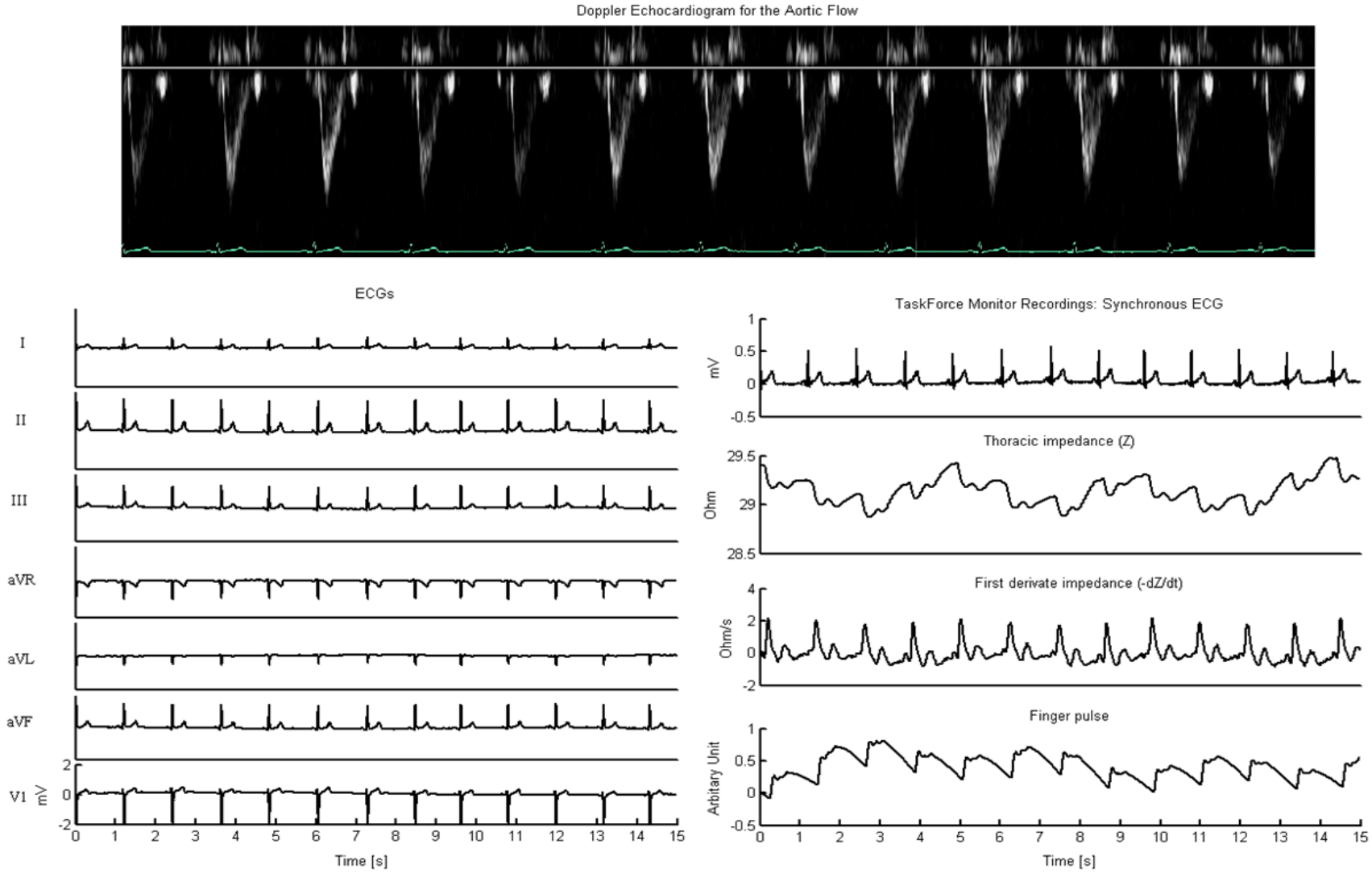

Figure 3-14. Example of synchronized Doppler image for aortic flow, ECGs and signals from the TaskForce Monitor system.

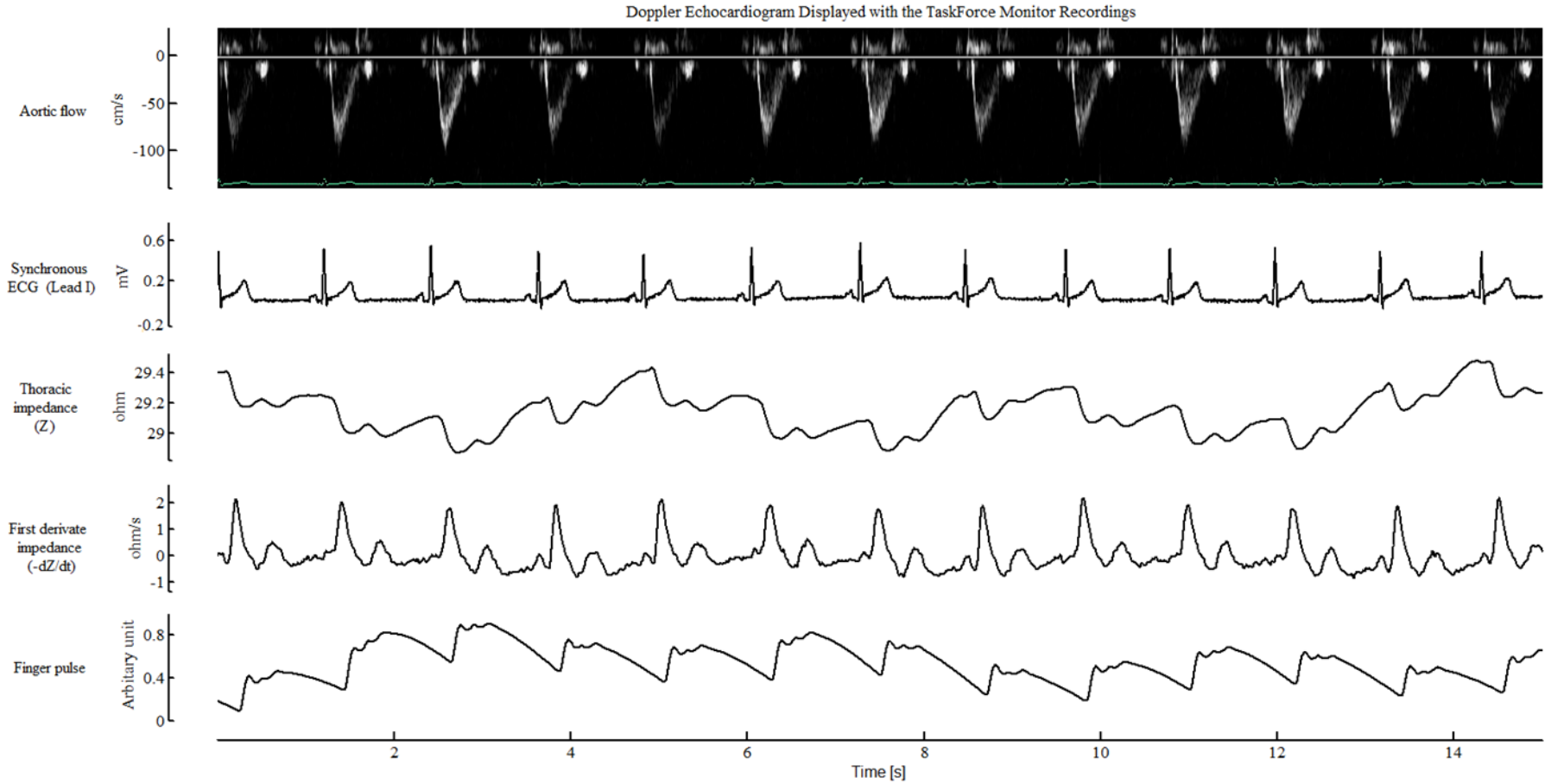

Figure 3-15. Example of synchronized Doppler echocardiogram for aortic flow displayed with synchronized physiological signals from the TaskForce Monitor system.

Chapter 4 Timing measurement and analysis

This chapter describes the methods developed for beat-to-beat identification of echocardiographic and physiological time features, and the analysis of these features.

4.1 Introduction

Techniques were developed to enable the previously synchronized echocardiograms and physiological signals to be analysed. Features were identified beat-by-beat from both images and physiological waveforms. While all the features on the images were detected manually, automatic algorithms were developed to identify features on the physiological signals. The features studied in this research, with their identification methods, are summarized in Table 4-1.

Software with a graphic user interface was developed in MATLAB (MathWorks Co., USA) to assist the feature identification. The software provided the following three main functions: 1) loading and displaying the signal; 2) enabling manual checking of the results given by automatic algorithms and identification of the other features; 3) saving the final results into excel sheets for further analysis.

The data and statistical analysis methods are also described in this chapter. As there were 10 recordings, which were taken over 1 hour in total, obtained on each subject, the stability of heart rate during this period were examined using the ANOVA test. In addition, times of the features measured from the ECG R wave were studied; the repeatability of feature identification on the simultaneous images and physiological signals was assessed with the Bland-Altman test and paired t-test; the timing sequence of cardiovascular events in single cycles was reconstructed with these measured times. Finally, the relationships between the echocardiography and physiological measurements were investigated based on the time features and the timing durations between two features.

Table 4-1. Summary of imaging and physiological features studied in this research.

Signals	***Features***	***Descriptions***	***Determination methods***
MV	open	during both early rapid filling and atrial contraction phases.	Manual
	max. opening		
	close		
AV	open	during the left ventricular ejection phase.	
	close		
MF	start	during both early rapid filling and atrial contraction phases.	
	peak		
	end		
AF	start	during the left ventricular ejection phase.	
	peak		
	end		
ECG	P_S, P_P, P_E	P wave start, peak and end.	Peaks: Auto*; others: Manual
	Q, R, S	QRS complex start, peak and end.	
	T_P, T_E	T wave peak and end.	
Impedance (Z)	Start	features of the systolic wave.	Auto
	Min.		
	End		
	2^{nd} min.	feature of the diastolic wave.	
Impedance (-dZ/dt)	Foot	features of the systolic wave.	
	1^{st} peak		
	End		
	2^{nd} peak	feature of the diastolic wave.	
Pulse (Ear & Finger)	Foot	features of the early systolic wave.	Auto
	Early systolic peak		
	Notch	notch before the diastolic wave.	
	Diastolic peak	peak of the diastolic wave.	

*: All the automatic identification results were manually checked.

In the following sections of this chapter, the MATLAB program for feature identification is first introduced, which is followed by feature determination on each signal. Then the data and statistical analysis methods are described.

4.2 Software for feature identification

Interactive software was developed in MATLAB Graphic User Interface (GUI) toolbox to assist in time feature identification on images and physiological signals beat-by-beat. Three independent components were designed for the analysis of the echocardiogram, ECGs and recordings from the TaskForce Monitor system separately. The following 5 stages were applied in sequence when using the software for the feature identification on each signal:

- Stage 1. Loading the signal to be analysed into the software;
- Stage 2. For physiological signals, pre-processing filtering procedures to remove the baseline wander caused by respiratory and motion and high frequency interference from main power supply were first implemented. Automatic feature identification algorithms were then applied;
- Stage 3. Displaying the signal beat-by-beat, with the automatically detected features marked on it;
- Stage 4. Manually checking the results from the automatic detection algorithms and identifying the other features;
- Stage 5. Saving the final results into an excel sheet for further analysis.

The interface of the component for echocardiographic feature identification is shown in Figure 4-1, which consisted of 6 main elements. The 1st component was a customized toolbar allowing the loading of the signal into the program and exporting identification results out to excel sheets. The 2nd element included a slide bar which was used for beat selection. The selected beat was displayed on the window provided by the 3rd element. The 4th element contained a set of editing boxes with each corresponding to a feature. A cursor was activated by right clicking a box to help to detect the position of the selected feature on the displayed signal. The box was then updated by the absolute position of the feature in pixels (each was 5 ms wide for M-mode and Doppler echocardiograms). The 5th element

was a table, which saved the identification results. The values given in this table were the relative position of the features in time (unit: ms) measured from the ECG R wave in the same beat, which were exported for further analysis. The 6th element had a series of check boxes and a window for result visualization.

An example is shown on Figure 4-1 of use of the software for the feature identification on aortic flow tracing from Doppler echocardiography. The start, peak and end points of the aortic flow were identified manually on each beat and indicated by solid vertical bars on the figure. The ECG R wave, indicated by the dashed bar on the plot, was identified automatically on the simultaneous recording from the ECG device. There were 12 beats contained in this recording. The times measured from each beat were listed in the table. A quick check of the variation of the identified features across all beats was enabled by the results displayed on the window of the right bottom.

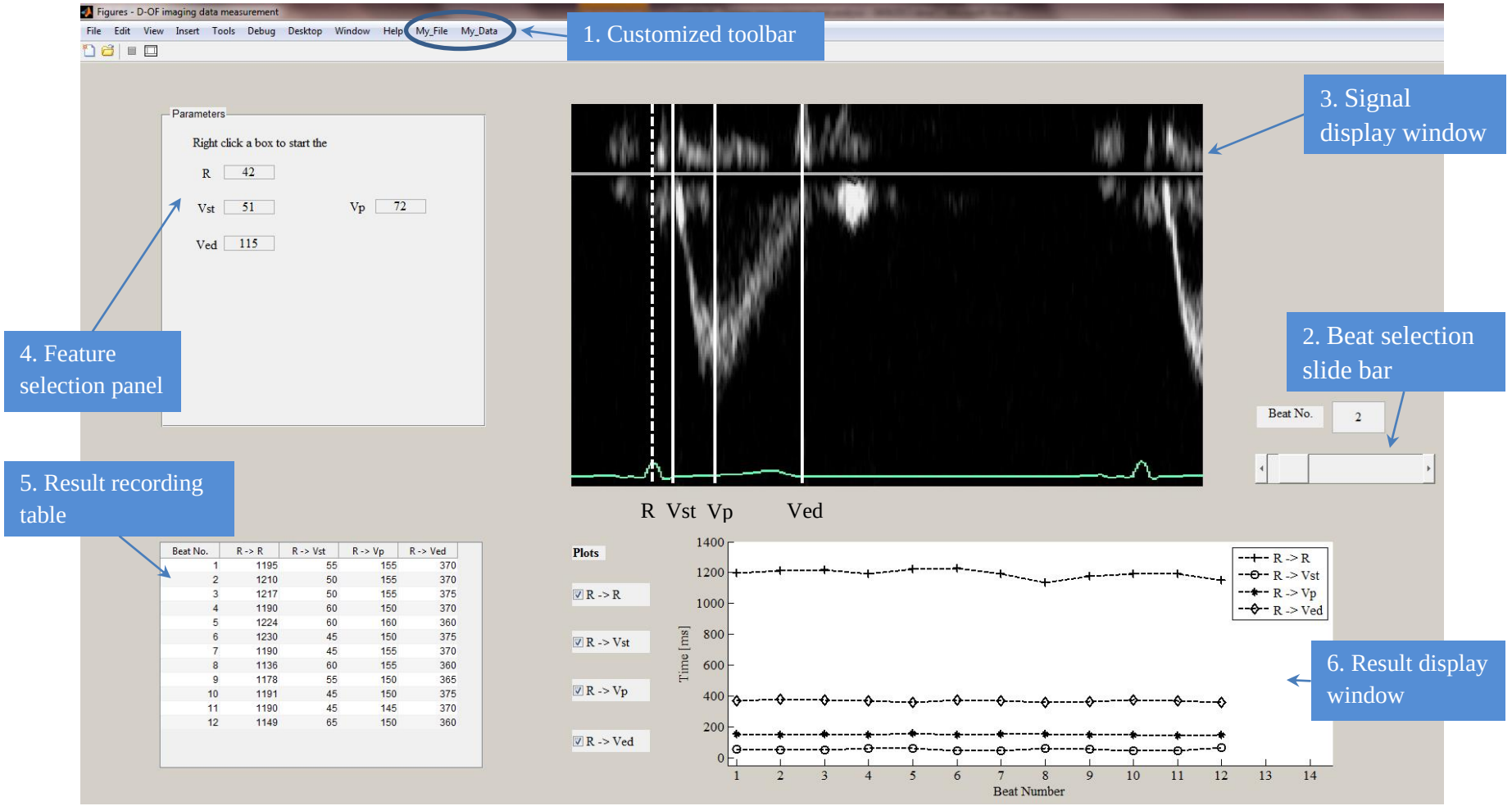

Beat No.	R -> R	R -> Vst	R -> Vp	R -> Ved
1	1195	55	155	370
2	1210	50	155	370
3	1217	50	155	375
4	1190	60	150	370
5	1224	60	160	360
6	1230	45	150	375
7	1190	45	155	370
8	1136	60	155	360
9	1178	55	150	365
10	1191	45	150	375
11	1190	45	145	370
12	1149	65	150	360

Figure 4-1. Illustration of the interface of the software developed for timing feature identification on echocardiograms. The software comprised 6 elements, which are labeled on the figure. An example is given to demonstrate the usage of the software for feature identification on Doppler image for aortic flow. Vst, Vp and Ved here denote the start, peak and end points of the flow respectively.

The interfaces of the components for timing feature identification on ECGs and the recordings from the TaskForce Monitor system were similar with that for the images. However, because there were multiple leads included in each ECG recording, a popup menu was added to allow selecting the lead to be analyzed. In addition, because the main ECG characteristic components, the P wave, QRS complex and the T wave have different frequency ranges, it was better to identify the features on them separately rather than deal with them as a whole. Therefore, another popup menu was designed to select the characteristic component to be analyzed. According to the selection, corresponding pre-processing procedure and the automatic feature identification algorithm were implemented.

The signal selection and display elements of the interface for the ECG feature identification, with an example for P wave analysis, are shown in Figure 4-2. Once the P wave was selected, its peak was identified by an automatic algorithm. Then the original waveform was displayed beat-by-beat, with the identified peak position on it. The plot was zoomed in order to give a large P wave. A smoothed waveform, generated by applying a smoothing filter on the original signal was also displayed, from which the start and end points of the P wave were detected. The design of filtering procedure and the identification methods are described in a later section of this chapter.

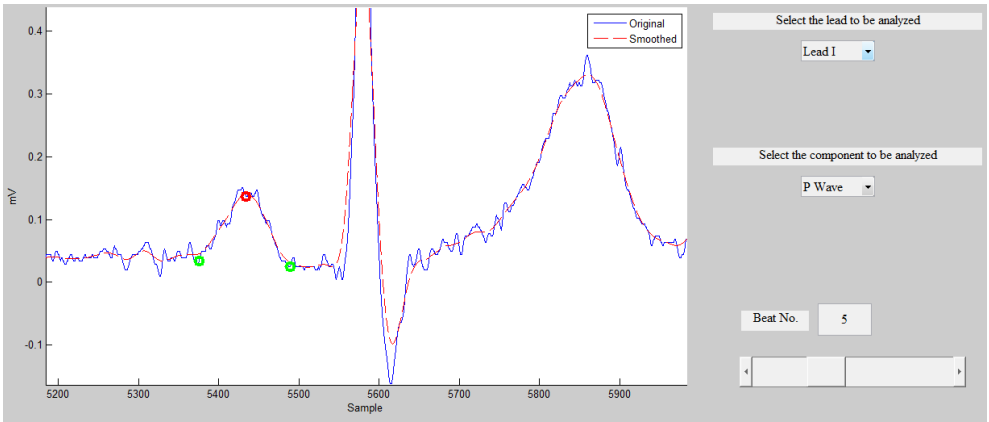

Figure 4-2. The signal selection and display elements of the software for ECG analysis. The selection of different leads and characteristic components to be analyzed was allowed by the two popup menus on the right side. An example of using the software for the feature detection on the P wave of Lead I is shown. The automatically identified P wave peak was indicated by the red circle, and the manually detected start and end of the P wave were indicated by the green circles.

As in the previous description, the signals recorded by the TaskForce Minitor system included a synchronous ECG, thoracic impedance and pulse waveforms. An integrated component was developed to assist feature identification on these signals. The selection of the signal to be analyzed was enabled by a popup menu. A pre-processing procedure and automatic feature identification algorithm were then applied to the selected signal. Because the identification of features on the impedance and pulse waveforms was referred to the ECG times, the synchronous ECG and automatically identified times were also displayed.

An example for the pulse analysis by using the software is shown in the Figure 4-3. The selected beat of the pulse waveform is displayed with the synchronous ECG. The automatically identified pulse foot, early systolic peak, notch and diastolic peak were marked by red markers on the pulse waveform. The ECG P peak, R wave and T peak were also identified automatically, and marked on the ECG waveform. The pre-processing procedure and automatic feature identification algorithm on each signal is described in a later section in this chapter.

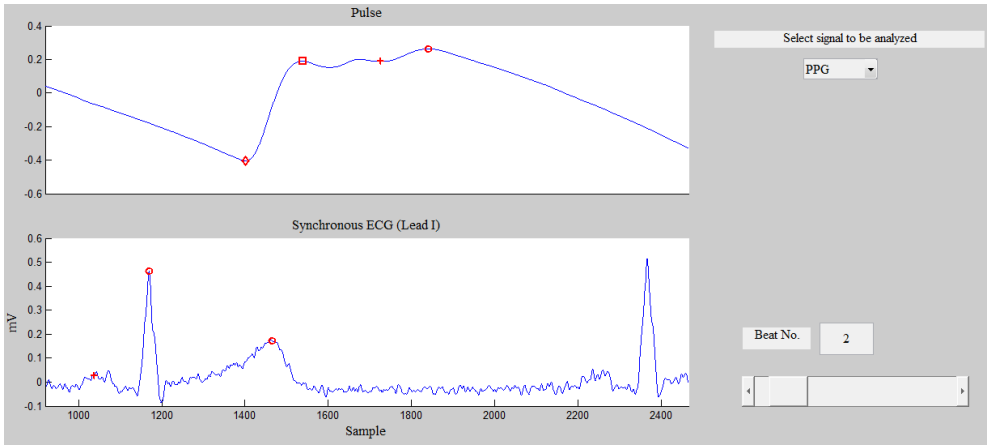

Figure 4-3. The signal selection and display elements of the software for the analysis of signals from the TaskForce Monitor system. The selection of the signal to be analyzed was allowed by the popup menu on the right side. The selected signal was displayed with the synchronous ECG. An example of using the software for pulse analysis is shown. The automatically identified time features on the pulse and ECG waveforms were indicated by the red markers.

4.3 Feature identification

4.3.1 Echocardiography

Time features were identified manually on the M-mode images for the mitral valve and aortic valve movement, and the Doppler images for the mitral flow and aortic flow under the assistance of the MATLAB software for the image analysis. The illustration of feature identification from the mitral valve movement tracing is shown in Figure 4-4. There were two characteristic components on each beat; a major component following the ECG T wave which corresponded to the left ventricular rapid filling phase, and a minor component after the ECG P wave which occurred during the atrial contraction phase. The opening, maximal opening and closing points of the valve were measured for both components. Because the larger anterior leaflet made a greater excursion than the smaller posterior leaflet, these points were measured from the anterior leaflet motion trace.

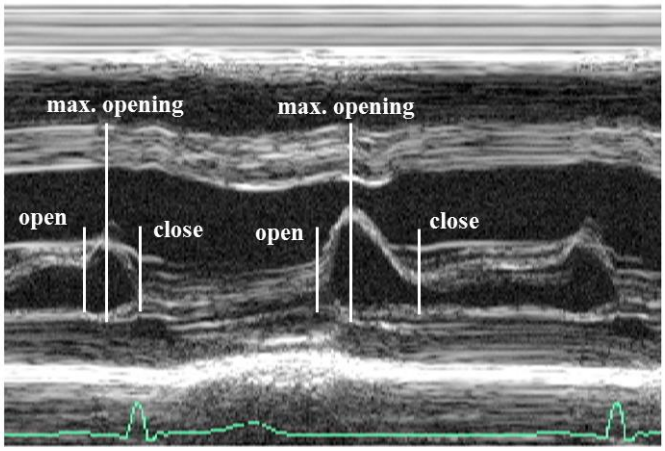

Figure 4-4. Illustration of the time feature identification from the M-mode echocardiography data for the mitral valve movement. The onset of valve opening, maximum opening and closing points during the rapid filling and left atrial contraction were determined from the anterior leaflet motion trace.

From the M-mode echocardiography, the leaflets of the aortic valve were seen separating and moving in parallel to form a box shape tracing during left ventricular ejection. The identification of the aortic valve opening and closing points is illustrated in Figure 4-5. The valve opening time was identified as the point when the leaflets started to separate and the valve closing time identified as the point when the leaflets touch together.

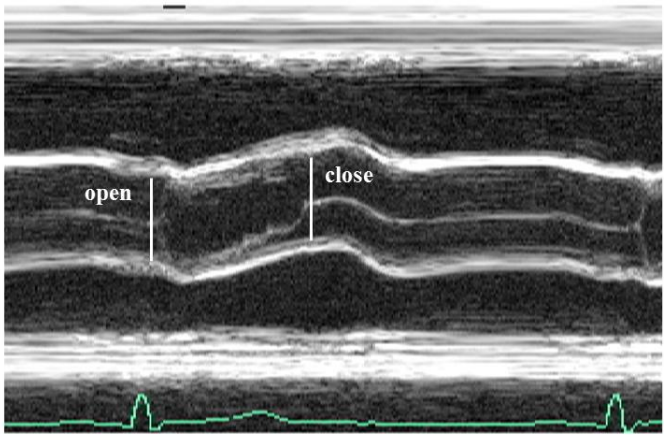

Figure 4-5. Illustration of time feature identification from the M-mode echocardiography for the aortic valve movement. The opening and closing points of the valve were determined.

The feature identification from the Doppler echocardiography for the mitral flow is illustrated in Figure 4-6. The image shows two characteristic components in each beat which reflected the blood velocity within the Doppler sample volume during the left ventricular passive filling phase and the left atrial contraction phase respectively. The flow start, peak and end points of both components were determined from the outer edge of the bright envelope of the velocity tracing.

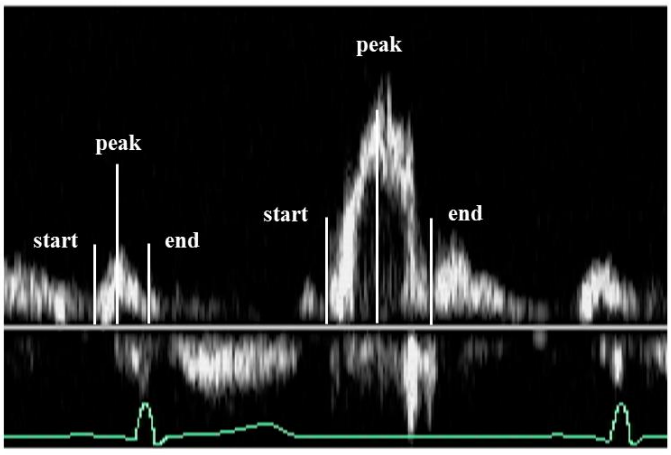

Figure 4-6. Illustration of time features identification from the Doppler echocardiography for the mitral flow. The start, peak and end points of the mitral flow during the passive filling and left atrial contraction were determined.

The feature identification on the Doppler echocardiography for the aortic flow is illustrated in Figure 4-7. A negative wave was recorded in each beat for the velocity of the aortic flow during the left ventricular ejection. The start, peak and end points of the wave were determined from the outer edge of the envelope.

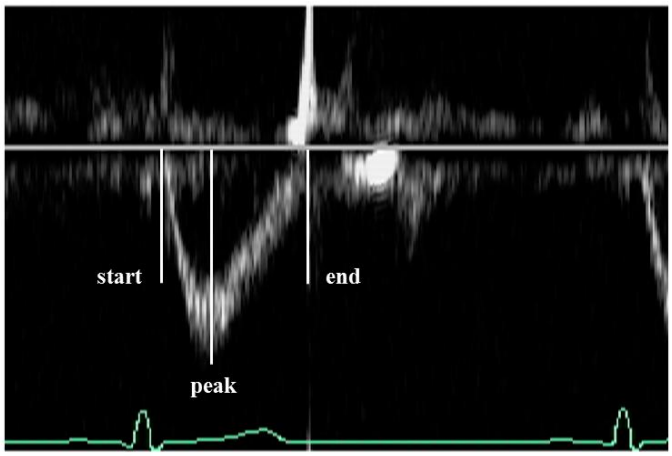

Figure 4-7. Illustration of feature identification from the Doppler echocardiography for the aortic flow. The start, peak and end of the aortic flow during left ventricular ejection were determined.

4.3.2 ECG

ECG waveform is characterized by the P-QRS-T waves in a single beat. The determination of time features, including the peaks and boundaries of the P wave, QRS complex and T wave, is illustrated in Figure 4-8. The MATLAB software for the ECG analysis was used to identify these features beat-by-beat on the lead I. Once the lead was selected, the P wave peak, R wave and T wave peak were identified automatically on each beat. The R waves were located by peak search method on the filtered waveform with a 2^{nd}-order Butterworth band-pass filter (bandwidth: 5 - 40 Hz). The low-frequency interference caused by respiration and movement and the high-frequency interference from mains power supply were removed from the processed signal. Additionally, according to Thakor et al.'s study (Thakor et al. 1984), the main power spectra of the P wave and T wave lie in the range lower than 5 Hz, while that of the QRS complex lie in the range from 5 to 30 Hz. Therefore, this filter was able to attenuate the P wave and T wave, but keep the QRS complex undistorted. In order to obtain zero-phase shift, all the filtering procedures in this

chapter were implemented bi-directionally. After the R wave was determined, the P wave peak was identified within a window before the R wave location and the T wave peak identified within window after the R wave on the filtered waveform by a 4^{th}-order Butterworth band-pass filter with the bandwidth between 2 and 15 Hz. In the next stage, when a characteristic wave was selected, the ECG original waveform was displayed beat-by-beat and automatically zoomed to the area of interest under the guidance of the determined peak position. For the P wave and T wave, a smoothed waveform by a 15-point smoothing filter was displayed with the original waveform, from which the start and end of the P wave, and the end of the T waves were determined manually.

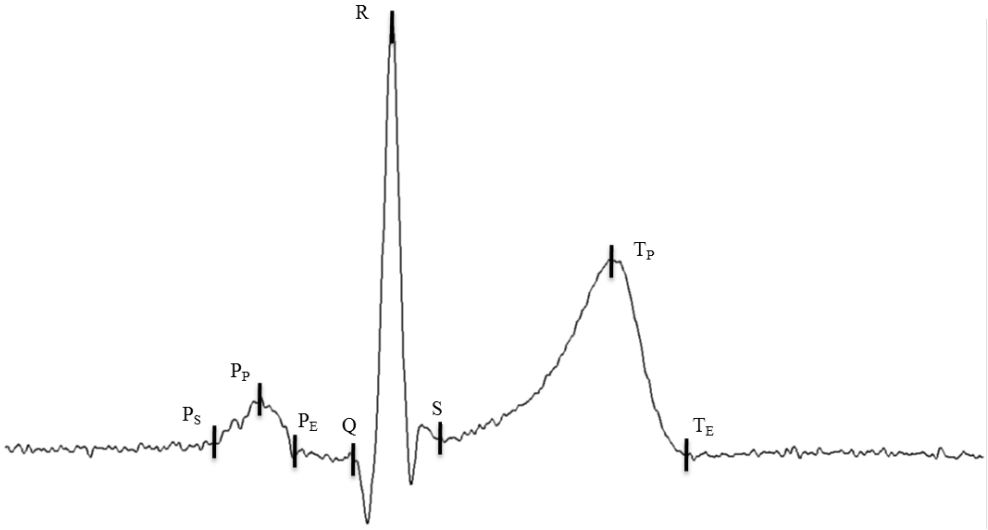

Figure 4-8. Illustration of time feature identification on ECG lead I.

4.3.3 Thoracic impedance waveforms

Features from the thoracic impedance (Z) and its negative first derivative (-dZ/dt) were identified by using the software component for the analysis of the recordings from the TaskForce Monitor system. In order to assist the feature identification on the impedance and pulse waveforms, ECG P wave peak, R wave and T wave peak were firstly determined on the synchronous ECG by the method described in the Section 4.3.2.

The impedance waveforms in a single beat and time feature identification are illustrated in Figure 4-9. Two characteristic components were seen on the impedance waveform (Z). The major component showed a decrease in impedance following the ECG QRS complex.

The other component was usually located on the upward limb of the major component. It also showed a decrease in impedance, but with a much smaller size. A 2^{nd}-order Butterworth high-pass filter with cutoff frequency at 0.5 Hz and a 4^{th}-order Butterworth low-pass filter with cutoff frequency at 20 Hz were applied to the signal. Afterwards, the time features of the major component, including the start, valley (the minimum) and end, were identified automatically on each beat with the reference of ECG times. The valley was determined as the minimum point on the impedance waveform within the window between the ECG R waves in the current beat and the following beat. The start was determined as the onset of the impedance fall, which was detected within the window between the ECG R wave and the determined valley, and the end was determined by searching forwards after the minimum till the first point when the sign of slope was changed from positive to negative. The valley of the minor component (the 2^{nd} minimum) was identified manually.

Corresponding to the Z waveform, there were also two components on the first derivative impedance waveform (-dZ/dt) in each beat; a major positive wave associated with the left ventricular ejection and a minor one associated with early diastole. A 4^{th}-order Butterworth band-pass filter with bandwidth of 0.7 to 40 Hz was applied to the derivative waveform. Then the time features, including the foot, peak (1^{st} peak) and end of the major wave and the peak of the minor wave (2^{nd} peak) were determined by an automatic algorithm. Again, ECG features were used as the time reference for impedance feature identification. The peak of the major wave was firstly obtained by searching the maximum on the impedance waveform within the window between ECG R wave and the T peak. Then the foot was determined by searching back from the peak till the 1^{st} point when the sign of slope changed, and the end was considered as the lowest point between the 1^{st} peak and the next ECG R wave. The 2^{nd} peak was determined as the highest peak between the end point of the major component and the next ECG R wave.

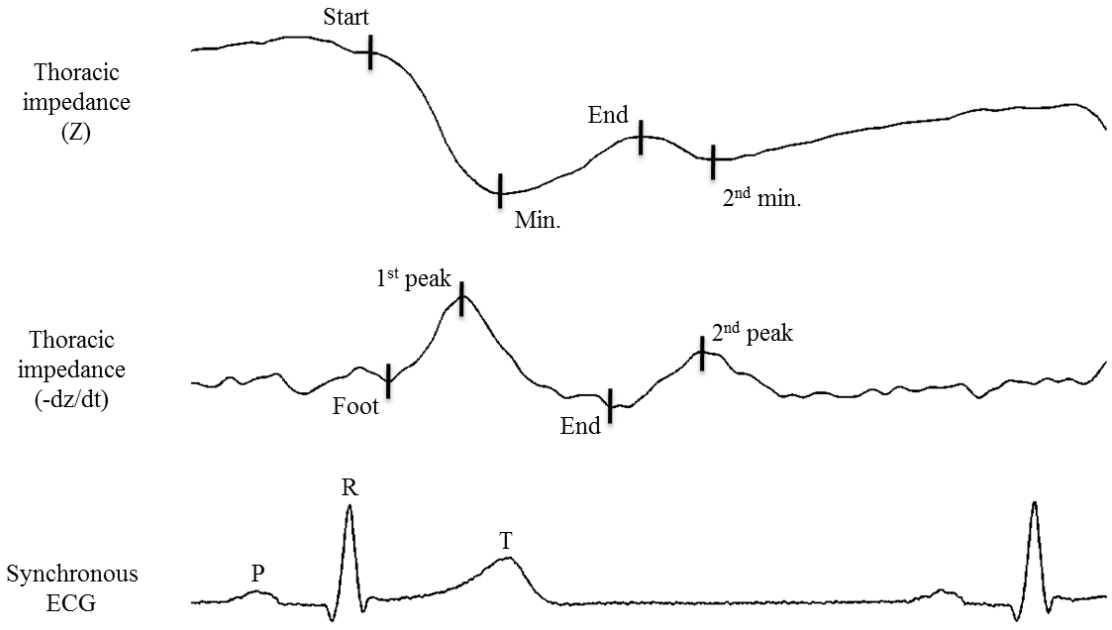

Figure 4-9. Illustration of time feature identification on impedance waveforms.

4.3.4 Pulse

Features from the pulses were also identified by using the software component for the analysis of the recordings from the TaskForce Monitor system. The ear and finger pulse waveforms in a single beat and the feature identification are illustrated in Figure 4-10. Both pulses were characterized by systolic and diastolic components. For the systolic component, early and late systolic waves were seen on both the ear and finger pulses. While the systolic component was usually dominated by the early wave on the finger pulse, it was the late wave or the two waves together that dominated the systolic component on the ear pulse. Because the late systolic wave was not always visible, especially on the finger pulse, only the early wave was researched in this study.

Because the main energy of pulse waveforms was located in the frequency range between 0.5 to 20 Hz (Allen 2007), a 4^{th}-order Butterworth high pass filter (cutoff frequency at 0.5 Hz) was applied. An automatic algorithm was then implemented to identify the time features, including the foot and peak of the early systolic peak, the peak of the diastolic wave and the notch point preceding the diastolic wave. The foot was determined as the lowest point within the current beat. Positive peaks were located by the peak detection methods. The 1^{st} peak following the foot was determined as the early

systolic peak, and the last peak was the diastolic peak. The notch point was determined by searching back from the diastolic peak till the point where the sign of the slope changed from negative to positive.

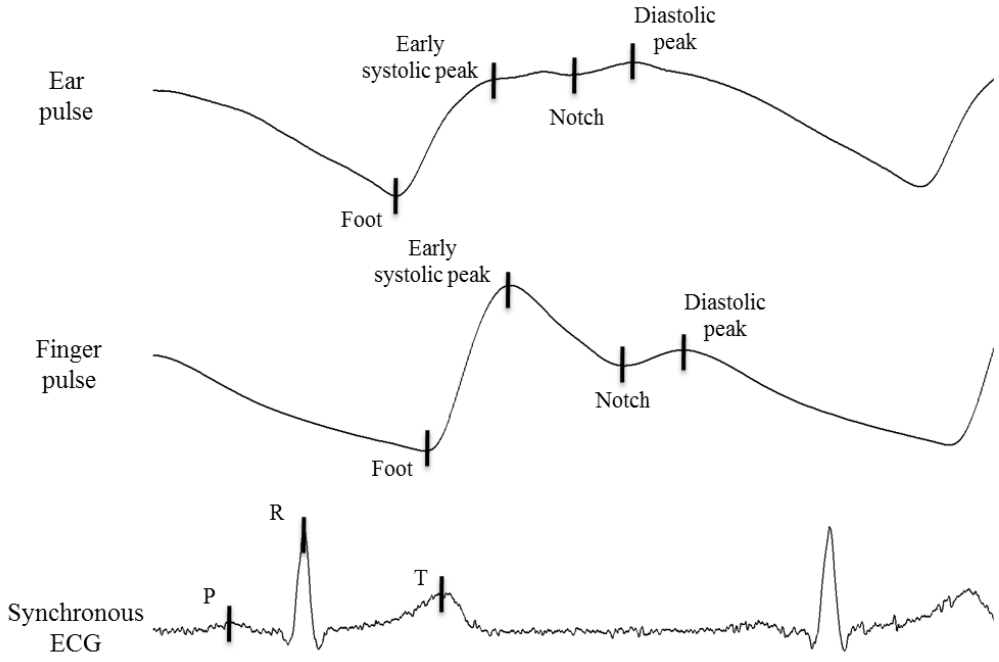

Figure 4-10. Illustration of time feature identification on ear and finger waveforms.

4.4 Statistical analysis

4.4.1 Statistical methods for repeatability assessment

The imaging data and physiological measurements were repeated within the same session. Time features were obtained on both the repeat recordings, which allowed the repeatability assessment on the measurements from the same session (within-session repeatability). Additionally, the thoracic impedance and finger pulse were recorded in both the session 2 and 3, while the limb leads ECGs were recorded in all the three sessions. The repeatability of the measurements from different sessions (between-session repeatability) was also assessed.

Bland-Altman plots

Bland-Altman plot is a very simple and direct visualizing statistical tool, which was originally proposed to assess the agreement between two different methods within clinical

studies (Bland and Altman 1986). It is also considered as a useful check when assessing the agreement of repeated measurements (Bland and Altman 2003).

A Bland-Altman plot is a scatter diagram, on which the difference of the values obtained from two measurements on each subject is displayed against the mean values. The line at the mean difference level, and a pair of lines representing the 95% limits of agreement, with one at the level of 1.96 × SD of the difference above and the other 1.96 × SD of the difference below the mean difference level, are added onto the scatter diagram. For the repeated measurement with a good agreement, it is expected that the mean difference level is close to zero, and the region between the 95% limits of agreement lines is narrow.

An example of using the Bland-Altman plot to assess the within-session repeatability for the ECG T wave peak (T_P) identification is shown in Figure 4-11. In the plot, the mean difference line was close to zero (within 1 ms), and the distance between the 95% limits of agreement lines was narrow (within 10 ms), which indicated a good repeatability of the T_P identification from the two repeat recordings. In this study, the Bland-Altman plots were made with SigmaPlot 11.0 (Systat Software, Inc., USA).

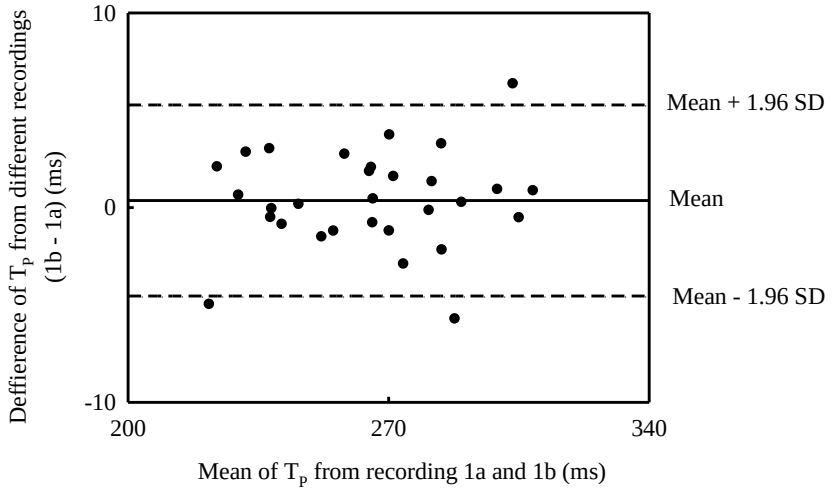

Figure 4-11. Example of Bland-Altman plot for within-session repeatability assessment. The data from the results of ECG T wave peak (T_P) identification on the repeat recordings in session 1.

Paired t-test

The Bland-Altman plot provides only a check rather than a formal statistical analysis on the repeatability of two measurements. In order to get a quantitative conclusion on the agreement between two repeated measurements, paired t-test was employed. The null hypothesis of the paired t-test is that the observed change in the two measurements is caused by chance, or alternatively, the mean difference between the two measurements is zero. This hypothesis is considered to be violated if the P value is less than 0.05. There are following two assumptions underlying the paired t-test:

- The difference between the two measurements follows a normal distribution;
- The variances of the two measurements are the same.

In this study, because the signals were recorded within one hour and analysed by the same person, these two assumptions were met in the most cases.

For example, according to the paired t-test results, there was no significant difference between the two ECG T wave end observations from the two repeat measurements in session 1 (Mean difference ± SEM: 0.4 ± 0.5 ms, P = 0.43).

Repeated measures ANOVA test

The paired t-test meets the repeatability assessment for the repeated measurements within the same session, and the average measurements from two sessions. However, it is unable to deal with the measurements from 3 sessions. In this case, the repeated measures ANOVA (analysis of variance) test was employed. The ANOVA test is a parametrical test to examine the equality of means of a group of measurements. The null hypothesis of the ANOVA test is that the tested measurements have the same mean values. The repeated measures ANOVA test is a special case of the general ANOVA test, where the repeated measurements are made on the same subjects. The most important assumptions underlying the repeated measures ANOVA test include:

- The difference between any two of the measurements follows a normal distribution;
- The variances of the difference between any two of the measurements are equal;

These two assumptions were always checked during the implementations of the ANOVA test in this study.

Both the paired t-test and the repeated measures ANOVA test were implemented in SPSS 16.0 (IBM Inc., USA). The paired t-test was always used for all the pair combinations of the tested measurements whenever the ANOVA test was implemented so that the repeatability between any two measurements can be also reported.

4.4.2 Statistical methods for comparison of difference

During the data analysis, the comparison between different features was usually of interest. The comparison of the time of features was helpful in obtaining a better understanding on the sequence of cardiovascular events, while the comparison of time intervals between features helped to quantify the duration of specific cardiac activity reflected on the imaging and physiological measurements. When the compared times or intervals were from the same subjects, the paired t-test was used. However, in some other cases, where variables from different groups of subjects were to be compared, when variables would not be expected to follow the normal distribution and the subject numbers in each group were not the same, a non-parametric testing method was employed to deal with these data.

Mann-Whitney test

Mann-Whitney test, also known as Wilcoxon rank-sum test, is a non-parametric test, which is used to compare a variable on subjects from two different groups. The comparison is based on the sum of rank codes within each group. Unlike the parametric tests, Mann-Whitney test does not need any assumption about the tested variable. The null hypothesis of the test is that the tested variable from the two groups have the same distribution. All the Mann-Whitney tests in this study were implemented in SPSS 16.0 (IBM Inc., USA).

4.4.3 Statistical methods for association examination

One of the most important purposes in this study was to investigate the relationships between cardiovascular events. Regression and correlation methods were employed to quantify the relations of physiological measurements with imaging data, and the effects of age, heart rate and blood pressures on the imaging and physiological measurements.

Linear regression

With linear regression analysis, how a variable (outcome or dependent variable) is associated to other one or more variables (predictors or independent variables) is examined. The regression is also known as simple linear regression if there is only one independent variable, or predictor. It was used to examine the relationship between two features in this study. The simple linear regression was visualized in a scatter diagram, with the dependent variable displayed against the independent variable. The scattered points were fitted with a straight regression line. The sum of distance of the scattered points to the line was minimized. The straight line is described by the equation below:

$$Y = a + \beta X$$

Where Y denotes the dependent variable, X denotes the predictor, a denotes the intersection of the line with the Y axis (intercept), and β presents the slope (known as regression coefficient). An example of the relationship between the left ventricular ejection duration (from aortic valve open to close) and ECG RR interval examined by simple linear regression is shown in Figure 4-12. As can be seen, the left ventricular ejection duration increases with RR interval lengthening, and the points lie tightly around the fitted line. The slope of the line is 0.141, which means every 1 ms increase in RR interval is associated with 0.141 ms increase in the left ventricular ejection duration.

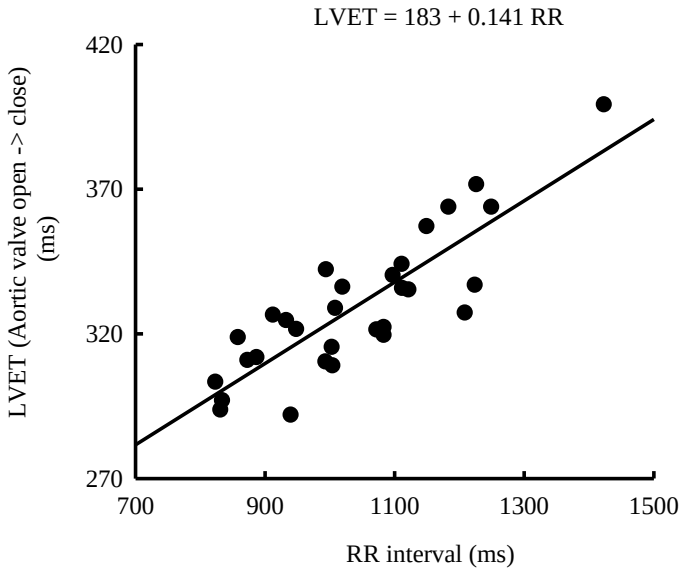

Figure 4-12. Example of simple linear regression model for the relationship between ECG RR interval (predictor) and left ventricular ejection time (LVET) (outcome). The data are from session 3.

While the simple linear regression method was used only for the examination of the relationship between two variables, multiple linear regression was used to examine the effects of multiple factors on one dependent variables. The multiple linear regression is a generalized linear regression model, which has one dependent variable but multiple predictors. The relationship between the dependent variable and the predictors is described by the equation below:

$$Y = a + \beta_1 X_1 + \beta_2 X_2 + \cdots + \beta_N X_N$$

Where Y and a denote the dependent variable and the intercept respectively, $X_{1\cdots N}$ denote the N independent variables, while $\beta_{1\cdots N}$ denote the regression coefficient for each independent variable.

Hypothesis testing was implemented for linear regression to assess the significance of the regression model and the significance of each predictor. The null hypothesis of the testing for the significance of the regression model was that none of the independent variable was correlated to the dependent variable, which is described by the following formula:

$$\beta_1 = \beta_2 = \cdots = \beta_N = 0$$

The null hypothesis of the testing for the significance of each independent variable in the regression model is that the tested variable is not correlated to the dependent variable.

Correlation

While the regression describes the form of the association between variables, correlation coefficient, r, is a statistic of the direction and strength of the association. The correlation coefficient is a coefficient within the interval between [-1, 1]. If the two variables are strongly associated, or correlated, the coefficient is close to 1 when they have positive correlation (increase or decrease together) or close to -1 if they have negative correlation (increase in one associated with a decrease in the other). If the two variables are not associated, or correlated, the coefficient is close to 0.

In addition to the correlation coefficient, another important statistic of correlation is coefficient of determination, R^2, which is a measure of the goodness of the linear regression model. It measures the proportion of variation in the dependent variable that is explained by the independent variable(s). In simple linear regression, R^2 equals the squared value of r. In the multiple linear regression, because R^2 increases with adding of new independent variables, adjusted R^2, which accounts for the number of independent variables was used in this work.

In this study, linear regression and correlation were implemented in SPSS 16.0 (IBM Inc., USA). When the linear regression was used, the regression coefficient of each independent variable β, the significance of the regression model and the significance of each independent variable were reported with coefficient of determination R^2.

Chapter 5 Repeatability and timing sequence

The main work of this chapter is to summarize the repeatability of the imaging and physiological data recorded from the three sessions, and to demonstrate the reconstruction of timing sequence of cardiovascular events with the times identified from the simultaneously recorded signals.

5.1 Introduction

Thirty male healthy subjects were studied in this research. The subject age, blood pressures and body mass index (BMI) are summarized at the beginning of this chapter.

As has been described in the previous chapter, images and physiological signals were recorded from each subject within three sequential sessions. Standard 12-lead ECG signals of 60s were recorded within the first session, and then 6 limb lead ECGs, impedance Z, minus derivative impedance -dZ/dt, ear pulse and finger pulse of 60 s were simultaneously recorded within the second session. For the signals recorded in these two sessions, only the first 15 s (1^{st} recording) and the last 15 s (repeat recording) were analysed. In the last session, 4 sets of imaging recordings for mitral and aortic valves, mitral and aortic flow were recorded with physiological signals. Two repeat recordings, 15 s long for each, were taken in the session. These recordings were coded as 1a and 1b, 2a and 2b, 3a and 3b, respectively. The heart rate stability across the three sessions is described first. Then the repeatability of time feature identification on the two recordings within the same session (within-session repeatability) is summarized. Furthermore, for those signals recorded within more than one session, the repeatability of the identification of the same feature on the recordings from different sessions (between-session repeatability) is also summarized.

At the end of this chapter, an example demonstrating the timing sequence of cardiovascular events is provided. The sequence is reconstructed with the times identified on the recorded signals within the three sessions on one subject.

5.2 Subject information

During the study period, a total of 30 staff from the Newcastle Hospitals NHS Foundation Trust and students from Newcastle University volunteered to participate in the study. All of the subjects were male, without any symptom or diagnosed cardiovascular disease. The demographic data of the subjects is summarized in Table 5-1. The average age was 41 years old and the average BMI was 24.7 kg/m^2. The average SBP and DBP were 122 and 76 mmHg respectively, with a calculated pulse pressure (PP) of 46 mmHg and a mean arterial pressure (MAP) of 91 mmHg.

Table 5-1. Demographic information of the subjects.

Parameters	Mean ± SD	Range
Age (years)	41 ± 13	23 - 66
Height (cm)	177 ± 6	165 - 190
Weight (kg)	77 ± 11	56 - 100
BMI (kg/m^2)	24.7 ± 3.6	17.7 - 33.8
SBP (mmHg)	122 ± 11	99 - 148
DBP (mmHg)	76 ± 8	58 - 94
PP (mmHg)	46 ± 8	30 - 60
MAP (mmHg)	91 ± 9	75 - 112

The histogram of subject age is shown in the Figure 5-1. Five age bands were used to classify the 30 subjects into the 5 groups, including 20 – 29, 30 – 39, 40 – 49, 50 – 59 and over 60 years. There were 7 subjects in each of the first 3 bands, 6 subjects in the band 50 – 59 years and 3 subjects in the last band.

The histogram of the BMI is shown in the Figure 5-2. The BMI was classified into four groups based on widely accepted values, including underweight (< 18.5 kg/m^2), normal (18.5 – 24.9 kg/m^2), overweight (25 – 29.9 kg/m^2) and obese (>= 30 kg/m^2). Most subjects were categorized as normal or overweight (83%). There was only 1 subject classified as underweight and another 4 as obese.

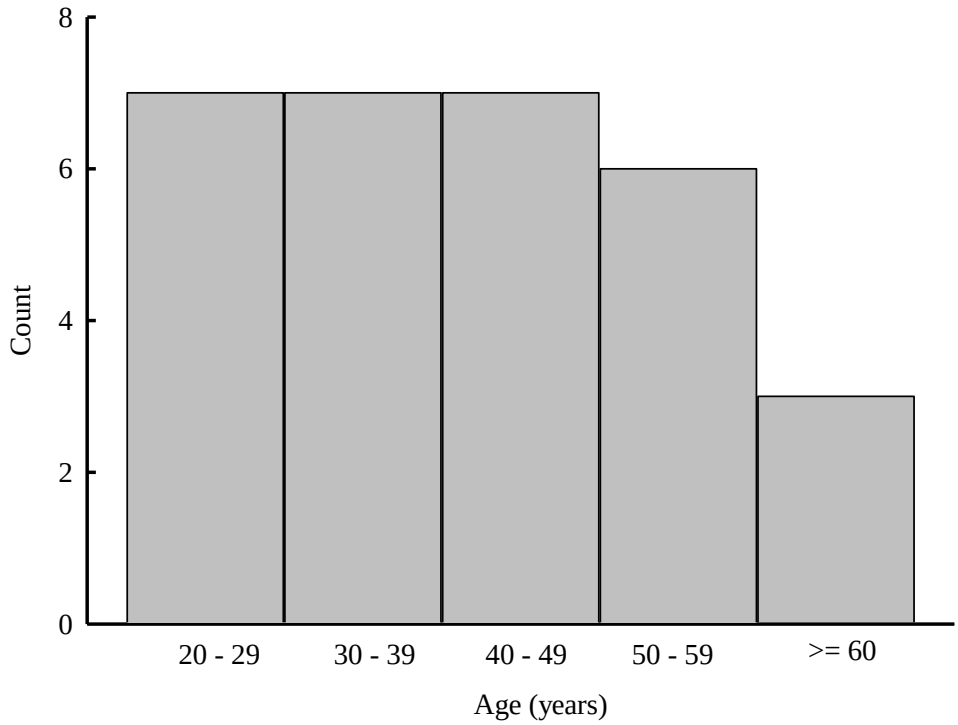

Figure 5-1. Histogram of subject age.

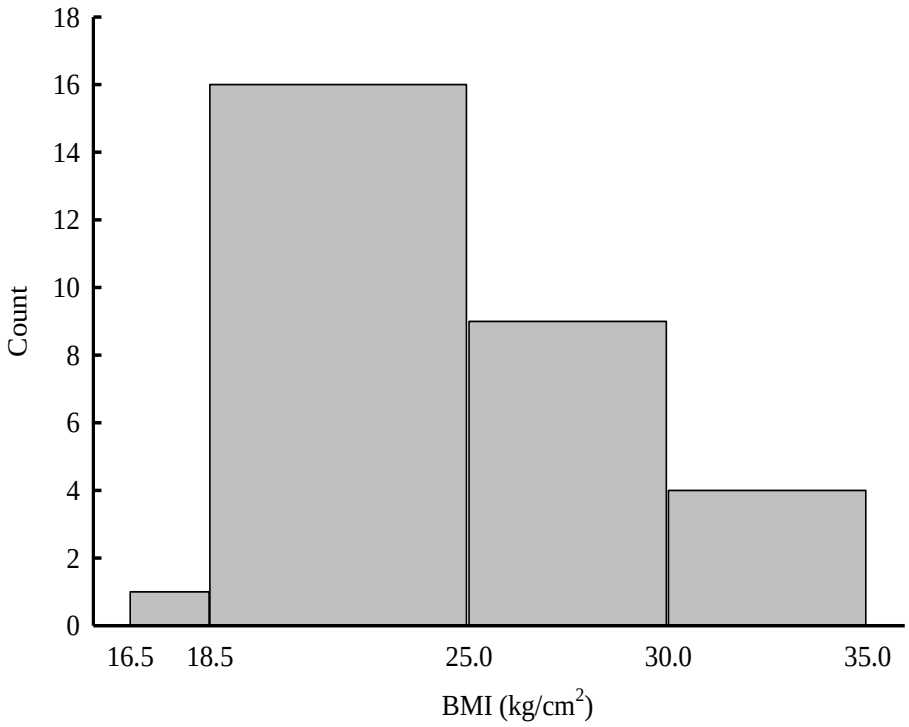

Figure 5-2. Histogram of subject BMI.

The histograms of subject blood pressures are shown in Figure 5-3. The SBP was classified into 4 groups, < 110, 110 – 119, 120 – 129, >= 130 mm Hg. There were 21 subjects (70%) located in the two groups of 110 – 119 and 120 – 129 mm Hg. The DBP was also classified into 4 groups, < 65, 65 – 74, 75 – 84, >= 85 mm Hg. There were 22 subjects (73%) with DBP between 65 and 75 mm Hg.

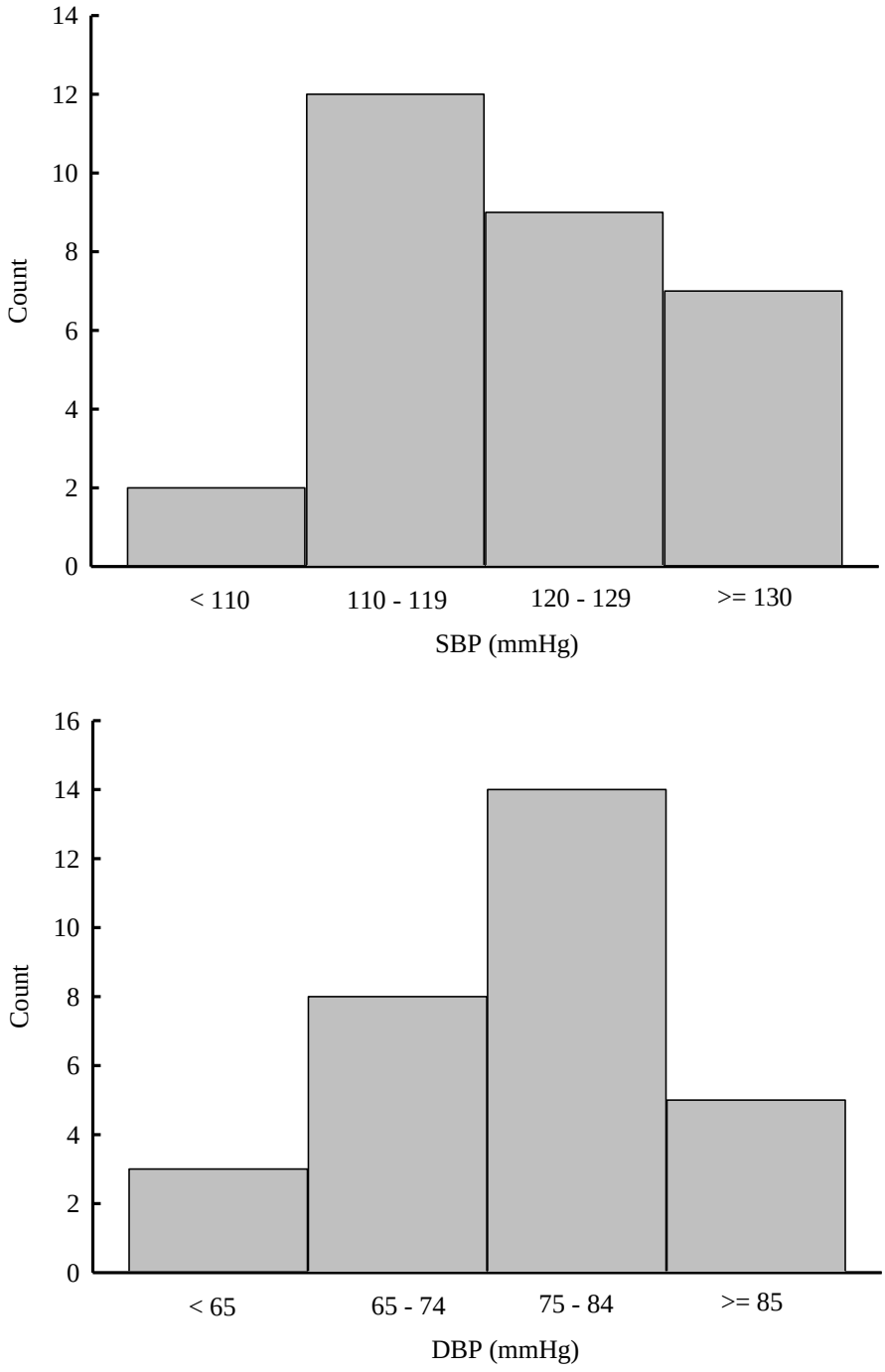

Figure 5-3. Histograms of subject blood pressures.

5.3 Heart rate stability

The average ECG RR interval in each session is summarized in Table 5-2 and visualized by the bar charts in Figure 5-4. The average RR interval increased gradually across the sessions, which started from 1016 ms (SD: 151 ms) within the first session to 1032 ms (SD: 162 ms) within the second session and to 1040 ms (SD: 146 ms) within the last session. However, according to the paired t-test results, this increasing was not statistically significant. There was no significant difference found between any of the three sessions. The further analysis of variance (ANOVA) test indicated that there was no significant difference in the RR interval overall across the three sessions.

Table 5-2. Average ECG RR intervals from the three sessions.

Session	Mean ± SD (ms)	Mean difference ± SEM (ms)	Pairwise significance	Significance from variance comparison
1	1016 ± 151	Ref.	Ref.	
2	1032 ± 162	16 ± 9	NS	NS
3	1040 ± 146	24 ± 12	NS	

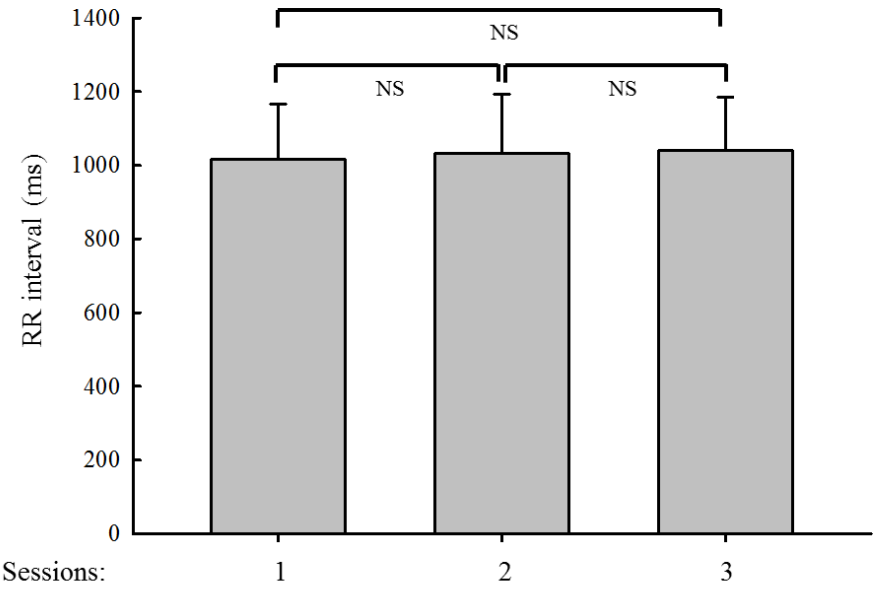

Figure 5-4. Comparison of the ECG RR intervals from different sessions. NS: no significant difference.

5.4 Within-session repeatability

5.4.1 Session 1: 12-lead ECG recordings

The times of the ECG P wave, QRS complex, T wave boundaries and peaks were obtained on lead I. On the lead with the largest T wave, times of the T wave (T_P and T_E) were measured. The individual means of these times for each 15 s recording were calculated for each subject, and then the overall means and the standard error of the means (SEM) across all the subjects were calculated.

The information of the ECG leads with the largest T wave is summarized in Table 5-3. All the largest T waves were observed on precordial leads V2 ~ V5. Lead V2 was the best site for the T wave, which provided 22 largest T waves out of 30 studied subjects. The lead V5 provided the second best site of the T wave, with 6 largest T waves. The largest T wave only happened once on each of the lead V3 and V4.

Table 5-3. Summary of the ECG lead with the largest T wave.

ECG wave	**Number of subjects on each lead**				**Total subject numbers**
	V2	**V3**	**V4**	**V5**	
T	22	1	1	6	30

The times, measured from the R wave, are summarized in Table 5-4. According to the paired t-test results, there was no significant difference between the RR intervals of the two repeat recordings (Mean Difference ± SEM: -18.3 ± 9.5 ms). Although mean differences of the other times between the two recordings were less than 2 ms, statistically significant differences were found for the P wave end and T wave end (both $P < 0.05$). This was because the between-subject variance of these two features was small (less than 32 ms), and the comparison was sensitive to small mean value change. That was why the mean differences within 2 ms still caused significant difference for the P wave end and T wave end identified on the repeat recordings. However, these tiny time differences were not considered as clinically significant.

Table 5-4. Repeatability of ECG feature identification within session 1.

Features	Subject numbers	Mean ± SD (ms)		Mean Difference ± SEM (ms)	Significance (difference)
		1a	1b		
†$\mathbf{P_S}$	30	-206 ± 22	207 ± 21	-0.5 ± 0.5	NS
†$\mathbf{P_P}$	30	-151 ± 21	-151 ± 21	0.5 ± 0.5	NS
†$\mathbf{P_E}$	30	-106 ± 22	-104 ± 22	1.2 ± 0.3	P < 0.05
†**Q**	30	-38 ± 6	-39 ± 6	-0.4 ± 0.2	NS
†**S**	30	47 ± 6	47 ± 6	-0.1 ± 0.3	NS
†$\mathbf{T_P}$	30	265 ± 25	265 ± 25	0.4 ± 0.5	NS
†$\mathbf{T_E}$	30	350 ± 31	352 ± 32	1.7 ± 0.6	P < 0.05
†**Next R**	30	1025 ± 155	1007 ± 152	-18.3 ± 9.5	NS
‡$\mathbf{T_P}$	30	253 ± 24	253 ± 25	0.1 ± 0.4	NS
‡$\mathbf{T_E}$	30	356 ± 32	356 ± 31	-0.2 ± 0.7	NS

†: features from lead I; ‡: features from the lead with the largest T.

The Bland-Altman plots for the within-session repeatability of the times from lead I are shown in Figure 5-5, and the plots for the features from the lead with largest T wave are shown in Figure 5-6. As can be seen, all the mean difference lines were close to the 0 level, and the distances of the 95% limits of agreement lines for other features were narrow. The points (pairs of difference against means) located within the regions between the 95% limits of agreement lines and laid along the mean difference lines. These observations confirmed again the good repeatability of ECG feature identification on the two repeat recordings within the session 1.

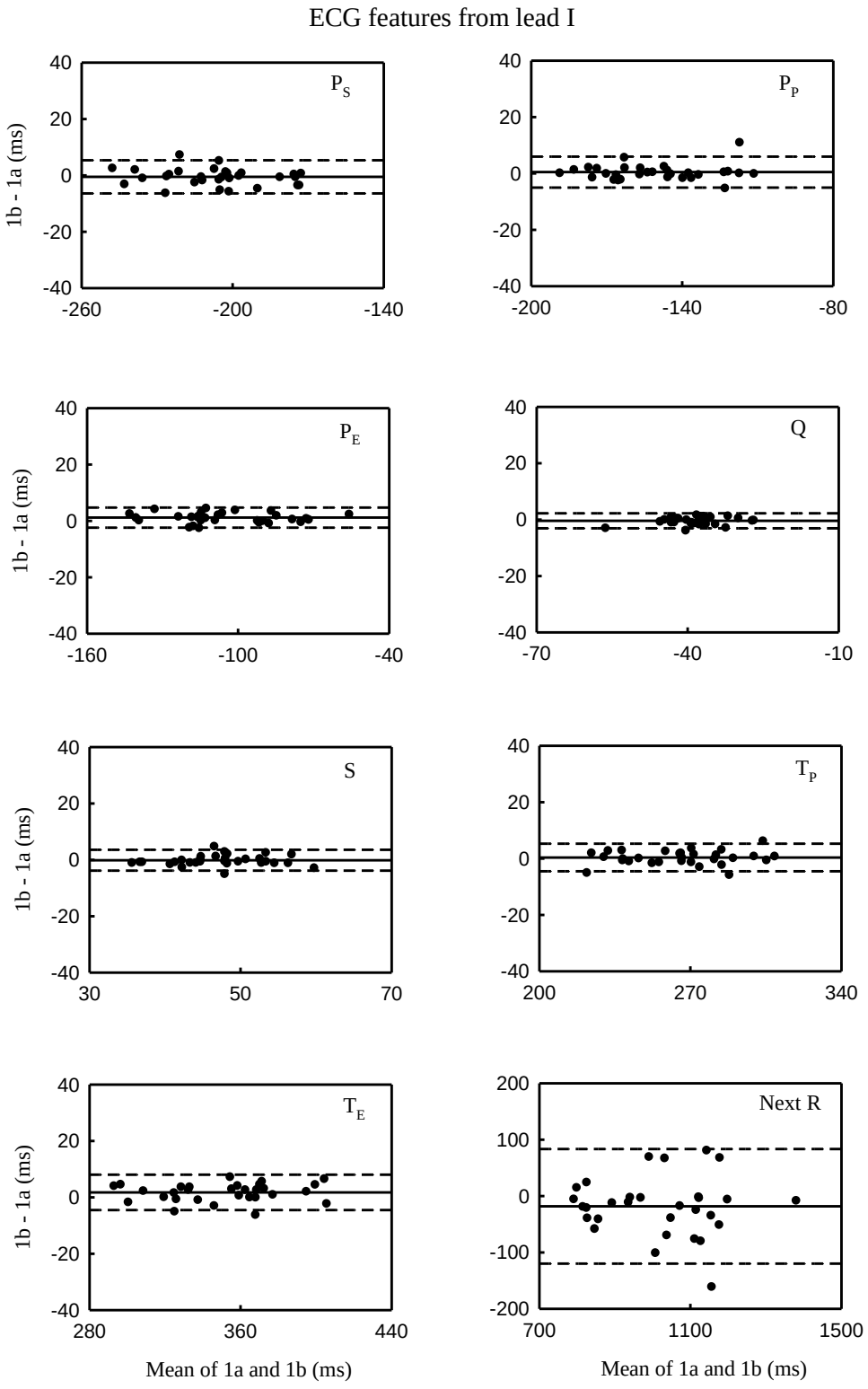

Figure 5-5. Within-session repeatability through Bland-Altman plots for ECG features on lead I from the two repeat recordings within session 1.

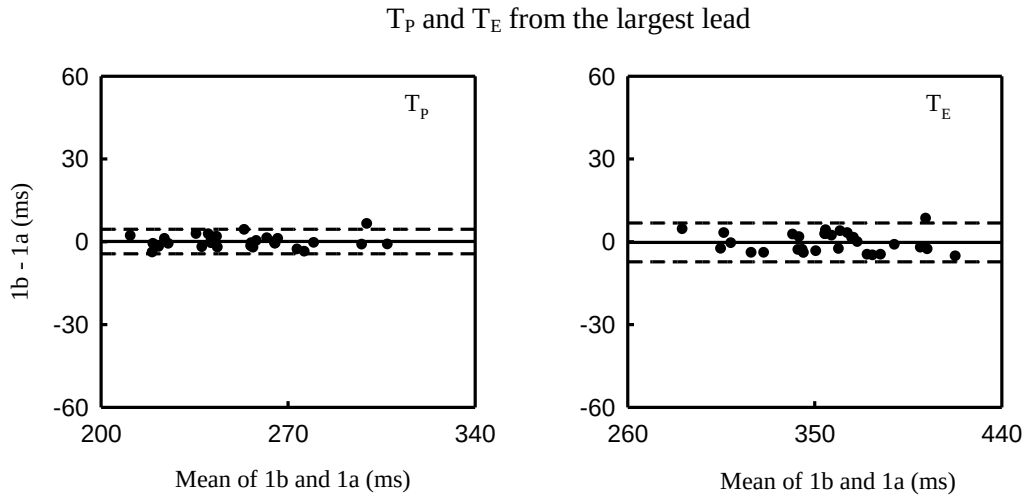

Figure 5-6. Within-session repeatability through Bland-Altman plots for the features of the largest T wave from the two repeat recordings within session 1.

Figure 5-7 shows an example of ECG time feature identification results from one subject within session 1. The average values and SD across all heart beats from the two repeat recordings were calculated and displayed in sequence. The average RR interval was 1153 ms, with a SD of 62 ms. The other features showed much smaller variance than that of RR interval. The smallest SD among these features was only 1 ms from the T wave peak (T_P) and the largest SD was 6 ms from the P wave peak (P_P).

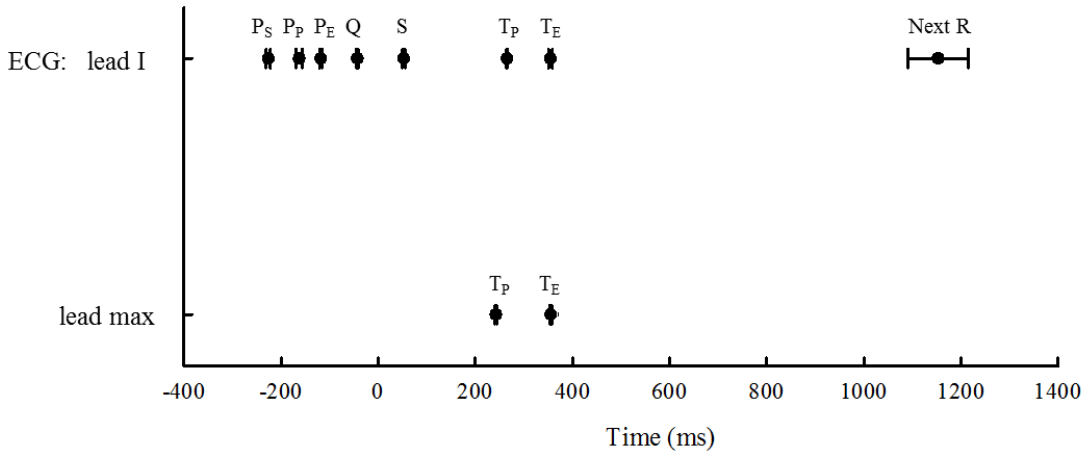

Figure 5-7. An example of the times identified on ECG lead I and on the lead with the largest T wave from one subject within session 1. The circle presents the mean and the error bar presents the SD across all the beats from the two repeat recordings.

5.4.2 Session 2: Simultaneous ECGs, impedance and pulses recordings

The 6 limb lead ECGs, impedance Z and the first derivative impedance -dZ/dt, ear pulse and finger pulse were simultaneously recorded within this session.

The overall means and SEMs of the feature times identified on ECG lead I is summarized in Table 5-5. The mean difference of the RR intervals between the two repeat recordings was -6.7 ms (SEM: 10.2 ms). The mean differences of the other times ranged from -0.1 to 1.0 ms. According to the paired t-test results, there was no significant difference found for any feature.

Table 5-5. Repeatability of ECG feature identification within session 2.

Features	Subject numbers	Mean ± SD (ms)		Mean Difference ± SEM (ms)	Significance (difference)
		2a	2b		
P_S	30	-208 ± 22	-207 ± 22	1.0 ± 0.5	NS
P_P	30	-153 ± 23	-152 ± 22	0.5 ± 0.5	NS
P_E	30	-106 ± 21	-106 ± 22	0.5 ± 0.4	NS
Q	30	-39 ± 6	-39 ± 6	-0.1 ± 0.2	NS
S	30	46 ± 6	46 ± 6	0.0 ± 0.2	NS
T_P	30	267 ± 27	267 ± 27	0.5 ± 0.4	NS
T_E	30	351 ± 33	351 ± 33	0.8 ± 0.6	NS
Next R	30	1035 ± 169	1028 ± 160	-6.7 ± 10.2	NS

The time features identified from the impedance Z and its minus first derivative -dZ/dt are provided in Table 5-6. The start and minimum points (Min.) of the systolic wave on the impedance Z waveform were obtained from all 30 subjects, while the end point was only obtainable on 28 subjects, and the minimum point of the diastolic wave (2^{nd} min.) from 23 subjects. The 2^{nd} minimum point had the largest mean difference -3.1 ms among all the times, and it was the only feature with statistically significant difference ($P < 0.05$) between the two recordings. The absolute values of the mean difference for the other three times were less than 0.5 ms and no significant difference was found.

The features of the systolic wave, including the foot, peak (1st peak) and end, were obtained from the derivative impedance -dZ/dt from all 30 subjects, but the peak of the diastolic wave (2nd peak) was identified from only 21 subjects. For all these 4 features, the absolute values of the mean difference between the two recordings were less than 1 ms, and no significant difference was found for any of them.

Table 5-6. Repeatability of feature identification on Z and -dZ/dt within session 2.

Signals	Features	Subject numbers	Mean ± SD (ms)		Mean Difference ± SEM (ms)	Significance (difference)
			2a	2b		
Z	**Start**	30	66 ± 18	66 ± 16	0.5 ± 1.0	NS
	Min.	30	262 ± 29	262 ± 29	0.0 ± 1.0	NS
	End	28	507 ± 40	507 ± 40	0.3 ± 1.2	NS
	2nd min.	23	644 ± 48	641 ± 47	-3.1 ± 1.4	P < 0.05
-dZ/dt	**Foot**	30	91 ± 18	90 ± 20	-0.8 ± 0.8	NS
	1st peak	30	189 ± 15	190 ± 14	0.6 ± 0.7	NS
	End	30	446 ± 26	446 ± 27	0.0 ± 1.1	NS
	2nd peak	21	614 ± 35	614 ± 35	0.2 ± 1.3	NS

The Bland-Altman plots for the within-session repeatability of the features from the impedance Z and -dZ/dt are shown in Figure 5-8. Except the 2nd minimum point on Z had the mean difference line 3.1 ms below the 0 level, the mean difference lines of other times were close to the 0 level . Points located within the region between the 95% limits of agreement lines confirmed the good repeatability showed by the paired t-test results.

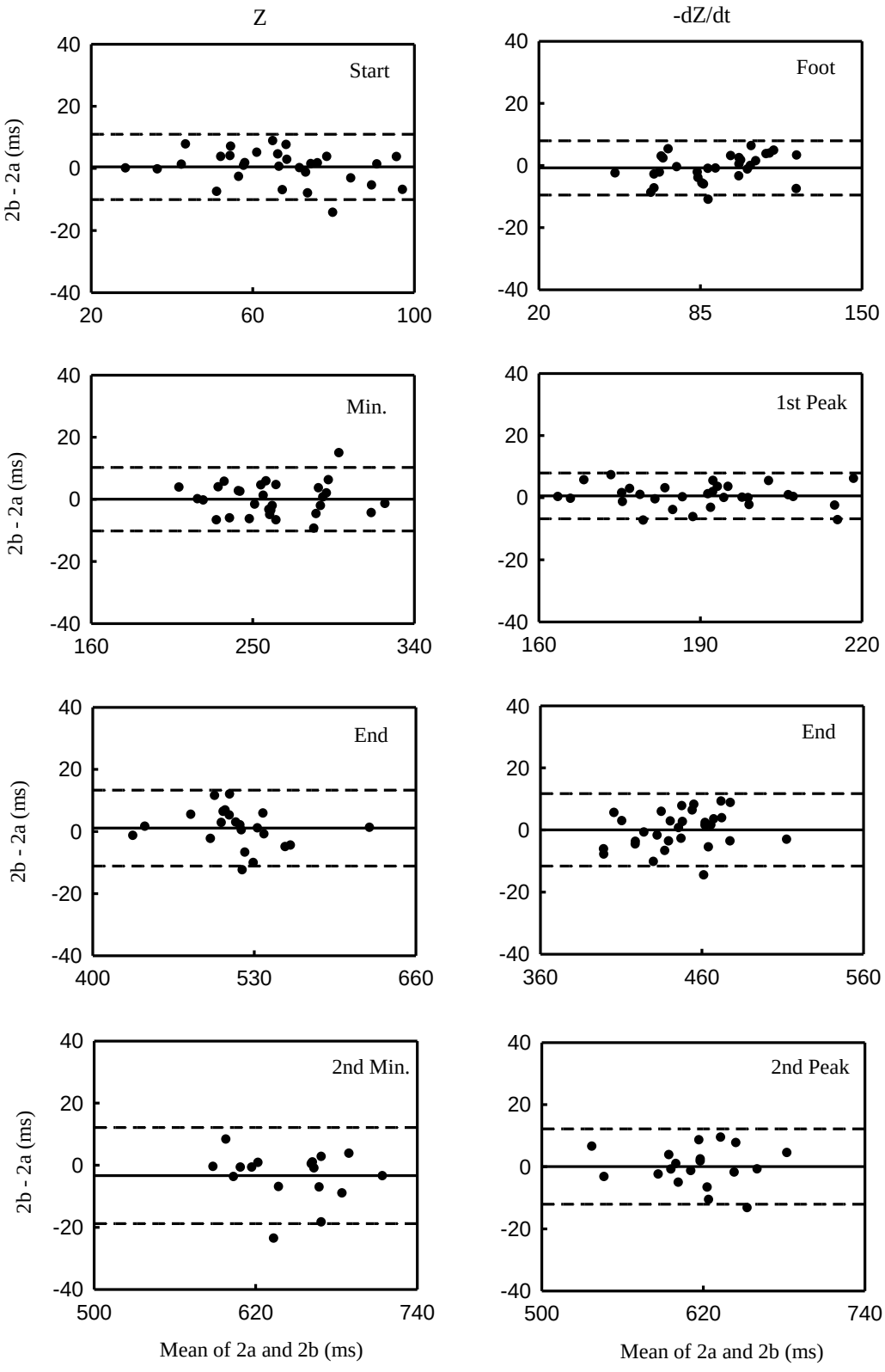

Figure 5-8. Within-session repeatability through Bland-Altman plots for impedance feature identification from the repeat recordings within session 2.

The repeatability of the time feature identification on the ear and finger pulse waveform is provided in Table 5-7. Good quality ear pulses were available on only 24 subjects. The notch point and diastolic peak were identifiable on 23 subjects. There was no significant difference between the recordings for the foot, notch point and diastolic peak identification, but for the systolic peak ($P < 0.05$), the mean difference was small at -3 ms. For the finger pulse, while the foot, systolic peak and notch point were obtained from all the studied 30 subjects, the diastolic peak was obtainable on only 21 subjects. The notch point identification provided the maximum mean difference 1.7 ms. There was no significant difference found between the recordings for any of the 4 features.

Table 5-7. Repeatability of feature identification on ear and finger pulses within session 2.

Signals	Features	Subject numbers	Mean ± SD (ms)		Mean Difference ± SEM (ms)	Significance (difference)
			2a	2b		
Ear pulse	**Foot**	24	162 ± 17	162 ± 19	-0.6 ± 0.7	NS
	Systolic peak	24	420 ± 43	417 ± 42	-3.0 ± 1.3	P < 0.05
	Notch	23	483 ± 34	483 ± 33	-0.1 ± 1.7	NS
	Diastolic peak	23	574 ± 63	572 ± 64	-1.8 ± 2.5	NS
Finger pulse	**Foot**	30	204 ± 18	205 ± 18	0.2 ± 0.6	NS
	Systolic peak	30	394 ± 59	394 ± 59	0.2 ± 1.3	NS
	Notch	30	557 ± 38	559 ± 34	1.7 ± 2.3	NS
	Diastolic peak	21	634 ± 45	633 ± 45	-0.8 ± 2.6	NS

The Bland-Altman plots for the between-recording repeatability of the features from the ear and finger pulses are shown in Figure 5-9, from which the good repeatability between the two recordings were visualized.

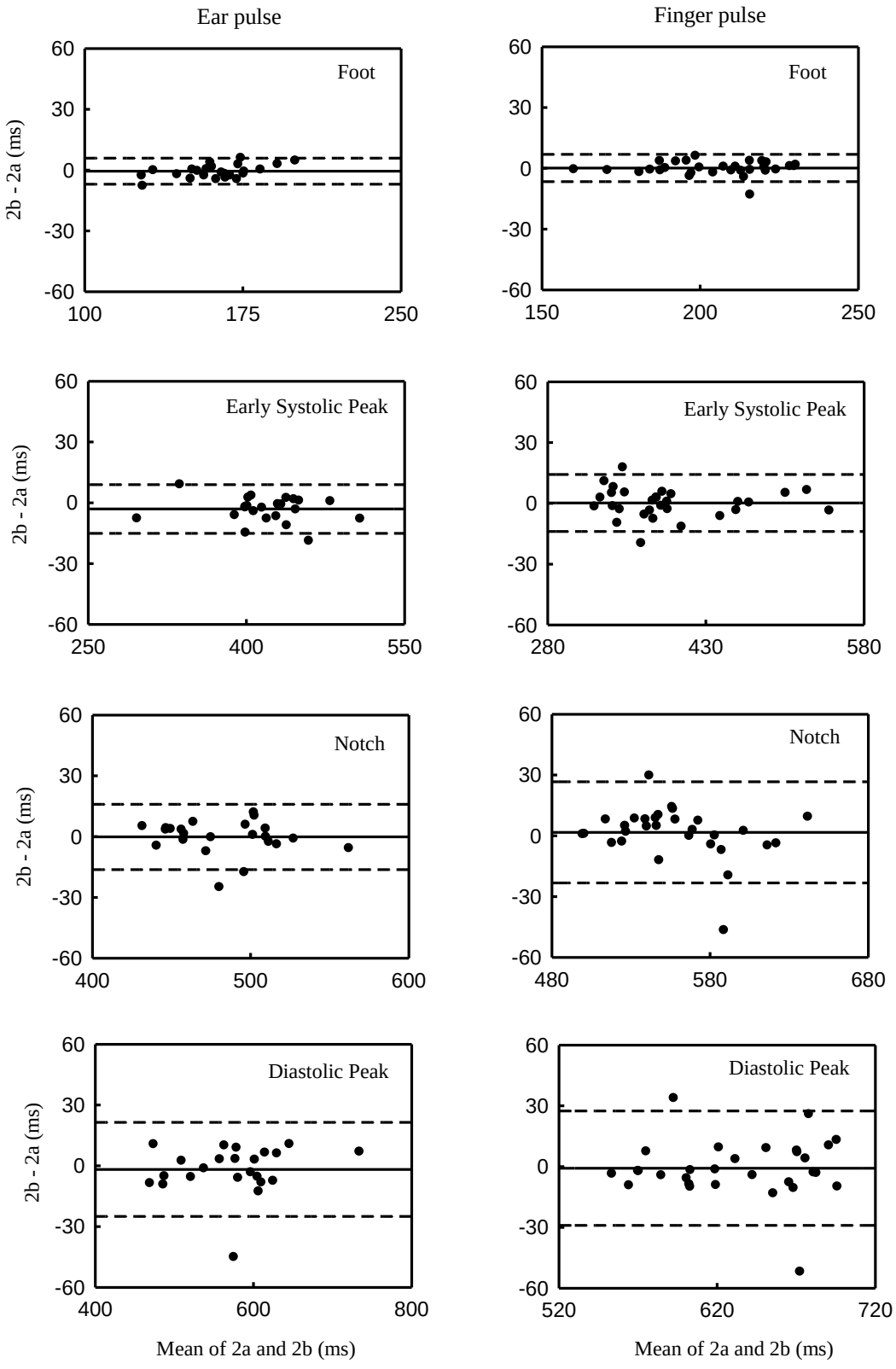

Figure 5-9. Within-session repeatability through Bland-Altman plots for the ear and finger pulse feature identification from the repeat recordings within session 2.

An example of the identified time features on the simultaneous ECG, impedance and pulses from one subject within the 2nd session is shown in Figure 5-10. The average RR interval across the two repeat recordings was 986 ms, with a SD of 30 ms. The 2nd peak on the derivative impedance provided the second largest variance, with a SD of 23 ms. The smallest variance was from the ECG T wave peak, with a SD of 3 ms.

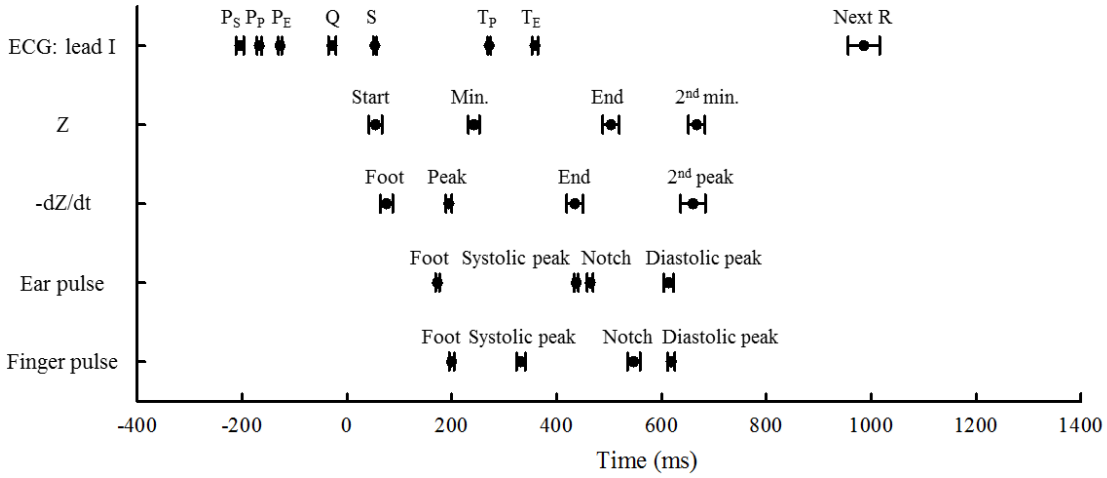

Figure 5-10. An example of the times identified on simultaneous ECG lead I, impedance Z, -dZ/dt, ear pulse and finger pulse for one subject within session 2. The circle presents the mean and the error bar presents the SD of the feature identification on all beats from the repeat recordings in the session.

5.4.3 Session 3: Echocardiograms with simultaneous physiological recordings

Within session 3, the echocardiograms were simultaneously recorded with ECGs, impedance Z , -dZ/dt and finger pulse.

The repeatability of ECG time feature identification on lead I of the ECG recordings within session 3 is summarized in Table 5-8. The mean difference of the RR intervals between the two repeat recordings was 10.9 ms (SEM: 6.9 ms). The mean differences of the other times ranged from -2.3 to 1.8 ms. According to the paired t-test results, the P wave start, Q wave and T peak identification had statistically significant differences between the recordings (all $P < 0.05$), with the mean differences within 3 ms.

Table 5-8. Repeatability of feature identification on the ECG lead I within session 3.

Features	Subject numbers	Mean ± SD (ms)		Mean Difference ± SEM (ms)	Significance (difference)
		3a	3b		
P_S	30	-211 ± 22	-214 ± 23	-2.3 ± 0.9	P < 0.05
P_P	30	-153 ± 22	-152 ± 24	-0.8 ± 0.6	NS
P_E	30	-104 ± 22	-104 ± 23	0.0 ± 1.0	NS
Q	30	-37 ± 6	-38 ± 6	-0.7 ± 0.2	P < 0.05
S	30	48 ± 7	48 ± 7	-0.2 ± 0.4	NS
T_P	30	269 ± 26	271 ± 27	2.2 ± 0.8	P < 0.05
T_E	30	357 ± 32	358 ± 32	1.2 ± 0.9	NS
Next R	30	1034 ± 149	1045 ± 145	10.9 ± 6.9	NS

The repeatability of time features from the valve movement and blood flow is provided in Table 5-9. The aortic opening and closure points were only measurable on 27 subjects and 29 subjects respectively, the other features were available on all 30 subjects. The mean differences of the features from the two recordings ranged from -3.6 to 4.3 ms. The mitral valve maximum opening time during the ventricular passive filling phase had the minimum absolute mean difference -0.1 ms (SEM: 1.9 ms), and the aortic valve closure time has the maximum absolute mean difference 4.3 ms (SEM: 2.1 ms). Besides the aortic valve closing time ($P < 0.05$), the mitral valve opening time during the active filling phase also was significantly different between the two recordings (Mean difference ± SEM: -2.8 ± 1.0 ms, $P < 0.05$).

The Bland-Altman plots for the within-session repeatability of the feature identification from the valve movement and blood flow are shown in Figure 5-11 to 5-14. For all imaging features, the mean difference lines were located close to the 0 level, and most pairs of difference against mean located in the narrow region between the 95% limits of agreement lines were distributed along the mean difference lines, which visualized the good repeatability of the imaging feature identification.

Table 5-9. Repeatability of feature identification on images within session 3.

Features		Subject numbers	Mean ± SD (ms)		Mean Difference ± SEM (ms)	Significance (difference)
			3a	3b		
Aortic and mitral valve movement						
MV (atrial contraction)	*Open*	30	-142 ± 27	-144 ± 27	-2.8 ± 1.0	P < 0.05
	Max. opening	30	-92 ± 21	-93 ± 23	-1.1 ± 1.3	NS
	Close	30	5 ± 15	6 ± 16	1.2 ± 1.1	NS
MV (passive filling)	*Open*	30	421 ± 30	424 ± 30	2.1 ± 1.7	NS
	Max. opening	30	497 ± 36	497 ± 35	-0.1 ± 1.9	NS
	Close	30	663 ± 48	667 ± 45	3.7 ± 3.2	NS
AV	*Open*	27	40 ± 11	38 ± 10	-2.3 ± 1.5	NS
	Close	29	368 ± 24	372 ± 26	4.3 ± 2.1	P < 0.05
Aortic and mitral flow						
MF (atrial contraction)	*Start*	30	-127 ± 24	-129 ± 24	-2.4 ± 1.9	NS
	Peak	30	-67 ± 20	-69 ± 20	-1.9 ± 1.0	NS
	End	30	-3 ± 16	0 ± 15	2.7 ± 1.6	NS
MF (passive filling)	*Start*	30	440 ± 33	441 ± 35	1.4 ± 2.5	NS
	Peak	30	528 ± 37	529 ± 37	1.2 ± 2.7	NS
	End	30	694 ± 47	695 ± 41	1.1 ± 5.8	NS
AF	*Start*	30	52 ± 13	53 ± 12	0.5 ± 1.3	NS
	Peak	30	151 ± 21	147 ± 21	-3.6 ± 1.9	NS
	End	30	362 ± 24	362 ± 26	0.2 ± 2.4	NS

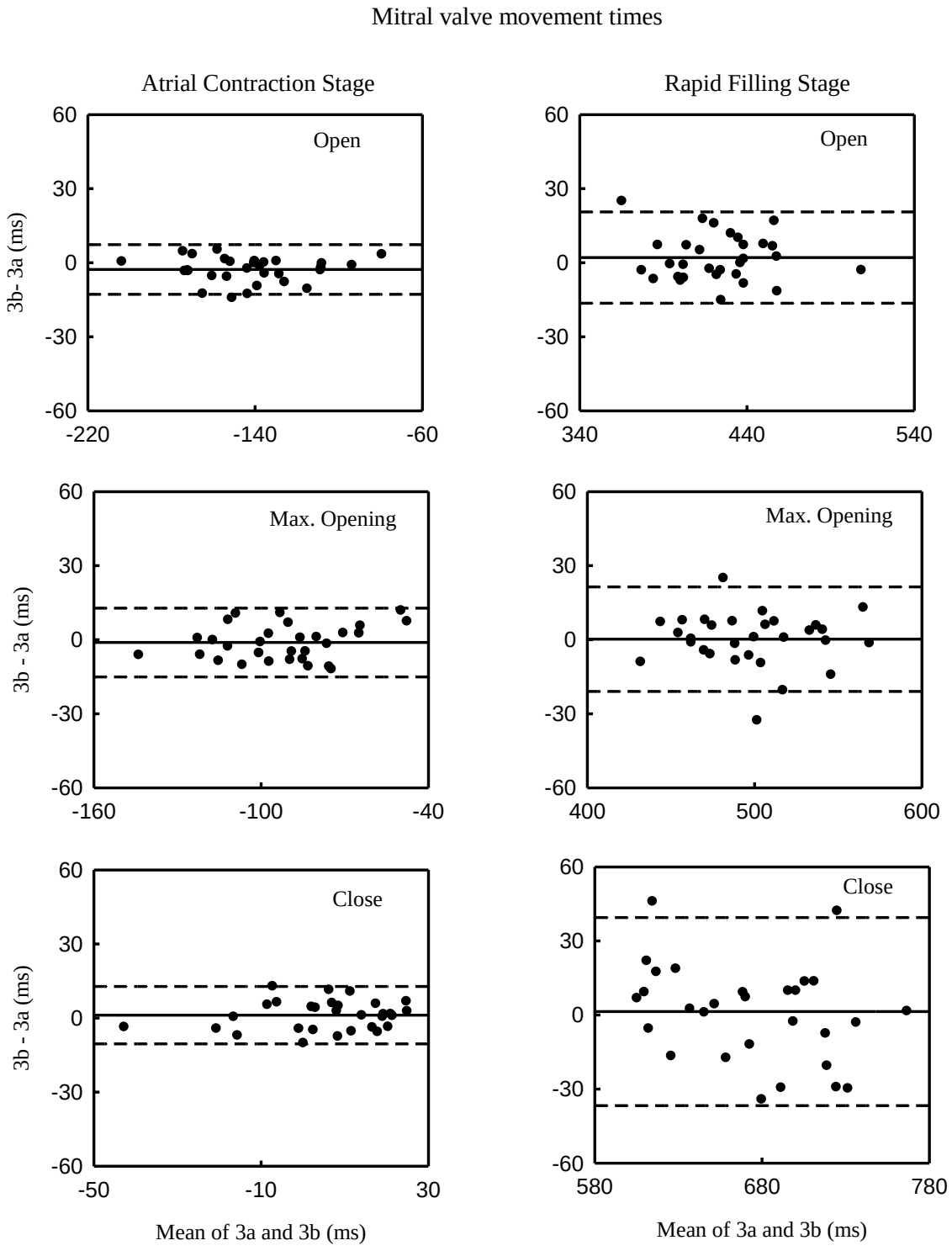

Figure 5-11. Within-session repeatability through Bland-Altman plots for the mitral valve opening, maximum opening and closing times during both atrial contraction (left panel) and ventricular passive filling (right panel) stages. The times were obtained from the repeat recordings within session 3.

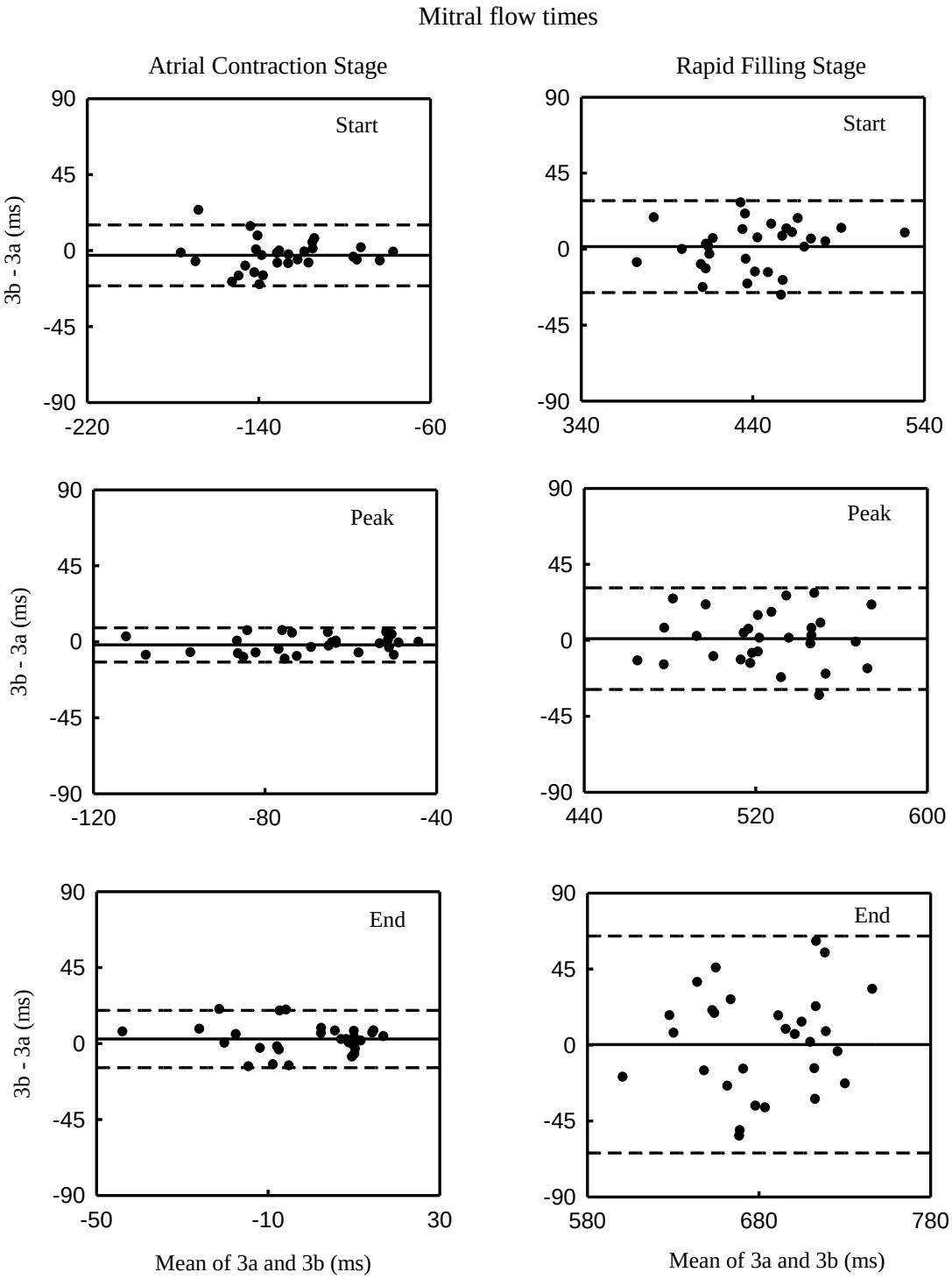

Figure 5-12. Within-session repeatability through Bland-Altman plots for the mitral flow start, peak and end times during both atrial contraction (left panel) and ventricular passive filling (right panel) stages. The times were obtained from the repeat recordings within session 3.

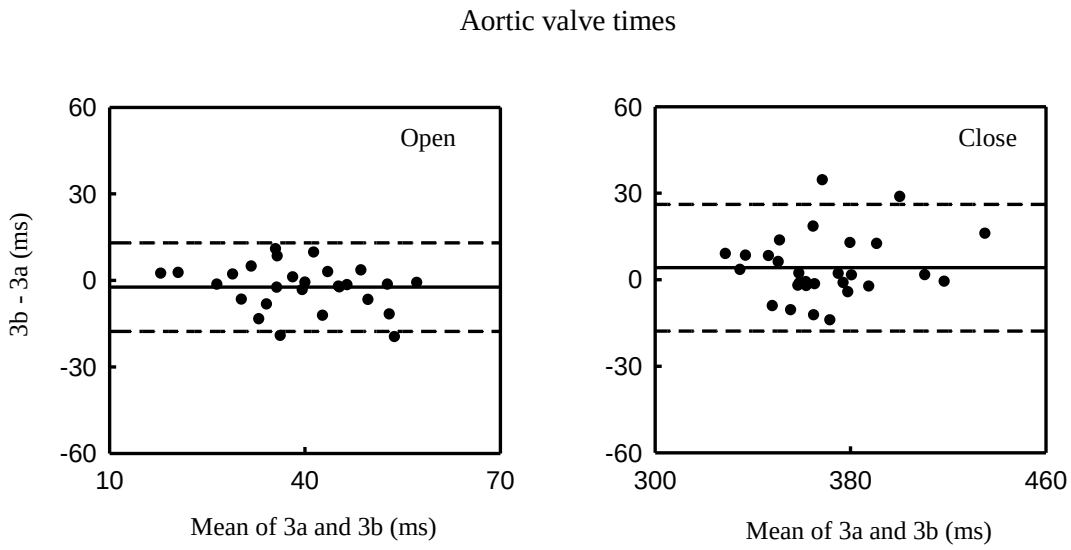

Figure 5-13. Within-session repeatability through Bland-Altman plots for the aortic valve opening and closing times, which were obtained from the repeat recordings within session 3.

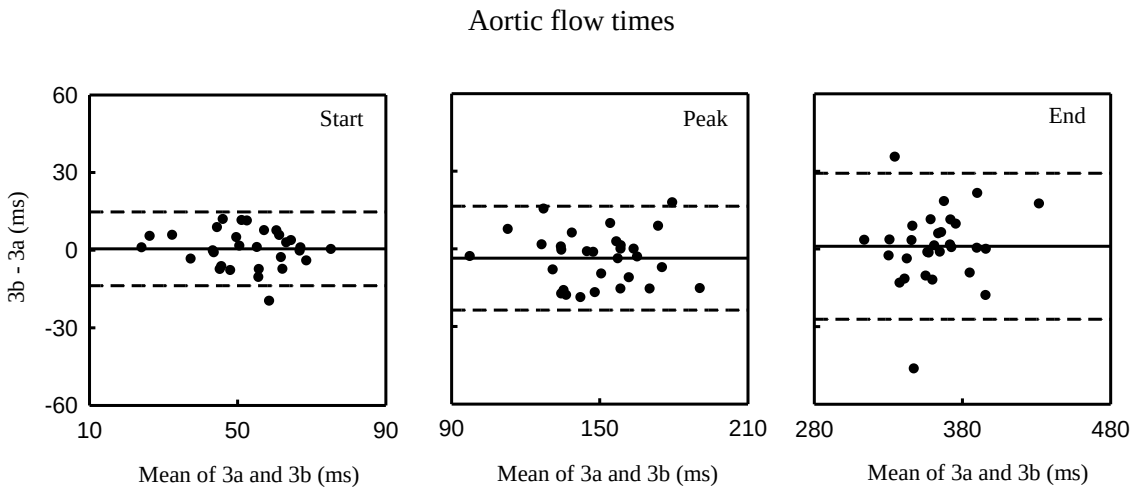

Figure 5-14. Within-session repeatability through Bland-Altman plots for the aortic flow start, peak and end times, which were obtained from the repeat recordings within session 3.

The repeatability of time feature identification on the impedance recordings within session 3 is provided in Table 5-10. The 2nd minimum point on the impedance Z was the only feature with significant difference between the recordings (Mean difference ± SEM: 3.8 ± 1.8 ms, $P < 0.05$).

Table 5-10. Repeatability of feature identification on the impedance within session 3.

Signals	Features	Subject numbers	Mean ± SD (ms)		Mean Difference ± SEM (ms)	Significance (difference)
			3a	3b		
Z	**Start**	30	66 ± 15	64 ± 15	-1.4 ± 1.1	NS
	Min.	30	260 ± 23	261 ± 23	0.5 ± 1.4	NS
	End	28	505 ± 41	508 ± 42	2.3 ± 1.7	NS
	2nd min.	23	641 ± 49	644 ± 50	3.8 ± 1.8	$P < 0.05$
-dZ/dt	**Foot**	30	87 ± 21	89 ± 21	1.7 ± 1.1	NS
	1st peak	30	189 ± 12	189 ± 12	-0.1 ± 0.8	NS
	End	30	448 ± 26	447 ± 28	-0.2 ± 1.5	NS
	2nd peak	21	611 ± 34	615 ± 34	4.3 ± 2.1	NS

The repeatability of time feature identification on the finger pulse recordings is provided in Table 5-11. Significant difference was found for the notch point identification between the recordings (Mean difference ± SEM: 5.0 ± 2.2 ms, $P < 0.05$).

Table 5-11. Repeatability of feature identification on finger pulse within session 3.

Features	Subject numbers	Mean ± SD (ms)		Mean Difference ± SEM (ms)	Significance (difference)
		3a	3b		
Foot	30	200 ± 18	201 ± 19	1.1 ± 0.9	NS
Systolic peak	30	386 ± 65	390 ± 63	3.7 ± 2.5	NS
Notch	30	547 ± 31	552 ± 31	5.0 ± 2.2	$P < 0.05$
Diastolic peak	30	628 ± 44	631 ± 47	2.4 ± 2.3	NS

Figure 5-15 shows an example of the time feature identification on images and simultaneous physiological measurements from one subject within session 3. The times of the mitral valve movement and flow conditions during the active filling phase, the aortic valve movement and flow conditions during the ventricular ejection phase and the mitral valve movement and flow conditions during the ventricular passive filling phase are displayed in sequence. The average RR interval across the session was 1108 ms (SD: 70 ms). The largest variance of the imaging feature identification was from the mitral valve closure time during the passive filling phase (SD: 17 ms), while the smallest variance of the imaging features was from the mitral flow ending during the active filling phase (SD: 5 ms).

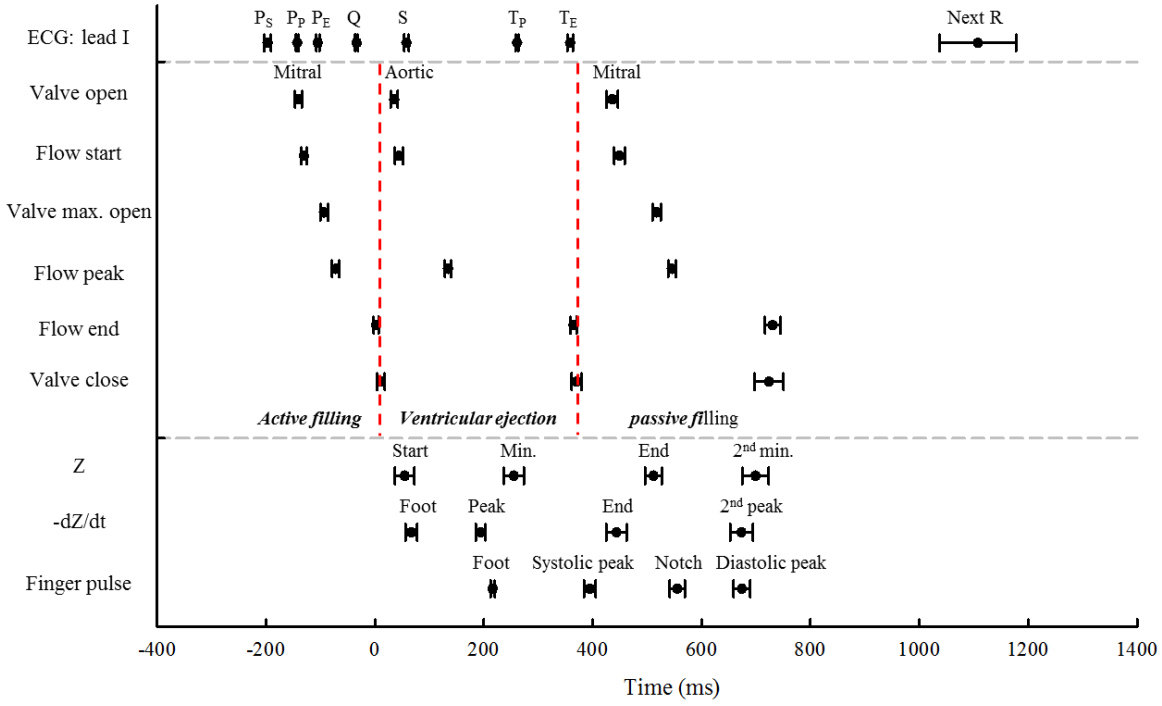

Figure 5-15. An example of the times identified on images and simultaneous ECG lead I, impedance Z, -dZ/dt and finger pulse from one subject within session 3. The times of the mitral valve movement and flow conditions during the active filling phase, the aortic valve movement and flow conditions during the left ventricular ejection phase and the mitral valve movement and flow conditions during the ventricular passive filling phase are displayed according to the time sequence. The circle presents the average value and the error bar presents the SD of the values of all beats from the two repeat recordings.

In summary, according to the within-session repeatability assessment results, most features identified from the two repeat recordings within the same session provided good repeatability. Among these features with a statistically significant difference, the maximum mean difference between the recordings was from the finger pulse notch point identification within session 3 (Mean difference ± SEM: 5.0 ± 2.2 ms, $P < 0.05$). This small difference was not considered as clinically significant. Therefore, when assessing the between-session repeatability in the following section, the average values from the two recordings within the same session were calculated and then compared.

5.5 Between-session repeatability

5.5.1 ECG recordings from session 1, 2 and 3

The ECG lead I was recorded within all the three sessions. Time features were identified on all these recordings. The repeatability of the feature identification across the sessions is summarized in Table 5-12. Because the average RR interval gradually increased from 1016 ms in the first session to 1040 ms in the last session, the effects of this change were studied. Corrections were made for the feature times identified in session 2 and 3 by multiplying the ratio of average RR interval within the session to that within session 1. The corrected values with comparison results are also summarized in the table.

Before the correction, while the RR intervals within the three sessions were not significantly different, the changes in RR interval caused significant influence on most ECG feature times, including P wave start and peak (P_S and P_E), Q, T wave peak and end (T_P and T_E) (all $P < 0.05$). The mean difference of the T_E between session 1 and 3 was as large at 7.3 ms (SEM: 2.3 ms, $P < 0.05$).

After the correction, the RR interval changing influence was alleviated. According to the paired t-test results, only the corrected P_E and Q from session 3, S wave from session 2 showed statistically significant differences with the values from session 1 (all $P < 0.05$), but the mean differences were smaller than 3 ms. According to the further ANOVA test results, only the Q wave was significant different across the three sessions ($P < 0.05$).

Table 5-12. Repeatability of time feature identification on ECG lead I on the recordings from session 1, 2 and 3.

Times	Original values					ANOVA test results	Corrected values				ANOVA test results
	Mean ± SD (ms)			Mean Difference ± SEM (ms)			Mean ± SD (ms)		Mean Difference ± SEM (ms)		
	S1	S2	S3	S2 – S1	S3 – S1		S2†	S3†	S2† – S1	S3† – S1	
P_S	-207 ± 21	-207 ± 22	-212 ± 23	-0.8 ± 0.6	-5.7 ± 1.5*	P < 0.05	-205 ± 22	-207 ± 23	2.2 ± 1.9	-0.6 ± 2.2	NS
P_P	-151 ± 21	-152 ± 22	-153 ± 23	-1.4 ± 0.7*	-2.3 ± 0.9*	P < 0.05	-150 ± 22	-149 ± 24	0.6 ± 1.3	1.4 ± 1.7	NS
P_E	-105 ± 22	-106 ± 21	-104 ± 22	-1.1 ± 0.5*	0.8 ± 0.9	NS	-105 ± 21	-102 ± 24	0.4 ± 1.0	3.0 ± 1.4*	NS
Q	-38 ± 6	-39 ± 6	-37 ± 6	-0.5 ± 0.4	0.9 ± 0.3*	P < 0.05	-38 ± 6	-37 ± 6	0.0 ± 0.6	1.8 ± 0.6*	P < 0.05
S	47 ± 6	46 ± 6	48 ± 7	-1.3 ± 0.3**	0.7 ± 0.9	NS	45 ± 7	47 ± 7	-1.9 ± 0.4*	-0.4 ± 1.0	NS
T_P	265 ± 25	267 ± 27	270 ± 27	2.3 ± 0.8*	4.8 ± 1.5*	P < 0.05	263 ± 27	264 ± 31	-1.6 ± 1.9	-1.2 ± 2.0	NS
T_E	351 ± 31	351 ± 33	358 ± 32	0.3 ± 1.2	7.3 ± 2.3*	P < 0.05	346 ± 31	350 ± 38	-4.4 ± 2.8	-0.8 ± 2.5	NS
Next R	1016 ± 151	1032 ± 162	1040 ± 146	15.6 ± 9.3	23.9 ± 11.8	NS	1016 ± 151	1016 ± 151	0.0 ± 0.0	0.0 ± 0.0	NS

†: Corrected values by the ratio of RR interval in the current session to RR interval in session 1; *: Significant difference with P < 0.05 when compared with the values from the session 1.

5.5.2 Impedance and finger pulse recordings from session 2 and 3

The impedance Z and -dZ/dt were recorded within session 2 and 3. The repeatability of the feature identification from the two sessions is provided in Table 5-13. The largest absolute mean difference between the sessions was from foot identification on the -dZ/dt waveform, which was 2.4 ms. No significant difference was found for any feature, which indicated good repeatability for the impedance feature identification between the sessions.

Finger pulse was also recorded within session 2 and 3. The repeatability of the feature identification from the two sessions is provided in Table 5-13. The largest absolute mean difference between the sessions was 8.4 ms resulted from the notch point identification, which caused a significant difference ($P < 0.05$). The pulse foot was also significantly different ($P < 0.05$) between the sessions, with mean difference -3.7 ms.

Table 5-13. Repeatability of feature identification on impedance and finger pulse within session 2 and 3.

Features		**Subject number**	**Mean ± SD (ms)**		**Mean Difference ± SEM (ms)**	**Significance (difference)**
			S2	**S3**		
Z	**Start**	30	66 ± 17	65 ± 15	-1.2 ± 1.1	NS
	Min.	30	262 ± 29	261 ± 23	-1.1 ± 2.2	NS
	End	28	507 ± 40	506 ± 41	-0.3 ± 2.9	NS
	2nd min.	23	642 ± 47	643 ± 50	0.2 ± 2.2	NS
-dZ/dt	**Foot**	30	91 ± 19	88 ± 21	-2.4 ± 1.6	NS
	1st peak	30	190 ± 15	189 ± 12	-1.1 ± 1.0	NS
	End	30	446 ± 26	448 ± 26	1.6 ± 2.1	NS
	2nd peak	21	614 ± 35	613 ± 34	-0.5 ± 2.5	NS
Finger pulse	**Foot**	30	205 ± 18	201 ± 18	-3.7 ± 1.2	P < 0.05
	Systolic peak	30	394 ± 59	388 ± 63	-6.0 ± 3.7	NS
	Notch	30	558 ± 35	549 ± 30	-8.4 ± 2.9	P < 0.05
	Diastolic peak	30	633 ± 45	630 ± 45	-3.7 ± 2.3	NS

In summary, according to the within-session repeatability assessment results, most feature times from images and physiological measurements had good repeatability. Significant difference was only found on a few features, with mean difference within 5 ms. However, because of the continuous increase in RR interval although not significant across the three sessions, between-session repeatability was poorer than the within-session repeatability. Significant differences were found on ECG and finger pulse features from different sessions. Therefore, in the further analysis in this study, the values of each time feature from the repeat recordings in the same session were combined. However, the values from different sessions were displayed and analysed separately.

5.6 An example of timing sequence of cardiovascular events

An example of the timing sequence of cardiovascular events, reconstructed with feature times on the imaging and physiological recordings from one subject, is illustrated in this section. The feature times from the three sessions were displayed in three parallel panels separately. For each feature, the average and SD of the values obtained from the repeat recordings within the same session were taken. The reconstructed timing sequence is shown in Figure 5-16. In this example, the average RR intervals increased from 1109 ms (SD: 73 ms) in the first session to 1208 ms (SD: 47 ms) in the last session.

The top panel shows the ECG timing sequence based on the data from session 1. The P-QRS-T wave sequence was reconstructed with the times identified on lead I, and the T wave sequence was also reconstructed with times identified on the lead with the largest T wave (lead max). The details of the times are summarized as following:

- the P wave identified on lead I started 174 ms and reached the peak 112 ms before the R wave. The whole duration of the P wave was 102 ms;
- the QRS complex identified on lead I started at 39 ms before the R wave, and ends at 45 ms, with a duration of 84 ms;
- the T wave peak on lead I occurred at 284 ms, which was later than that on the lead with the largest T wave (256 ms). The end of the T wave identified on lead I (372 ms) was also slightly later than that on the largest T wave (361 ms). The decreasing

duration of T wave on lead I was 18 ms shorter than that of the largest T wave (88 ± 6 ms vs. 105 ± 3 ms, $P < 0.001$);

The middle panel of the Figure 5-16 illustrates the sequence of times from the simultaneously recorded ECGs, impedance and pulses within session 2. The details of the sequence are summarized as following:

- the thoracic impedance started to fall at 91 ms, which was after the ECG S wave (42 ms), and achieved the minimum (Min.) at 289 ms, which was almost at the same time with the ECG T wave peak (289 ms). The impedance then rose up and ended at 510 ms. The minimum of the diastolic wave (2^{nd} min.) was observed at 669 ms;
- as expected, the foot of the first derivate impedance -dZ/dt was observed (101 ms) soon after the start of impedance falling during systole. The peak of the systolic wave was observed (203 ms) before the minimum impedance point and its end point observed 70 ms before the systolic end of impedance Z. The 2^{nd} peak of -dZ/dt was observed at 633 ms, before the 2^{nd} minimum point of Z;
- the foot of the ear pulse occurred at 174 ms, which was 56 ms before the foot of the finger pulse. Because of the shape difference, the dominant systolic peak on the ear pulse (445 ms) was seen later than that on the finger pulse (393 ms). The notch point (475 ms) and the diastolic peak (629 ms) on the ear pulse preceded the corresponding features on the finger pulse by 83 ms and 39 ms respectively.

The sequence of times obtained from the images and simultaneous physiological signals within session 3 are illustrated in the bottom panel of the Figure 5-13. The valve movements and corresponding blood flow conditions during the active filling phase, ventricular ejection phase and passive filling phase were connected by connection lines. The time sequence of these three phases is as following:

- the active filling phase started with the mitral valve opening 67 ms after the start of the ECG P wave, and finished with the mitral valve closing 25 ms after the ECG R wave;
- the left ventricular ejection phase then started with the aortic valve opening 87 ms after the ECG Q wave, and ended with the valve closing at 377 ms, which was right before the ECG T wave end (390 ms);

- the passive filling phase started with the mitral valve opening 47 ms later than the aortic valve closing, and ended with the mitral flow stopping at 669 ms.

5.7 Discussion and conclusions

The within-session repeatability and between-session repeatability of time features identification on the recordings from the three sessions were assessed in this chapter. Both the imaging and physiological time features showed good repeatability between the repeat recordings within the same session. There was no significant difference found on most features. For the ECG P wave end and T wave end, and the 2nd minimum point on the impedance Z waveform, significant difference was found between the values from the repeat recordings. However, because all the mean differences between the recordings were less than 5 ms, they were not considered as clinically significant. This allowed the combination of the values from the repeat recordings for each time feature. On the other hand, significant difference usually found when comparing the time features from different sessions, especially on the ECG and finger pulse features. The alleviation of the significant difference on ECG times after the correction by RR intervals indicated that the difference was mainly caused by the heart rate changes across the sessions. Based on these observations, time features from different sessions were analysed separately in this study.

Timing sequence of cardiovascular events was demonstrated with the data from one subject. The times from the three sessions were displayed in three parallel panels, and briefly described separately.

In the following chapter, the details of dynamic relations between the valve movements and corresponding blood flow conditions are described. The relationships between the imaging features with the impedance features and pulse features is investigated in Chapter 7 and Chapter 8 respectively.

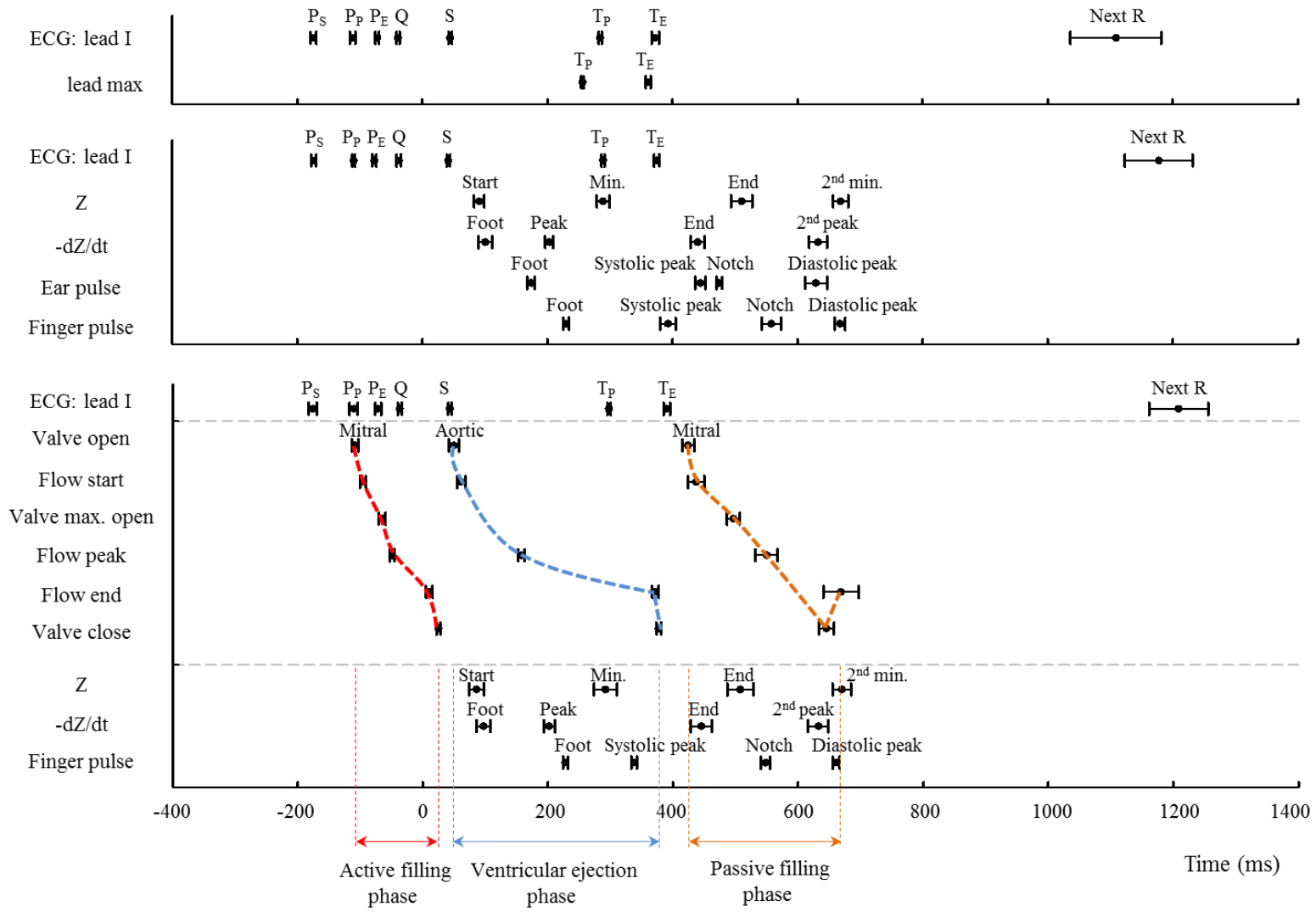

Figure 5-16. An example of the timing sequence of cardiovascular events from one subject. The plots from the top to the bottom showed the data from session 1 to 3. The circle presents the mean and error bar presents SD of the values of all beats from the repeat recording within the same session. On the bottom panel, the valve movements and the corresponding blood flow conditions during the ventricular active filling, left ventricular ejection and passive filling phases were connected by the red, blue and brown lines in sequence.

Chapter 6 Dynamic relations between valve movement and blood flow and ECG

The dynamic relation of valve movements with corresponding blood flow conditions and ECG features are described in this chapter.

6.1 Introduction

Cardiac mechanical functions are initiated by electrical activity. The atrial depolarization stimulates atrial myocardial contraction, and results in active filling of the ventricles. Afterwards, the ventricular depolarization stimulates ventricular contraction, which makes the blood eject from the ventricles into the arterial system. Following the repolarization of the ventricles, the ventricular myocardium relaxes and then passive filling of the ventricles starts, driven by the pressure gradient between the atria and ventricles. During these three ventricular filling and ejecting phases, cardiac valves open to allow the blood to flow from one chamber to another, or to the aorta.

In this chapter, the timing sequence of the mitral and aortic valve movement (open, maximum opening and close) and corresponding blood flow conditions (start, peak and end) during the active filling, ventricular ejection and passive filling phases are measured. The corresponding durations from the valve movement and blood flow through the valve are compared, and the relationships between them are investigated.

The relation between the valve movement and ECG components are also investigated. The timing sequence of the valve movement features are compared with the corresponding ECG features, and the relationships are investigated.

6.2 Overview of valve movement and blood flow timing sequence

For the study in this chapter, the average values of the two repeat recordings in session 3 were used. The times of the mitral valve and aortic valve movement during the active filling, ventricular ejection and passive filling phases are provided in Table 6-1.

Table 6-1. Times of valve movement and blood flow conditions from the imaging data recorded in session 3 (all times were measured from ECG R wave).

Features		Mean ± SD (ms)
Active ventricular filling phase		
Mitral valve	open	-143 ± 27
	max. opening	-92 ± 22
	close	5 ± 15
Mitral flow	start	-128 ± 24
	peak	-68 ± 20
	end	-1 ± 15
Ventricular ejection phase		
Aortic valve	open	39 ± 10
	close	368 ± 25
Aortic flow	start	52 ± 12
	peak	149 ± 20
	end	362 ± 24
Passive ventricular filling phase		
Mitral valve	open	423 ± 30
	max. opening	497 ± 35
	close	665 ± 46
Mitral flow	start	440 ± 33
	peak	529 ± 36
	end	694 ± 41

The means and SDs of the timing sequence of ECG features, valve movement and blood flow from all the 30 subjects are shown in Figure 6-1. The valve movement and corresponding flow conditions during the active filling phase, left ventricular ejection phase and passive filling phase are connected by three dotted connection lines in sequence. The overview of the sequence is summarized as follows:

- The active filling phase started after the ECG P wave (-212 ms). The mitral valve opened at -143 ms, and achieved the maximum opening at -92 ms. The phase ended with the valve closing at 5 ms. The mitral flow onset was detected at -128 ms, and the peak flow occurred at -68 ms. It ended 6 ms before the valve closed;
- The left ventricular ejection phase started after the ECG Q wave (-37 ms). The aortic valve opened at 39 ms, and closed at 368 ms. The aortic flow started at 52 ms and then kept accelerating till the peak flow at 149 ms. After that it started to decelerate and ended at 362 ms;
- The passive filling phase started after the ECG T wave end (358 ms). The mitral valve opened at 423 ms, followed by the mitral flow onset (440 ms). The valve maximum opening occurred at 497 ms, which was before the peak flow (529 ms). The flow end was observed later than the valve close (694 ms *vs.* 665 ms), indicating that the valve, although it had stopped moving, had not completely closed.

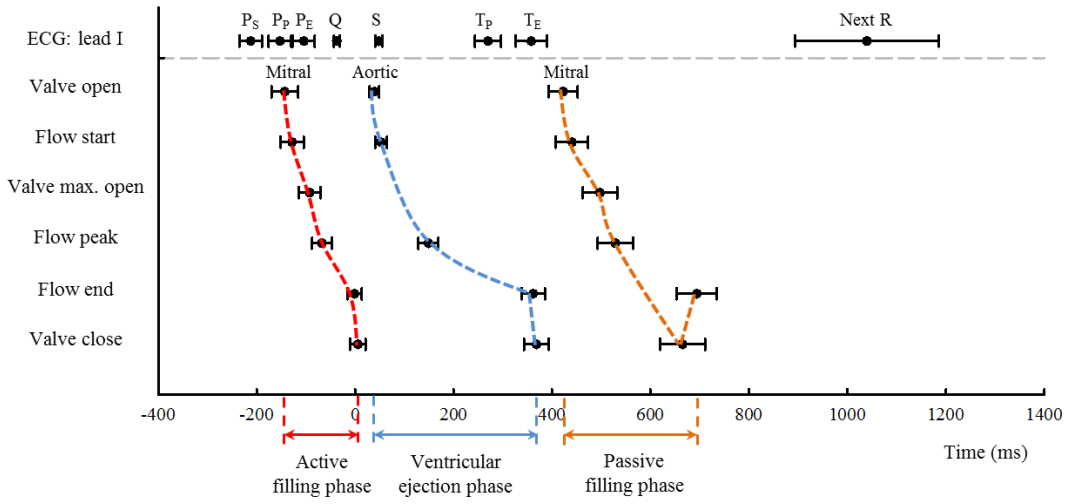

Figure 6-1. Timing sequence of ECG features, valve movement and flow during the active filling, ventricular ejection and passive filling phases. Circles present the means and error bars presents the SDs across the subjects.

The details of the comparison of the ECG times, valve movement and blood flow, and the investigation on the relationships among them are described in the following sections.

6.3 Dynamic relation between valve movement and blood flow

6.3.1 Time difference between valve movement and corresponding flow conditions

The composite diagram of valve movement from M-mode images and blood flow velocity tracing from Doppler images in a cardiac cycle is shown in Figure 6-2.

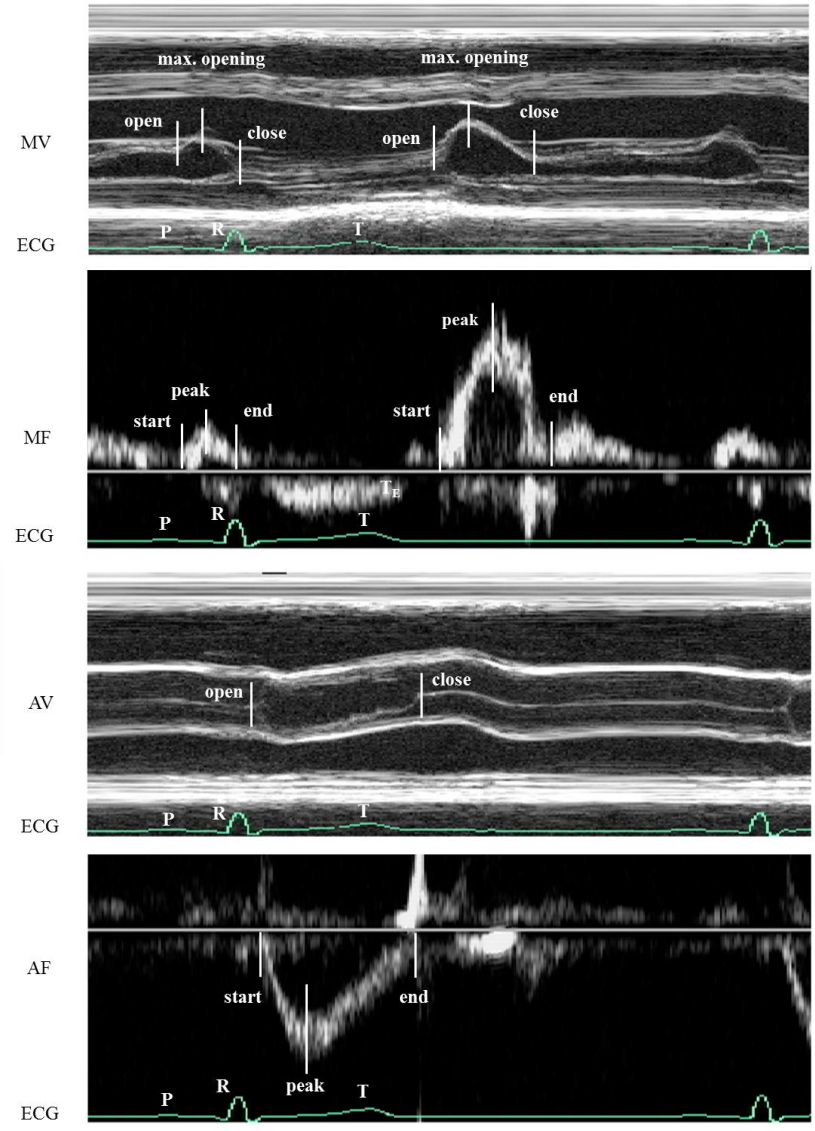

Figure 6-2. Composite diagram of valve movement and blood flow in a cardiac cycle. From top to bottom are mitral valve, mitral flow, aortic valve and aortic flow.

The time difference between valve movement and corresponding flow conditions is summarized in Table 6-2. The valves consistently opened before the onset of flow detection (all $P < 0.001$). The initial opening of the mitral valve occurred 15 ms earlier during the active filling phase and 18 ms earlier during the passive filling phase than when mitral flow was detected. During the ventricular ejection phase, the aortic valve initial opening was 13 ms before the onset of the flow detection.

The maximum opening of the mitral valve preceded the peak mitral flow during both ventricular filling phases (both $P < 0.001$). The time differences between the point of maximal valve opening and peak mitral flow were 25 ms during the active filling phase and 32 ms during the passive filling phase. These striking results showed that the blood flow was still speeding up when the mitral valve had already started to close from the maximum opening.

The complete closure of the valves occurred after the flow ended, but the flow was still detectable when the mitral valve closed incompletely (all $P < 0.001$). Both the mitral valve during the active filling phase and the aortic valve during the ventricular ejection closed 7 ms later than the flow end detection. However, the mitral flow was still detectable 29 ms after the point of the minimal mitral valve opening at the end of passive filling phase.

Table 6-2. Time difference between valve movement and corresponding flow conditions.

Time difference	**Mean difference ± SEM (Range) (ms)**		
	Active filling Mitral	**Ventricular ejection Aortic**	**Passive filling Mitral**
Valve opens to Flow starts	$15 \pm 2^{**}$ (-5, 32)	$13 \pm 2^{**}$ (-5, 30)	$18 \pm 2^{**}$ (-4, 45)
Valve max. opening to Flow peak	$25 \pm 2^{**}$ (11, 72)	N/A	$32 \pm 4^{**}$ (-22, 78)
Flow ends to Valve closes	$7 \pm 1^{**}$ (-2, 19)	$7 \pm 2^{**}$ (-13, 23)	$-29 \pm 5^{**}$ (-104, 4)

**: Significant difference with $P < 0.001$.

6.3.2 Comparison between time durations from valve movement and flow

The comparison between time intervals measured from the valve movement and blood flow is shown in Figure 6-3 and summarized in Table 6-3.

The mitral valve opening durations, measured from the initial opening of the valve to its maximum opening, were always shorter than the corresponding mitral flow accelerating durations, measured from the onset to the peak flow. The valve opening duration during the active filling phase was 51 ms, which was 10 ms shorter than the flow accelerating duration 61 ms ($P < 0.001$). The opening duration during the passive filling phase was 75 ms, which was 14 ms shorter than the flow accelerating duration 88 ms ($P < 0.05$). The lagging of the valve maximum opening behind the peak flow made the valve opening periods shorter than the flow accelerating periods, although the valve opening point occurred before the onset of mitral flow detection.

The mitral closing duration (from the maximum opening point to the closure) was compared with the mitral flow decelerating duration (from the maximum opening point to the closure) for the active ventricular filling phase and passive filling phase. The comparison results were different for different phases. During the active filling, the valve closing duration was 98 ms, which was significantly longer than the flow decelerating duration 66 ms (Mean difference ± SEM: -31 ± 2 ms, $P < 0.001$). However, these two durations were comparable during the passive filling phase (168 ± 22 ms *vs.* 165 ± 27 ms, $P > 0.05$).

The overall mitral valve open duration (from the valve opening to closing) during the active filling phase was longer than the measured flow duration (from the flow start to end) (Mean difference ± SEM: -22 ± 2 ms, $P < 0.001$), while the valve open duration during the passive filling phase was shorter than the flow duration (Mean difference ± SEM: 11 ± 5 ms, $P < 0.05$). This was because the mitral valve closed after the flow offset at the end of active filling, while the flow was still detectable after the valve apparently closed at the end of passive filling phase. The aortic valve opening duration during ventricular ejection was 20 ms longer than the flow duration during the left ventricular ejection phase ($P < 0.001$).

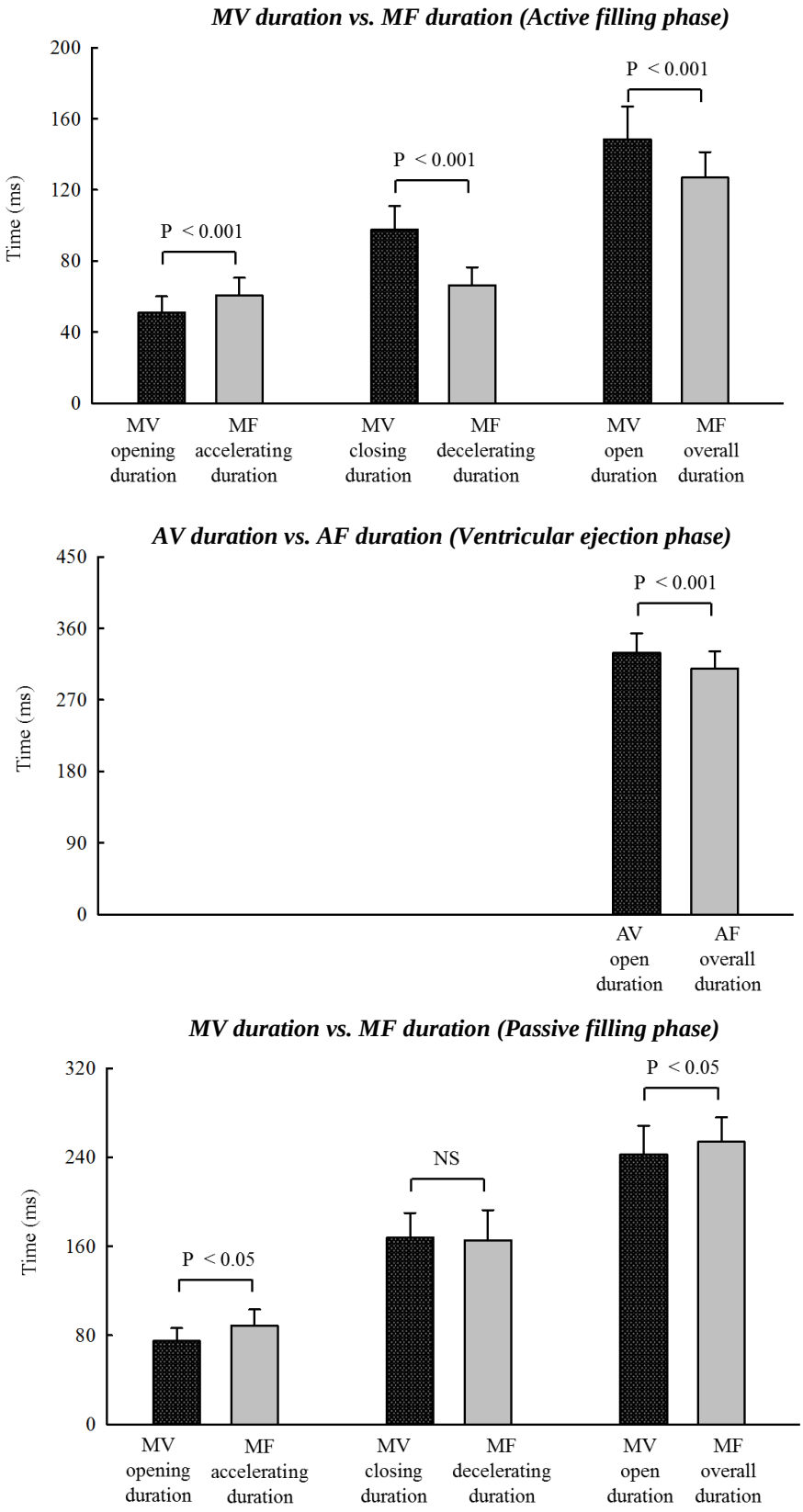

Figure 6-3. Comparison of valve movement and flow durations.

Table 6-3. Comparison between time intervals measured from valve movement and flow.

Durations	Mean difference ± SEM (ms)		
	Active filling Mitral	**Ventricular ejection Aortic**	**Passive filling Mitral**
Valve opening - Flow accelerating	$-10 \pm 2^{**}$	N/A	$-14 \pm 4^{*}$
Valve closing - Flow decelerating	$31 \pm 2^{**}$	N/A	2 ± 5
Valve open duration - Flow overall duration	$22 \pm 2^{**}$	$20 \pm 2^{**}$	$-11 \pm 5^{*}$

*: significant difference with $P < 0.05$; **: Significant difference with $P < 0.001$.

6.3.3 Relationship between time durations from valve movement and flow

Figure 6-4 shows the linear relationship between the valve open durations and corresponding flow overall durations during different phases. The mitral flow duration during the active filling phase showed strong linear relationships with the valve open duration ($R^2 = 0.809$, $P < 0.001$). The aortic flow duration during the left ventricular ejection phase was also strongly related with the aortic valve open duration ($R^2 = 0.754$, $P < 0.001$). These strong relationships during these two phases suggest that the left ventricular active filling duration and ejection duration may be obtained from either M-mode or Doppler images. It can be noted, however, that the flow was still detectable after the valve incomplete closing, and the mitral flow during the passive filling phase showed a relatively weak relationship with the valve open duration ($R^2 = 0.151$, $P < 0.05$).

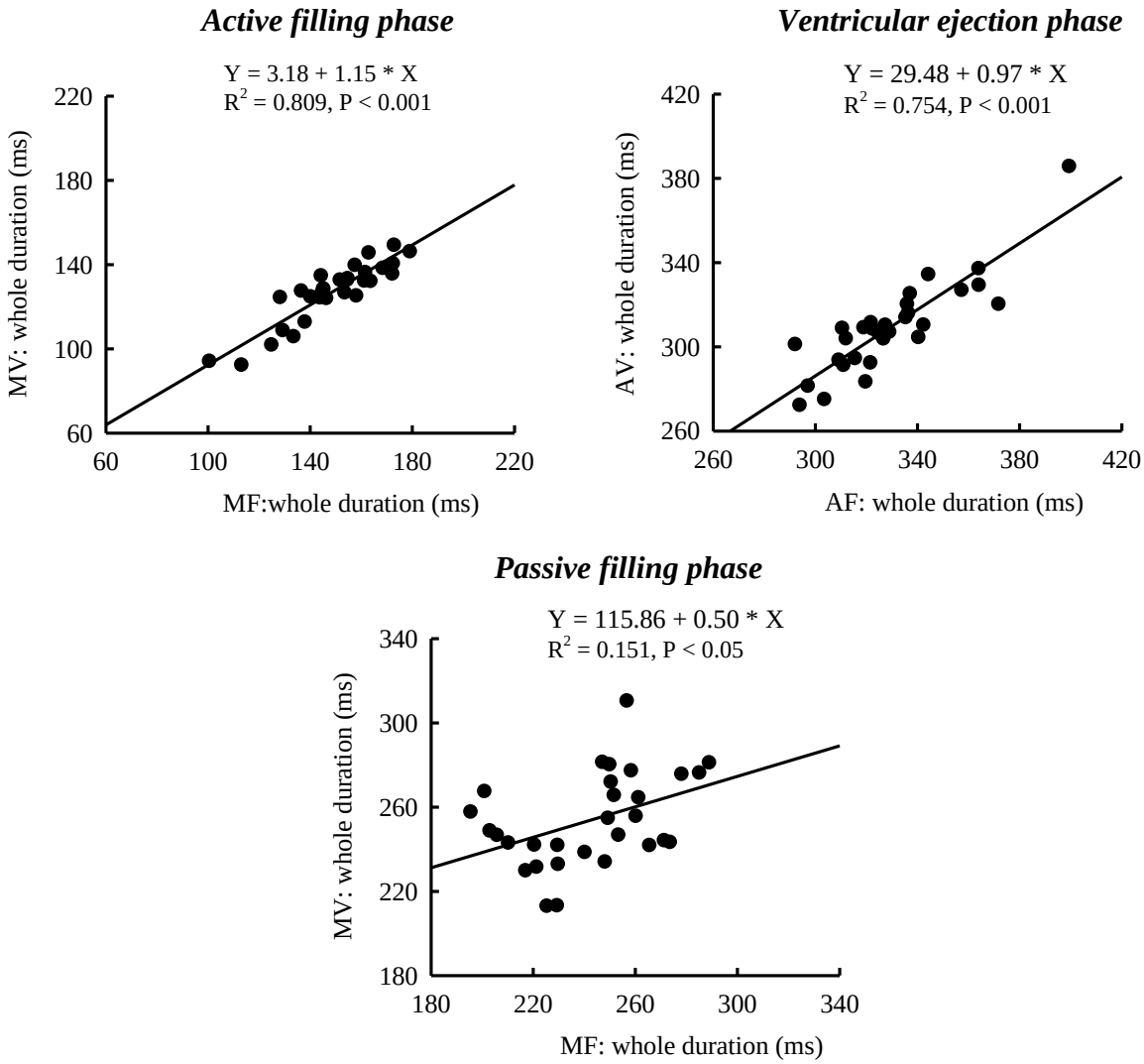

Figure 6-4. Relationship between the valve open durations and flow overall durations during the left ventricular active filling, ejection and passive filling phases.

6.4 Relationships between valve movement and ECG features

6.4.1 Time difference between valve movement and corresponding ECG features

The left ventricular active filling phase is initiated by atrial depolarization. The mitral valve movement times during the active filling phase referred to the ECG P wave onset are illustrated in Figure 6-5. The valve started to open 69 ms after the P wave onset, and achieved the maximum opening 51 ms later. The valve closed 217 ms after the P wave.

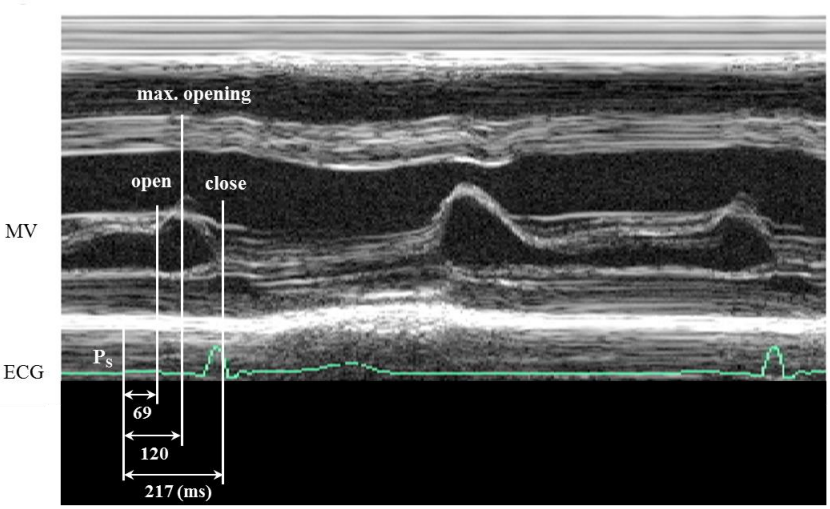

Figure 6-5. Illustration of the time features of the mitral valve movement during the active filling phase referred to the ECG P wave start.

The comparison of the mitral valve opening, maximum opening and closing times with the related ECG times is shown in Figure 6-6. All the times were measured referred to the ECG P wave onset. The valve initial opening point was soon after the ECG P wave peak (Mean difference ± SEM: 10 ± 2 ms, $P < 0.001$). The valve fully opened following the end of the P wave (Mean difference ± SEM: 12 ± 2 ms, $P < 0.001$). The valve stayed open till the ventricular depolarization started and closed 43 ms after the ECG Q wave.

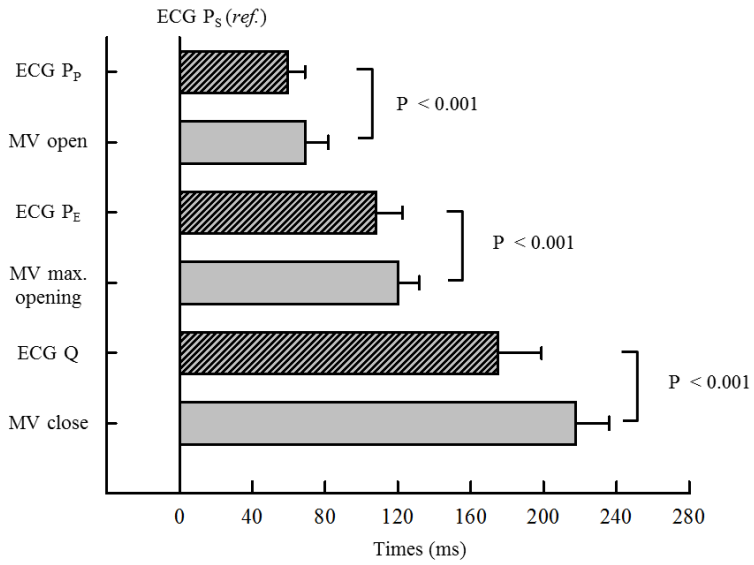

Figure 6-6. Comparison between the mitral valve movement during the active filling phase and the corresponding ECG times. The times were measured from the reference ECG P wave start. The error bars present the SDs of the times across the subjects.

Left ventricular ejection is initiated by ventricular depolarization. Figure 6-7 illustrates the aortic valve opening and closing times referred to the ECG Q wave. The duration from the ECG Q wave to the aortic valve opening (pre-ejection duration) was 76 ms (SD: 10 ms). The duration from the Q wave to the valve closure (electromechanical systole duration) was 405 ms (SD: 24 ms). The duration from the aortic valve open to close (left ventricular ejection duration) was 329 ms (SD: 24 ms).

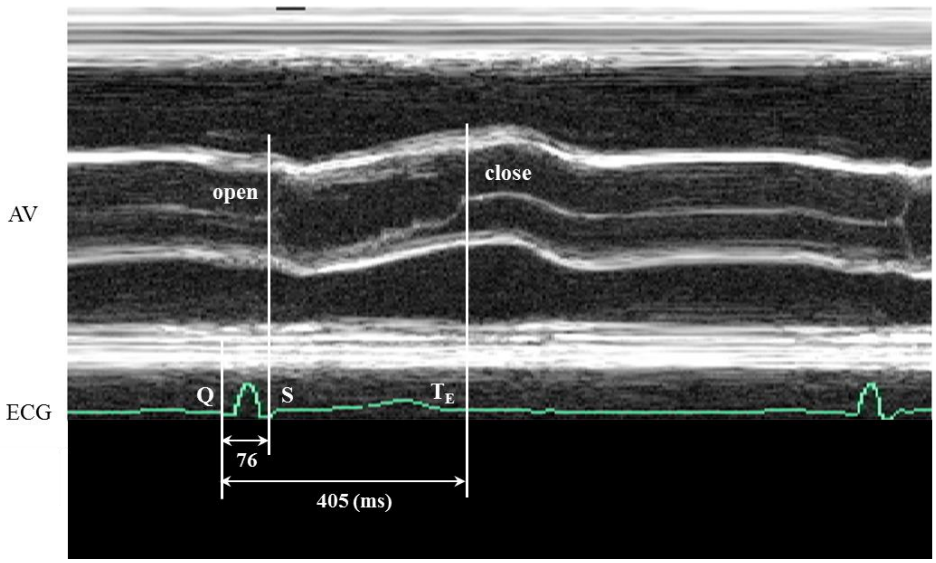

Figure 6-7. Illustration of aortic valve movement times with reference to the ECG Q wave.

Figure 6-8 shows the comparison between the aortic valve movement and related ECG times. All times were measured from the ECG Q wave. The means and SDs of the times are displayed on the plot. As can be seen, the aortic valve started to open before the end of ventricular depolarization, and stayed open till the end of ventricular repolarization. Its initial opening was 9 ms before the ECG S wave, while its closure was observed 11 ms later than the T wave end. Both comparisons were statistically significant ($P < 0.001$).

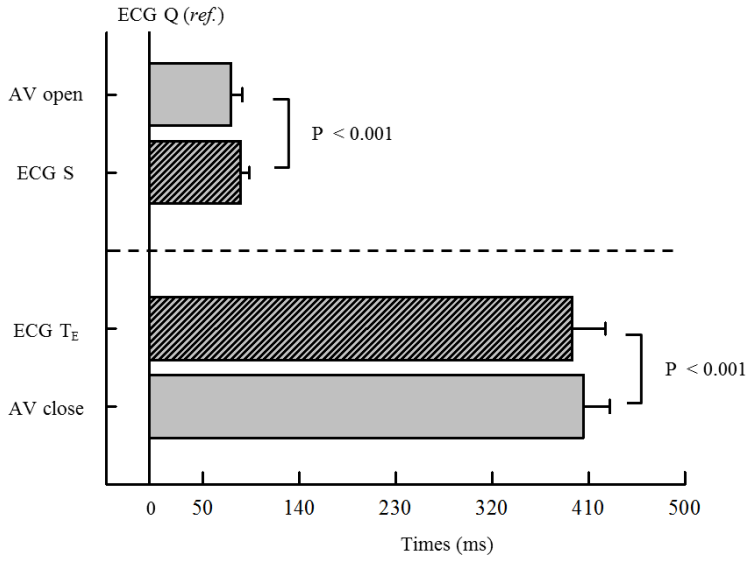

Figure 6-8. Comparison between the aortic valve times and the corresponding ECG times. The error bars represent the SDs of the times across the subjects.

Left ventricular diastole results from ventricular repolarization. The left ventricular passive filling phase occurred during early ventricular diastole, following the ECG T wave. The mitral valve movement times referred to the ECG T wave end during the passive filling phase are illustrated in Figure 6-9. The valve started to open 65 ms after the T wave end. It achieved the maximum opening 75 ms later, and incompletely closed 308 ms after the T wave end.

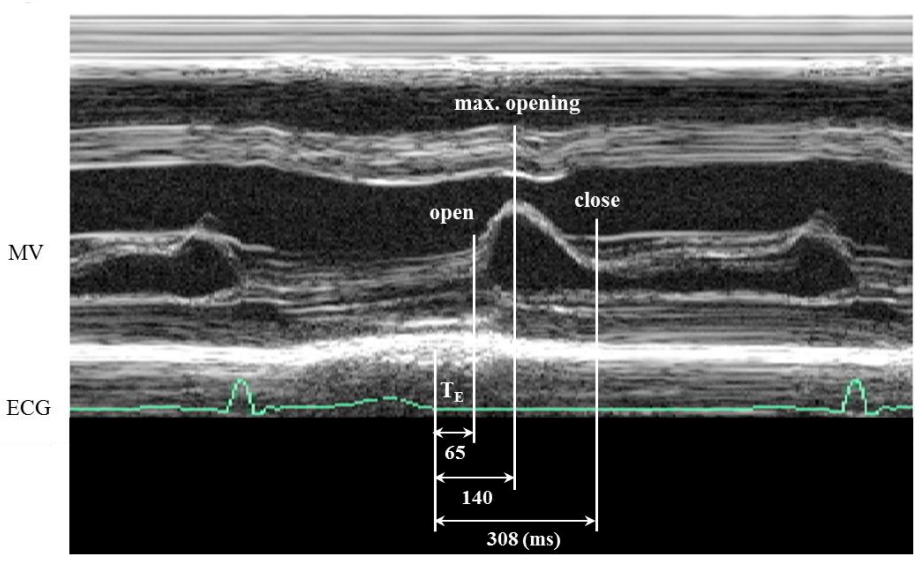

Figure 6-9. Illustration of the time features of the mitral valve movement during the ventricular passive filling phase with reference to the ECG T wave end (T_E).

The bar chart in Figure 6-10 shows the mitral valve movements following ECG T wave end. There is no other ECG feature on lead I that occurred during this phase.

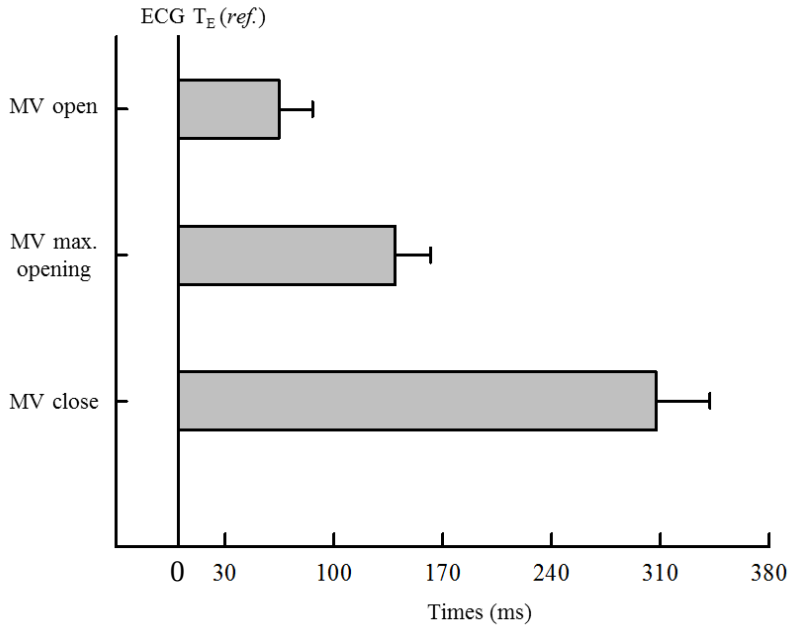

Figure 6-10. Comparison between the mitral valve movement times during passive filling phase and the corresponding ECG times. The times were measured with reference to ECG T wave end (T_E). The error bars represent the SDs of the times across the subjects.

6.4.2 Relationship between valve movement and ECG feature times

Mitral valve movement during active filling and ECG P wave

The relationships of the mitral valve movement times during the active filling phase with ECG P wave times are shown in Figure 6-11. All the valve open, maximum opening and close times showed strongly positive linear correlations with the P wave start, peak and end. The strongest correlation was observed between the mitral valve initial opening and the P wave peak ($R^2 = 0.868$, $P < 0.001$). The valve closure showed less strong correlations with the P wave times, but all the correlations were significant ($P < 0.001$). These results are as expected, because the left ventricular active filling is initiated by the atrial depolarization.

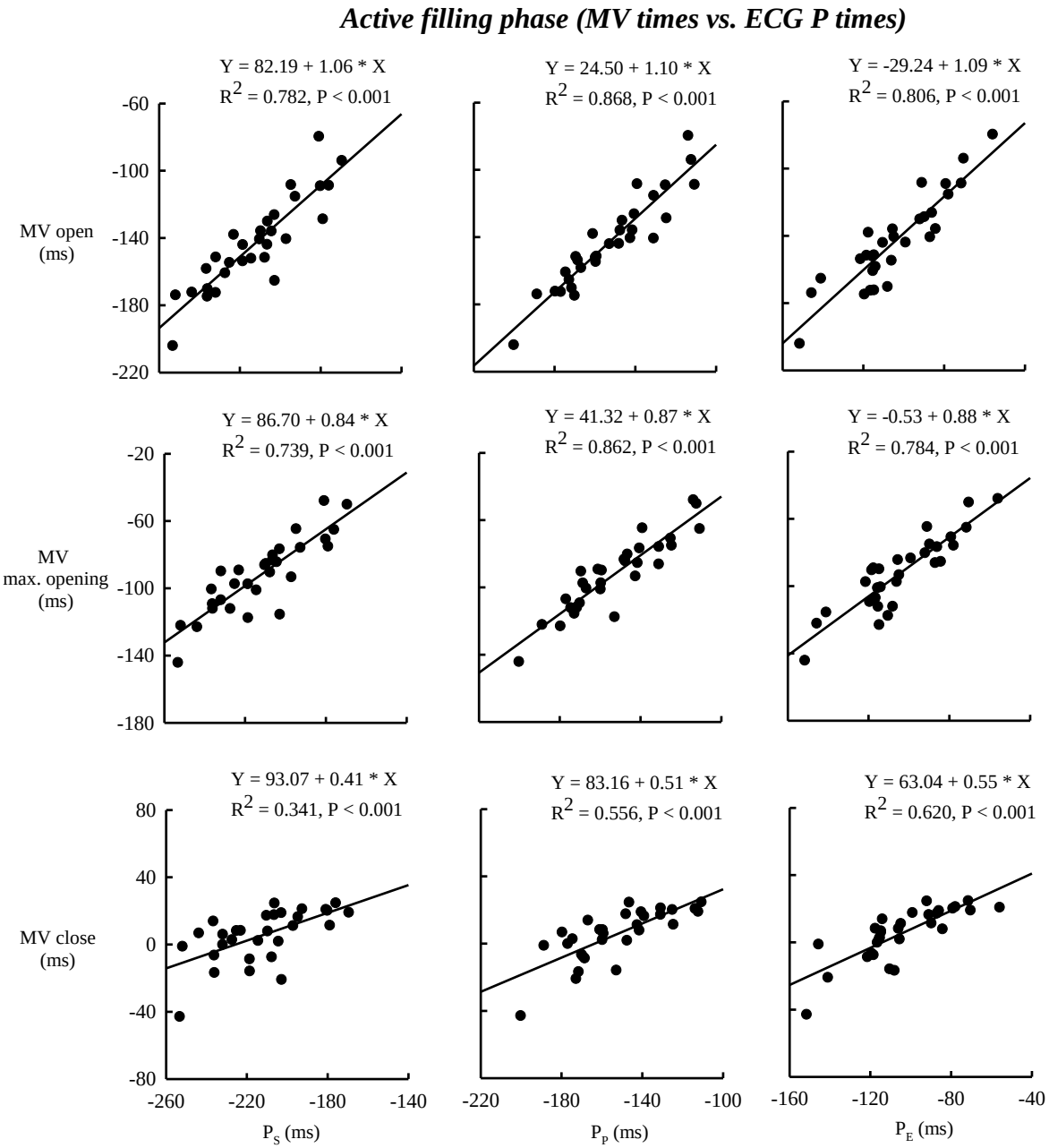

Figure 6-11. Relationship between mitral valve movement times during the active filling phase with ECG P wave times.

Multiple linear regression analysis results are given in Table 6-4. As described above, before any adjustment for RR interval the valve movement times were strongly correlated to P wave times ($R^2 \geq 0.341$, $P < 0.001$). As the valve times were not associated with ECG RR interval ($R^2 \leq 0.072$, $P > 0.05$), the adjustment for RR interval did not influence the strong correlation between mitral valve movement and the ECG P wave. This observation suggests that the relationship between the mitral valve movement during the active filling phase and ECG P wave times is independent of heart rate.

Table 6-4. Correlation of mitral valve movement during active filling and ECG P wave.

ECG Times	Measure	MV open		MV max. opening		MV close	
		Un-adjusted	Adjusted[a]	Un-adjusted	Adjusted[a]	Un-adjusted	Adjusted[a]
P_S	R^2	0.782**	0.775**	0.739**	0.731**	0.341**	0.452**
	P	< 0.001	< 0.001	< 0.001	< 0.001	< 0.001	< 0.001
P_P	R^2	0.868**	0.865**	0.862**	0.821**	0.556**	0.696**
	P	< 0.001	< 0.001	< 0.001	< 0.001	< 0.001	< 0.001
P_E	R^2	0.806**	0.804**	0.784**	0.776**	0.620**	0.759**
	P	< 0.001	< 0.001	< 0.001	< 0.001	< 0.001	< 0.001
Next R	R^2	0.072	--	0.029	--	0.000	--
	P	0.082	--	0.182	--	0.716	--

[a]: the linear regression model was adjusted for RR interval; * or **: the linear regression model is significant with $P < 0.05$ or $P < 0.001$ respectively. P: represents the significance of the independent variable.

Aortic valve movement and ECG QRS complex

The relationships between the aortic valve movement and the ECG QRS complex features are shown in Figure 6-12. By contrast with the strong relationship between the mitral valve movement during the active filling and the ECG P wave, neither the valve opening nor closing time showed a linear relationship to ECG Q or S wave times ($P > 0.05$). The valve opening time did not show any significant linear relationship with the RR interval. However, its closing time was strongly correlated with the RR interval ($R^2 = 0.758$, $P < 0.001$).

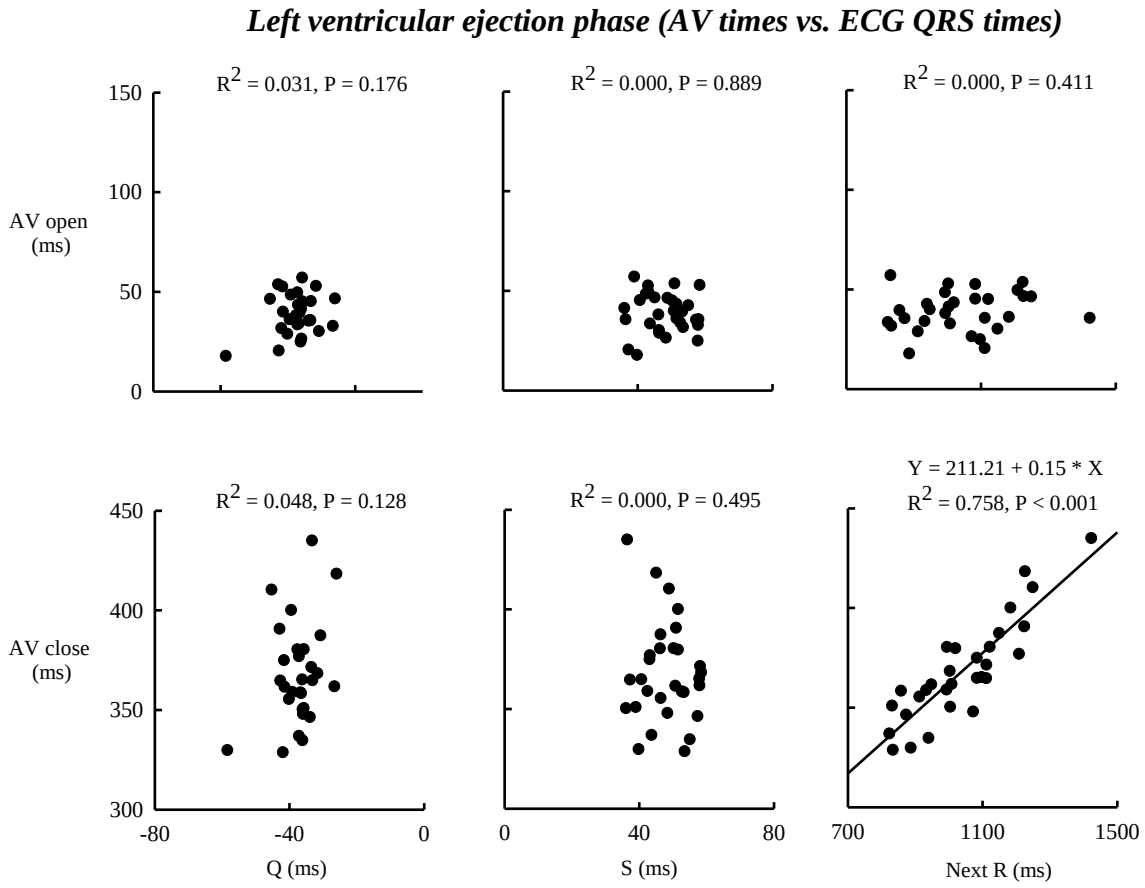

Figure 6-12. Relationship between aortic valve movement times during the ventricular ejection phase with ECG QRS complex times.

Further multiple linear regression analysis results are provided in Table 6-5. The adjustment for the RR interval did not improve the coefficient of determination of the linear regression models for predicting the aortic valve opening time with the ECG QRS times ($R^2 \leq 0.165$, $P > 0.05$), which suggests that the valve opening time had not significant linear relationships with the ventricular depolarization times. Additionally, a large increase in the coefficient of determination after the adjustment for RR interval confirmed that heart rate was a major factor correlated to the aortic valve closure.

Table 6-5. Correlation of aortic valve movement and ECG QRS complex times.

		AV open		**AV close**	
ECG Times	**Measure**	Un-adjusted	Adjusted[a]	Un-adjusted	Adjusted[a]
Q	R^2	0.031	0.008	0.048	0.765**
	P	0.176	0.227	0.128	0.181
S	R^2	0.000	0.000	0.000	0.750**
	P	0.889	0.991	0.495	0.722
Next R	R^2	0.000	--	0.758**	--
	P	0.411	--	< 0.001	--

[a]: the linear regression model was adjusted for RR interval; * or **: the linear regression model is significant with $P < 0.05$ or $P < 0.001$ respectively. P: represents the significance of the independent variable.

Mitral valve movement during passive filling phase and ECG T wave

The relationships between the mitral valve movement during the passive filling phase and the ECG T wave times are shown in Figure 6-13. All the valve open, maximum opening and close times showed strongly positive relationships with the ECG T wave end and RR interval ($R^2 \geq 0.406$, $P < 0.001$).

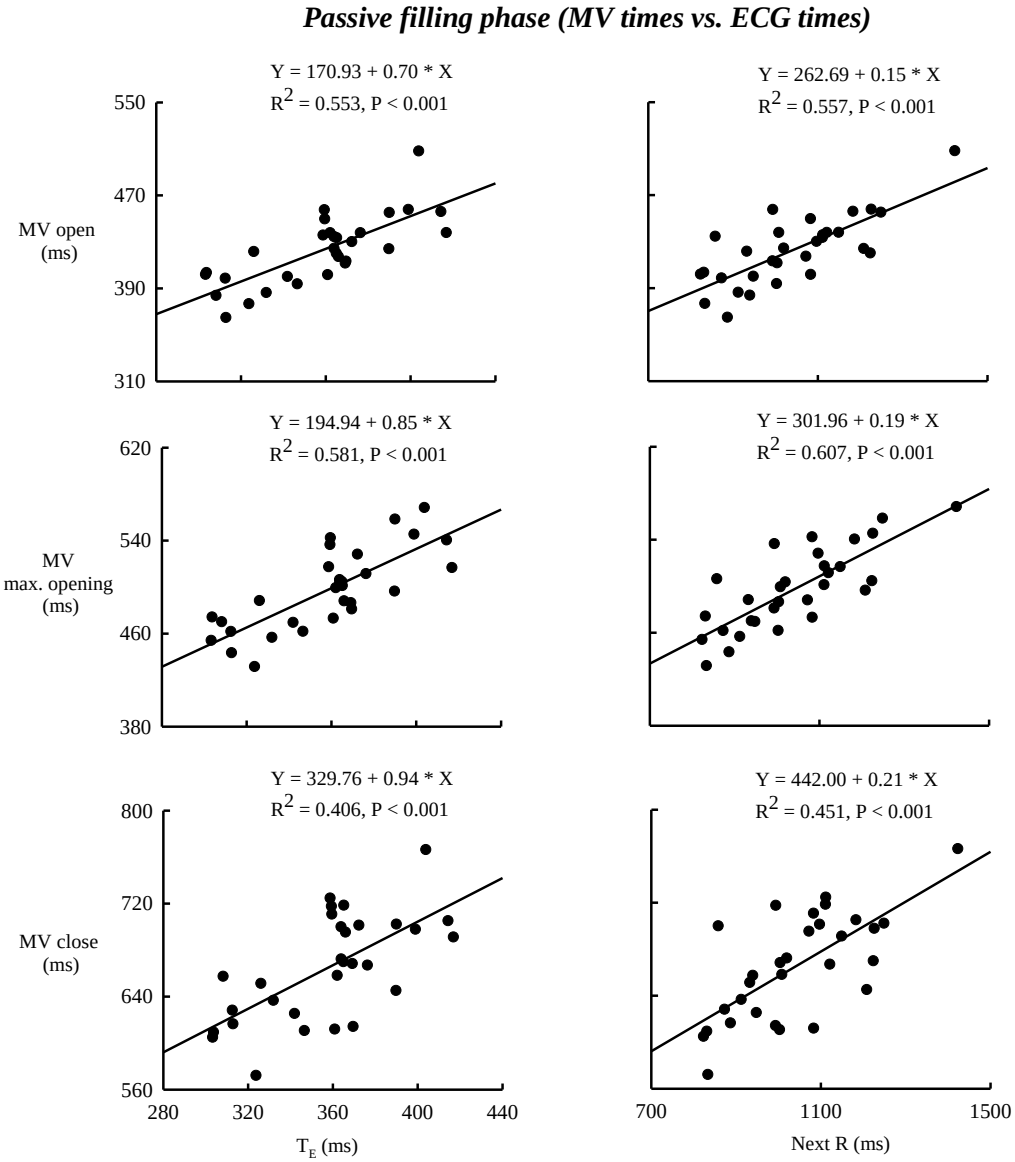

Figure 6-13. Relationship between mitral valve movement times during the passive filling phase with ECG T wave end RR interval.

Further multiple linear regression analysis results are provided in Table 6-6. As described above, before the adjustment for RR interval, both the T wave end and the RR interval were significantly correlated to the valve times ($P < 0.001$). However, after the adjustment, the coefficients of determination of the linear regression models increased, but the T wave end was no longer a significant factor in the regression model ($P > 0.05$). This suggests that the T wave end is linked to heart rate and its relationship with mitral valve movement is not independent of RR interval.

Table 6-6. Correlation of mitral valve movement during passive filling and ECG T wave.

		MV open		**MV max. opening**		**MV close**	
ECG Times	**Measure**	Un-adjusted	Adjusted [a]	Un-adjusted	Adjusted [a]	Un-adjusted	Adjusted [a]
T_E	R^2	0.553**	0.593**	0.581**	0.638**	0.406**	0.454**
	P	< 0.001	0.072	< 0.001	0.075	< 0.001	0.301
Next R	R^2	0.557**	--	0.607**	--	0.451**	--
	P	< 0.001	--	< 0.001	--	< 0.001	--

[a]: the linear regression model was adjusted for RR interval; * or **: the linear regression model is significant with $P < 0.05$ or $P < 0.001$ respectively. P: represents the significance of the independent variable.

6.4.3 Relationship between valve movement and related ECG time durations

The relationships between the valve open durations between different phases and corresponding ECG time intervals are shown in Figure 6-14. There was no significant linear relationship found between the mitral valve open duration during the active filling phase ECG P wave duration, and between the aortic valve open duration and ECG QRS duration ($P \geq 0.177$). By contrast, the mitral valve open duration during the passive filling phase showed a significantly positive linear relationship with the ECG QT interval (ventricular depolarization and repolarization duration) ($R^2 = 0.394$, $P < 0.001$).

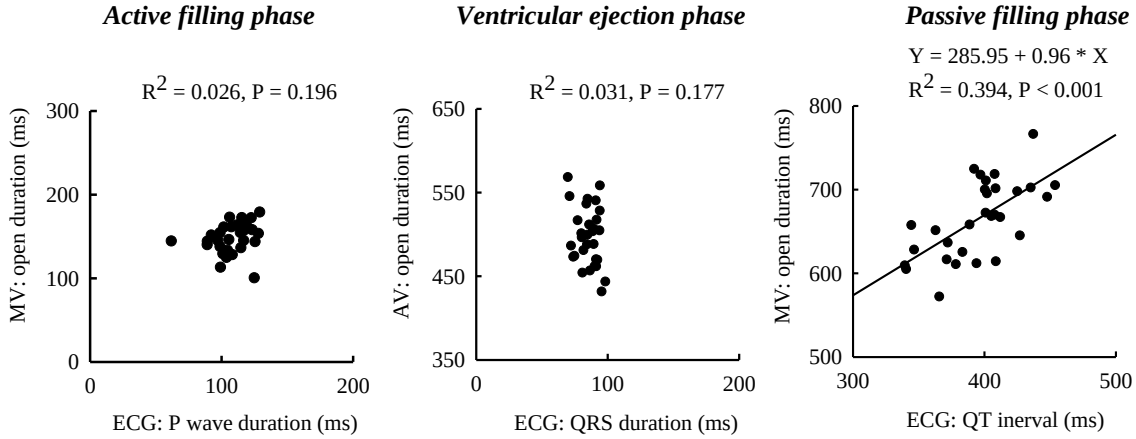

Figure 6-14. Relationships between valve open durations and ECG time intervals.

Further multiple linear regression analysis results for the relationships between valve movement durations and ECG time intervals are given Table 6-8. It can be noted that all the valve open durations showed significantly positive relationships with the RR interval ($R^2 \geq 0.328$, $P < 0.001$). After the adjustment for the RR interval, the ECG QT interval was no longer a significant independent variable of the mitral valve open duration during passive filling phase ($P = 0.523$). Therefore, although the cardiac mechanical events were initiated by electric activity, the relationships between valve open durations were not apparently associated with the corresponding electric durations (mitral valve during active filling *vs.* ECG P wave, aortic valve during ventricular ejection *vs.* ECG QRS duration), or the relationship was linked to heart rate (mitral valve during passive filling *vs.* ECG QT interval).

Table 6-8. Correlation of valve movement durations and ECG durations.

		Active filling MV open duration		**Ejection AV open duration**		**Passive filling MV open duration**	
ECG Intervals	**Measure**	Un-adjusted	Adjusted [a]	Un-adjusted	Adjusted [a]	Un-adjusted	Adjusted [a]
P_S -> P_E	R^2	0.026	0.345**	--	--	--	--
	P	0.196	0.201	--	--	--	--
Q -> S	R^2	--	--	0.031	0.592**	--	--
	P	--	--	0.177	0.907	--	--
Q -> T_E	R^2	--	--	--	--	0.394**	0.450**
	P	--	--	--	--	< 0.001	0.341
R -> Next R	R^2	0.328**	--	0.607**	--	0.451**	--
	P	< 0.001	--	< 0.001	--	< 0.001	--

[a]: the linear regression model was adjusted for RR interval; * or **: the linear regression model is significant with $P < 0.05$ or $P < 0.001$ respectively. P: represents the significance of the independent variable.

6.5 Discussion and conclusions

In this chapter, the timing differences between the aortic and mitral valve movement features and corresponding blood flow conditions were investigated. The key findings of the time difference include:

- The valves consistently opened before the onset of flow detection (mean difference ranged from 13 ms to 18 ms);
- The mitral valve always achieved the maximum opening preceding the mitral peak flow by 25 ms during the active filling phase and 32 ms during the passive filling phase;
- The valves closed 7 ms before the flow end was detected during the active filling phase and left ventricular ejection phase, but the mitral flow ended 29 ms after the mitral valve apparent closure at the end of the passive filling phase.

In addition, the valve movement time durations were compared with corresponding flow durations. The overall valve open durations (from open to close) during the active filling phase and the ventricular ejection phase were around 20 ms longer than the overall measurable flow durations (from start to end), but the mitral valve open duration was 11 ms shorter than the flow duration in the passive filling phase.

The relationship between the valve movement related time durations and the flow related durations were investigated. The overall valve open durations during the active filling phase and the left ventricular ejection phase were strongly correlated with the overall flow durations in the corresponding phase ($R^2 \geq 0.754$, $P < 0.001$). The relationship between the overall mitral valve open and flow duration was relatively weak ($R^2 = 0.151$, $P < 0.05$).

The relationship between the valve movement and corresponding ECG features were investigated. Firstly, the time sequence of the valve movement feature times during the active filling phase, left ventricular ejection phase and the passive filling phase were investigated with reference to ECG P wave, QRS complex and T wave respectively. The linear relationships between the valve movement features and the ECG features were also examined. The key findings are summarized as follows:

- During the active filling phase, the mitral initially opened following the ECG P wave peak (Mean difference: 12 ms), and closed after the ECG Q wave (Mean difference: 43 ms). All the mitral valve movement feature times (open, maximum open and close) were strongly related to ECG P wave times (start, peak and end) ($R^2 \geq 0.341$, $P < 0.001$);
- During the left ventricular ejection phase, the aortic valve initially opened right before the ECG S wave (Mean difference: 9 ms), and closed following the ECG T wave end (Mean difference: 11 ms). The aortic valve closing was strongly related to RR interval ($R^2 = 0.758$, $P < 0.001$);
- During the passive filling phase, the mitral valve initially opened 65 ms later than the ECG T wave end. All the mitral valve movement feature times (open, maximum open and close) were strongly related to RR interval ($R^2 \geq 0.451$, $P < 0.001$).

The findings in the present study that the valves have already opened before the onset of blood flow detection are consistent with the findings from the previous studies (Thubrikar et al. 1977, Higashidate et al. 1995). By dynamically measuring the aortic valve orifice area with a technique involving electromagnetic induction in anesthetized dogs, Higashidata et al. (1995) found that the aortic valve initially opened before the aortic flow onset and elevation of aortic pressure. The similar results were also obtained by computer simulation from Howard et al's study (Howard et al. 2003). Based on these observations, the initial opening mechanism of the aortic valve was attributed to the aortic root expansion during the early left ventricular systole (Higashidate et al. 1995, Howard et al. 2003). However, by the work of Laniado et al. (1975), the mitral valve movement and transmitral flow were simultaneously recorded with echocardiography and electromagnetic flowmeter on chest-opened adult mongrel dogs. It was reported that the initial opening motion of the mitral valve was coincidently with the beginning of the mitral flow. This result is conflicting with the findings in the present study and other literature.

In Laniado el al.'s study (Laniado et al. 1975) on the relation between the mitral valve movement and flow, the valve maximum opening was reported occurring on average 44 ms before the peak flow on anesthetized dogs. In their later study on the relation between the aortic valve movement and flow, the aortic valve fully opened before the peak aortic flow (Laniado et al. 1978). Higashidate et al. (1995) also reported that the maximum aortic valve orifice area preceded peak aortic flow. These results agree with the findings in this study.

The preceding of the valve leaflet closing motion than the flow decelerating was attributed to the combination of the internal forces stored by the displacement of the cusps and the vortexes in the sinuses (Higashidate et al. 1995).

At the end of the active filling phase and the ventricular ejection phase, the valves were observed to be completely closed soon after the corresponding flow ended. However, at the end of passive filling phase, because the mitral valve did not close completely, mitral flow was still seen a short time after the valve leaflets appeared to be closed.

In this study, the cardiac excitation-contraction coupling was assessed by linking the ECG times to the valve movement times. The duration from the ECG P wave onset to the mitral valve initial opening during the active filling phase, which reflected the atrial electromechanical delay, was 69 ms, and the duration from the ECG Q wave onset to the aortic valve initial opening during the ventricular ejection phase, which reflected the ventricular electromechanical delay, was 76 ms. However, because the valve opening is normally after the onset of myocardial contraction, the durations referred to the valve initial opening would be expected to be longer than the real electromechanical delay. According to the linear regression analysis results, while the mitral valve movement times during the active filling phase showed significantly linear relationships, which were independent of the RR interval, with the ECG P wave times, the aortic valve movement did not show any significant linear relationship with the QRS complex times. The causes of these different patterns of the relationship between cardiac electric activity and valve movement need further studies.

Chapter 7 Relationship between impedance and imaging data

The relationships of thoracic impedance with valve movement and flow are described in this chapter.

7.1 Introduction

The resistance, or impedance, to electrical current in the thorax varies with the thoracic blood content. During the left ventricular ejection phase, the blood in the ventricles is pumped from the heart through the semilunar valves into the arterial system. During the passive filling phase, the blood in the atria returns from the venous system and fills into the ventricles through the atrioventricular valves. These phases lead to the re-distribution of blood in the thorax, and hence result in thoracic impedance variation.

In the 3rd data recording session of this study, two impedance signals, impedance Z and the first derivative impedance -dZ/dt, were recorded with 4 sets of images, including two sets of M-mode echocardiograms for mitral and aortic valve movement and another two sets of Doppler echocardiograms for mitral and aortic flow. While the Z waveform reflects the dynamic thoracic impedance variation, the -dZ/dt waveform represents the rate of change of Z.

The relations of the impedance Z and -dZ/dt with the valve movement and blood flow through the valves are investigated in this chapter; the timing sequence of impedance features, valve movement and flow conditions are reconstructed; the corresponding times and durations from the impedance and images are compared; the systolic time intervals measured from the impedance and images are also compared; additionally, the association between these time features of impedance and images are examined by regression analysis.

7.2 Overview of timing sequence of thoracic impedance

During the 3rd session, impedance Z and the first derivative impedance -dZ/dt were recorded simultaneously with images. On the Z waveform, the start, minimum and end points of the major systolic wave were identified and related to ventricular ejection, and the minimum point of the diastolic wave (2nd min.) related to ventricular passive filling. Similarly, the foot, peak and end points of the major systolic wave and the peak of the diastolic wave (2nd peak) were identified on the -dZ/dt waveform. These features were identified on all subjects. As described in Table 7-1, except for the systolic wave end point (28 subjects) and the 2nd minimum point (23 subjects) on the Z waveform, and the 2nd peak (21 subjects) on the -dZ/dt waveform, all other times were from on all 30 subjects.

Table 7-1. Summary of subject number of impedance features measurement.

Impedance Z		**Derivative impedance -dZ/dt**	
Features	**Subject numbers**	**Features**	**Subject numbers**
Start	30	*Foot*	30
Min.	30	*Peak*	30
End	28	*End*	30
2nd min.	23	*2nd peak*	21

An example of the Z and -dZ/dt waveforms is displayed with the synchronous ECG in Figure 7-1. The feature times showed in the figure are the average values from all subjects studied in session 3, which are summarized in Table 7-2. As illustrated in the Figure 7-1, all the times were measured from ECG R waves. The impedance Z started to fall 65 ms after the ECG R wave, and achieved the minimum 196 ms later. Afterwards, the impedance kept rising till the end of the major wave at 506 ms, which was followed by another falling phase with smaller amplitude. After the minimum at 643 ms, the impedance recovered slowly during the rest of the cycle.

As can be seen in the figure, an increase in the Z generated a positive upward wave on the -dZ/dt waveform, while a decrease in the Z corresponded to a negative downward wave on the -dZ/dt waveform. The foot of the acceleration of the Z falling was 88 ms after the R

wave, and achieved the peak at 189 ms. The major systolic wave of the -dZ/dt ended at 448 ms, and the 2nd peak was observed at 613 ms.

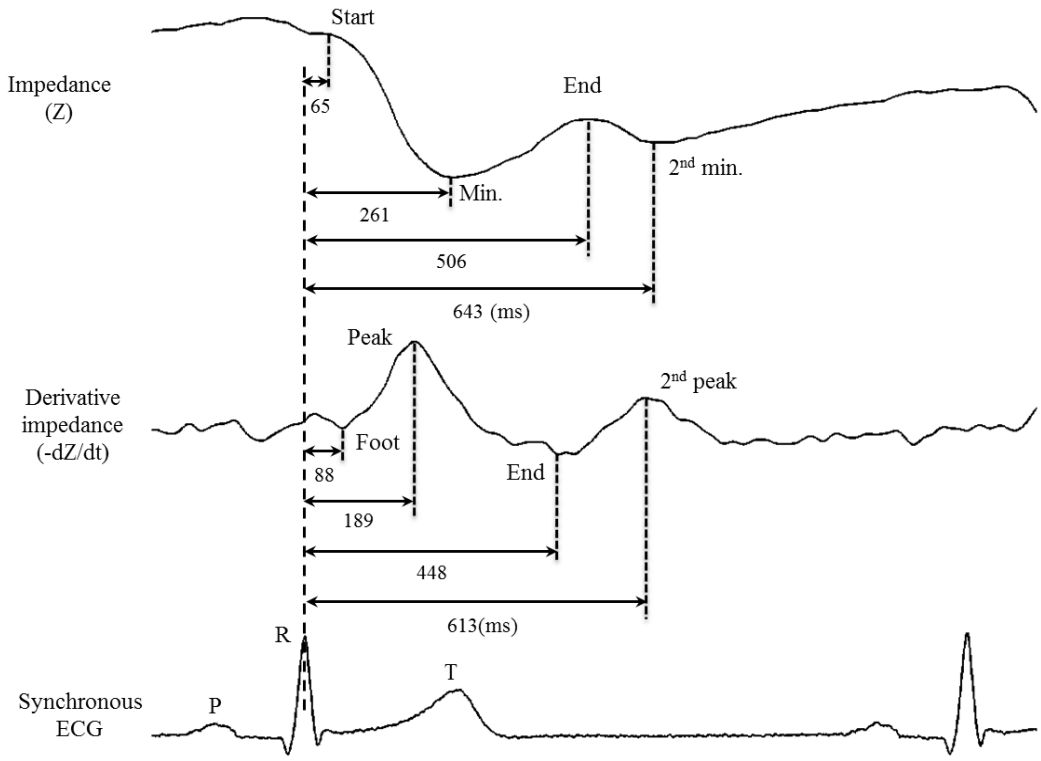

Figure 7-1. Impedance signals with synchronized ECG. The impedance feature times were measured from the ECG R wave. The values were means across all the subjects.

This brief quantitative analysis agrees with Karnegis and Kubicek's (1970) qualitative description about the characteristic components of the impedance waveform referred to the ECG waveform; they described the largest deflection in Z (the systolic wave) as a systolic event synchronized with the ECG QRS complex, which is followed by a smaller deflection (the diastolic wave) that occurred in early diastole.

The comparison between the Z times and the corresponding -dZ/dt times is also provided in the Table 7-2. The systolic foot of the -dZ/dt waveform was detected 23 ms after the onset of the Z falling phase. The maximum -dZ/dt was 72 ms before the Z achieved the minimum. The end point of the major systolic wave on the -dZ/dt waveform occurred 59 ms before that on the Z, and the 2nd peak on the -dZ/dt occurred 28 ms before the 2nd minimum point on Z. All the differences were statistically significant with $P < 0.001$.

Table 7-2. Summary of time features on impedance Z and -dZ/dt from data in session 3.

Features		**Mean ± SD (ms)**		**Mean difference ± SEM (ms)**
Z	**-dZ/dt**	**Z**	**-dZ/dt**	
Start	*Foot*	65 ± 15	88 ± 21	-23 ± 4**
Min.	*Peak*	261 ± 23	189 ± 12	72 ± 3**
End	*End*	506 ± 41	448 ± 26	59 ± 4**
2nd min.	*2nd peak*	643 ± 50	613 ± 34	28 ± 5**

**: significant difference with $P < 0.001$.

Figure 7-2 shows the timing sequence of the impedance features with the ECG features, valve movement features and flow conditions which have been reported in the previous chapter. The start and the minimum points of the Z systolic wave, and the foot and the peak of -dZ/dt systolic wave were located within the left ventricular ejection phase. The end of the Z systolic waves and its 2nd minimum, the end of the -dZ/dt systolic end and the 2nd peak were located in the passive filling phase. More details about the timing sequence between the impedance and imaging features are provided in the following sections.

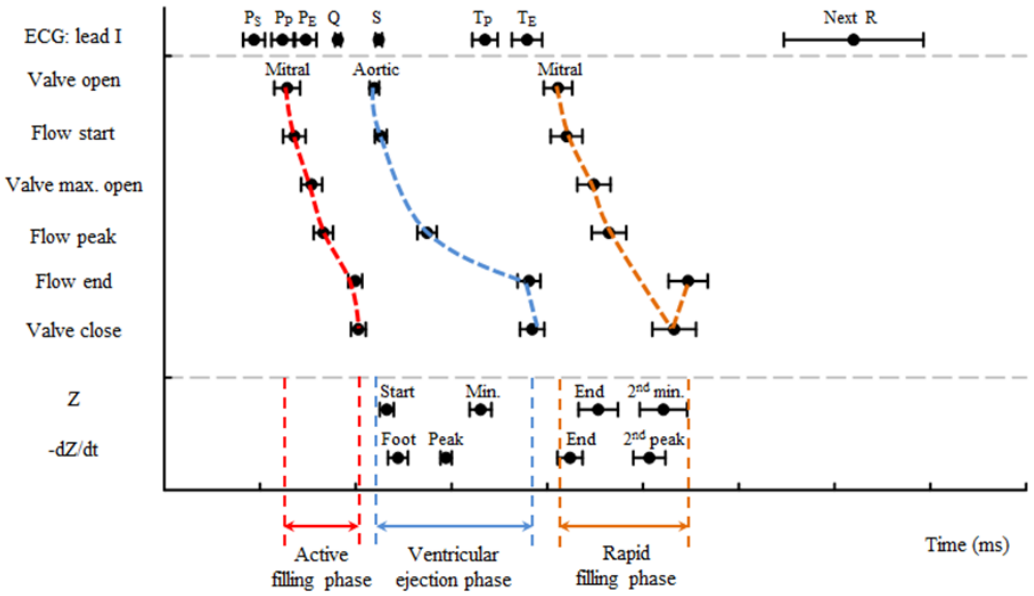

Figure 7-2. Timing sequence of impedance features with ECG and imaging features. Circle represents the mean and error bar represents SD across all the studied subjects.

7.3 Dynamic relationship between valve movement and impedance

7.3.1 Timing sequence of valve movement and impedance features

Figure 7-3 shows the impedance signals with the synchronous ECG and M-mode echocardiograms for aortic valve and mitral valve movement. The impedance feature times measured from the aortic valve opening are also shown. The values were means across all the subjects. As can be seen, the impedance Z started to fall 26 ms after the aortic valve opening, and achieved the minimum at 222 ms. The end of the impedance systolic wave was seen at 467 ms, and close to the mitral valve maximum opening time during the passive filling phase. The 2nd minimum point on the Z was observed soon before the mitral valve closed. The foot the systolic wave of -dZ/dt occurred 49 ms after the aortic valve opened, and achieved the peak at 150 ms. The end of the systolic wave on -dZ/dt (409 ms) was close to the initial opening of the mitral valve during the passive filling phase.

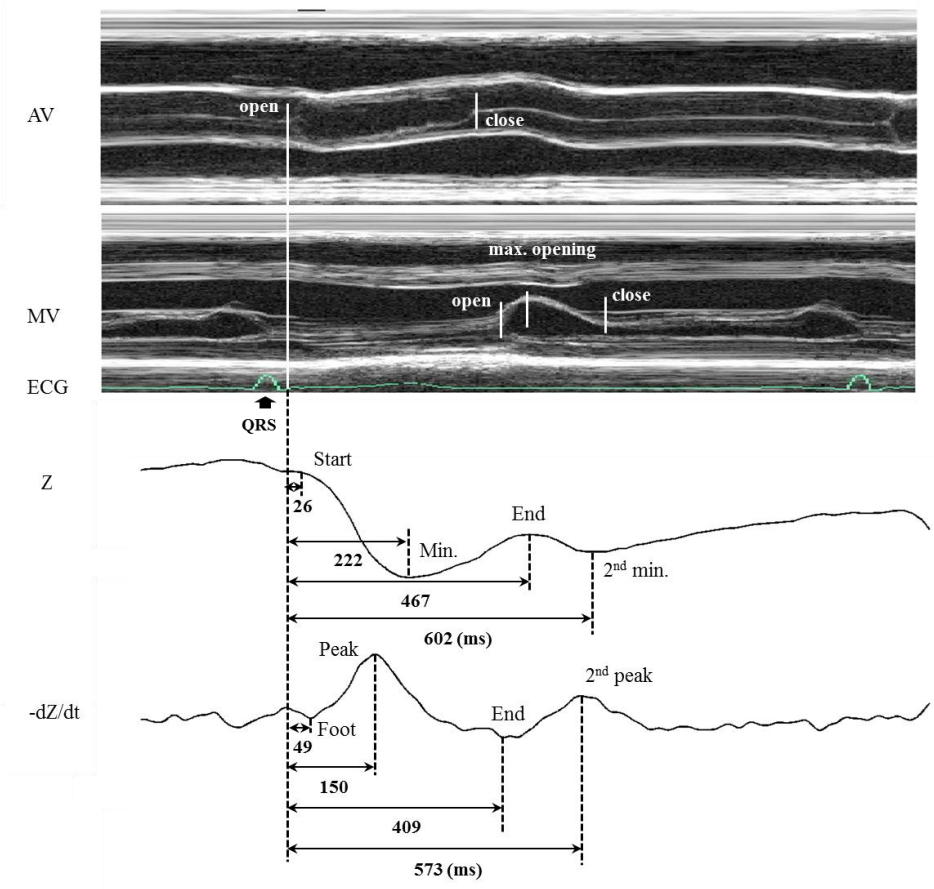

Figure 7-3. Impedance signals with synchronized ECG and valve movement images. The impedance feature times were measured from the aortic valve opening. The values were means across all the subjects.

In Figure 7-4, features from the impedance Z and the derivative impedance -dZ/dt are displayed with valve movement features in a timing sequence. All the times were measured from the aortic valve opening. Comparison was made for impedance feature times and corresponding imaging times.

The Figure 7-4 (A) shows the means and SDs of the time features from impedance Z, aortic valve movement and the mitral valve movement during the passive filling phase, and the comparison of corresponding times. Following the aortic valve opening, the impedance Z started to fall and achieved the minimum 108 ms before the valve closed ($P < 0.001$). Afterwards, the impedance Z started to rise even when the left ventricle was still in ejection. The rising period lasted till the ventricular passive filling phase started. Around the time when the mitral valve reached the maximum opening, the increase in Z stopped. There was no significant difference found between the end of the systolic wave on Z and the mitral valve maximum opening time (Mean difference: 11 ms, $P = 0.054$). The impedance started to fall at the beginning of the diastolic wave, and achieved the 2^{nd} minimum point 16 ms before the mitral valve closed ($P < 0.05$). According to these results, both the ventricular ejection and filling resulted in a decrease in the impedance. However, a difference was observed, as Z started to restore when the left ventricular ejection was still in progress during ventricular systole, and it stopped falling before the end of the passive filling during ventricular diastole. These striking observations suggest that the blood volume changes in great vessels in the thorax rather than the volume changes in the heart would probably be the main contributor to thoracic impedance variation.

The Figure 7-4 (B) shows the means and SDs of the time features from the derivative impedance -dZ/dt, aortic valve movement and mitral valve movement during the passive filling phase, and the comparison of corresponding times. The foot of the derivative impedance systolic wave was 49 ms later than the aortic valve opening, and its peak occurred 179 ms before the aortic valve closed (both $P < 0.001$). The end of the systolic wave on the -dZ/dt was 79 ms later than the aortic valve closure ($P < 0.001$), and was observed between the mitral valve initial opening and maximum opening during the passive filling phase ($P < 0.001$). The diastolic peak occurred 52 ms before the mitral valve closed ($P < 0.001$).

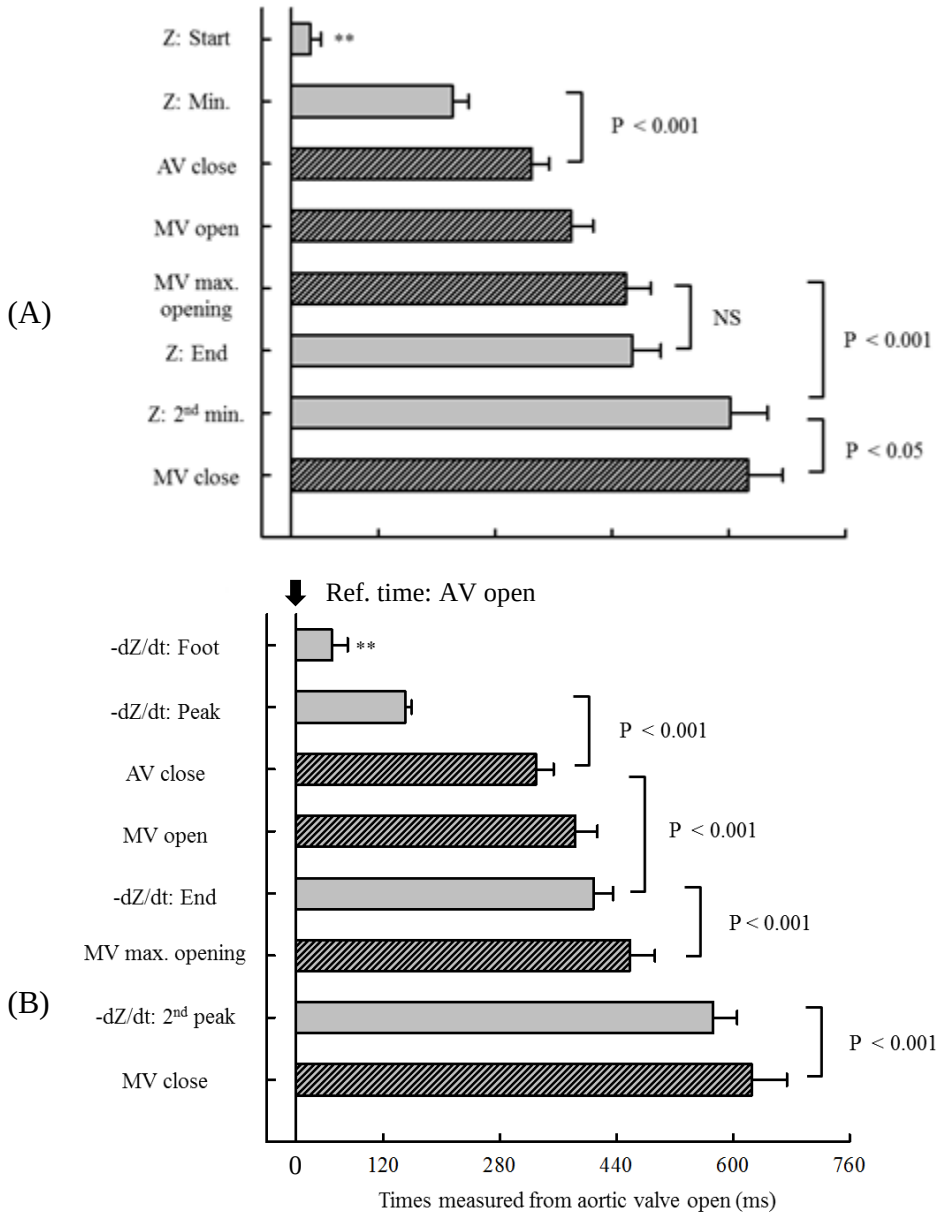

Figure 7-4. Timing sequence of features from impedance Z (A) and -dZ/dt (B) with valve movement times. **: significant difference from the reference time (aortic valve open) with $P < 0.001$. Error bars represent the SDs between subjects.

The comparison between feature times of the derivative impedance -dZ/dt and cardiac mechanical events reported in the previous studies are summarized in Table 7-3. The data from the current study are summarized in Table 7-4. According to Lababidi et al. (1970), the -dZ/dt systolic foot was synchronous with the mitral valve closing at the end of active filling phase, its systolic end synchronous with aortic valve opening, and the diastolic peak synchronous with the mitral valve closing at the beginning of passive filling phase. Surprisingly, these impedance times were perfectly synchronized with the heart sound

times with a mean difference of zero even though the phonocardiograph is an indirect measurement technique of cardiac mechanical events. These results were questioned in the later studies. Sherwood et al. (1990) pointed out that -dZ/dt systolic foot should be considered as the indicator of aortic valve open rather than mitral valve close. However, the relevant data to support this point was limited. Carvalho et al. (2011) compared the -dZ/dt feature times with aortic valve opening and closing times from Doppler images, which showed that -dZ/dt systolic foot occurred soon (12 ms) after the aortic valve opened, while its end occurred 32 ms later than the valve closing. In this section, the valve movement times were obtained from M-mode images, which is a more direct measurement for valve movement. The results showed that -dZ/dt systolic foot occurred 49 ms after the aortic valve initial opening, much later than the mitral valve closing (83 ms), while its systolic end occurred 79 ms after the aortic valve closing. Additionally, -dZ/dt diastolic peak was much later (194 ms) than the mitral valve opening time. Actually, the diastolic peak occurred even much later than the mitral valve maximum opening.

There are numerous studies that have been made to investigate the relationship between blood volumetric change in the thorax and the amplitude of the impedance Z waveform. However, the timing information of the Z waveform was usually ignored. The comparison between feature times on the impedance Z and valve movement times in this study are summarized in Table 7-5. The synchronization of the aortic valve opening and the onset of impedance falling (26 ms later) confirmed that the largest Z deflection in each cardiac cycle is a systolic event. However, the impedance Z started to recover far (108 ms) before the end of left ventricular ejection, which agrees with the observations from previous studies that the volume change in the left ventricle is not the only factor for the Z change; the blood volume change in the central great veins could affect the thoracic impedance (Patterson 1989). The increase in Z during late ventricular ejection would, because of the drainage of blood volume from the central aorta to the periphery, be overwhelmed by the incoming volume from the left ventricle during the late ejection phase. The Z decreased again 220 ms after the mitral valve opening during the early passive filling phase, and stopped (16 ms) before the mitral valve closed. It thus can be noted that a significant decrease in the Z can be associated with both ventricular ejection and filling. However, the response of Z change to the ejection was quicker than to the filling, which would be explained by the larger volume with faster distribution by the ejection than that by the filling.

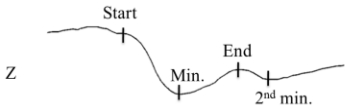

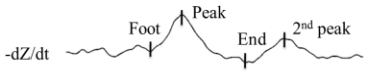

Table 7-3. Summary of literature on comparison between time features measured from derivative impedance (-dZ/dt) and reference techniques.

		Mean (SD) and Mean difference (SD) between techniques (ms)												
		MV close (after active filling)			AV open			AV close			MV open (before passive ventricular filling)			
References	***Subject No.***	R -> -dZ/dt foot	R-> MV close	diff.	R -> -dZ/dt foot	R -> AV open	diff.	R -> -dZ/dt end	R -> AV close	diff.	R -> -dZ/dt 2nd peak	R -> MV open	diff.	***Reference techniques***
Lababidi et al. 1970	37	--	--	0 (1)	--	--	--	--	--	0 (2)	--	--	0 (7)	PCG
Schieken et al. 1978	10	--	--	--	--	--	--	--	--	-20	--	--	--	M-mode
Carvalho et al. 2011	17	--	--	--	--	--	12 (9)	--	--	32 (25)	--	--	--	Doppler

Table 7-4. Summary of comparison between time features measured from derivative impedance (-dZ/dt) and M-mode echocardiograms.

	Mean (SD) and Mean difference (SD) between techniques (ms)												
	MV close (after active filling)			AV open			AV close			MV open (before passive ventricular filling)			
Subject No.	R -> -dZ/dt foot	R-> MV close	diff.	R -> -dZ/dt foot	R -> AV open	diff.	R -> -dZ/dt end	R -> AV close	diff.	R -> -dZ/dt 2nd peak	R -> MV open	diff.	***Reference techniques***
30	88 (21)	5 (15)	83 (27)	88 (21)	39 (10)	49 (22)	448 (26)	368 (25)	79 (17)	613 (34)	423 (30)	194 (22)	M-mode

Table 7-5. Summary of comparison between time features measured from impedance (Z) and M-mode echocardiograms.

	Mean (SD) and Mean difference (SD) between techniques (ms)												
	MV close (after active filling)			AV open			AV close			MV open (before passive ventricular filling)			
Subject No.	R -> Z start	R-> MV close	diff.	R-> Z start	R -> AV open	diff.	R-> Z end	R -> AV close	diff.	R -> Z 2nd min.	R -> MV open	diff.	***Reference techniques***
30	65 (15)	5 (15)	59 (23)	65 (15)	39 (10)	26 (16)	506 (41)	368 (25)	138 (27)	643 (50)	423 (30)	220 (32)	M-mode

7.3.2 Comparison of time durations from valve movement and impedance

The comparison between time durations from impedance and valve movement is shown in Figure 7-5. Both the systolic waves on the impedance Z (mean ± SD: 441 ± 40 ms) and the -dZ/dt (mean ± SD: 359 ± 33 ms) were significantly longer than the aortic valve open duration (mean ± SD: 329 ± 24 ms, both $P < 0.001$). The mitral valve closing duration (from maximum opening to close) during the passive filling phase was longer than the 2nd falling duration of impedance Z (from end to 2nd minimum) ($P < 0.001$), but comparable to the duration from the end of the systolic wave to the 2nd peak on the -dZ/dt (mean ± SD: 168 ± 22 ms *vs.* 166 ± 22 ms, $P = 0.459$).

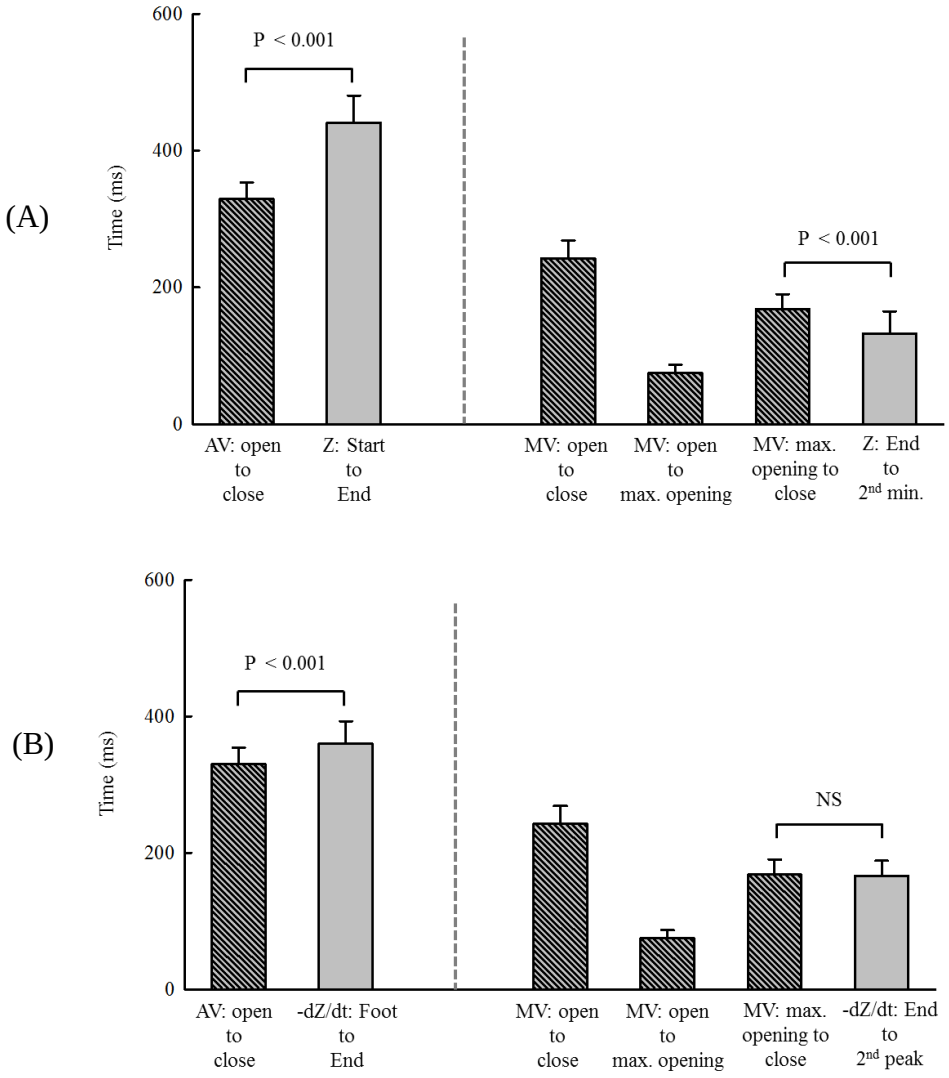

Figure 7-5. Comparison of impedance Z durations (A) and -dZ/dt durations (B) with valve movement durations. Error bars represent the SDs between subjects.

7.3.3 Comparison between systolic time intervals measured from derivative impedance and M-mode echocardiograms

One of the most important potential applications of the impedance technique is to provide a quick and easy way to measure systolic time intervals, which were usually obtained from the combination of ECG, phonocardiogram (PCG) and carotid arterial pulse, or from echocardiograms. Once the systolic foot and end had been identified on the derivative impedance -dZ/dt, systolic time intervals were calculated. These intervals were pre-ejection period (PEP, from ECG Q wave to the impedance systolic foot), electromechanical delay (EMD, from ECG Q wave to the impedance systolic end) and left ventricular ejection time (LVET, from the impedance systolic foot to the end).

The relevant data from previous studies are summarized in Table 7-6, while the comparison of the measurements from impedance with those from M-mode echocardiograms is summarized in Table 7-7. According to the Table 7-7, all the systolic time intervals measured from the impedance were longer than those measured from the images in this study. The PEP measured from the impedance was 126 ms, which was 49 ms longer than that measured from the images (76 ms). The EMD measured from the impedance was 485 ms, which was 79 ms longer than that from the images (406 ms). The LVET measured from the impedance was 359 ms, which was 30 ms longer than that from the images (329 ms). The LVET measurement provided the closest agreement between the two techniques among the three systolic time intervals.

For both the PEP and EMD measurements, the differences between the values given by the impedance and those by the reference images were longer than those from the literature. It was reported that for the PEP measurement the difference between the impedance and the images ranged from -20 to 12 ms, while for the EMD the difference ranged from -20 to 32 ms (Schieken et al. 1978, Kizakevich et al. 1993, Cybulski et al. 2004, Carvalho et al. 2011). However, for the LVET measurement, the difference between the impedance and the M-mode images in this study (Mean difference $\pm$ SD: 30 $\pm$ 27 ms) was close to that reported by Fellahi et al. (2009) (Mean difference $\pm$ SD: 32 $\pm$ 37 ms) and that reported by Carvalho et al. (2011) (Mean difference $\pm$ SD: 35 $\pm$ 38 ms). This probably suggests that the measurement of relative time intervals (LVET) from impedance would be more reliable than the measurement of instant time based features, including PEP and EMD.

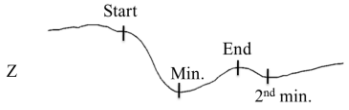

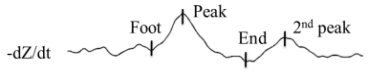

Table 7-6. Summary of literature on comparison between systolic time intervals measured from impedance and reference techniques (provided in the last column).

		Mean (SD) and Mean difference (SD) between techniques (ms)									
		PEP (Q -> aortic valve open)			EMD (Q -> aortic valve close)			LVET (aortic valve open -> close)			
References	***Subject No.***	-dZ/dt (Q ->foot)	Ref.	(-dZ/dt) - Ref.	-dZ/dt (Q ->end)	Ref.	(-dZ/dt) - Ref.	-dZ/dt (foot ->end)	Ref.	(-dZ/dt) - Ref.	***Reference techniques***
Lababidi et al. 1970	37	--	--	--	--	--	0 (2)	--	--	--	PCG
Schieken et al. 1978	10	--	--	--	340 (6)	360 (8)	-20	--	--	--	M-mode
Kizakevich et al. 1993	17	--	--	-20	--	--	21	--	--	--	Doppler
Cybulski et al. 2004	13	104 (21)	97 (13)	7 (19)	--	--	--	294 (27)	311 (27)	-16 (20)	Doppler
Fellahi et al. 2009	25	--	--	--	--	--	--	317 (36)	286 (23)	32 (37)	Doppler
Carvalho et al. 2011	17	--	--	12 (9)	--	--	32 (25)	--	--	35 (38)	Doppler
Ulbrich et al. 2013	6	--	--	--	--	--	--	307	--	--	None

Table 7-7. Summary of comparison between systolic time intervals measured from impedance and M-mode images based on data from this study.

	Mean (SD) and Mean difference (SD) between techniques (ms)									
	PEP (Q -> aortic valve open)			EMD (Q -> aortic valve close)			LVET (aortic valve open -> close)			
Subject No.	-dZ/dt (Q -> foot)	Ref.	(-dZ/dt) - Ref.	-dZ/dt (Q -> end)	Ref.	(-dZ/dt) - Ref.	-dZ/dt (foot -> end)	Ref.	(-dZ/dt) - Ref.	***Reference techniques***
30	126 (22)	76 (10)	49 (22)	485 (25)	406 (24)	79 (16)	359 (33)	329 (24)	30 (27)	M-mode

7.3.4 Relationship between valve movement and impedance feature times

Figure 7-6 shows the linear regression analysis results for the impedance times with the aortic valve opening time. Only the systolic peak of -dZ/dt showed a significant linear relationship with the aortic valve opening time ($R^2 = 0.394$, $P < 0.001$).

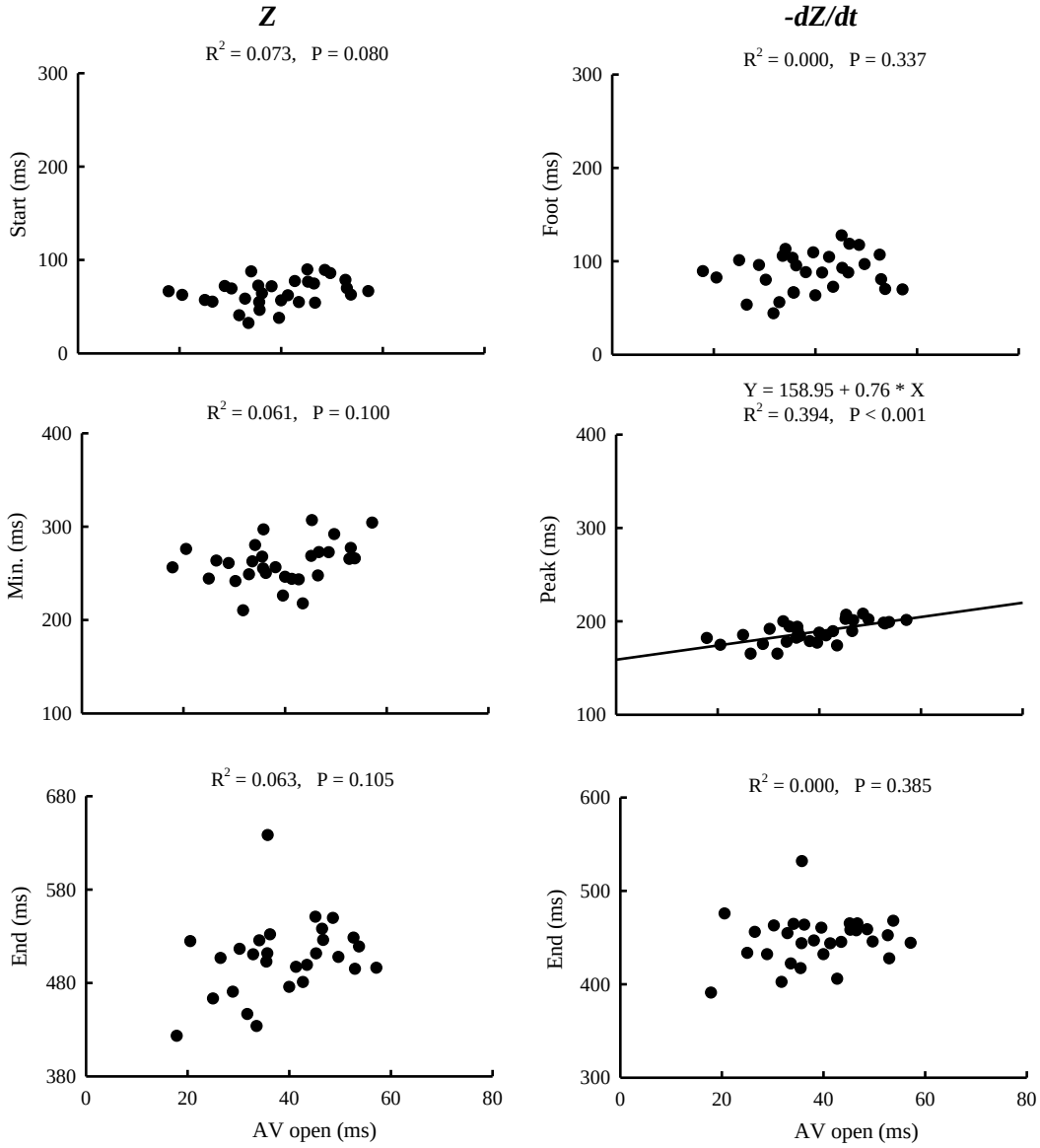

Figure 7-6. Relationship between aortic valve open and impedance times. All times were measured from ECG R wave.

Figure 7-7 shows the linear regression analysis results for the impedance times with the aortic valve closing time. The end of the systolic wave and the 2nd minimum point on the Z, and the end of systolic wave and the 2nd peak on the -dZ/dt showed significant linear relationships with the valve closing time ($R^2 \geq 0.371$, $P < 0.05$).

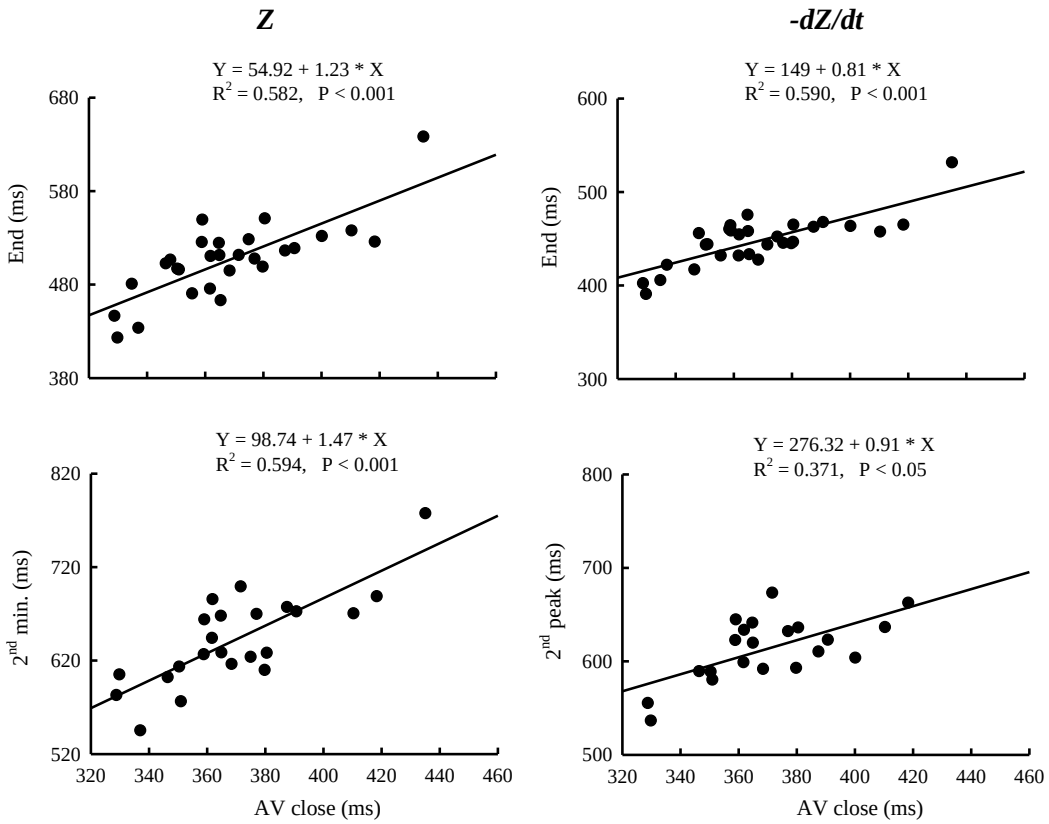

Figure 7-7. Relationship between aortic valve close and impedance times. All times were measured from ECG R wave.

Figure 7-8 shows the linear regression analysis results for the impedance times with the mitral valve movement times during the passive filling phase. Interestingly, all the impedance times showed significantly positive linear relationships with the valve open, maximum opening and closing times. The impedance Z end and 2nd minimum point, derivative impedance -dZ/dt end and 2nd peak ($R^2 \geq 0.566$, $P < 0.001$) showed stronger correlations with the valve initial opening than the other two valve times.

The linear regression analysis results for the assessment of the relation of the Z and -dZ/dt times with the valve movement times, are summarized in Table 7-8 and Table 7-9. After accounting for the RR interval, the aortic valve closing was still a significant variable in the regression model for the predicting of -dZ/dt end of systolic wave ($R^2 = 0.586$, $P < 0.05$), and the mitral valve open still showed a strong linear regression relationship with Z end, -dZ/dt end and 2nd peak ($R^2 \geq 0.560$, $P < 0.05$). The relationships between the mitral valve opening and the impedance diastolic features suggest the impedance diastolic wave would be initiated by ventricular passive filling.

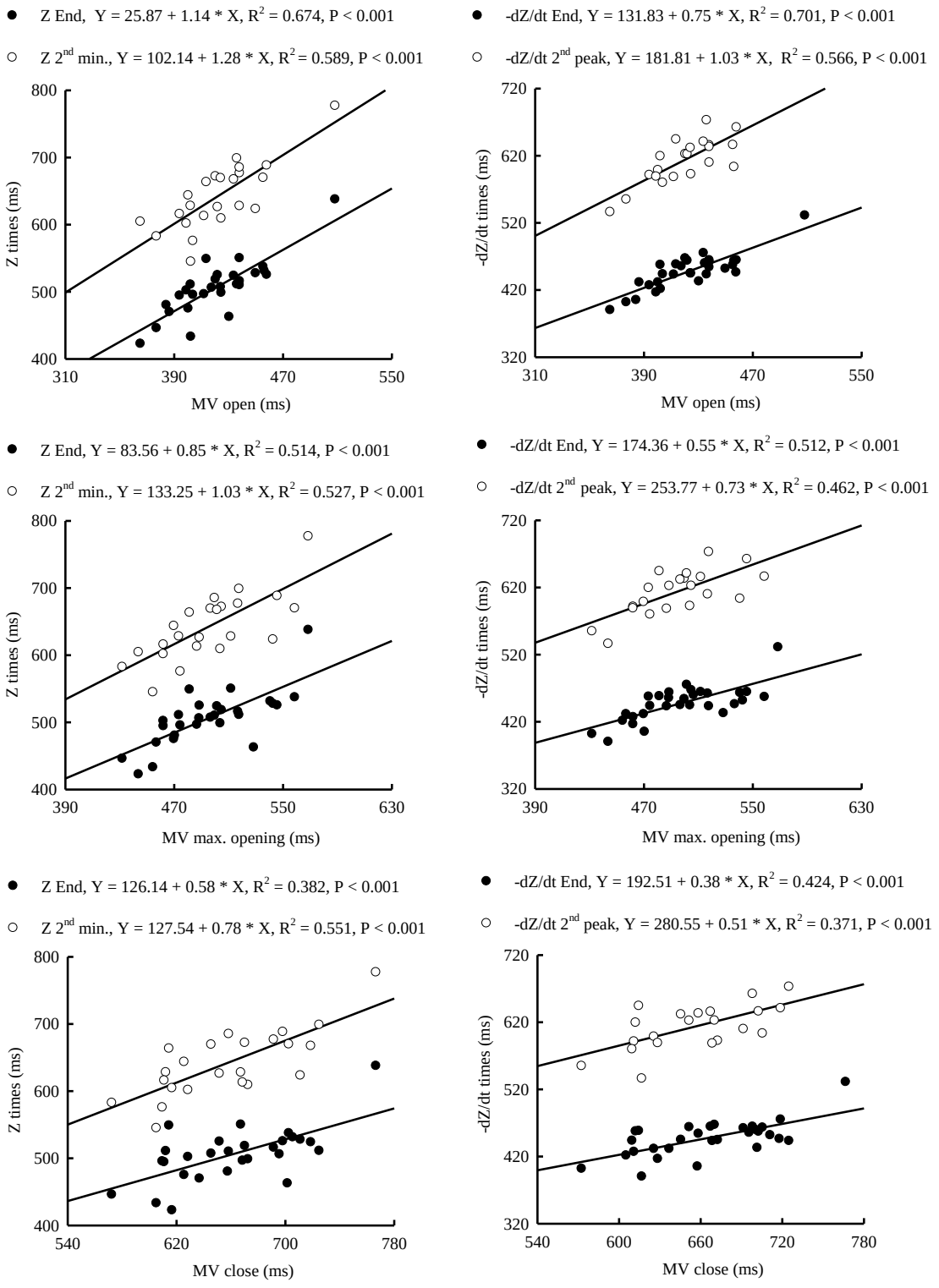

Figure 7-8. Relationship between impedance and mitral valve movement times during passive filling phase. All times were measured from ECG R wave.

Table 7-8. Summary of linear regression analysis results for impedance Z and valve movement times.

Valve movement times		Measure	Impedance Z times							
			Start		Min.		End		2nd min.	
			Un-adjusted	Adjusted[a]	Un-adjusted	adjusted[a]	Un-adjusted	adjusted[a]	Un-adjusted	adjusted[a]
AV	open	R^2	0.073	0.046	0.061	0.087	0.063	0.570**	0.000	0.755**
		P	0.080	0.101	0.100	0.146	0.105	0.139	0.872	0.061
	close	R^2	---	---	---	---	0.582**	0.584**	0.594**	0.707**
		P	---	---	---	---	< 0.001	0.084	< 0.001	0.912
MV	open	R^2	---	---	---	---	0.674**	0.673**	0.589**	0.725**
		P	---	---	---	---	< 0.001	< 0.05	< 0.001	0.266
	max. opening	R^2	---	---	---	---	0.514**	0.558**	0.527**	0.707**
		P	---	---	---	---	< 0.001	0.215	< 0.001	0.128
	close	R^2	---	---	---	---	0.382**	0.536**	0.551**	0.724**
		P	---	---	---	---	< 0.001	0.579	< 0.001	0.272

[a]: the linear regression model is adjusted for RR interval; * or **: the linear regression model is significant with $P < 0.05$ or $P < 0.001$.

P: represents the significance of the independent variable.

Table 7-9. Summary of linear regression analysis results for the derivative impedance (-dZ/dt) and valve movement times.

Valve movement times		Measure	Derivative impedance times (-dZ/dt)							
			Foot		Peak		End		2nd peak	
			Un-adjusted	Adjusted[a]	Un-adjusted	adjusted[a]	Un-adjusted	adjusted[a]	Un-adjusted	adjusted[a]
AV	open	R^2	0.000	0.000	0.394**	0.430**	0.000	0.502**	0.004	0.408*
		P	0.086	0.326	< 0.001	< 0.001	0.062	0.698	0.311	0.638
	close	R^2	---	---	---	---	0.590**	0.586**	0.371*	0.407*
		P	---	---	---	---	< 0.001	< 0.05	< 0.05	0.674
MV	open	R^2	---	---	---	---	0.701**	0.711**	0.566**	0.560**
		P	---	---	---	---	< 0.001	< 0.001	< 0.001	< 0.05
	max. opening	R^2	---	---	---	---	0.512**	0.565**	0.462**	0.464**
		P	---	---	---	---	< 0.001	0.054	< 0.001	0.162
	close	R^2	---	---	---	---	0.424**	0.555**	0.371*	0.447*
		P	---	---	---	---	< 0.001	0.079	< 0.05	0.234

[a]: the linear regression model is adjusted for RR interval; * or **: the linear regression model is significant with $P < 0.05$ or $P < 0.001$.

P: represents the significance of the independent variable.

7.3.5 Relationship between valve movement and impedance durations

The relationships between the aortic valve open duration and impedance durations are shown in Figure 7-9. Significant linear relationships were observed between the valve open duration and the Z systolic rising duration (from the minimum to the end) and overall duration of the systolic wave ($R^2 \geq 0.444$, $P < 0.001$), and the -dZ/dt systolic decelerating duration (from peak to end) and whole duration of the major wave ($R^2 \geq 0.324$, $P < 0.001$).

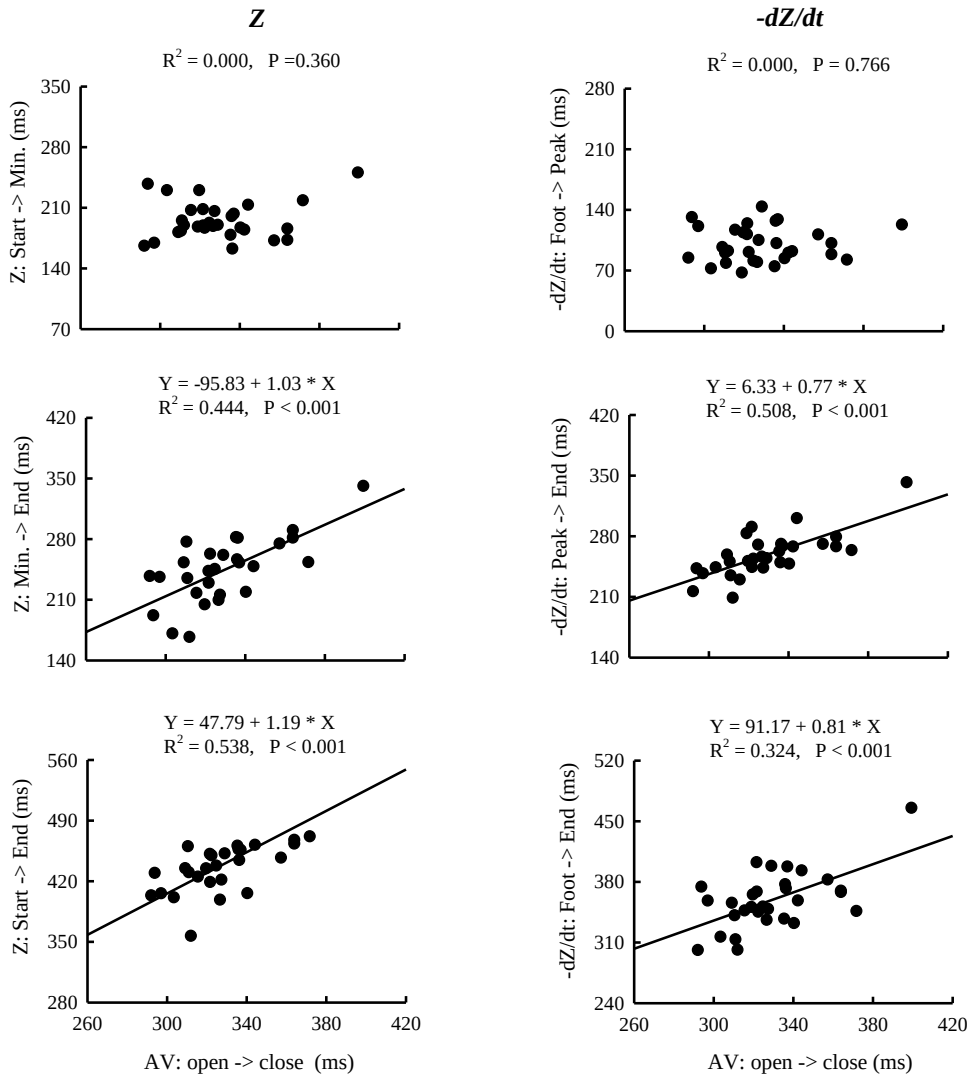

Figure 7-9. Relationship between aortic valve open and impedance durations.

The linear regression analysis results, adjusted for RR interval, for the relation of the impedance durations with the aortic valve open duration are summarized in Table 7-10. After accounting for the RR interval, the aortic valve open duration showed a significantly positive relationship with the -dZ/dt systolic decelerating duration ($R^2 = 0.491$, $P < 0.05$).

This relationship suggests that the rate of impedance variation during ventricular systole is related to the left ventricular ejection.

Table 7-10. Summary of linear regression analysis results for the relationships between impedance time durations and aortic valve opening duration.

Impedance durations (ms)		**Measure**	**AV open -> close (ms)**	
			Un-adjusted	Adjusted[a]
Z	Start -> Min.	R^2	0.000	0.000
		P	0.360	0.959
	Min. -> End	R^2	0.444**	0.459**
		P	< 0.001	0.223
	Start -> End	R^2	0.538**	0.571**
		P	< 0.001	0.167
-dZ/dt	Foot -> Peak	R^2	0.000	0.050
		P	0.766	0.172
	Peak -> End	R^2	0.508**	0.491**
		P	< 0.001	< 0.05
	Foot -> End	R^2	0.324**	0.333**
		P	< 0.001	0.301

[a]: the linear regression model was adjusted for RR interval; * or **: the linear regression model is significant with $P < 0.05$ or $P < 0.001$. P: represents the significance of the independent variable.

The linear relations of the Z diastolic falling duration (from systolic end to 2nd min.) and the corresponding accelerating duration on the -dZ/dt (from end to 2nd peak) with the mitral valve opening duration (from open to max. opening), closing duration (from max. opening to close) and overall duration (from open to close) during the passive filling phase are shown in Figure 7-10. However, as can be seen, there was no mitral valve movement duration showing a significantly linear relationship with the impedance diastolic durations.

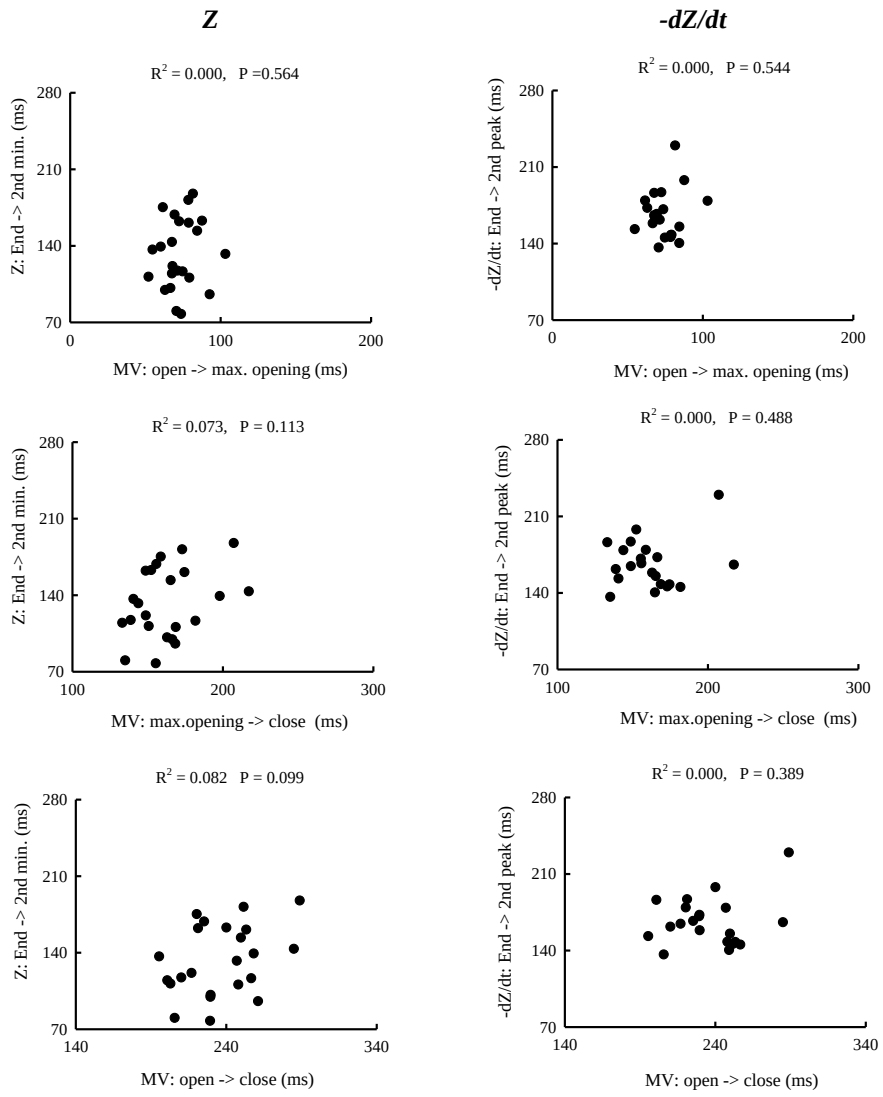

Figure 7-10. Relationship between impedance durations and mitral valve movement durations during the passive filling phase.

7.4 Dynamic relationship between blood flow and impedance

7.4.1 Timing sequence of flow conditions and impedance features

The impedance signals are displayed with the synchronized Doppler images for mitral flow and aortic flow in Figure 7-11. The impedance time features measured from the aortic flow start are also shown. The foot of the -dZ/dt occurred 36 ms after the flow onset, and the systolic peak was observed 100 ms later. The systolic wave on the -dZ/dt ended 395 ms after the aortic flow offset, which was close to the mitral flow start during the passive filling phase. The 2nd peak on the -dZ/dt was between the mitral flow peak and end.

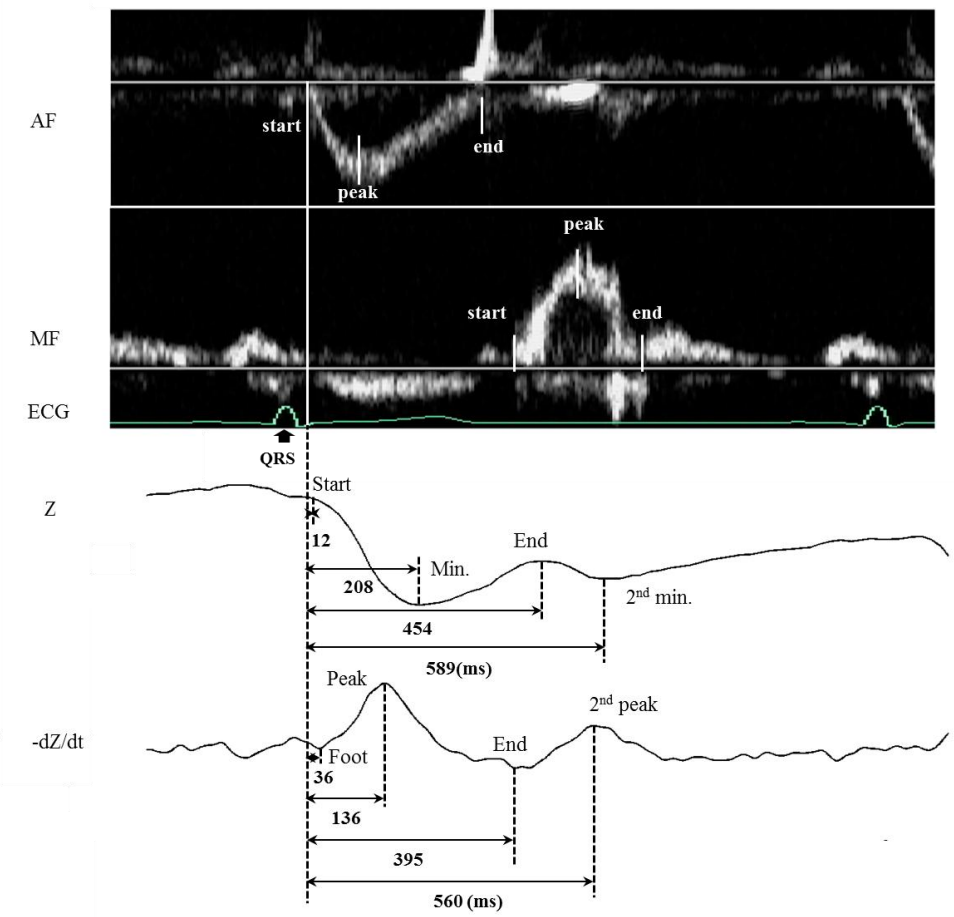

Figure 7-11. Impedance signals with synchronized ECG and blood flow traces. The impedance feature times were measured from the aortic flow start. The values are the means across all subjects.

Figure 7-12 (A) shows the sequence of time features from impedance Z, aortic flow and mitral flow during the passive filling phase, and the comparison results of corresponding times. All times were measured from the aortic flow start. After the onset of the aortic flow, the impedance Z started to fall. The minimum point of the Z occurred between the aortic flow peak and end ($P < 0.001$). Afterwards, the Z systolic wave ended between the mitral flow peak and end, and the 2nd minimum occurred before the mitral flow end during the passive filling phase ($P < 0.001$).

The sequence of time features from derivative impedance -dZ/dt and the blood flow conditions is shown in Figure 7-12 (B). The foot of the -dZ/dt systolic wave was significantly later than the aortic flow start ($P < 0.001$). Its first peak occurred 40 ms after the aortic flow peak ($P < 0.001$). The end of the systolic wave on -dZ/dt was observed

around the mitral flow start (Mean difference ± SEM: 7 ± 4 ms, P = 0.06), while the 2nd peak occurred 81 ms before the flow end during the passive filling phase (P < 0.001).

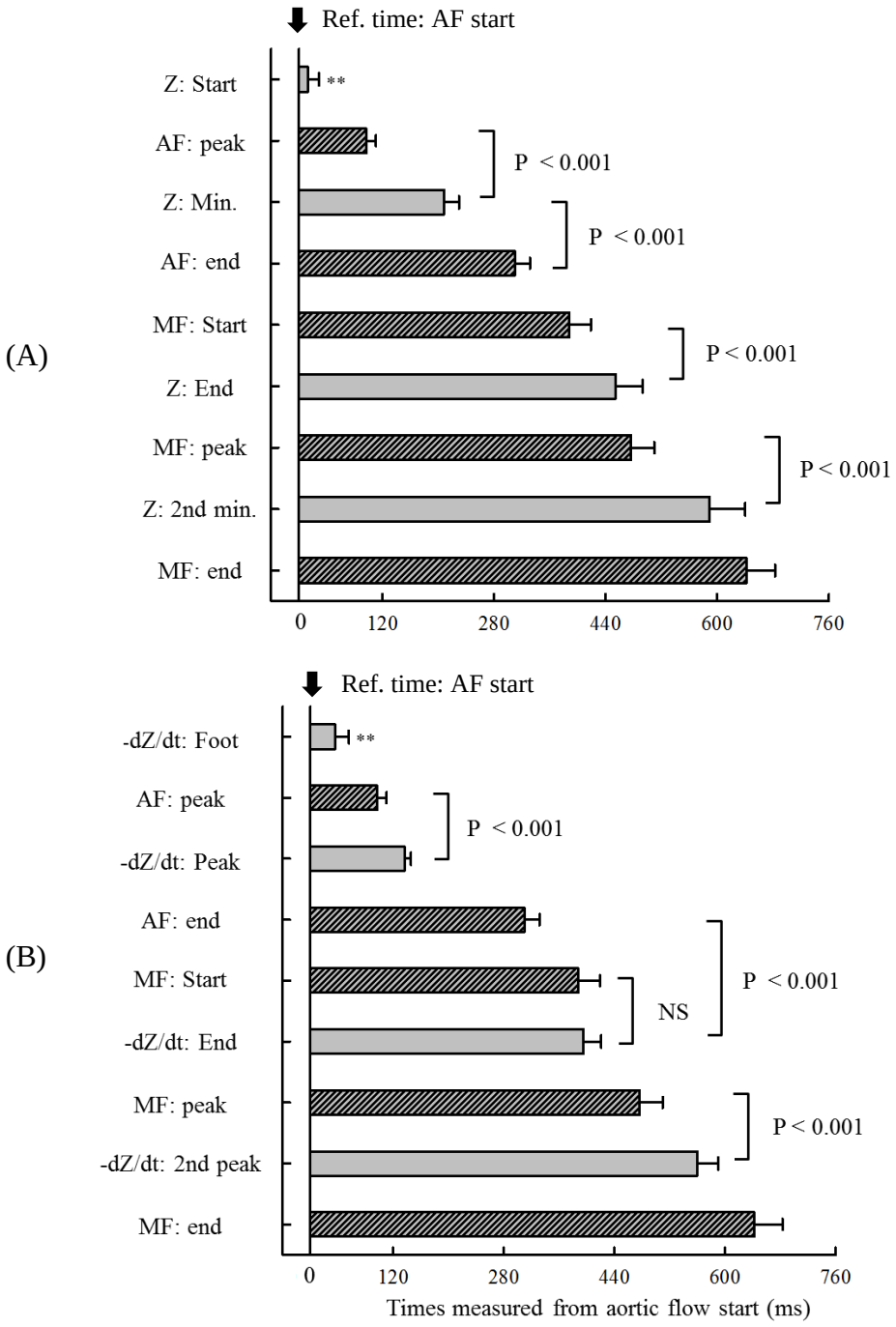

Figure 7-12. Timing sequence of features from impedance Z (A) and derivative impedance -dZ/dt (B) with blood flow times. **: significantly different from the reference time (aortic flow start) with P < 0.001.

The comparison between the feature times of the derivative impedance -dZ/dt and blood flow conditions would be expected to be more straightforward because both signals represent the velocities of change. The literature on the comparison of time features of -dZ/dt and blood flow conditions are summarized in Table 7-11, while the comparison using the data in this study are summarized in Table 7-12. It was reported by Kizakevich et al. (1993) that the impedance systolic foot occurred 20 ms before the aortic flow start. However, the authors argued that the phase delay of the Doppler device might be the main contributor to the delay. In this study, the impedance systolic foot occurred 36 ms after the aortic flow onset, which agreed with Cybulski et al. (2004). Kubicek (1989) reported that the systolic peak of the -dZ/dt occurred precisely at the peak flow velocity measured with an electromagnetic flowmeter. However, a time delay was found between the impedance systolic peak and the aortic flow peak measured with Doppler imaging. The delay reported by Carvalho et al. (2011) was 12 ms, while it was 40 ms in this study. The systolic end of the -dZ/dt showed a time delay of 86 ms after the aortic flow end in this study which was longer than that reported in the literature. In this study, the impedance diastolic peak was compared with the mitral flow peak during the passive filling phase. A delay of 87 ms was found for the impedance peak after the flow peak.

The comparison of feature times of impedance Z with blood flow conditions could provide additional information about the association between impedance change and cardiac mechanical events. However, it has rarely been investigated in the past. The key findings of comparison between the impedance Z time features and blood flow conditions in this study are summarized in Table 7-13. The decrease in the impedance during the ventricular ejection phase followed the onset of aortic flow by 12 ms. This reinforces the results reported in the previous section where the decrease of impedance started following the valve opening. A more important message here was that the impedance started to recovery 112 ms after the peak aortic flow during the ventricular ejection phase, which supported the previous finding that an increase in the impedance is caused by the drainage of more volume in the aorta to the periphery than the incoming volume from the left ventricle after the passive ventricular ejection phase. Interestingly, the time delay of the minimum of the impedance in diastole (2^{nd} minimum) with the mitral flow peak was 111 ms, which was very close to the delay of the impedance systolic minimum after the aortic flow peak.

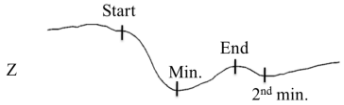

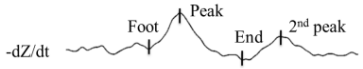

Table 7-11. Summary of literature on comparison between time features measured from derivative impedance (-dZ/dt) and reference techniques (in the last column).

		Mean (SD) and Mean difference (SD) between techniques (ms)												
		AF start			AF peak			AF end			MF start (before passive ventricular filling)			
References	***Subject No.***	R-> -dZ/dt foot	R -> AF start	diff.	R-> -dZ/dt peak	R -> AF peak	diff.	R-> -dZ/dt end	R -> AF end	diff.	R-> -dZ/dt 2nd peak	R -> MF start	diff.	***Reference techniques***
Kubicek 1989	--	--	--	--	--	--	0	--	--	--	--	--	--	Electro-magnetic
Kizakevich et al. 1993	17	--	--	-20	--	--	--	--	--	21	--	--	--	Doppler
Cybulski et al. 2004	13	--	--	7 (19)	--	--	--	--	--	--	--	--	--	Doppler
Carvalho et al. 2011	17	--	--	12 (9)	--	--	--	--	--	32 (25)	--	--	--	Doppler

Table 7-12. Summary of comparison between time features measured from derivative impedance (-dZ/dt) and Doppler images in this study.

	Mean (SD) and Mean difference (SD) between techniques (ms)												
	AF start			AF peak			AF end			MF start (before passive ventricular filling)			
Subject No.	R-> -dZ/dt foot	R -> AF start	diff.	R-> -dZ/dt peak	R -> AF peak	diff.	R-> -dZ/dt end	R -> AF end	diff.	R-> -dZ/dt 2nd peak	R -> MF start	diff.	***Reference techniques***
30	88 (21)	52 (12)	36 (20)	189 (12)	149 (20)	40 (17)	448 (26)	362 (24)	86 (15)	613 (34)	529 (36)	81 (24)	Doppler

Table 7-13. Summary of comparison between time features measured from impedance (Z) and Doppler images in this study.

	Mean (SD) and Mean difference (SD) between techniques (ms)												
	AF start			AF peak			AF end			MF start (before passive ventricular filling)			
Subject No.	R-> Z start	R -> AF start	diff.	R-> Z min.	R -> AF peak	diff.	R-> Z end	R -> AF end	diff.	R-> Z 2nd min.	R -> MF start	diff.	***Reference techniques***
30	65 (15)	52 (12)	12 (16)	261 (23)	149 (20)	112 (28)	506 (41)	362 (24)	144 (24)	643 (50)	529 (36)	111 (31)	Doppler

7.4.2 Comparison of time durations from blood flow and impedance

The comparison of time durations from the impedance signals with durations from flow is shown in Figure 7-13. The overall aortic flow duration was less than the durations of the systolic wave on the impedance Z and -dZ/dt ($P < 0.001$). For the systolic wave, the aortic flow accelerating duration (from start to peak) was comparable to the impedance accelerating duration (from -dZ/dt foot to peak) (Mean difference ± SEM: 4 ± 5 ms, $P = 0.386$). For the diastolic wave, the mitral flow decelerating duration (from flow peak to end) during the passive filling phase was significantly shorter than the Z falling duration ($P < 0.001$), but close to the impedance accelerating duration (from -dZ/dt end to 2nd peak) (Mean difference ± SEM: 6 ± 8 ms, $P = 0.520$).

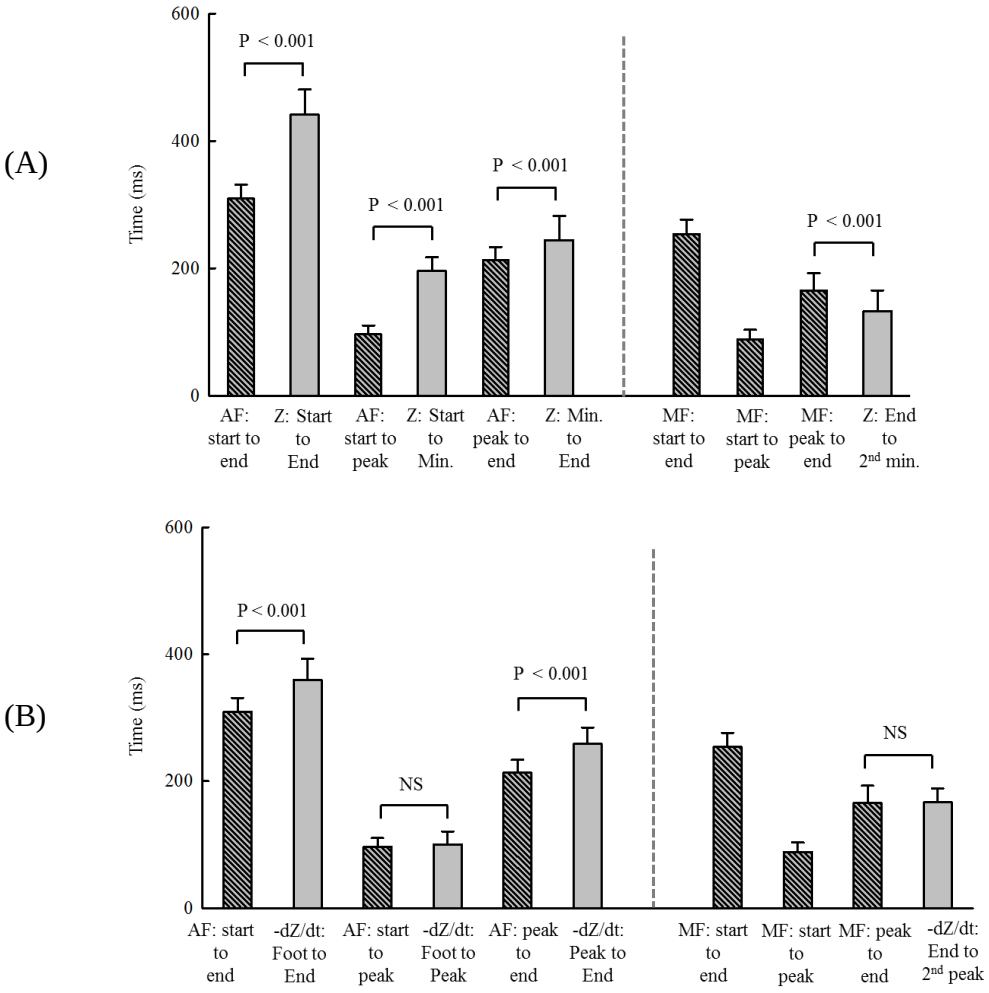

Figure 7-13. Comparison of impedance Z durations (A) and -dZ/dt durations (B) with blood flow durations. Error bars represent SDs between subjects.

7.4.3 Comparison between systolic time intervals measured from derivative impedance and Doppler echocardiograms

The relevant data from previous studies on the comparison between systolic time intervals measured from the derivative impedance -dZ/dt and reference techniques are summarized in Table 7-14, while the data about the comparison of the measurements from impedance with those from M-mode and Doppler echocardiograms are summarized in Table 7-15. As has been described in the previous chapter, the aortic flow started soon after the aortic valve opened, while the flow ended shortly before the valve closed. Therefore, the PEP measured from the Doppler images (49 ms) was a little longer than that from the M-mode images (36 ms), while the EMD from the Doppler images (79 ms) was shorter than that from the M-mode images (86 ms). The LVET measured from the Doppler images 20 ms shorter than that from the M-mode images (Mean Doppler LVET *vs.* Mean M-mode LVET: 30 ms *vs.* 50 ms).

For the PEP, the measurement provided by the impedance was 36 ms longer than that from the Doppler images. The time difference was more significant for the EMD measurement. The estimation from the impedance was 86 ms longer than that from the Doppler images. The LVET measured from the impedance was 50 ms longer than that from the Doppler images. However, it can be noted that the impedance accelerating time (measured from the systolic foot to the peak) was comparable to the aortic flow accelerating time (measured from the aortic flow start to peak), which means that the difference of LVET measurement from impedance and Doppler image was mainly contributed by the difference between the decelerating times of the impedance (measured from the systolic peak to end) and the aortic flow (measured from the peak to end) (Mean difference: 46 ms). This observation suggests that the current definition of the systolic end of the derivative impedance (the minimum point between the systolic wave and diastolic wave) would probably not be the best for LVET measurement. Carvalho et al. (2011) proposed using the onset of the descending part before the minimum point as the new definition of the impedance systolic end. By employing this new definition, the difference of LVET measured from the impedance and Doppler images was reduced to 35 ms in their study.

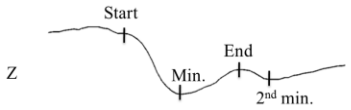

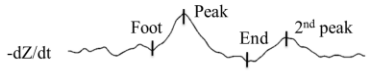

Table 7-14. Summary of literature on the comparison between systolic time intervals measured from impedance and reference techniques (in the last column).

		Mean (SD) and Mean difference (SD) between techniques (ms)												
		PEP (Q -> aortic valve open)			EMD (Q -> aortic valve close)			LVET (aortic valve open -> close)			Accelerating time (aortic flow start -> peak)			
References	***Subject No.***	-dZ/dt (Q-> foot)	Ref.	(-dZ/dt) - Ref.	-dZ/dt (Q-> end)	Ref.	(-dZ/dt) - Ref.	-dZ/dt (foot-> end)	Ref.	(-dZ/dt) - Ref.	-dZ/dt (foot-> peak)	Ref.	(-dZ/dt) - Ref.	***Reference techniques***
Lababidi et al. 1970	37	--	--	--	--	--	0 (2)	--	--	--	--	--	--	PCG
Schieken et al. 1978	10	--	--	--	340 (6)	360 (8)	-20	--	--	--	--	--	--	M-mode
Kizakevich et al. 1993	17	--	--	-20	--	--	21	--	--	--	--	--	--	Doppler
Cybulski et al. 2004	13	104 (21)	97 (13)	7 (19)	--	--	--	294 (27)	311 (27)	-16 (20)	--	--	--	Doppler
Fellahi et al. 2009	25	--	--	--	--	--	--	317 (36)	286 (23)	32 (37)	--	--	--	Doppler
Carvalho et al. 2011	17	--	--	12 (9)	--	--	32 (25)	--	--	35 (38)	--	--	--	Doppler
Ulbrich et al. 2013	6	--	--	--	--	--	--	307	--	--	--	--	--	None

Table 7-15. Summary of the comparison between systolic time intervals measured from impedance and echocardiograms in this study.

	Mean (SD) and Mean difference (SD) between techniques (ms)												
	PEP (Q -> aortic valve open)			EMD (Q -> aortic valve close)			LVET (aortic valve open -> close)			Accelerating time (aortic flow start -> peak)			
Subject No.	-dZ/dt (Q-> foot)	Ref.	(-dZ/dt) - Ref.	-dZ/dt (Q-> end)	Ref.	(-dZ/dt) - Ref.	-dZ/dt (foot-> end)	Ref.	(-dZ/dt) - Ref.	-dZ/dt (foot-> peak)	Ref.	(-dZ/dt) - Ref.	***Reference techniques***
30	126 (22)	76 (10)	49 (22)	485 (25)	406 (24)	79 (16)	359 (33)	329 (24)	30 (27)	--	--	--	M-mode
	126 (22)	90 (11)	36 (20)	485 (25)	399 (23)	86 (15)	359 (33)	309 (22)	50 (27)	100 (20)	96 (14)	-4 (25)	Doppler

7.4.4 Relationship between blood flow conditions and impedance feature times

The relationship between the impedance Z and aortic flow features is shown in Figure 7-14. Most Z features had no significant linear relationship with the flow features. The minimum point of the Z systolic wave showed significant relationship with aortic flow start (R^2 = 0.138, P < 0.05). The end of the systolic wave on the Z waveform showed a significant relationship with the flow peak (R^2 = 0.158, P < 0.05), and a very strong positive linear relationship with the flow end (R^2 = 0.703, P < 0.001).

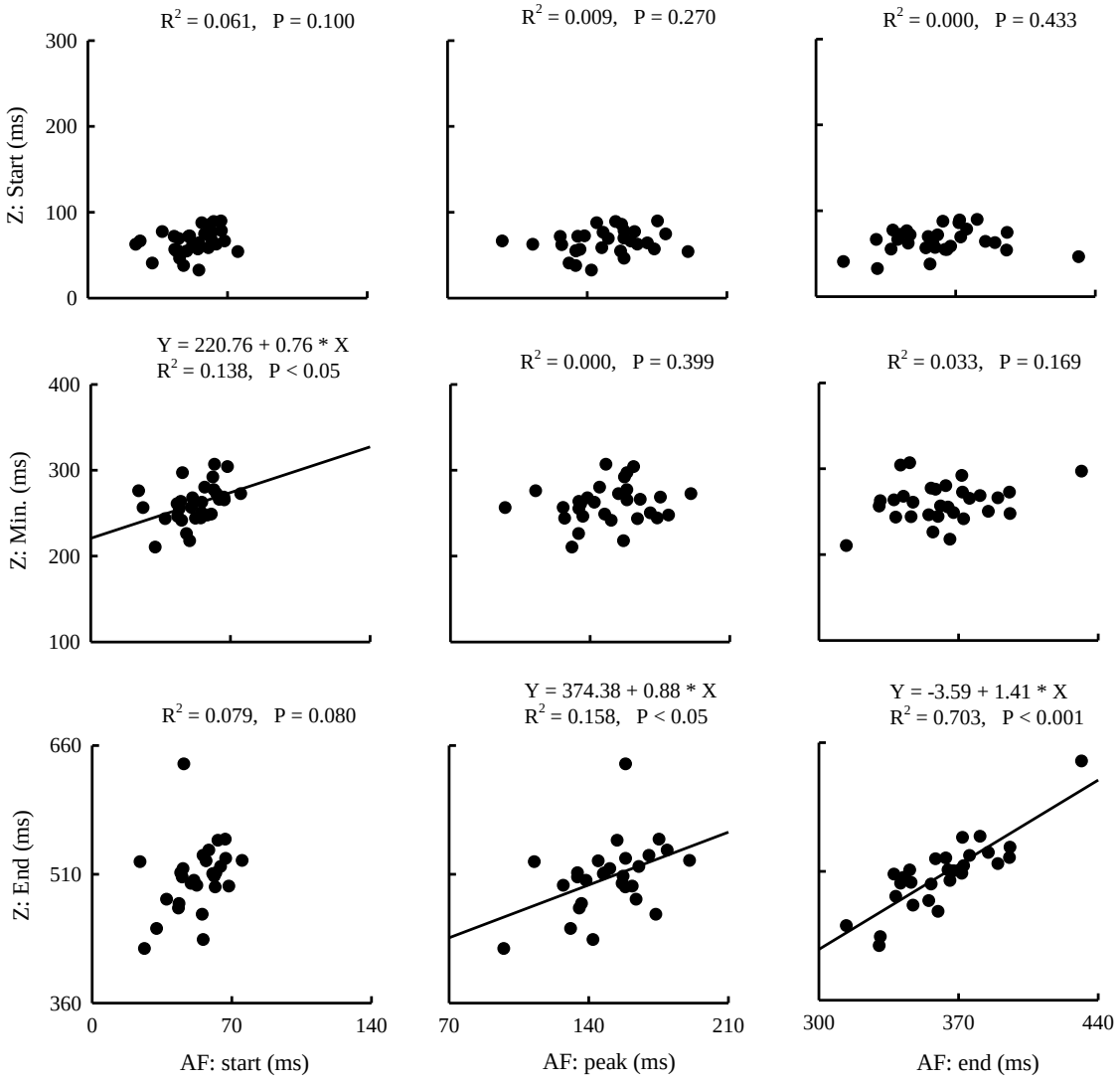

Figure 7-14. Relationship between impedance Z and aortic flow times. All times were measured from ECG R wave.

The relationship between the derivative impedance -dZ/dt and aortic flow features is shown in Figure 7-15. The -dZ/dt foot showed a positive linear relationship with the flow

start (R^2 = 0.112, P < 0.05). The -dZ/dt peak showed significant relationships with all the flow times, especially with the flow start (R^2 = 0.484, P < 0.001). The strongest relationship was observed between the -dZ/dt end and the flow end (R^2 = 0.657, P < 0.001).

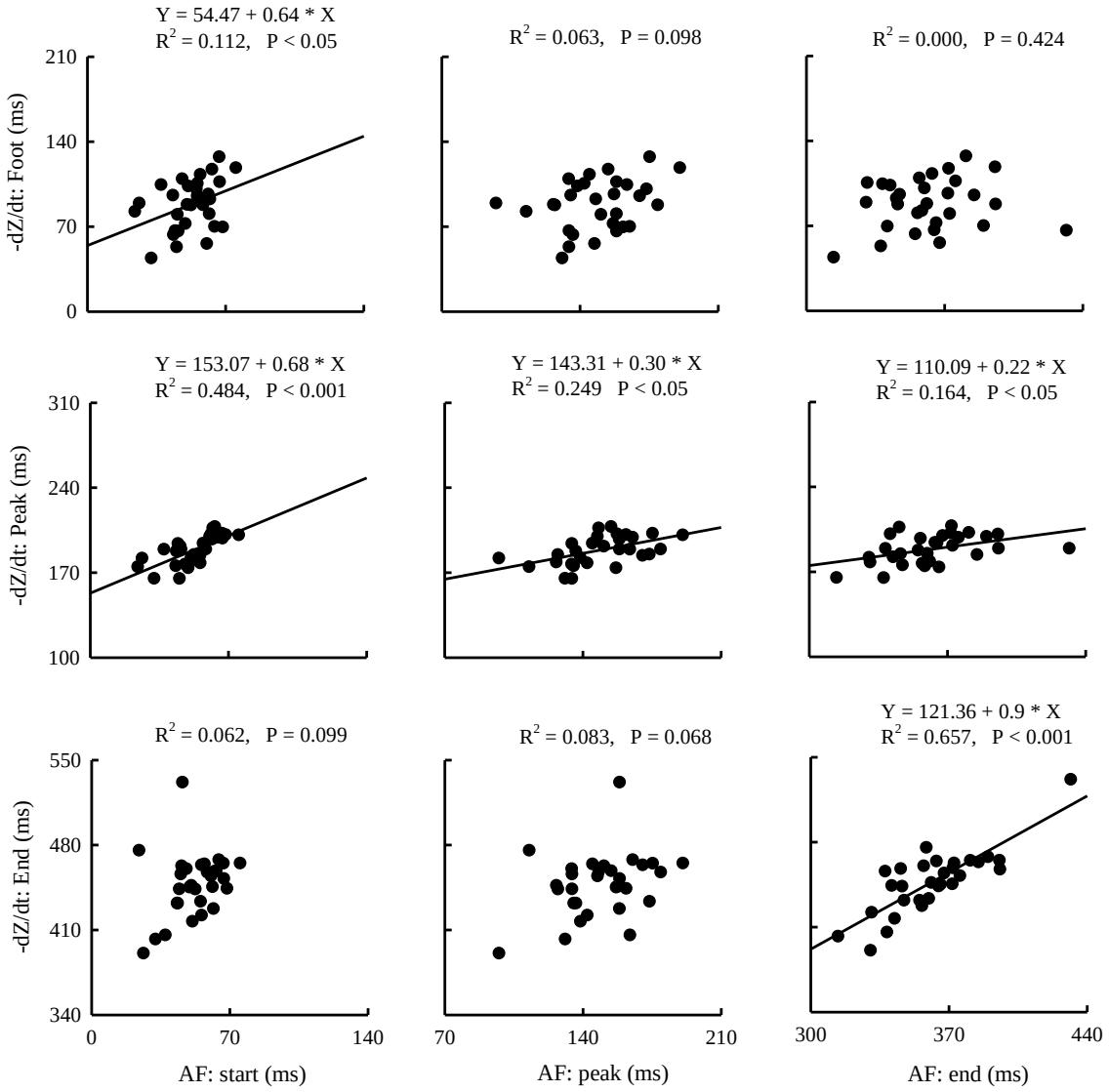

Figure 7-15. Relationship between derivative impedance -dZ/dt and aortic flow times. All times were measured from ECG R wave.

The relationship between the impedance and mitral flow features is shown in Figure 7-16. As can be noted, all the flow times showed significant relationships with the impedance Z end and 2nd minimum points, and -dZ/dt end and 2nd peak (all P < 0.001). For a given impedance time, the flow start always provided the best fit for the linear regression model with the largest R^2 value.

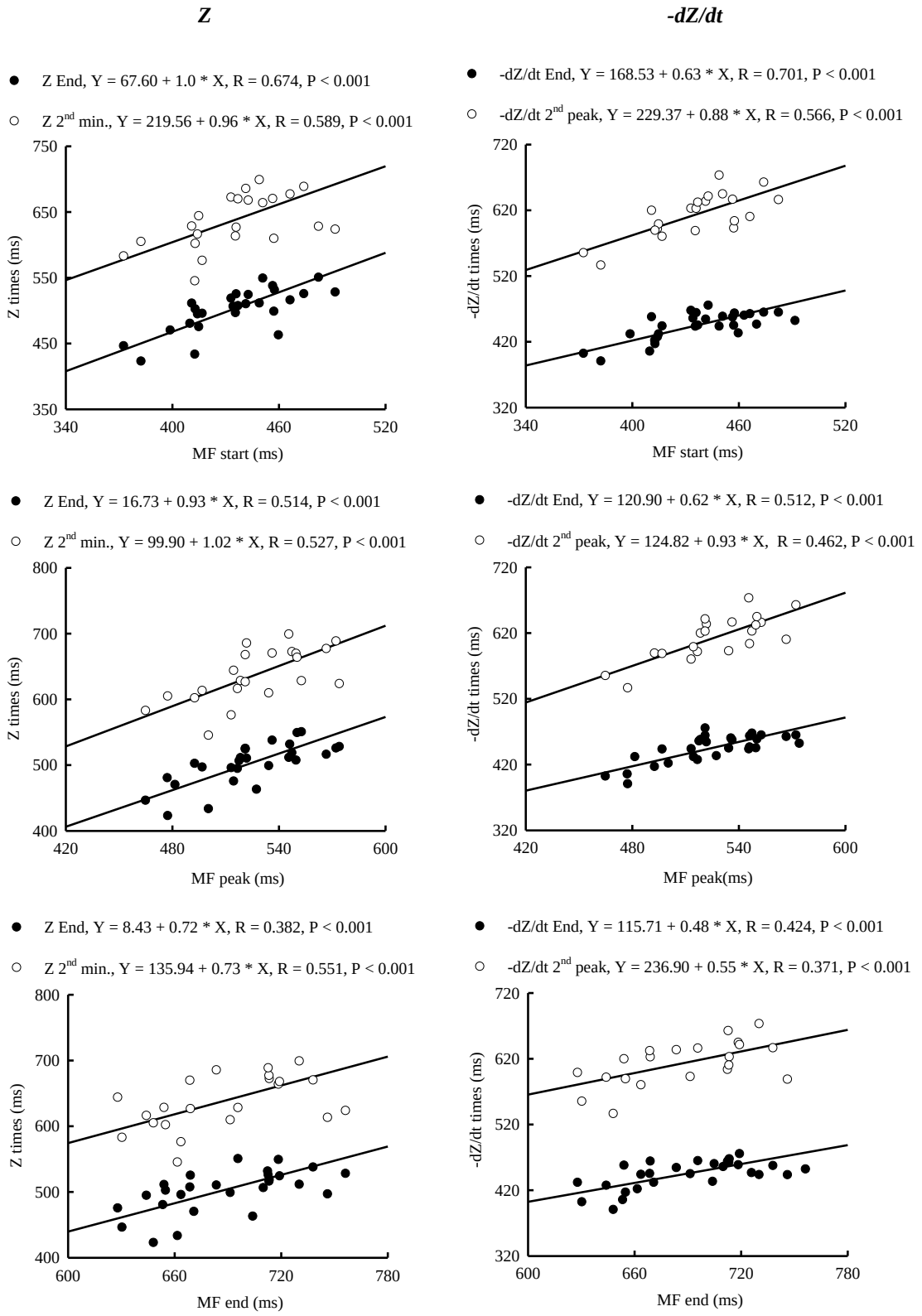

Figure 7-16. Relationship between impedance and mitral flow times during the passive filling phase. All times were measured from ECG R wave.

The linear regression analysis results for the relation of flow times with impedance Z and -dZ/dt times are summarized in Table 7-16 and Table 7-17. After accounting for the RR interval, while none of the aortic flow times was found as a significant variable for any regression model, all the mitral flow times were significant in the regression models for predicting of the Z systolic wave end (all $P < 0.05$).

There were more flow times keeping the significant linear relationships with the -dZ/dt times than Z times after the adjustment for RR interval. In the regression models for the predicting of the -dZ/dt systolic peak, the aortic flow started ($R^2 = 0.491$, $P < 0.001$) and peak ($R^2 = 0.227$, $P < 0.05$) were still significant variables in each model. The aortic flow end was strongly related with -dZ/dt end ($R^2 = 0.647$, $P < 0.05$). The mitral flow time also showed a significant relationship with the -dZ/dt end. The coefficients of determination for the mitral flow start and peak in the corresponding models were 0.677 and 0.712 respectively (both $P < 0.001$). The mitral flow end had less strong influence on the -dZ/dt end ($R^2 = 0.619$, $P < 0.05$).

According to the linear regression analysis results in this section, the flows were more related to the derivative impedance -dZ/dt than the impedance Z. The times of the aortic flow were strongly related to the times of the -dZ/dt systolic wave. The -dZ/dt systolic end, as the connection of the systolic wave and diastolic wave, was strongly related to both aortic flow during ventricular systole and mitral flow during ventricular early diastole.

Table 7-16. Summary of linear regression analysis results for impedance (Z) and blood flow times.

			Impedance times (Z)							
			Start		Min.		End		2nd min.	
Flow times		**Measure**	Un-adjusted	Adjusted[a]	Un-adjusted	adjusted[a]	Un-adjusted	adjusted[a]	Un-adjusted	adjusted[a]
AF	start	R^2	0.061	0.030	0.138*	0.142*	0.079	0.557‡	---	---
		P	0.100	0.135	< 0.05	0.052	0.080	0.225	---	---
	peak	R^2	0.009	0.000	0.000	0.012	0.158*	0.537‡	---	---
		P	0.270	0.390	0.399	0.909	< 0.05	0.544	---	---
	end	R^2	0.000	0.000	0.033	0.012	0.703**	0.692**	---	---
		P	0.431	0.714	0.101	0.868	< 0.001	< 0.001	---	---
MF	start	R^2	---	---	---	---	0.653**	0.677**	0.437**	0.709**
		P	---	---	---	---	< 0.001	< 0.05	< 0.001	0.711
	peak	R^2	---	---	---	---	0.695**	0.692**	0.596**	0.723**
		P	---	---	---	---	< 0.001	< 0.001	< 0.001	0.285
	end	R^2	---	---	---	---	0.515**	0.604**	0.409**	0.711**
		P	---	---	---	---	< 0.001	< 0.05	< 0.001	0.616

[a]: the linear regression model is adjusted for RR interval; * or **: the linear regression model is significant with $P < 0.05$ or $P < 0.001$.

P: represents the significance of the independent variable.

Table 7-17. Summary of linear regression analysis results for the derivative impedance (-dZ/dt) and blood flow times.

			Derivative impedance times (-dZ/dt)							
			Foot		Peak		End		2nd peak	
Flow times		**Measure**	Un-adjusted	Adjusted[a]	Un-adjusted	adjusted[a]	Un-adjusted	adjusted[a]	Un-adjusted	adjusted[a]
AF	start	R^2	0.112*	0.098	0.484**	0.491**	0.062	0.516**	---	---
		P	< 0.05	< 0.05	< 0.001	< 0.001	0.099	0.338	---	---
	peak	R^2	0.063	0.077	0.249*	0.227*	0.083	0.501**	---	---
		P	0.098	< 0.05	< 0.05	< 0.05	0.068	0.809	---	---
	end	R^2	0.000	0.058	0.164*	0.142*	0.657**	0.647**	---	---
		P	0.424	0.063	< 0.05	0.088	< 0.001	< 0.05	---	---
MF	start	R^2	---	---	---	---	0.627**	0.677**	0.516**	0.548**
		P	---	---	---	---	< 0.001	< 0.001	< 0.001	< 0.05
	peak	R^2	---	---	---	---	0.512**	0.712**	0.575**	0.565**
		P	---	---	---	---	< 0.001	< 0.001	< 0.001	< 0.05
	end	R^2	---	---	---	---	0.535**	0.619**	0.313*	0.446*
		P	---	---	---	---	< 0.001	< 0.05	< 0.05	0.240

[a]: the linear regression model is adjusted for RR interval; * or **: the linear regression model is significant with $P < 0.05$ or $P < 0.001$.

P: represents the significance of the independent variable.

7.4.5 Relationship between blood flow and impedance durations

The relationships between the impedance durations and aortic flow durations are shown in Figure 7-17. Significant relationships of impedance durations with the flow decelerating duration and the overall flow duration are observed. Specifically, the flow decelerating duration is significantly related to the impedance Z increasing duration (R^2 = 0.247, P < 0.05) and the -dZ/dt decelerating duration (R^2 = 0.390, P < 0.001). The overall flow duration is significantly related to the overall duration of the major wave on Z (R^2 = 0.568, P < 0.001) and -dZ/dt (R^2 = 0.334, P < 0.001).

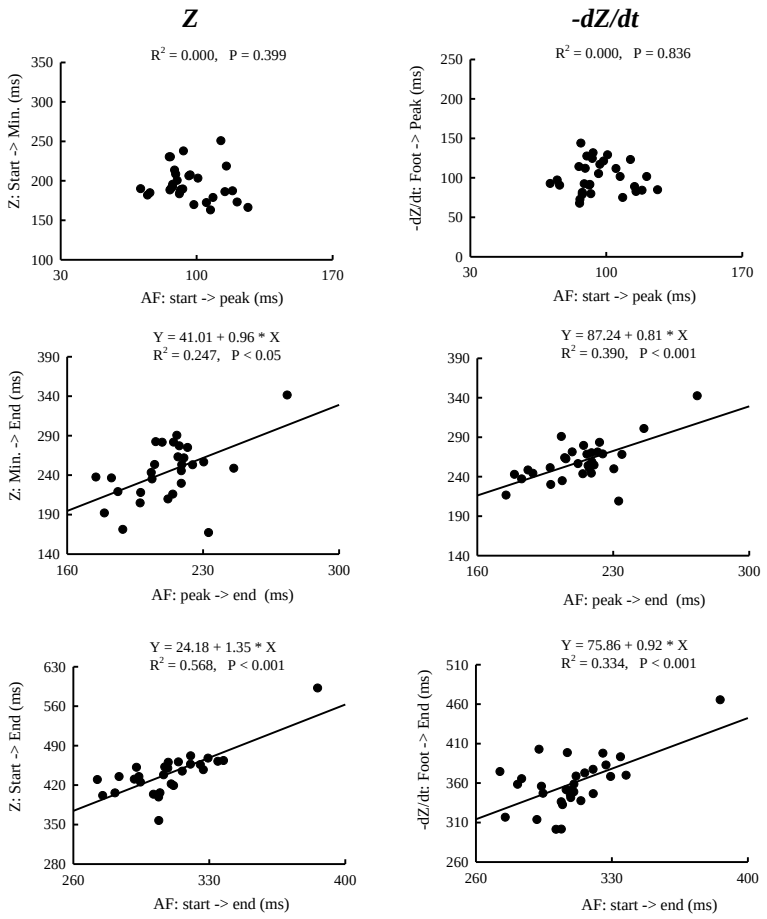

Figure 7-17. Relationship between aortic flow and impedance time durations.

The linear regression analysis results, adjusted for RR interval, for the relation of the impedance durations with the aortic flow durations are summarized in Table 7-18. After the adjustment, the flow decelerating duration is still significantly correlated with the impedance decelerating duration (R^2 = 0.475, P < 0.05), and the overall flow duration is significantly correlated with the duration of the major wave of Z (R^2 = 0.604, P < 0.05).

Table 7-18. Summary of linear regression analysis results for the relationships between impedance time durations and aortic flow durations.

Impedance durations (ms)		Measure	AF durations (ms)					
			Accelerating duration start to peak		Decelerating duration peak to end		Whole duration start to end	
			Un-adjusted	Adjusted[a]	Un-adjusted	Adjusted[a]	Un-adjusted	Adjusted[a]
Z	Start to Min.	R^2	0.000	0.076	---	---	---	---
		P	0.399	0.132	---	---	---	---
	Min. to End	R^2	---	---	0.247*	0.453**	---	---
		P	---	---	< 0.05	0.271	---	---
	Start to End	R^2	---	---	---	---	0.568**	0.604**
		P	---	---	---	---	< 0.001	< 0.05
-dZ/dt	Foot to Peak	R^2	0.000	0.015	---	---	---	---
		P	0.836	0.342	---	---	---	---
	Peak to End	R^2	---	---	0.390**	0.475**	---	---
		P	---	---	< 0.001	< 0.05	---	---
	Foot to End	R^2	---	---	---	---	0.334**	0.350*
		P	---	---	---	---	< 0.001	0.184

[a]: the linear regression model is adjusted for RR interval; * or **: the linear regression model is significant with $P < 0.05$ or $P < 0.001$.

P: represents the significance of the independent variable.

The relationships between the impedance durations and mitral flow durations during the passive filling phase are shown in Figure 7-18. There was no flow duration showing a significant relationship with the impedance Z or -dZ/dt duration.

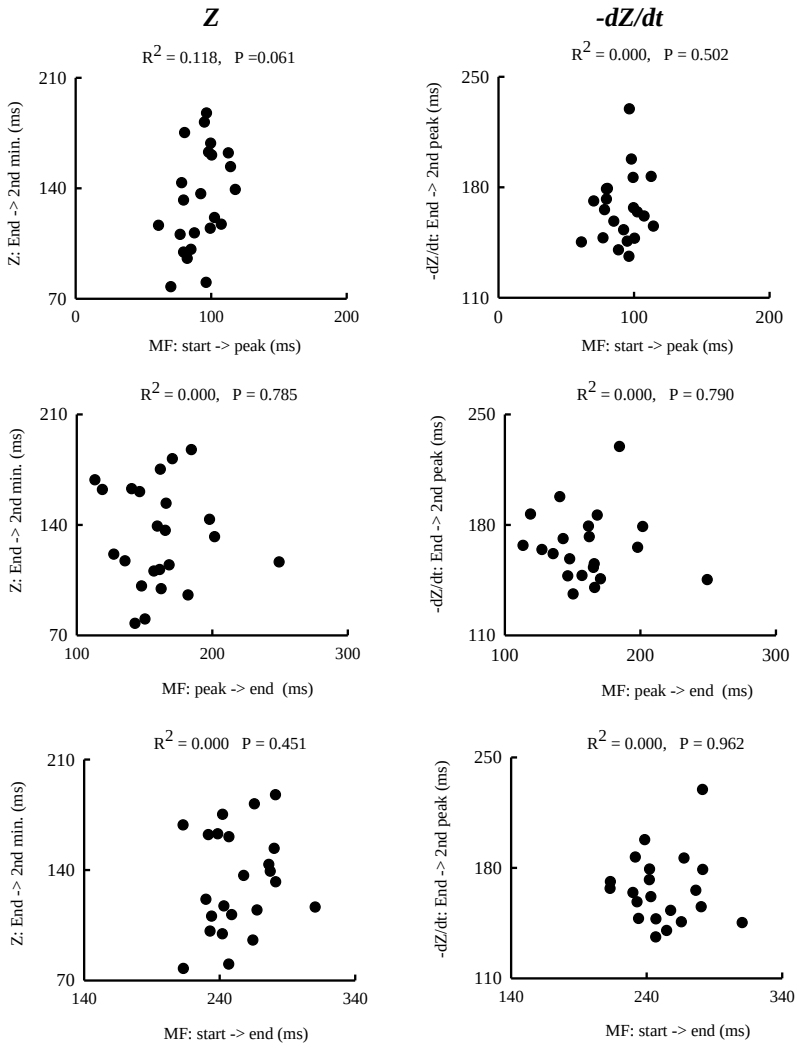

Figure 7-18. Relationship between mitral flow and impedance time durations.

7.4.6 Summary of relationships between impedance times and flow time features

According to linear regression analysis results, the systolic times of the impedance Z did not show significant correlations with aortic flow conditions. However, the systolic end from Z (also considered as the start of the diastolic falling) was strongly correlated with the mitral flow start during the passive filling phase ($R^2 = 0.653$, $P < 0.001$). This correlation is independent of heart rate change ($R^2 = 0.677$, $P < 0.001$, after adjustment by RR interval).

The impedance diastolic minimum was strongly correlated with the mitral peak flow (R^2 = 0.596, $P < 0.001$).

All the time features of the derivative impedance -dZ/dt showed strong correlations with the blood flow conditions. In contrast to the weak relationship with the aortic valve opening, the impedance systolic foot was significantly correlated with the aortic flow start (R^2 = 0.112, $P < 0.05$). The impedance systolic peak, although it had a time delay, was strongly correlated with the peak aortic flow (R^2 = 0.484, $P < 0.001$). Because the impedance systolic foot and end were significantly correlated with the aortic flow start and end respectively, the LVET measured from the -dZ/dt showed a strongly positive correlation with that from the Doppler images. In addition to the significant association between the impedance systolic times with aortic flow conditions, its diastolic peak also strongly correlated with the peak mitral flow during the passive filling phase (R^2 = 0.575, $P < 0.001$). All these results suggest that the derivative impedance is more related with the flow than valve movement.

7.5 Discussion and conclusions

In this chapter, the time features of the impedance Z and the first derivative impedance -dZ/dt were investigated, with reference to valve movement times and blood flow conditions from simultaneously recorded images. The time durations from the impedance signals, especially the systolic time intervals measured from the derivative impedance -dZ/dt, were compared with the corresponding durations from images. The relationships between the impedance time features and imaging time features were examined. The key results of the comparison and the linear relationship examination between the impedance features and corresponding imaging features are summarized in Table 7-19.

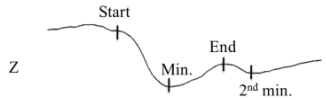

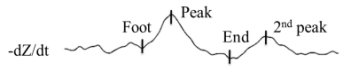

Table 7-19. Summary of key results of the comparison and linear relationship examination between impedance features and imaging features.

Imaging features	***Impedance features***	**Comparison**			**Significance of linear regression analysis‡**
		Mean difference ± SD† (ms)	**Range (ms)**	**Significance**	
AV open	Z start	26 ± 15	(-2, 53)	P < 0.001	P = 0.101
AV close	Z min.	-108 ± 30	(-163, -47)	P < 0.001	--
AF start	-dZ/dt foot	36 ± 20	(-4, 67)	P < 0.001	P < 0.05
AF peak	-dZ/dt peak	40 ± 17	(10, 85)	P < 0.001	P < 0.05
AF peak	Z min.	112 ± 28	(61, 163)	P < 0.001	P = 0.909
AF end	-dZ/dt end	86 ± 15	(61, 118)	P < 0.001	P < 0.05
MV open (passive filling)	Z end	86 ± 23	(32, 136)	P < 0.001	P < 0.05
MF peak (passive filling)	-dZ/dt 2nd peak	87 ± 21	(44, 128)	P < 0.001	P < 0.05

†: Mean difference = impedance features (measured from ECG R wave) – imaging features (measured from ECG R wave); ‡: Adjusted for RR interval;

Linking the time features of the impedance Z with valve movement and blood flow conditions is helpful in providing a better understanding of the origins of the pulsatile Z in each cardiac cycle. The key findings from the investigation are:

- The impedance Z started to fall at the beginning of the left ventricular ejection, but started to recover during the late ventricular ejection phase. Another Z falling period, with a smaller amplitude, was observed during the ventricular passive filling phase;
- During the ventricular ejection phase, the impedance started to fall soon (26 ms) after the aortic valve opened. The minimum of the impedance was observed 112 ms after the aortic flow peak and 146 ms before the valve closed. During ventricular passive filling phase, the impedance started to fall around the mitral valve maximum opening time ($P > 0.05$), and stopped 23 ms before the valve closed;
- The overall duration of the impedance Z systolic wave was 82 ms longer than the left ventricular ejection duration measured from aortic valve open to close on M-mode echocardiograms;
- The impedance Z systolic start was linked by a short difference from the aortic valve opening and aortic flow start even there was no significant linear relationship between the Z start and any of the valve opening or flow start. The Z systolic end (the start of falling during diastole) was strongly related to mitral valve opening during ventricular passive filling phase ($R^2 = 0.673$, $P < 0.05$).

The three characteristic components of the pulsatile impedance Z were firstly described by Karnegis and Kubicek (1970) with reference of the ECG waveform; a small upward wave associated with the ECG P wave, a major downward wave synchronous with the ECG QRS complex followed by a second downward wave during early diastole. Because the small upward wave was not always visible, only the two downwards waves were investigated in this study. The major decrease in the impedance Z occurred during the ventricular ejection phase, while the second decrease occurred within the ventricular passive filling phase, which confirmed that these two waves were a systolic event and a diastolic event respectively.

A series of studies investigating the effects of blood volumetric change in the thorax on the impedance Z waveform were performed by Patterson and Kubicek et al. (1964, 1966, 1970, 1978 and 1989). By controlling the pulmonary arterial flow and aortic flow with

balloon catheters placed in the right and left atria of dogs, the investigator found that the Z systolic wave was abolished when the left ventricular ejection was disabled. In addition, during spontaneous left mechanical alternans, where the left ventricle ejects blood on every other beat while the right ventricular ejection does not change, the Z systolic wave only followed the aortic flow. Based on these observations, the investigators concluded that the ejection of blood into the aorta is the main factor causing the systolic pulsatile Z wave (Kubicek et al. 1967). According to the work of Patterson (1978), the contributions of volume changes in various regions in the thorax on the pulsatile Z during systole were compared. It was found that the volume changes in lungs, atria, aorta and ventricles can make significant contribution to the impedance changes. As compared to other regions, the volume change in the ventricles made the least contribution (Patterson 1978). Unfortunately, timings were ignored in these studies. In this study, the impedance Z feature times were linked to valve movement times and blood flow conditions. The results are able to provide additional information on the origins of the pulsatile impedance waveform. Firstly, a decrease in the impedance was observed during both the ventricular ejection and passive filling phase, which confirmed that the volume change in the ventricles would not be the only contributor to the impedance change. Impedance falling during systole was found soon after the start of ventricular ejection, but stopped during the late ejection phase. This observation suggests that the volume change in the aorta rather than in the ventricle is the main generator of the impedance falling during systole. During the late ejection phase, the blood volume from the left ventricle into the aorta was reduced and slowed down. The volume change in the thorax is dominated by the drainage of volume from the central aorta to the periphery, which would result in a reduction of the blood volume in the thorax thus causing the impedance to restore. Attention was drawn by Karnegis et al. (1970) to the central venous return contributing to the pulsatile Z. There is no direct evidence showing the links between the Z waveform and the venous return so far. However, it was known that the central venous flow was augmented by the pressure gradient during the ventricular passive filling phase (Wexler et al. 1968). The strong relationship between the starting point of Z falling during diastole and the mitral valve movement during the passive filling phase might indicate that the venous return in this phase could be the main generator of the Z diastolic falling.

The first derivative impedance -dZ/dt represents the velocity of impedance change. The relationships between the time features of the derivative impedance and the blood flow conditions from Doppler echocardiograms were of interest in this study. The key findings for the investigation are:

- As with the impedance Z, the derivative impedance -dZ/dt systolic foot and peak were located within the ventricular ejection phase, while the systolic wave end and the diastolic peak were located within the passive filling phase;
- During the ventricular ejection phase, the systolic foot of the -dZ/dt occurred shortly (36 ms) after the aortic flow onset, and the systolic peak occurred 40 ms after the aortic peak flow. During the passive filling phase, the systolic wave of the -dZ/dt ended around the mitral flow onset ($P > 0.05$), and the diastolic peak of the -dZ/dt occurred 81 ms after the mitral flow peak;
- The derivative impedance -dZ/dt systolic foot was linked by a short difference from the aortic flow start although there was no significant linear relationship between the -dZ/dt foot and the flow start. The systolic peak of the derivative impedance -dZ/dt was significantly related to aortic flow peak ($R^2 = 0.227$, $P < 0.05$), and the end of the -dZ/dt systolic wave was strongly related to aortic flow end ($R^2 = 0.647$, $P < 0.05$);
- The diastolic peak of the -dZ/dt was strongly related to mitral flow peak ($R^2 = 0.565$, $P < 0.05$) during the ventricular passive filling phase.

According to Lababidi et al. (1970), the feature times of the derivative impedance -dZ/dt were perfectly synchronized with the cardiac mechanical events measured from phonocardiograms; the systolic foot of the -dZ/dt was synchronous with the maximal deflection of the first heart sound (mitral valve close), the systolic end was synchronous with the maximal deflection of the aortic second heart sound (aortic valve close), the diastolic peak of the -dZ/dt was found around the maximal vibration of the phonocardiographic opening snap (mitral valve open). These results were questioned in the later studies. Sherwood et al. (1990) pointed out that the impedance systolic foot should be considered as the indicator of aortic valve open rather than mitral valve close. However, the relevant data to support this point was limited. Carvalho et al. (2011) compared the time instant of the -dZ/dt features with aortic valve open and close times estimated from Doppler

echocardiograms, which showed that the impedance systolic foot occurred soon (12 ms) after the aortic valve opening, while its end occurred 32 ms later than the valve closing. In this study, the feature times of the derivative impedance -dZ/dt were carefully linked to the aortic flow conditions during ventricular ejection and mitral flow conditions during ventricular passive filling. A time delay ranged from 36 ms to 86 ms was found when comparing the impedance systolic times (foot, peak and end) with the corresponding aortic flow conditions (start, peak and end). The impedance diastolic peak was also found to occurr 81 ms later than the mitral flow peak. It can be noted that these time delays were higher than the values reported in other relevant literature (Kizakevich et al. 1993, Cybulski et al. 2004, Carvalho et al. 2011). This could partially result from the intrinsic difference of the impedance recording devices. As reported by Sherwood et al. (1990), because of a lack in methodological standardization, signals recorded by different impedance cardiography could vary a lot. The associations between the derivative impedance times and blood flow conditions were demonstrated by the significantly linear regression results.

One of the most important potential applications of the impedance technique is to provide a quick and easy way to measure systolic time intervals. The three common systolic time intervals, including pre-ejection period (PEP), electromechanical delay (EMD) and left ventricular ejection time (LVET), and the aortic flow accelerating time were measured on the -dZ/dt and compared with those measured from images. The key findings in this investigation are:

- The PEP measured from the impedance -dZ/dt was 126 ms, which was significantly longer ($P < 0.001$) than that from M-mode images (76 ms) and Doppler images (90 ms). No significant relationship was found for the impedance PEP with either M-mode PEP or Doppler PEP;
- The EMD measured from the impedance -dZ/dt was 485 ms, which was also significantly longer ($P < 0.001$) than that from M-mode images (406 ms) and Doppler images (399 ms). Strong linear relationships were found for the impedance EMD with both the M-mode EMD ($R^2 = 0.590$, $P < 0.001$) and the Doppler EMD ($R^2 = 0.657$, $P < 0.001$);
- The LVET measured from the impedance -dZ/dt was 359 ms, which was significantly longer ($P < 0.001$) than that from M-mode images (329 ms) and Doppler images (309 ms). Significantly linear relationships were found for the

impedance LVET with both the M-mode LVET (R^2 = 0.324, P < 0.001) and the Doppler LVET (R^2 = 0.334, P < 0.001);

- The systolic accelerating time measured from the impedance -dZ/dt was 100 ms, which was comparable (P > 0.05) with the aortic flow accelerating time (96 ms). However, no significant relationship was found between them.

It can be noted that for all the PEP, EMD and LVET measurements, the impedance provided significantly higher values than those from the images. For those intervals based on the instant time of impedance features, including PEP and EMD, the differences between the values given by the impedance and those by the reference images in this study were longer than those from the literature. It was reported that for the PEP measurement the difference between the impedance and the images ranged from -20 to 12 ms, while for the EMD the difference ranged from -20 to 32 ms (Schieken et al. 1978, Kizakevich et al. 1993, Cybulski et al. 2004, Carvalho et al. 2011). Again, this would result from the difference of the impedance recording devices. However, for the LVET measurement, the difference between the impedance and the M-mode images in this study (Mean difference ± SD: 30 ± 27 ms) was close to that reported by Fellahi et al. (2009) (Mean difference ± SD: 32 ± 37 ms) and that reported by Carvalho et al. (2011) (Mean difference ± SD: 35 ± 38 ms). This probably suggests that the measurement of relative time intervals (LVET) from impedance would be more reliable against differences than the measurement of instant time based features, including PEP and EMD. As the impedance accelerating time (measured from the systolic foot to the peak) was comparable to the aortic flow accelerating time (measured from the aortic flow start to peak), the difference of LVET measurement from impedance and Doppler image was mainly due to the difference between the decelerating parts of the impedance and the aortic flow (Mean difference: 46 ms). This observation suggests that the current definition of the systolic end of the derivative impedance (the minimum point between the systolic wave and diastolic wave) would probably not be the best for LVET measurement. Carvalho et al. (2011) proposed using the onset of the descending part before the minimum point as the new definition of the impedance systolic end. By employing this new definition, the difference of LVET measured from the impedance and Doppler images was reduced to 35 ms in their study.

Chapter 8 Relation of peripheral pulse with imaging and impedance data

The relation of peripheral pulses with the imaging and impedance data is investigated in this chapter.

8.1 Introduction

A peripheral pulse is initiated by the ejection of blood from the left ventricle to the aorta, which is then transmitted to peripheral sites along the arterial system. In session 3, finger pulse was recorded with M-mode echocardiograms for aortic valve movement and Doppler images for aortic flow. Based on these data, the relation of pulse features with aortic valve movement and aortic flow conditions is investigated in this chapter.

As described in the previous chapter, the pulsatile change in impedance in each cardiac cycle is another physiological phenomenon resulting from ventricular ejection. The shape of the impedance waveform in each heart beat was similar to that of the peripheral volume pulse; both of them consist of two waves in each beat, a major wave corresponding to the systole and a smaller wave corresponding to diastole. In session 2, ear and finger pulses were recorded with impedance on each subject, which allowed the investigation of the relationship between these two peripheral pulses and impedance changes presented in this chapter.

8.2. Overview of timing sequence of finger pulse

The ECG data and echocardiographic data recorded in session 3 have been introduced in Chapter 6. The feature times of the finger pulse recorded in the same session are summarized in Table 8-1. The features, including the pulse foot, systolic peak, notch and the diastolic peak, were identified from all the 30 subjects and measured with reference to the ECG R wave.

Table 8-1. Summary of finger pulse feature times from the data recorded in session 3.

Features	Subject numbers	Mean ± SD (ms)
Foot	30	201 ± 18
Systolic peak	30	388 ± 63
Notch	30	549 ± 30
Diastolic peak	30	630 ± 45

The pulse features are displayed with ECG features and imaging features in timing sequence in Figure 8-1. The dots represented the mean values of the feature times across all subjects, while the error bars represented the SDs. As can be seen, the aortic valve opened within 100 ms after the ECG R wave and the pulse foot occurred approximately 200 ms after the ECG R wave, which means that it took more than 100 ms for the pulse to be transmitted to the finger tip after left ventricle ejection started. The pulse systolic peak was observed approximately at the end of the ejection phase, with the notch and diastolic peak occur during the passive filling phase.

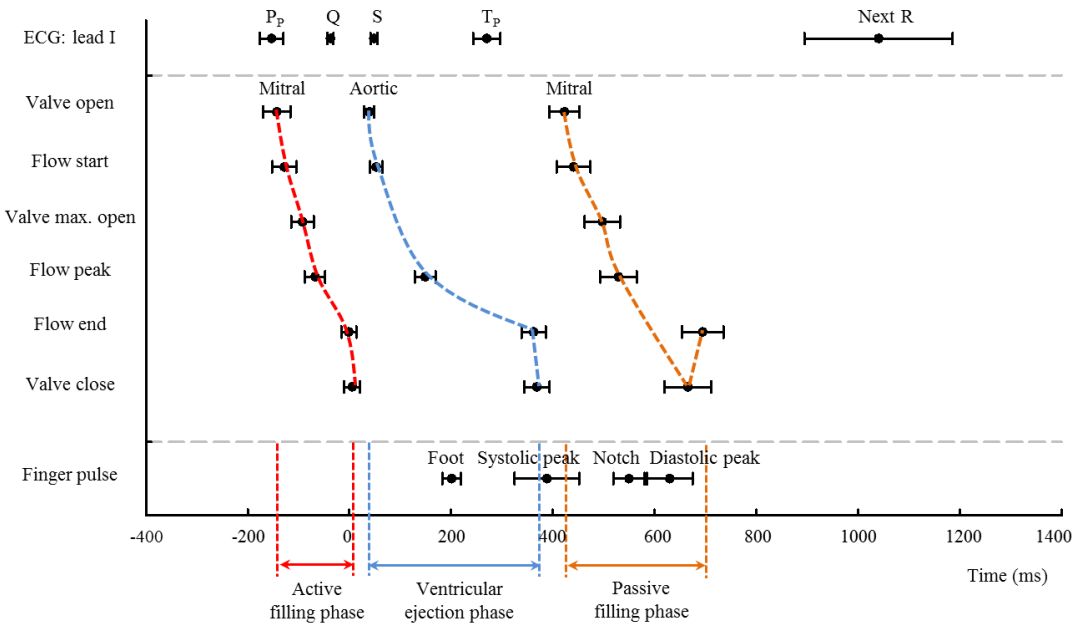

Figure 8-1. Timing sequence of ECG, imaging and finger pulse features. All times were measured from ECG R wave. Circle represents the mean and error bar represents SD across all subjects.

8.3 Dynamic relation of finger pulse with aortic valve movement and flow

8.3.1 Timing sequence of finger pulse and imaging features

Figure 8-2 shows the finger pulse waveform with a time aligned M-mode image for aortic valve movement and a Doppler image for aortic flow in a single beat. The average pulse feature times across all subjects, measured from the aortic valve opening time, are also illustrated. The pulse foot was detected on average 162 ms (SD: 15 ms) after the aortic valve initially opened, and achieved its systolic peak 349 ms and the diastolic peak 591 ms after the valve opened. Between the two peaks, the pulse notch point was detected at 510 ms with reference to the valve opening.

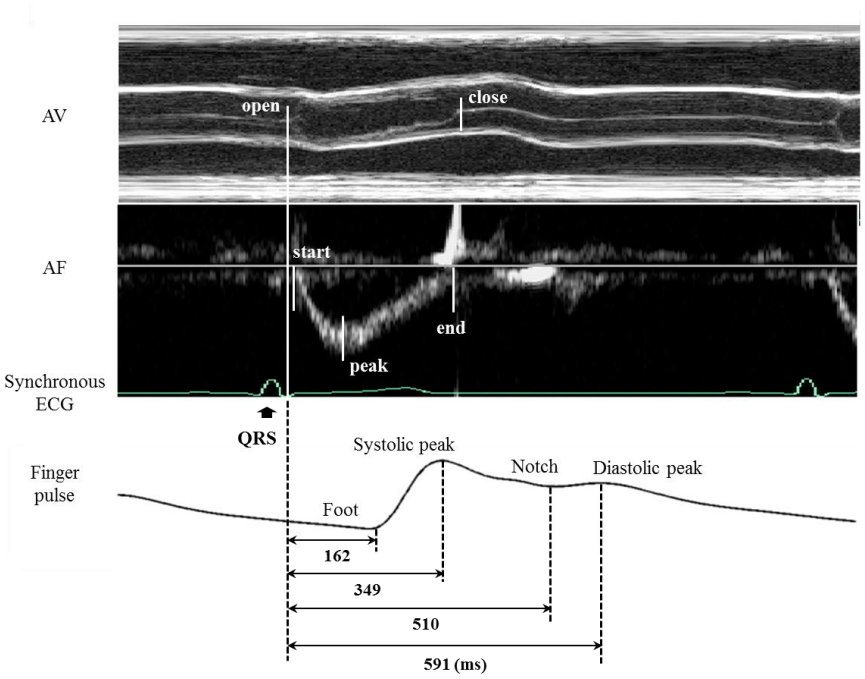

Figure 8-2. An example of finger pulse waveform with simultaneous aortic valve movement and aortic flow with average pulse feature times (measured from aortic valve opening) across all subjects.

Figure 8-3 shows the comparison of the pulse features with the aortic valve movement and flow condition times. Statistically, the finger pulse foot occurred significantly after the peak aortic flow (Mean difference ± SD: 52 ± 16 ms) and before the aortic valve closed (Mean difference ± SD: 168 ± 25 ms) (both $P < 0.001$). The systolic peak of the pulse occurred 20 ms after the aortic valve closed ($P < 0.05$).

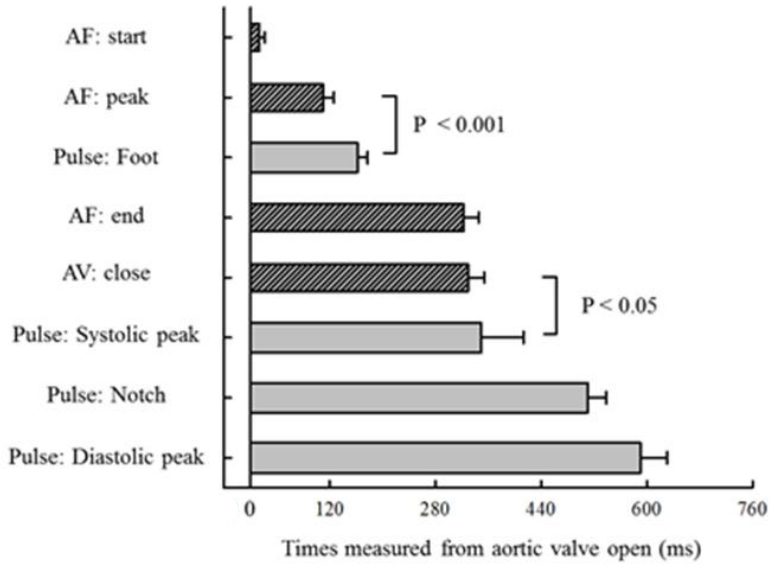

Figure 8-3. Timing sequence of finger pulse and valve movement features.

8.3.2 Comparison between finger pulse and imaging time durations

Figure 8-4 shows the comparisons of the pulse durations with aortic valve movement and flow durations. The overall duration of the pulse systolic wave (measured from pulse foot to the notch) (Mean ± SD: 348 ± 24 ms) was slightly longer than the left ventricular ejection duration measured from the aortic valve opening to closing (Mean ± SD: 329 ± 24 ms) or from the aortic flow start to end (Mean ± SD: 309 ± 22 ms) (both $P < 0.001$). In addition, the pulse rise time (from pulse foot to the systolic peak) was slightly shorter (26 ms) than the aortic flow decelerating time (from aortic flow peak to end) ($P < 0.05$).

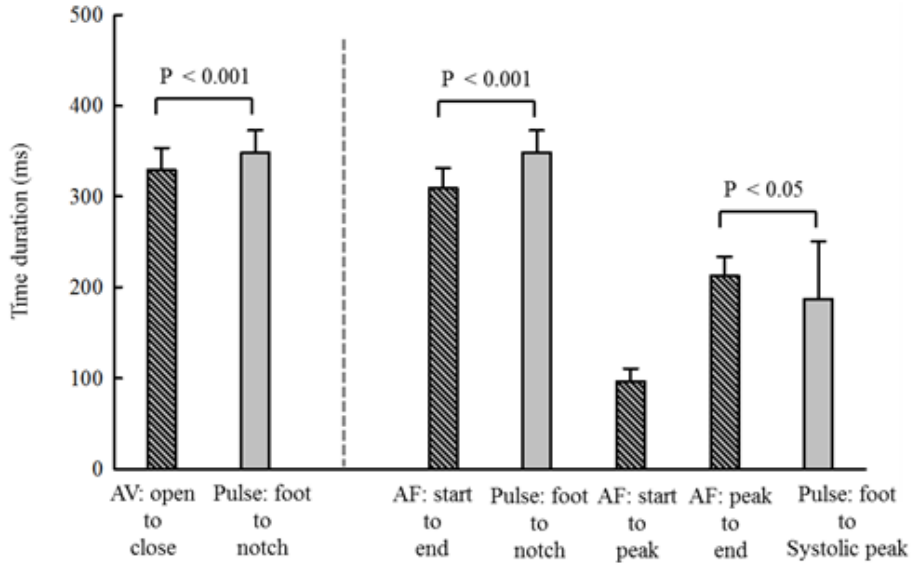

Figure 8-4. Comparison between time durations of finger pulse durations with aortic valve and flow durations.

8.3.3 Relationship between finger pulse and imaging features

The linear regression results for the relations of the pulse systolic feature times (foot, peak and notch) with the aortic valve opening and closing times are shown in Figure 8-5. Only the pulse foot showed a significant linear relationship with the valve initial opening ($R^2 = 0.270$, $P < 0.05$), while the pulse foot, systolic peak and notch showed a strongly linear relationship with the valve closing time ($R^2 \geq 0.336$, all $P < 0.001$).

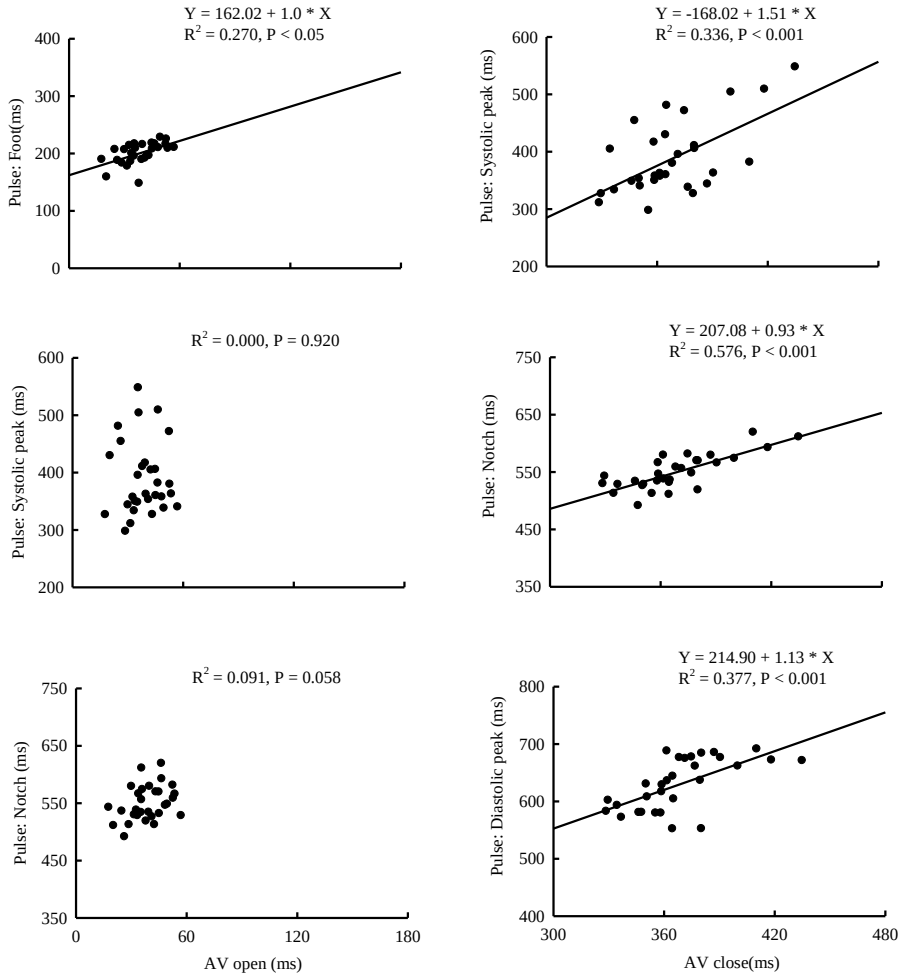

Figure 8-5. Relationship between aortic valve movement and feature times of the finger pulse systolic wave. All times were measured from ECG R wave.

The relations of the pulse systolic times (foot, peak and notch) with the aortic flow conditions are shown in Figure 8-6. The pulse foot did not show a significant linear relationship with any flow condition time. The pulse systolic peak showed strongly positive

linear relationships with the flow start, peak and end ($R^2 \geq 0.512$, $P < 0.001$), while the pulse notch was significantly related only with flow start and peak ($R^2 \geq 0.300$, $P < 0.001$).

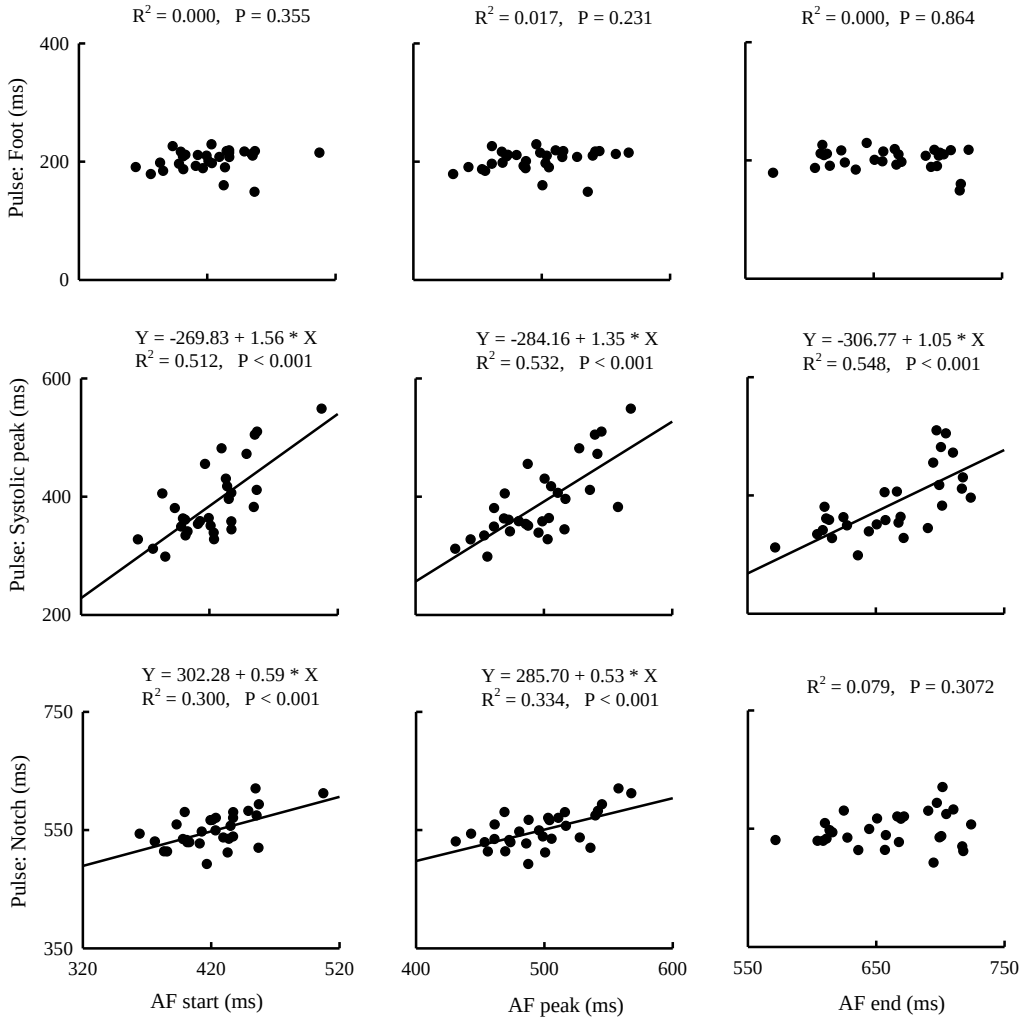

Figure 8-6. Relationship between aortic flow conditions and finger pulse times. All times were measured from ECG R wave

The multiple linear regression analysis results for the investigation of the relations of pulse feature times with aortic valve and flow times are summarized in Table 8-2. After accounting for the RR interval, the valve opening time still showed a significant relationship with the pulse foot ($R^2 = 0.361$, $P < 0.05$), and the valve closing time showed a strong relationship with the pulse notch ($R^2 = 0.579$, $P < 0.001$). The pulse systolic peak kept a significant relationship with the flow start ($R^2 = 0.504$, $P < 0.05$) and peak ($R^2 = 0.518$, $P < 0.05$). The significant correlations between the pulse times and imaging times confirmed that the pulse systolic features originated from left ventricular ejection.

Table 8-2. Summary of linear regression analysis results for the finger pulse times and valve movement times.

Imaging times (R ->) (ms)		Measure	Finger pulse times (R ->) (ms)					
			Foot		Systolic peak		Notch	
			Un-adjusted	Adjusted[a]	Un-adjusted	adjusted[a]	Un-adjusted	adjusted[a]
AV	open	R^2	0.270*	0.361**	0.000	0.345**	0.091	0.397**
		P	< 0.05	< 0.05	0.920	0.446	0.058	0.084
	close	R^2	---	---	0.336**	0.348**	0.576**	0.579**
		P	---	---	< 0.001	0.404	< 0.001	< 0.001
AF	start	R^2	0.000	0.155*	0.512**	0.504**	0.300**	0.355**
		P	0.355	0.231	< 0.001	< 0.05	< 0.001	0.277
	peak	R^2	---	---	0.532**	0.518**	0.334**	0.370**
		P	---	---	< 0.001	< 0.05	< 0.001	0.178
	end	R^2	---	---	0.548**	0.370**	0.079	0.340**
		P	---	---	< 0.001	0.178	0.072	0.447

[a]: the linear regression model is adjusted for RR interval; * or **: the linear regression model is significant with $P < 0.05$ or $P < 0.001$.

8.3.4 Relationship between finger pulse and imaging time durations

The relations of the pulse time duration with the aortic valve movement and flow durations are shown in Figure 8-7. The correlations of the pulse systolic rise time with the aortic flow accelerating time (from flow start to peak) and decelerating time were examined, but there was no significant relationship found. By contrast, the overall duration of the pulse systolic wave showed a strongly positive relationship with the left ventricular ejection time (LVET) obtained from aortic valve open duration ($R^2 = 0.461$, $P < 0.001$) or from aortic flow duration ($R^2 = 0.444$, $P < 0.001$).

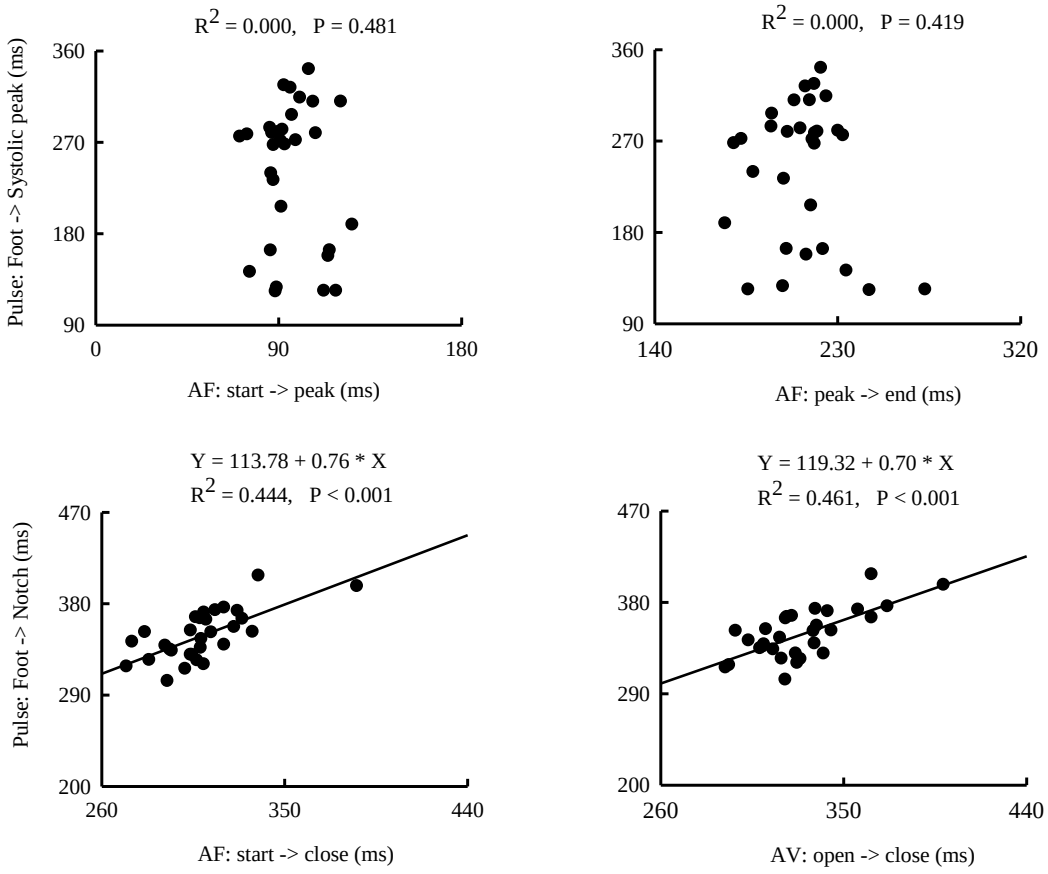

Figure 8-7. Relations of finger pulse systolic time durations with aortic valve movement and flow durations.

The multiple linear regression results, adjusted for the RR interval are provided in Table 8-3. After accounting for the RR interval, the overall duration of the finger pulse systolic wave still had a strong linear relationship with the left ventricular ejection time obtained from the images ($R^2 \geq 0.446$, $P < 0.001$). These observations suggested that a potential simple measurement of the LVET can be provided by the PPG technique.

Table 8-3. Summary of linear regression analysis results for the relationships between finger pulse durations and valve open durations.

Pulse durations (ms)	Imaging durations (ms)	Measure	Values	
			Un-adjusted	Adjusted[a]
Foot -> Systolic peak	AF start -> peak	R^2	0.000	0.000
		P	0.481	0.737
Foot -> Systolic peak	AF peak -> end	R^2	0.000	0.000
		P	0.419	0.650
Foot -> Notch	AF start -> end	R^2	0.444^{**}	0.446^{**}
		P	< 0.001	< 0.001
Foot -> Notch	AV open -> close	R^2	0.461^{**}	0.509^{**}
		P	< 0.001	< 0.001

[a]: the linear regression model is adjusted for RR interval; * or **: the linear regression model is significant with $P < 0.05$ or $P < 0.001$.

8.4 Dynamic relation of peripheral pulses with thoracic impedance

8.4.1 Overview on timing sequence of pulse and impedance features

In session 2, the ear and finger pulses were recorded with limb lead ECG, impedance Z and the first derivative impedance -dZ/dt. While the other signals were obtained on all the 30 subjects, the ear pulse was only measurable on 24 subjects.

The feature times from these simultaneous recorded physiological signals are summarized in Table 8-4. All the ECG and finger pulse features were obtainable on the 30 subjects. While the ear pulse foot and systolic peak were available on the studied 24 subjects, the notch and diastolic peak were unavailable on 1 of them. Being accordant with the impedance signals recorded in session 3, which were described in the previous chapter, the impedance Z systolic wave end was identifiable on 28 subjects, while the 2^{nd} minimum point was identifiable on 23 subjects. The 2^{nd} peak of the derivative impedance -dZ/dt was identifiable on 21 subjects.

Table 8-4. Summary of times from physiological data recorded in session 2.

Features		Subject numbers	Mean ± SD (ms)
ECG	**P_P**	30	-152 ± 22
	Q	30	-39 ± 6
	T_P	30	267 ± 27
	Next R	30	1032 ± 162
Z	**Start**	30	66 ± 17
	Min.	30	262 ± 29
	End	28	507 ± 40
	2nd min.	23	642 ± 47
-dZ/dt	**Foot**	30	91 ± 19
	1st peak	30	190 ± 15
	End	30	446 ± 26
	2nd peak	21	614 ± 35
Ear pulse	**Foot**	24	162 ± 18
	Systolic peak	24	419 ± 43
	Notch	23	483 ± 33
	Diastolic peak	23	573 ± 63
Finger pulse	**Foot**	30	205 ± 18
	Systolic peak	30	394 ± 59
	Notch	30	558 ± 35
	Diastolic peak	30	633 ± 45

The timing sequence of features from ECG, impedance and pulses, illustrated in Figure 8-8, was reconstructed based on the values provided in the Table 8-4. For the systolic components, the pulse feet were detected after the onset of the impedance Z falling, and the pulse systolic peaks occurred after the impedance Z systolic minimum point respectively.

The pulse notch points were observed around the Z end. For the diastolic components, the pulse diastolic peaks were seen before the Z 2nd minimum point. Further details of the comparison between the feature times of the pulses and impedance signals are provided in the following sections.

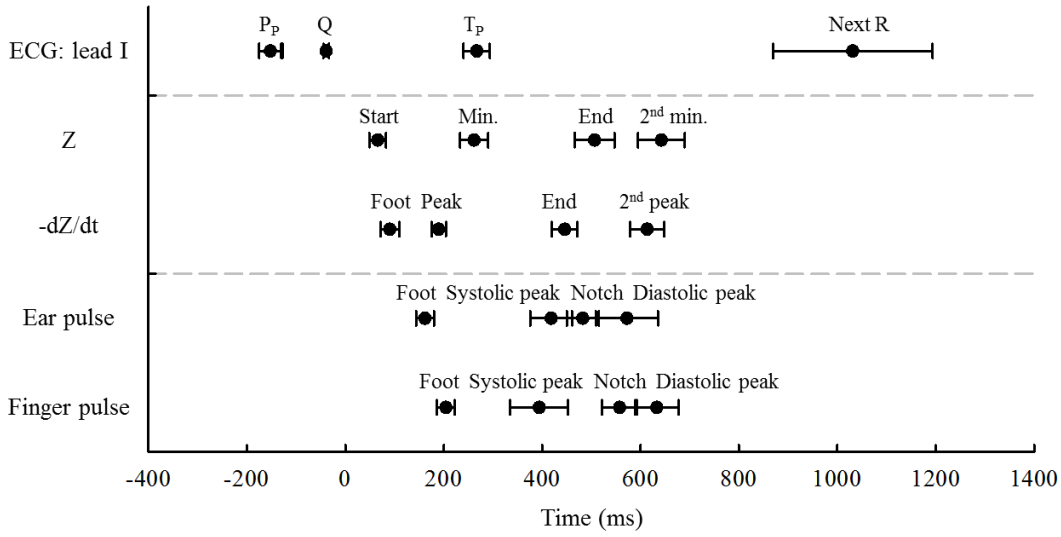

Figure 8-8. Timing sequence of ECG, impedance and pulse features. All times were measured from ECG R wave. Circle represents the mean and error bar represents SD across all subjects.

8.4.2 Time difference between pulse and impedance features

The synchronized ECG, impedance and pulse waveforms in a cardiac cycle are displayed in Figure 8-9. The relative times of the pulse features, measured from the time point when impedance Z started to fall, are also illustrated in the figure. As can be seen, the ear pulse foot occurred 95 ms and finger pulse foot occurred 138 ms after the impedance Z start. The dominant systolic peak of the finger pulse (328 ms after the Z start) occurred earlier than that of the ear pulse (352 ms after the Z start). The notch point and the diastolic peak of the ear pulse occurred earlier than the corresponding features on the finger pulse. The notch point and the diastolic peak of the ear pulse were 416 ms and 505 ms after the Z start, while those of the finger pulse were 492 ms and 567 ms after the Z start.

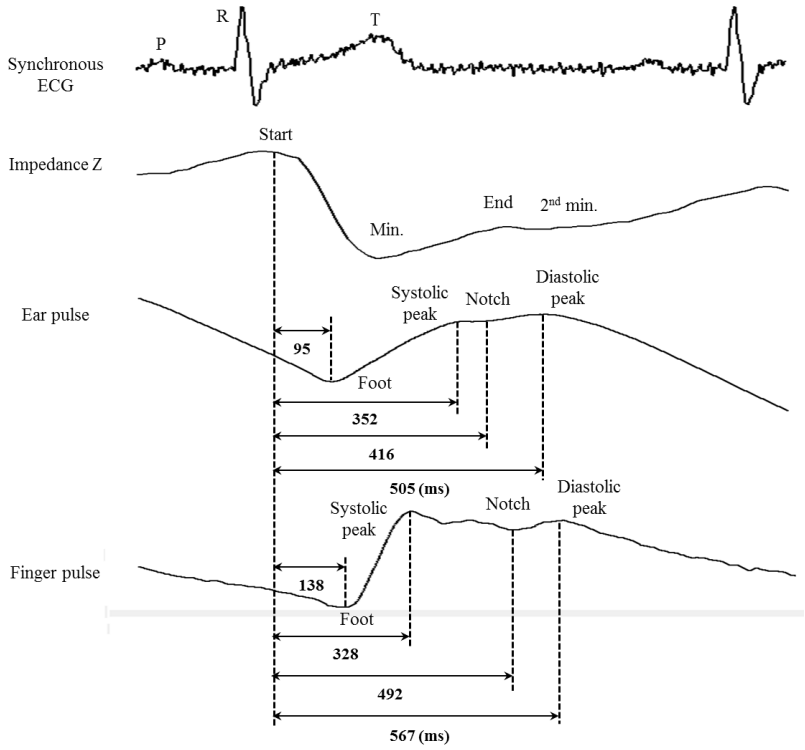

Figure 8-9. Synchronized ECG, impedance Z and pulse waveforms. The average pulse feature times across all subjects were measured from Z staring point.

The comparison of the impedance Z features with ear pulse and finger pulse features are shown in Figure 8-12 (A) and (B). Both the pulse feet were significantly later than the Z start ($P < 0.001$), and the pulse systolic peaks were significantly later than the Z minimum point ($P < 0.001$). While the ear pulse notch point was close to the Z end (Mean difference $\pm$ SD: -15 $\pm$ 46 ms, $P = 0.136$), the finger pulse notch point was significantly later than the Z end (Mean difference $\pm$ SD: 53 $\pm$ 37 ms, $P < 0.001$). The 2nd minimum point of the impedance Z occurred 49 ms later than the ear pulse diastolic peak ($P < 0.05$), but was close to the finger pulse diastolic peak (Mean difference $\pm$ SD: 1 $\pm$ 40 ms, $P = 0.862$).

These observations provided additional information about the generation of the pulse and impedance waveforms. The blood is ejected into the central aorta during the systole, and from where it is distributed to the smaller arterioles in the peripheral sites. During the early systole, a large amount of blood enters into the aorta, which causes the impedance to drop rapidly. However, with ejection slowing, the dominance of blood volume to the aorta is gradually lost to the periphery. Therefore, the impedance was recovering while the peripheral blood volume was increasing.

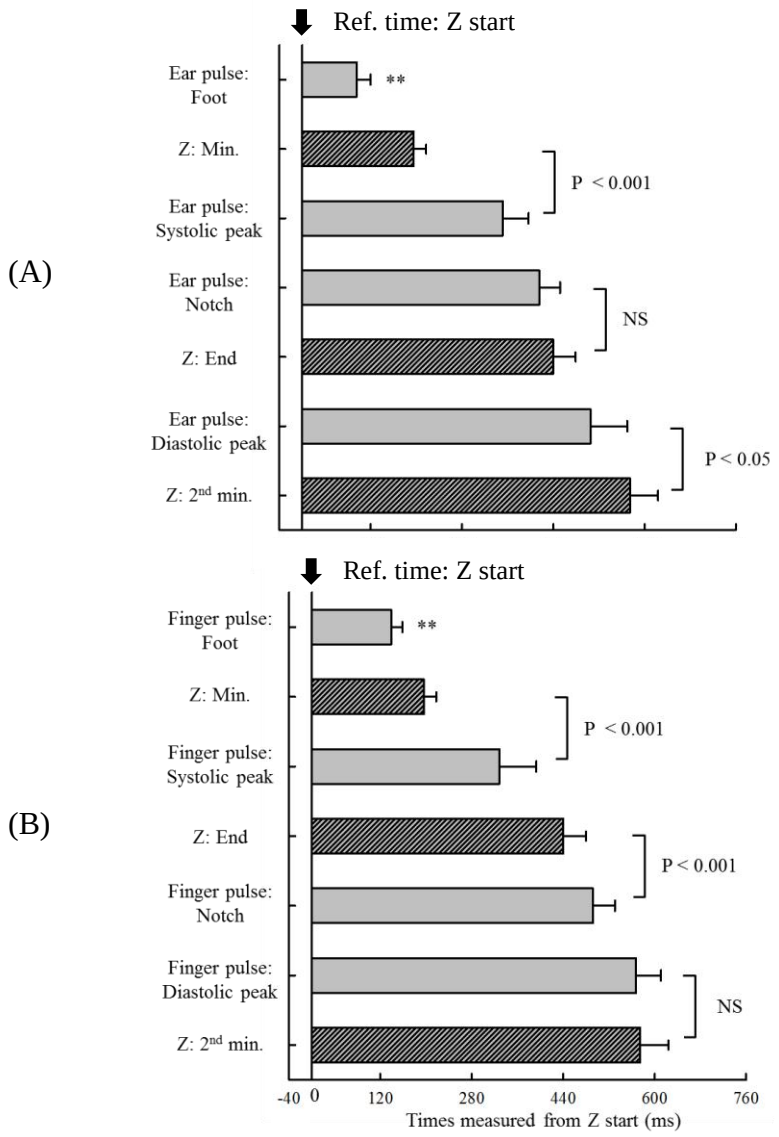

Figure 8-10. Timing sequence of impedance and pulse features. The means and SDs were from all subjects.

8.4.3 Comparison between pulse and impedance time durations

The comparison between the time durations of the impedance Z and pulses is shown in Figure 8-11. For the systolic components, the overall systolic wave durations (from the pulse foot to notch) of the ear and finger pulses were significantly shorter than the Z systolic wave durations (from Z start to end) (both $P < 0.001$). While the ear pulse rising time (from foot to systolic peak) was longer than the Z falling time (from the start to the minimum point) ($P < 0.001$), the finger pulse rising time was comparable with the Z falling time (Mean difference ± SD: -6 ± 56 ms, $P = 0.552$). For the diastolic components, the

rising times (from the end of systolic wave to diastolic peak) of the pulses were shorter than the impedance Z falling time (from the end of systolic wave to the 2nd minimum) (both $P < 0.05$). The peak-to-peak time of the pulses (from the systolic peak to the diastolic peak) was also significantly shorter than the distance between the systolic minimum point and the diastolic minimum point of the impedance ($P < 0.001$).

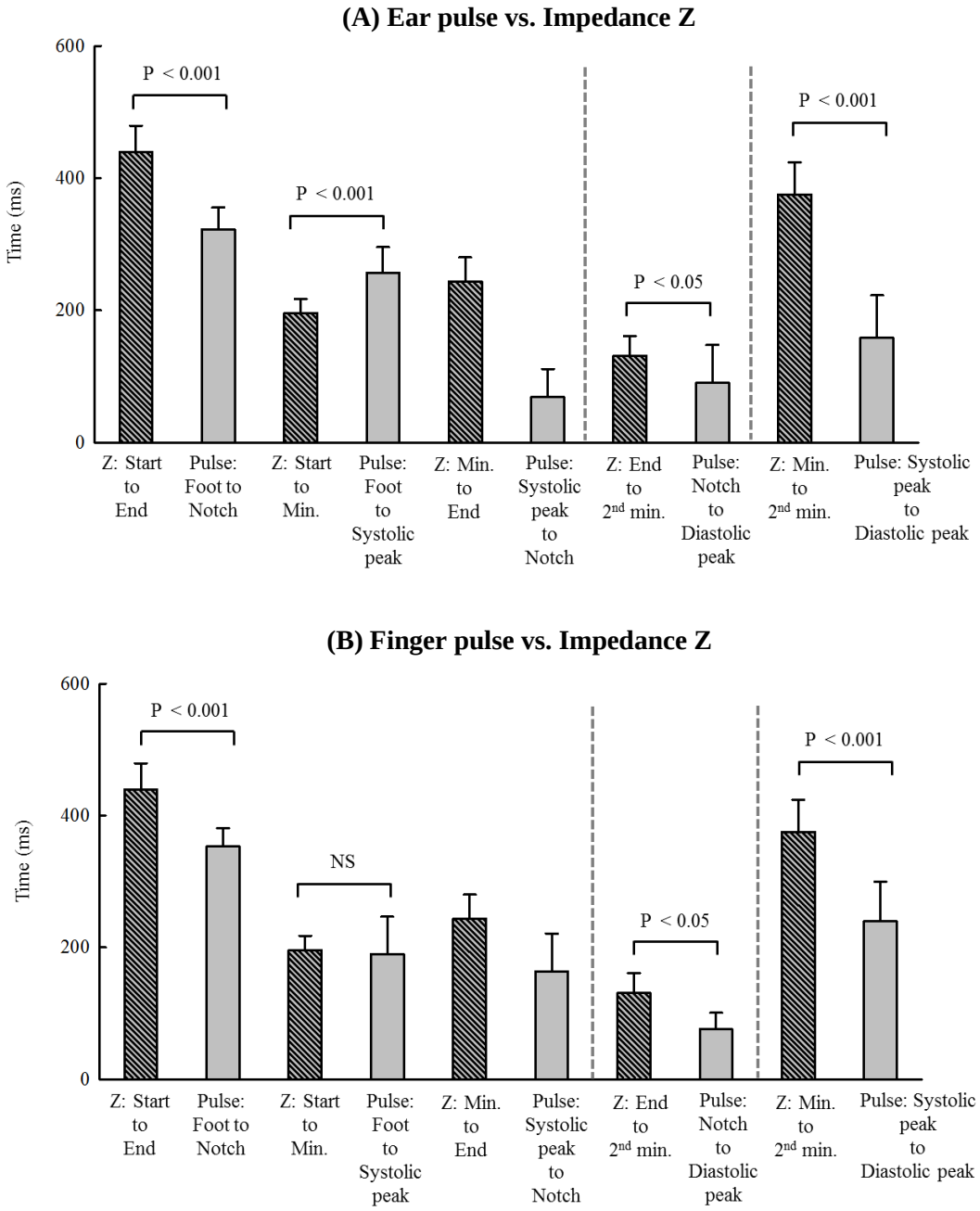

Figure 8-11. Comparison between pulse and impedance time durations. The means and SDs were from all subjects.

8.4.4 Relationship between pulse and impedance features

The relationships between the feature times of the finger pulse and impedance are displayed in Figure 8-12. None of the pulse features showed a significant relationship with any of the Z start or systolic minimum points. However, the pulse systolic peak, notch and diastolic peaks showed significantly linear relationships with Z end and 2nd minimum point ($R^2 \geq 0.247$, $P < 0.05$).

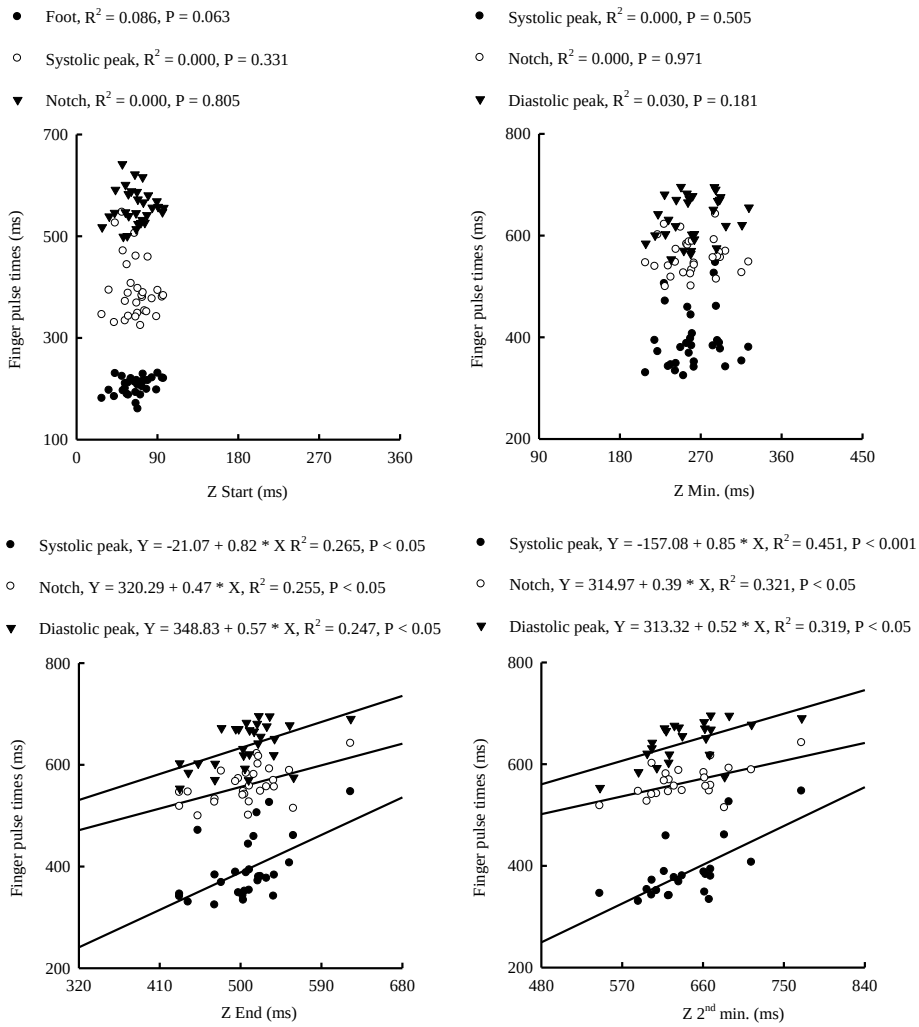

Figure 8-12. Relationship between impedance and finger pulse features. All times were measured from ECG R wave.

The multiple linear regression results for the relations of the impedance with the pulses are summarized in Table 8-5 and Table 8-6. No pulse feature time showed a significant linear relationship with any of the impedance time after accounting for the RR interval.

Table 8-5. Summary of linear regression analysis results for the finger pulse times and impedance times.

		Finger pulse times (ms)							
		Foot		**Systolic peak**		**Notch**		**Diastolic peak**	
Impedance times (ms)	**Measure**	Un-adjusted	Adjusted[a]	Un-adjusted	adjusted[a]	Un-adjusted	adjusted[a]	Un-adjusted	adjusted[a]
Start	R^2	0.086	0.269*	0.000	0.497**	0.000	0.314*	---	---
	P	0.063	0.063	0.331	0.082	0.805	0.995	---	---
Min.	R^2	---	---	0.000	0.437**	0.000	0.327*	0.030	0.458**
	P	---	---	0.505	0.964	0.971	0.473	0.181	0.389
End	R^2	---	---	0.265*	0.475**	0.255*	0.337*	0.247*	0.455**
	P	---	---	< 0.05	0.548	< 0.05	0.266	< 0.05	0.605
2^{nd} min.	R^2	---	---	0.451**	0.497**	0.321*	0.423*	0.319*	0.523**
	P	---	---	< 0.001	0.263	< 0.05	0.791	< 0.05	0.731

[a]: the linear regression model is adjusted for RR interval; * or **: the linear regression model is significant with $P < 0.05$ or $P < 0.001$.

Table 8-6. Summary of linear regression analysis results for the ear pulse times and impedance times.

		Ear pulse times (ms)							
		Foot		**Systolic peak**		**Notch**		**Diastolic peak**	
Impedance Z times (ms)	**Measure**	Un-adjusted	Adjusted[a]	Un-adjusted	adjusted[a]	Un-adjusted	adjusted[a]	Un-adjusted	adjusted[a]
Start	R^2	0.000	0.072	0.000	0.358*	0.000	0.000	---	---
	P	0.497	0.742	0.683	0.890	0.726	0.784	---	---
Min.	R^2	---	---	0.290	0.361*	0.000	0.000	0.048	0.345*
	P	---	---	0.207	0.716	0.367	0.408	0.161	0.470
End	R^2	---	---	0.190*	0.346*	0.000	0.000	0.128	0.320*
	P	---	---	< 0.05	0.938	0.646	0.512	0.062	0.917
2^{nd} min.	R^2	---	---	0.431*	0.419*	0.000	0.000	0.128	0.318*
	P	---	---	< 0.001	0.228	0.421	0.549	0.080	0.620

[a]: the linear regression model is adjusted for RR interval; * or **: the linear regression model is significant with $P < 0.05$ or $P < 0.001$.

8.4.5 Relationship between pulse and impedance time durations

The relations of the impedance durations with finger pulse durations and ear pulse durations are shown in Figure 8-13 and Figure 8-14 respectively. No significance was found for the relation of the pulse rising time with Z falling time during systole, the relation of the pulse rising time with the Z falling time during diastole, or the relation of the pulse peak-to-peak duration with the duration between the two minimum points of the impedance. The only significant relationship was from the finger pulse systolic wave duration with the Z systolic wave duration. The pulse systolic wave duration increased with the Z duration ($R^2 = 0.230$, $P < 0.05$). However, after accounting for the RR interval, the Z duration was not a significant variable in the linear regression model ($P = 0.185$).

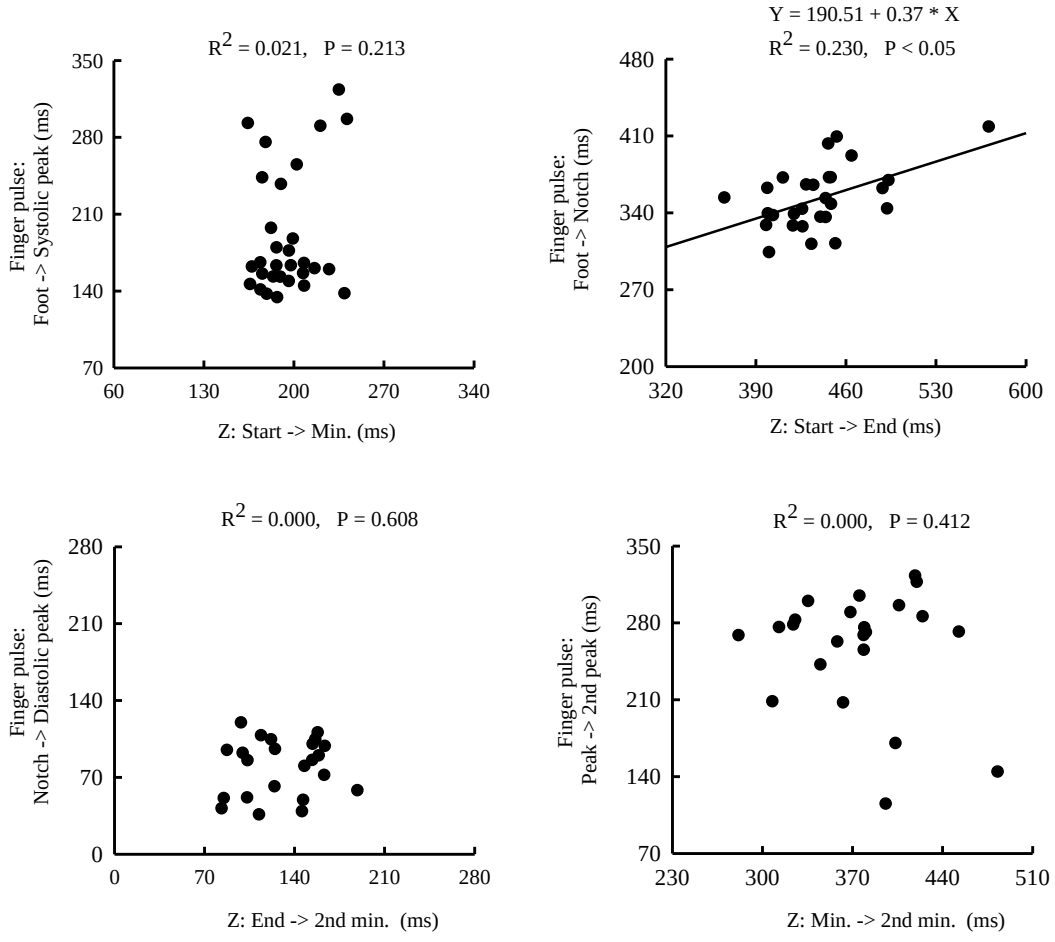

Figure 8-13. Relationship between impedance and finger pulse time durations.

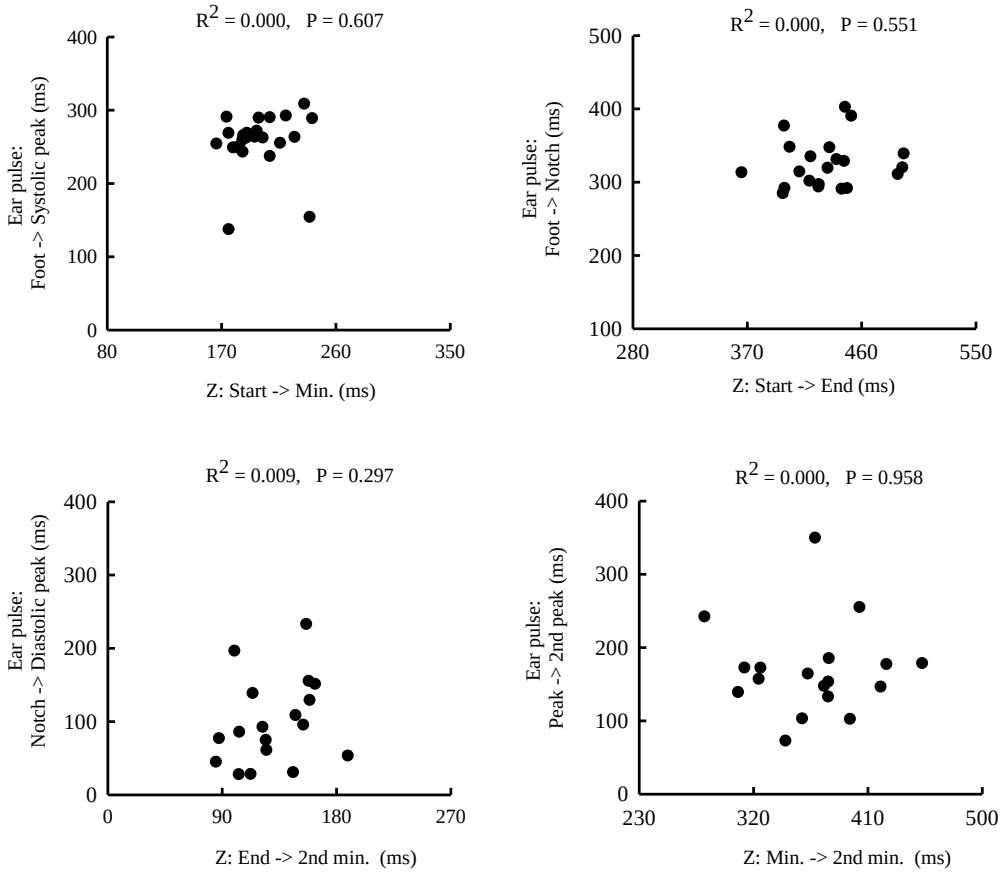

Figure 8-14. Relationship between impedance and ear pulse time durations.

8.4.6 Comparison between time features of ear pulse and finger pulse

The comparison between the corresponding feature times from the ear pulse and finger pulse is shown in Figure 8-15. The foot, notch and diastolic peak on the ear pulse were proceeding the corresponding times on the finger pulse. More specifically, the ear pulse foot occurred on average 41 ms before the finger pulse foot. The notch point and diastolic peak of the ear pulse were 67 ms and 51 ms before those of the finger pulse respectively. All the comparisons were statistically significant ($P < 0.001$). However, because the systolic wave of the finger pulse was more likely to be dominated by the early systolic component while that of the ear pulse was mainly dominated by the late systolic component, the systolic peak of the ear pulse was significantly later than that of the finger pulse (Mean difference $\pm$SEM: -28 $\pm$8 ms, $P < 0.05$).

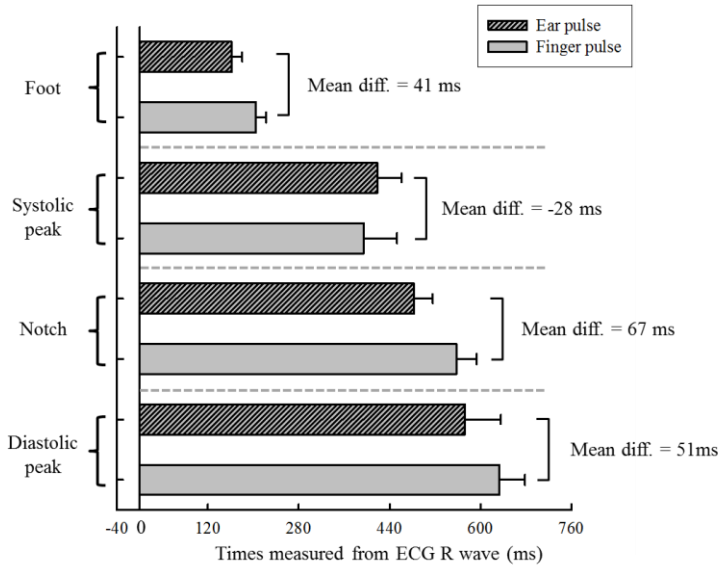

Figure 8-15. Comparison of feature times from ear and finger pulses. All times were measured from ECG R wave. The means and SDs were measured across all subjects.

The comparison between the time durations of the ear pulse and finger pulse is shown in Figure 8-16. Due to the significant difference between systolic peaks, the rising time of the ear pulse (256 ms) was significantly longer than that of the finger pulse (190 ms) ($P < 0.001$), and the peak-to-peak duration of the ear pulse (158 ms) was significantly shorter than that of the finger pulse (239 ms) ($P < 0.001$). The overall systolic wave duration of the ear pulse was slightly shorter (21 ms) than that of the finger pulse ($P < 0.05$).

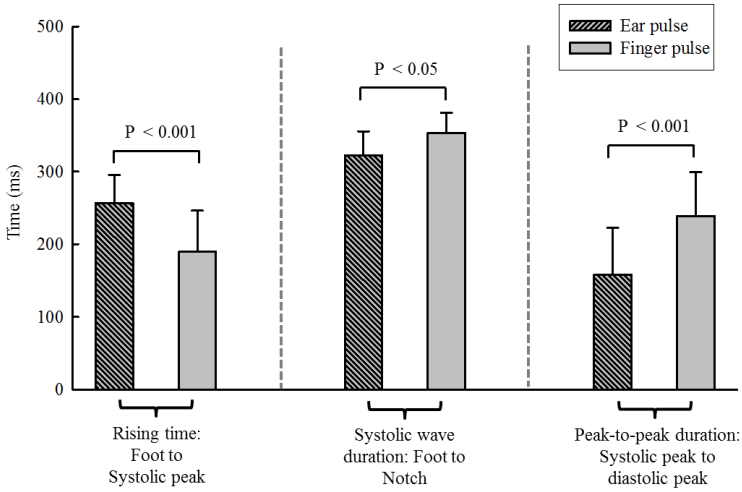

Figure 8-16. Comparison of time durations from ear and finger pulses. The means and SDs were measured across all subjects.

8.5 Clinical indices measured from peripheral pulse

Clinical indices, reflecting the cardiovascular function, can be obtained from the peripheral volume pulse waveforms. The commonly used clinical indices from pulse included the pulse foot transit time (PTT_f, from ECG R wave to the pulse foot), pulse peak transit time (PTT_p, from ECG R wave to the pulse systolic peak), pulse rise time (from the pulse foot to systolic peak) and the stiffness index (SI, the subject height in meter divided by pulse peak-to-peak time in s). The reference values of these 4 indices from the literature are summarized in Table 8-7. Their mean values and SDs, calculated with the data from session 2, are provided in Table 8-8. To facilitate the comparison between the data from the present study and the literature, the median and range of the values are also provided.

As described in the Table 8-8, the average PTT_f of the finger pulse (Mean ± SD: 205 ± 18 ms) was longer than that of the ear pulse (Mean ± SD: 162 ± 18 ms). The median of the ear pulse PTT_f from this study was 30 ms longer than that reported by Allen and Murray (2000), while the medians of the finger pulse PTT_f from these two studies were comparable (Difference: 9 ms). The average PTT_p of the finger pulse (Mean ± SD: 394 ± 59 ms) was 25 ms shorter than that of the ear pulse (Mean ± SD: 419 ± 43 ms) in this study. The median of the finger pulse PTT_p was 42 ms shorter than the ear pulse PTT_p. This observation disagreed with that reported in Allen and Murray's study (Allen and Murray 2000), where the median of the finger pulse PTT_p was 39 ms longer than that of the ear pulse PTT_p. This difference could have resulted from the different criteria for the systolic peak identification and the difference in distinguishing the systolic peaks. The average ear pulse rise time obtained in this study was 256 ms, which was 66 ms longer than the finger pulse rise time (Mean: 190 ms). The average SI obtained from the ear pulse in this study was 13.1 m/s, which was 64% higher than that obtained from the finger pulse (Mean: 8.0 m/s). The coefficient of variation (ratio of SD to the mean) of the SI was 43% for the ear pulse and 31% for the finger pulse, which suggested that the measurement of SI from peripheral pulses had high dispersion. This also reflected by the reference values reported in the literature. Although all the finger volume pulses were recorded on normal subjects, the SI reported by Brumfield and Andrew (2005) was almost twice than that reported by Millasseau et al. (2003). The high variance of the SI measurement would restrict its clinical application. The effect of age, heart rate and RR interval on these 4 indices will be discussed in the following chapter.

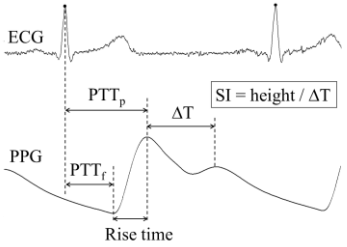

Table 8-7. Summary of commonly used indices from PPG signal with their reference values from literature.

References	*Subject No.*	*Mean (SD)*[†] */ Median (Range)*[‡]				*Measurement sites*
		PTT$_f$ (R -> foot) (ms)	**PTT$_p$ (R -> peak) (ms)**	**Rise time (foot -> peak) (ms)**	**SI (height / ΔT) (m/s)**	
Allen and Murray 2000	20	133[‡]	397[‡]	--	--	Ear
Allen and Murray 2000	20	199[‡]	436[‡]	--	--	Finger
Millasseau et al. 2002	87	--	--	--	8.4[†]	Finger
Millasseau et al. 2003	124	--	--	--	6.3[†]	Finger
Brumfield and Andrew 2005	44	--	--	--	12.3[†]	Finger
Allen et al. 2008	52	259 (242 – 273) [‡]	493 (465 – 521) [‡]	234 (215 – 255) [‡]	--	Toes

Table 8-8. Summary of commonly used indices from PPG signal with their reference values from this study.

Subject No.	*Mean (SD)*[†] */ Median (Range)*[‡]				*Measurement sites*
	PTT$_f$ (R -> foot) (ms)	**PTT$_p$ (R -> peak) (ms)**	**Rise time (foot -> peak) (ms)**	**SI (height / ΔT) (m/s)**	
24	162 (18) [†] 163 (127 – 200) [‡]	419 (43) [†] 423 (296 – 507) [‡]	256 (39) [†] 262 (137 – 308) [‡]	13.1 (5.6) [†] 11.2 (5.0 – 24.8) [‡]	Ear
30	205 (18) [†] 208 (160 – 230) [‡]	394 (59) [†] 381 (324 – 547) [‡]	190 (57) [†] 163 (134 – 323) [‡]	8.0 (2.5) [†] 6.8 (5.7 – 14.8) [‡]	Finger

8.6 Discussion and conclusions

In this chapter, the timing sequence of finger pulse features was studied with reference to the M-mode echocardiograms for aortic valve movement times and Doppler images for aortic flow recorded in session 3. The finger pulse foot was observed 162 ms after the aortic valve initial opening. The pulse systolic peak was on average 20 ms after the aortic valve closed ($P < 0.05$).

In addition, the pulse timing durations were also compared with the corresponding durations of aortic valve movement and aortic flow conditions. According to the comparison results, the overall duration of the finger pulse systolic wave (from foot to notch) was slightly longer (19 ms) than the left ventricular ejection duration measured from the aortic valve open duration ($P < 0.001$). The finger pulse rising time (from foot to systolic peak) was slightly (26 ms) shorter than the aortic flow decelerating time (from aortic flow peak to end) ($P < 0.05$).

Finally, the relations of the finger pulse time features with the aortic valve movement times and the aortic flow conditions were investigated by linear regression analysis. The key findings for the investigation included:

- The pulse foot was significantly related to the aortic valve opening ($R^2 = 0.361$, $P < 0.05$), and the pulse notch point was strongly related to the valve closing ($R^2 = 0.579$, $P < 0.001$);
- The pulse systolic peak was strongly related to the peak aortic flow ($R^2 = 0.518$, $P < 0.001$);
- The overall duration of the pulse systolic wave was strongly correlated with the left ventricular ejection duration measured from aortic valve open duration ($R^2 = 0.509$, $P < 0.001$) or from aortic flow duration ($R^2 = 0.446$, $P < 0.001$);

It is evident from the work to date that the pulse is caused by the left ventricular ejection of blood volume into the aorta during systole. Hearzman and Spealman (1937) described the characteristics of the peripheral volume pulse waveform in the two phases; a rising phase concerning systole and a decreasing phase concerning diastole and reflection wave from the periphery. However, the origins of the features on the pulse waveform are still not clear, which restricts its clinical application (Allen 2007). It was known that the closing of

the aortic valve generates a characteristic notch point on the pressure pulse (O'Rourke et al. 1992, Levick 2010). In this study, by linking the volume pulse to the simultaneous M-mode echocardiograms for the aortic valve movement, it was found that the notch point on the peripheral volume pulse was strongly correlated with the aortic valve closing. This observation suggested that the occurrence of the notch point on the volume pulse would be also caused by the aortic valve closing. This point agreed with Millasseau et al.'s studies (Millasseau et al. 2000, 2003b), in which it was reported that the peripheral volume pulse and the peripheral pressure pulse would be determined by a similar mechanism because they can be well predicted by each other with a generalized transfer function. Furthermore, the strongly linear relationship between the pulse systolic peak and the aortic flow peak also suggests that the peripheral pulse features would be directly associated with the cardiac mechanical events. However, the principles underlying these associations need further investigation.

The strong relationships between the pulse feature times and the aortic valve movement and flow feature times indicates the possibility of estimating the left ventricular ejection time (LVET) from the pulse waveform. The method to detect the LVET from high order (3^{rd} and 4^{th} order) derivative of finger pulse waveform was implemented on the data recorded on 13 healthy subjects in Chan et al.'s study (Chan et al. 2007). A small difference and strong correlation between the LVET derived from the pulse and that from the Doppler echocardiogram (from aortic flow start to end) was found (Mean difference $\pm$ SD: -14 $\pm$ 14 ms, $R^2 = 0.805$, $P < 0.05$). The most important limitation of such methods was from the unclear physiological meaning of the high order derivative of the pulse waveform. The present study showed that the duration from the pulse foot to notch was close to the LVET from M-mode image with a strong correlation (Mean $\pm$ SD: 19 $\pm$ 16 ms, $R^2 = 0.534$, $P < 0.001$). This was a much simpler and more intuitive method, based on the observation of the strong association between the pulse and aortic valve movement times.

Based on the data recorded in session 2, the timing sequence of features from peripheral pulses and the impedance Z was investigated. The pulse feet occurred after the onset of the impedance falling during systole (Mean difference: 95 ms for ear pulse, 138 ms for finger pulse), and the pulse systolic peaks occurred after the impedance systolic minimum (Mean difference: 157 ms for ear pulse, 132 for finger pulse). Statistically, the pulse notch points

were close to the end of the impedance systolic wave, and the pulse diastolic peaks were close to the impedance diastolic minimum.

The pulse timing durations were also compared with the impedance duration. The overall durations of the ear pulse and finger pulse systolic waves (from pulse foot to notch) were significantly shorter than the impedance systolic wave duration (from Z start to end), but the systolic rising time of the finger pulse (from pulse foot to systolic peak) was comparable to the impedance systolic falling time (from Z start to the systolic minimum) (Mean difference $\pm$ SD: 6 $\pm$ 56 ms, P = 0.552). The diastolic rising time of the finger pulse (from notch to diastolic peak) was, however, significantly shorter than the impedance diastolic falling duration (from Z end to the 2nd minimum) (Mean difference: 41 ms for ear pulse, 55 ms for finger pulse).

The pulsatile change in thoracic impedance reflected the blood volume change in the central great vessels, while the peripheral pulse reflected the blood volume change at the peripheral sites. The inverted impedance waveform was similar to the waveforms of the pulses in shapes: a major upwards wave during systole and a relatively minor upwards wave superimposed on the decaying limb of the systolic wave. To my best knowledge, no study has been done to link the peripheral pulses to the thoracic impedance. In the present study, the ear and finger pulses were linked to the simultaneous impedance recordings. This investigation was helpful to provide further evidence about the generation of pulse and impedance waveforms. The pulse rising phase followed the impedance falling phase during systole, and the impedance started to recover before the peripheral pulse achieved a peak. These observations reflected the blood distribution process in the arterial system; the blood is ejected into the central aorta during the left ventricular systole, and from where it is distributed to the smaller arterioles in the peripheral sites. During the early ventricular ejection, because a large amount of blood entered into the aorta, the impedance dropped rapidly. Meanwhile, the peripheral blood volume started to increase when receiving blood volume from the central great vessels. With the ejection slowing, the dominance of blood volume to the aorta is reduced by the out-flowing blood. The impedance was restored with the reduction of blood volume in the central vessels. After that the blood volume in the peripheral sites was maintained at a relatively high level, while the impedance recovered gradually.

According to the linear regression analysis results, no significant linear relation of the times from the pulses and impedance was found, although they showed a similar waveform shapes. These results indicated that the features on the pulse waveform and impedance waveform could originate from different mechanisms. The association between the peripheral pulses and thoracic impedance needs further investigation.

At the end of this chapter, the feature times of the ear pulse and finger pulse were compared. The ear pulse foot, notch and diastolic peak preceded the corresponding features from the finger pulse by 41 ms, 67 ms and 51 ms respectively. However, the systolic peak of the ear pulse was observed later than that of the finger pulse (Mean difference $\pm$ SD: 28 $\pm$ 39 ms, $P < 0.05$). This was because the systolic wave of the finger pulse was more likely to be dominated by the early systolic component, while that of the ear pulse was mainly dominated by the late systolic component.

Four indices, including pulse foot transit time (PTT_f), peak transit time (PTT_p), rise time and stiffness index (SI), were obtained from the pulses. These indices were considered as the potential clinical indicators for vascular function (Allen and Murray 2000, Millasseau et al. 2002, 2003, Allen et al. 2008). The effects of age, heart rate and blood pressure on these indices are discussed in the following chapter.

Chapter 9 Effects of age, heart rate and blood pressure on image and physiological measurements

The effects of age, heart rate and blood pressure on ECG, echocardiographic, impedance and pulse measurements are described in this chapter.

9.1 Introduction

Age, heart rate and blood pressure are the three important factors influencing the cardiovascular function. These influences are reflected on the cardiac images and physiological signals. In this chapter, the effects of age, heart rate and blood pressure on the echocardiographic, ECG, thoracic impedance and peripheral pulse signals are investigated.

9.2 Effects of age, heart rate and blood pressure on ECG measurement

Time intervals from the ECG waveform of clinical importance include the PR interval (from P wave start to Q wave), QRS duration (from Q wave to S wave), QT interval (from the Q wave to T wave end) and ST interval (from S wave to T wave end). The relationships of these time intervals with age, heart rate and systolic blood pressure are shown in Figure 9-1. As can be seen, the PR interval, representing the duration for the action potential transferring from the SA node to the ventricles, increased with aging advance ($R^2 = 0.225$, $P < 0.05$). The PR interval also increased when the RR interval was prolonged. The QT interval, representing the overall duration for ventricular depolarization and repolarization showed a significantly positive relationship with RR interval ($R^2 = 0.680$, $P < 0.001$). The ST interval, representing the ventricular repolarization duration, was also strongly correlated with RR interval ($R^2 = 0.680$, $P < 0.001$). None of the time intervals showed a significant relationship with systolic blood pressure.

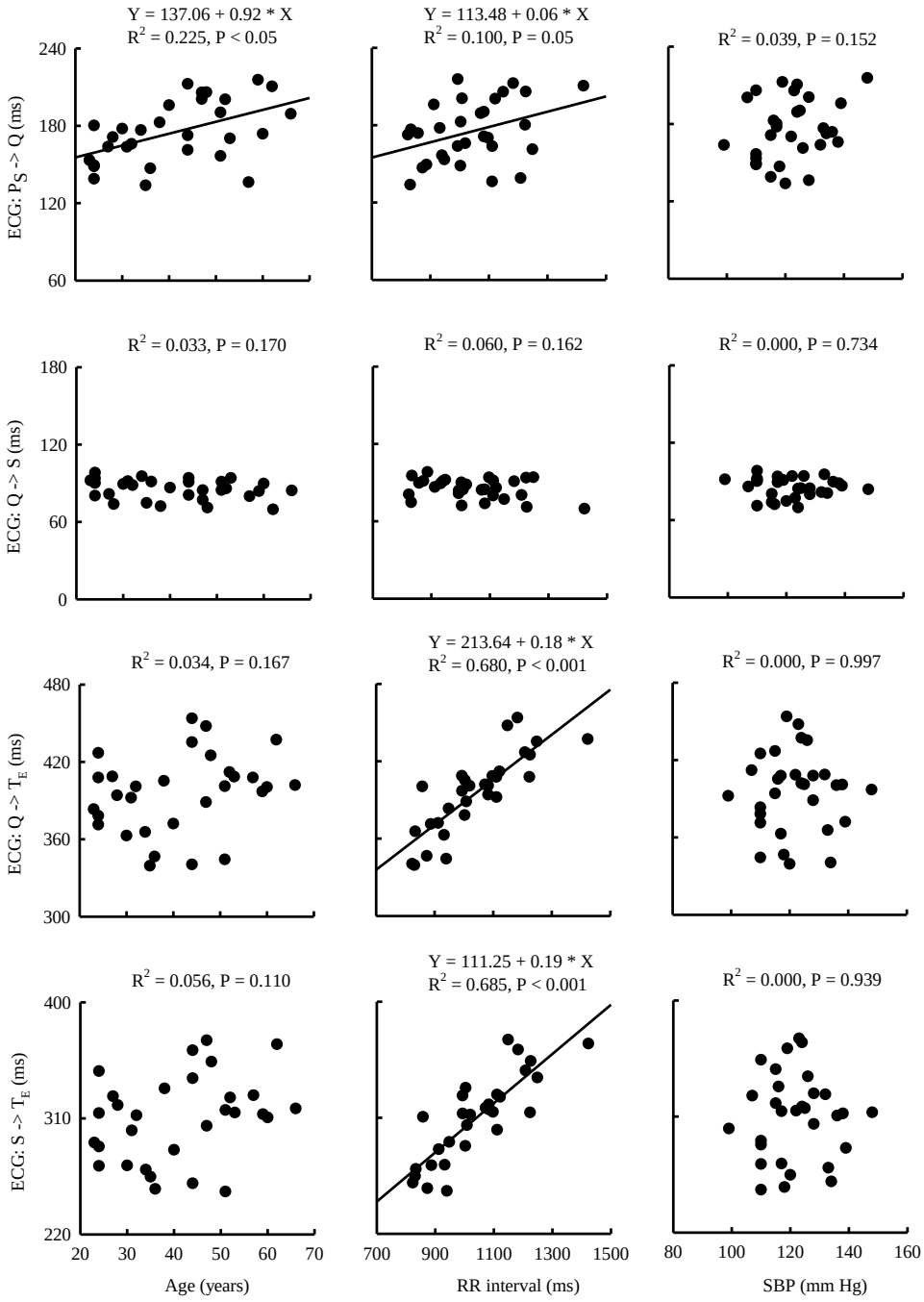

Figure 9-1. Relationships of ECG timing intervals with age, RR interval and systolic blood pressure.

The multiple linear regression results, which were used to examine the combination effects of the age, heart rate and blood pressure on the ECG intervals, are summarized in Table 9-1. The PR interval, QT interval and ST interval can be well predicted by the combined variables ($R^2 \geq 0.278$, $P < 0.05$). While age and RR interval played similar significance in the model for PR interval (P values around 0.06), RR interval was the only

significant factor in the models for the QT interval and ST interval. The QRS duration slightly decreased with an increase in any of the three variables ($\beta < 0$), but the association was not significant ($P \geq 0.169$).

Table 9-1. Summary of multiple linear regression results for the combination effects of age, RR interval and systolic blood pressure on ECG time intervals.

Demographic data (Variables)	Measure	ECG time intervals (Outcomes)			
		PR interval P_S -> Q (ms)	QRS duration Q -> S (ms)	QT interval Q -> T_E (ms)	ST interval S -> T_E (ms)
Overall	Adj. R^2	0.278	0.034	0.699	0.713
	P	P < 0.05	0.283	< 0.001	< 0.001
Age (years)	β	0.636	-0.102	-0.040	0.766
	P	0.067	0.428	0.884	0.110
RR interval (ms)	β	0.055	-0.015	0.186	0.191
	P	0.063	0.169	< 0.001	< 0.001
SBP (mm Hg)	β	0.470	-0.048	0.585	0.044
	P	0.238	0.746	0.081	0.939

9.3 Effects of age, heart rate and blood pressure on imaging measurements

9.3.1 Aortic valve movement and flow

From the M-mode images for aortic valve movement, systolic time intervals, including the pre-ejection period (PEP, from ECG Q wave to the valve opening), the left ventricular ejection time (LVET, from the valve opening to closing) and the electromechanical delay (EMD, from ECG Q wave to the valve closing), and the ratio of the PEP to the ejection duration, were measured. The relationships of these systolic intervals with age, RR interval and systolic blood pressure are shown in Figure 9-2. The PEP showed a significantly negative relationship with age ($R^2 = 0.175$, $P < 0.05$). The LVET was strongly related to the RR interval ($R^2 = 0.709$, $P < 0.001$) and weakly related with age ($R^2 = 0.107$, $P < 0.05$). The EMD was only correlated with RR interval ($R^2 = 0.741$, $P < 0.001$). Because of the

decrease in PEP and increase in LVET with advancing age, the ratio of the PEP to the LVET was negatively related to age (R^2 = 0.239, P < 0.05). None of the systolic time intervals was significantly correlated with the systolic blood pressure.

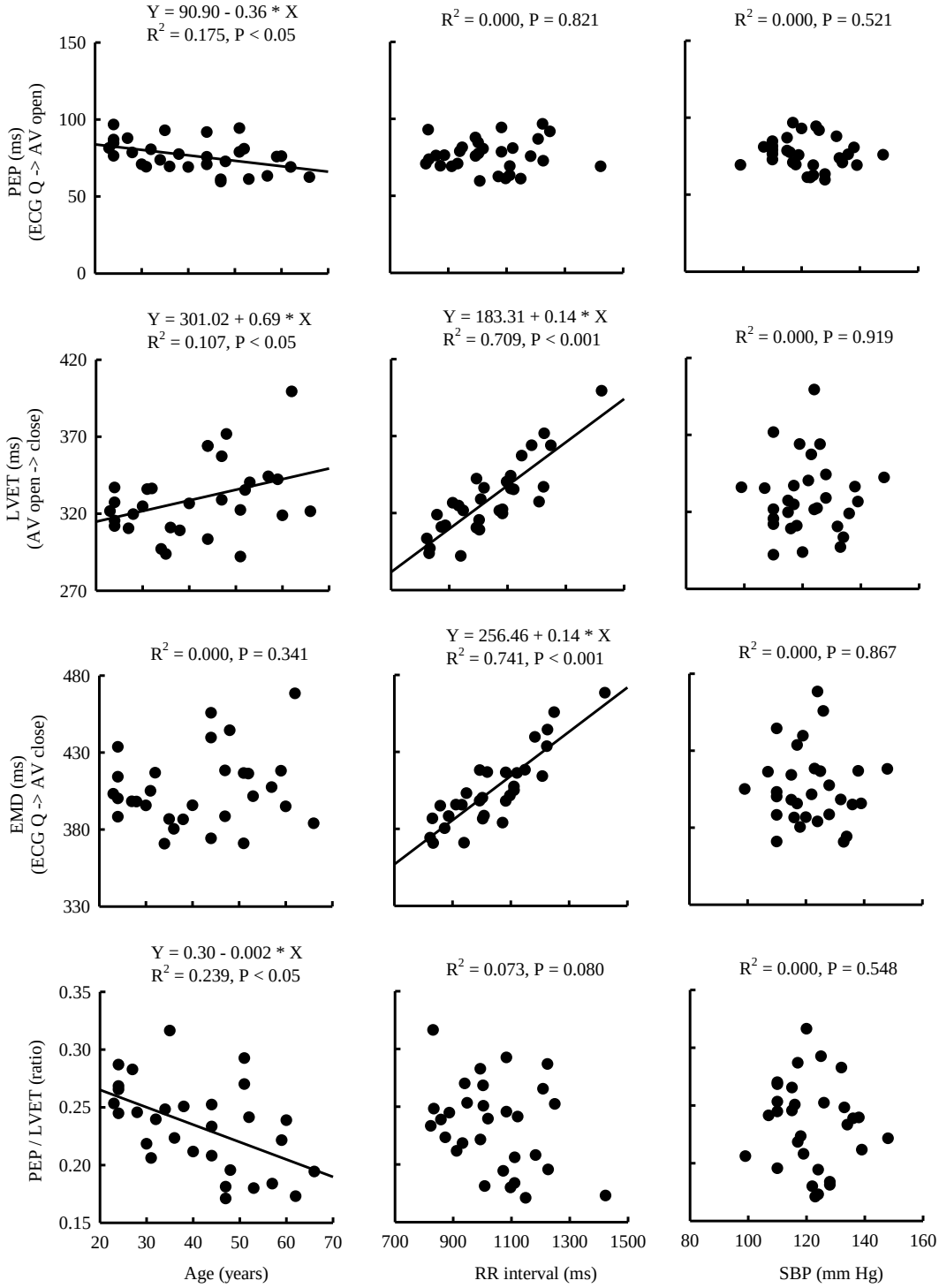

Figure 9-2. Relationships of aortic valve movement with age, RR interval and systolic blood pressure.

The multiple linear regression results, for the investigation on the relationships of the aortic valve movement with age, heart rate and blood pressure, are summarized in Table 9-2. The LVET and EMD were well predicted by the combination of the three variables ($R^2 \geq 0.753$, $P < 0.001$) with RR interval as the main significant predictor. The regression model for the ratio of the PEP to LVET was also significant ($R^2 = 0.232$, $P < 0.05$). However, age was the main factor of the regression mode.

Table 9-2. Summary of multiple linear regression results for the relationships of aortic valve movement with age, RR interval and systolic blood.

		Aortic valve movement time intervals (Outcomes)			
Demographic data (Variables)	**Measure**	**PEP Q -> AV open (ms)**	**LVET AV open -> close (ms)**	**EMD Q -> AV close (ms)**	**PEP / LVET (ratio)**
Overall	**Adj. R^2**	0.148	0.753	0.767	0.232
	P	0.068	< 0.001	< 0.001	< 0.05
Age (years)	**β**	-0.424	0.206	-0.218	-0.001
	P	< 0.05	0.304	0.265	< 0.05
RR interval (ms)	**β**	0.014	0.143	0.157	-0.000
	P	0.316	< 0.001	< 0.001	0.233
SBP (mm Hg)	**β**	0.112	0.393	0.504	0.000
	P	0.542	0.101	< 0.05	0.965

In terms of the Doppler imaging for the aortic flow, the flow accelerating duration (from flow start to peak), the decelerating duration (from flow peak to end) and the ratio of the decelerating duration to the accelerating duration were of interest. The relationships of these flow times with age, heart rate and blood pressure are shown in Figure 9-3. As can be seen, the RR interval showed a significantly positive relationship with both the flow accelerating duration ($R^2 = 0.230$, $P < 0.05$) and decelerating duration ($R^2 = 0.231$, $P < 0.05$)

in similar level. There was no significant influence found for age or systolic blood pressure on any of the three flow times.

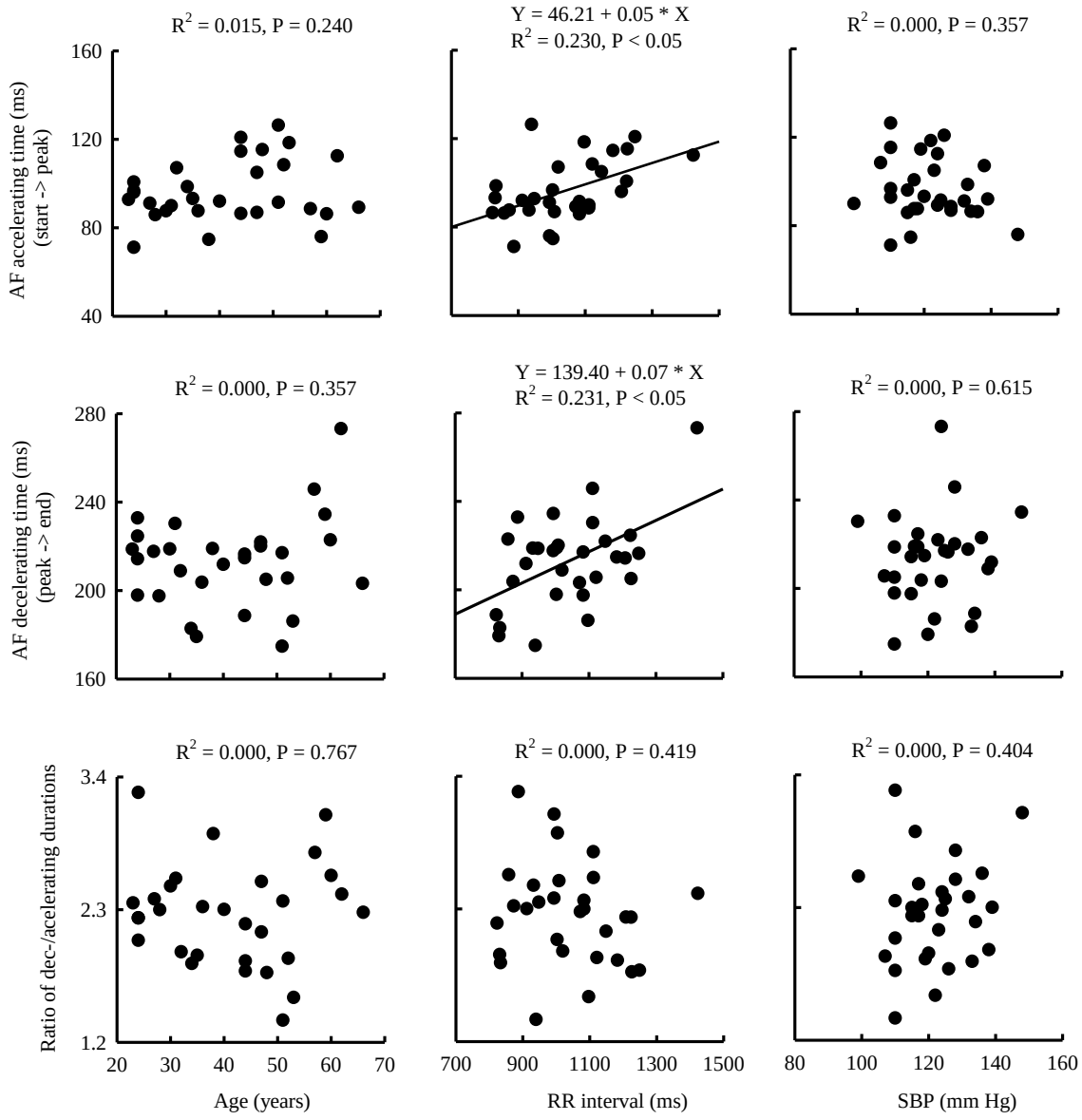

Figure 9-3. Relationships of age, RR interval and blood pressure with aortic flow durations.

The multiple linear regression results for the combination effects of age, RR interval and systolic blood pressure on the aortic flow times are summarized in Table 9-3. As expected, both the regression models for the flow accelerating and decelerating durations were significant ($R^2 \geq 0.200$, $P < 0.05$) with the RR interval as the main factor.

Table 9-3. Summary of multiple linear regression results for the relationships of age, RR interval and systolic blood pressure with aortic flow durations.

		Aortic flow time intervals (Outcomes)		
Demographic data		**Accelerating duration**	**Decelerating duration**	**Dec-/accelerating durations**
(Variables)	**Measure**	**Start -> peak (ms)**	**Peak -> end (ms)**	**(ratio)**
Overall	**Adj. R^2**	0.200	0.227	0.000
	P	< 0.05	< 0.05	0.735
Age (years)	**β**	0.187	-0.071	-0.003
	P	0.367	0.810	0.650
RR interval (ms)	**β**	0.042	0.080	-0.000
	P	< 0.05	< 0.05	0.671
SBP (mm Hg)	**β**	-0.172	0.451	0.007
	P	0.478	0.200	0.435

9.3.2 Mitral valve movement and flow

From the M-mode images for mitral valve movement during the ventricular passive filling phase, the valve opening duration (from valve initial opening to maximum opening), the valve closing duration (from valve maximum opening to closing) and the overall valve open duration (from valve initial opening to closing) were measured. In addition, the mitral valve open duration during active filling phase was also measured. The relationships of these mitral valve durations with age, RR interval and blood pressure are shown in Figure 9-4. While the valve opening duration was positively related to RR interval ($R^2 = 0.149$, $P < 0.05$), its closing duration increased with increasing age ($R^2 = 0.291$, $P = 0.001$). The overall mitral valve open duration during the ventricular passive filling phase was significantly correlated to only age ($R^2 = 0.261$, $P < 0.05$), but the valve open duration during the active filling phase was significantly correlated to both age ($R^2 = 0.296$, $P = 0.001$) and RR interval ($R^2 = 0.320$, $P < 0.001$). The systolic blood pressure did not show any significant influence on the mitral valve movement times.

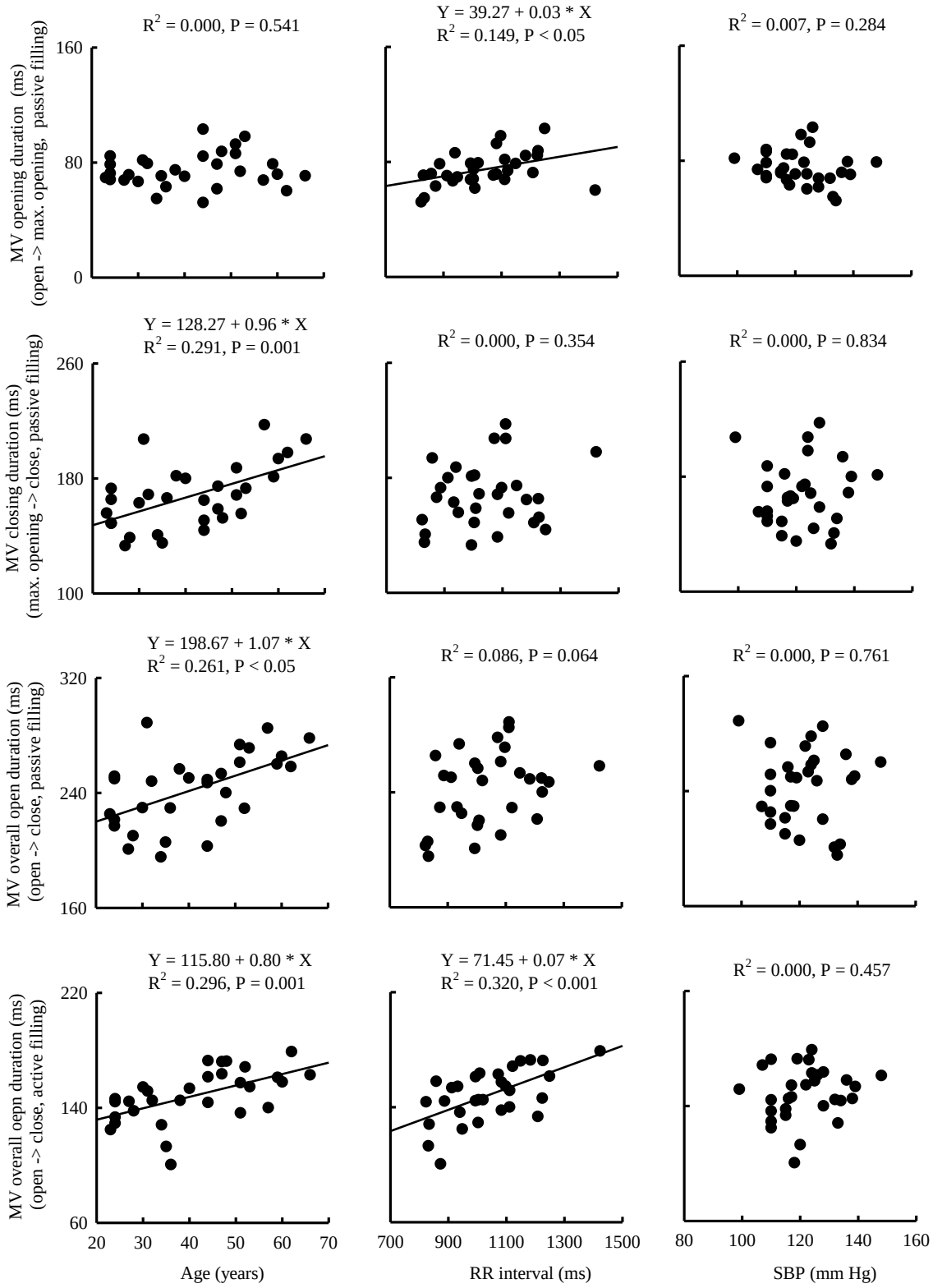

Figure 9-4. Relationships of mitral valve movement with age, RR interval and systolic blood pressure.

According to the multiple linear regression results provided in Table 9-4, the combination effects of age, RR interval and systolic blood pressure on the mitral valve closing duration and overall open duration during the ventricular passive filling phase, and the overall open duration during the active filling phase were significant ($R^2 \geq 0.273$, $P < 0.05$). Age shows strong influence on the three valve durations as a significant factor in the models ($P < 0.05$). In all the regression models for these three mitral valve durations, age was a significant factor. The RR interval was the main factor in the model for the valve open duration during the active filling phase ($P < 0.001$).

Table 9-4. Summary of multiple linear regression results for the relationships of age, RR interval and systolic blood pressure with mitral valve movement durations.

		Mitral valve movement time intervals (Outcomes)			
Demographic data (Variables)	**Measure**	**Opening duration (passive filling) open -> max. opening (ms)**	**Closing duration (passive filling) max. opening -> close (ms)**	**Open duration (passive filling) open -> close (ms)**	**Open duration (active filling) open -> close (ms)**
Overall	**Adj. R^2**	0.103	0.273	0.310	0.508
	P	0.124	< 0.05	< 0.05	< 0.001
Age (years)	**β**	0.081	1.090	1.170	0.569
	P	0.663	< 0.05	< 0.05	< 0.05
RR interval (ms)	**β**	0.030	-0.002	0.028	0.066
	P	0.067	0.937	0.365	< 0.001
SBP (mm Hg)	**β**	-0.158	-0.397	-0.555	0.189
	P	0.467	0.284	0.190	0.448

From the Doppler images for the mitral flow recording, the flow accelerating duration (from start to peak) and the flow decelerating duration (from peak to end) during the ventricular passive filling phase were measured. Additionally, the overall flow duration

(from start to end) during the ventricular active filling phase and the ratio of the overall flow duration during the active filling phase to that during the rapid filling phase were also obtained. The relationships of these aortic flow times with age, RR interval and systolic blood pressure are shown in Figure 9-5. The flow accelerating duration during the ventricular passive filling phase was negatively associated with age ($R^2 = 0.184$, $P < 0.05$) and positively associated with RR interval ($R^2 = 0.110$, $P < 0.05$). The decelerating duration was independent of RR interval, but increased with advancing age ($R^2 = 0.115$, $P < 0.05$). The overall flow duration during the passive filling phase was positively influenced by both age and RR interval ($R^2 \geq 0.196$, $P < 0.05$). The ratio of overall flow duration during the active filling phase to that during the passive filling phase was positively correlated to age ($R^2 = 0.143$, $P < 0.05$), but independent of RR interval or systolic blood pressure.

The multiple linear regression results for the combination effects of age, RR interval and systolic blood pressure on the mitral flow times are summarized in Table 9-5. As can be noted, the regression models for the mitral flow accelerating duration during the passive filling phase ($R^2 = 0.398$, $P < 0.001$) and the overall flow duration during the active filling phase ($R^2 = 0.368$, $P < 0.001$) were significant. In these two models, both age and RR interval were the significant predictors ($P < 0.05$).

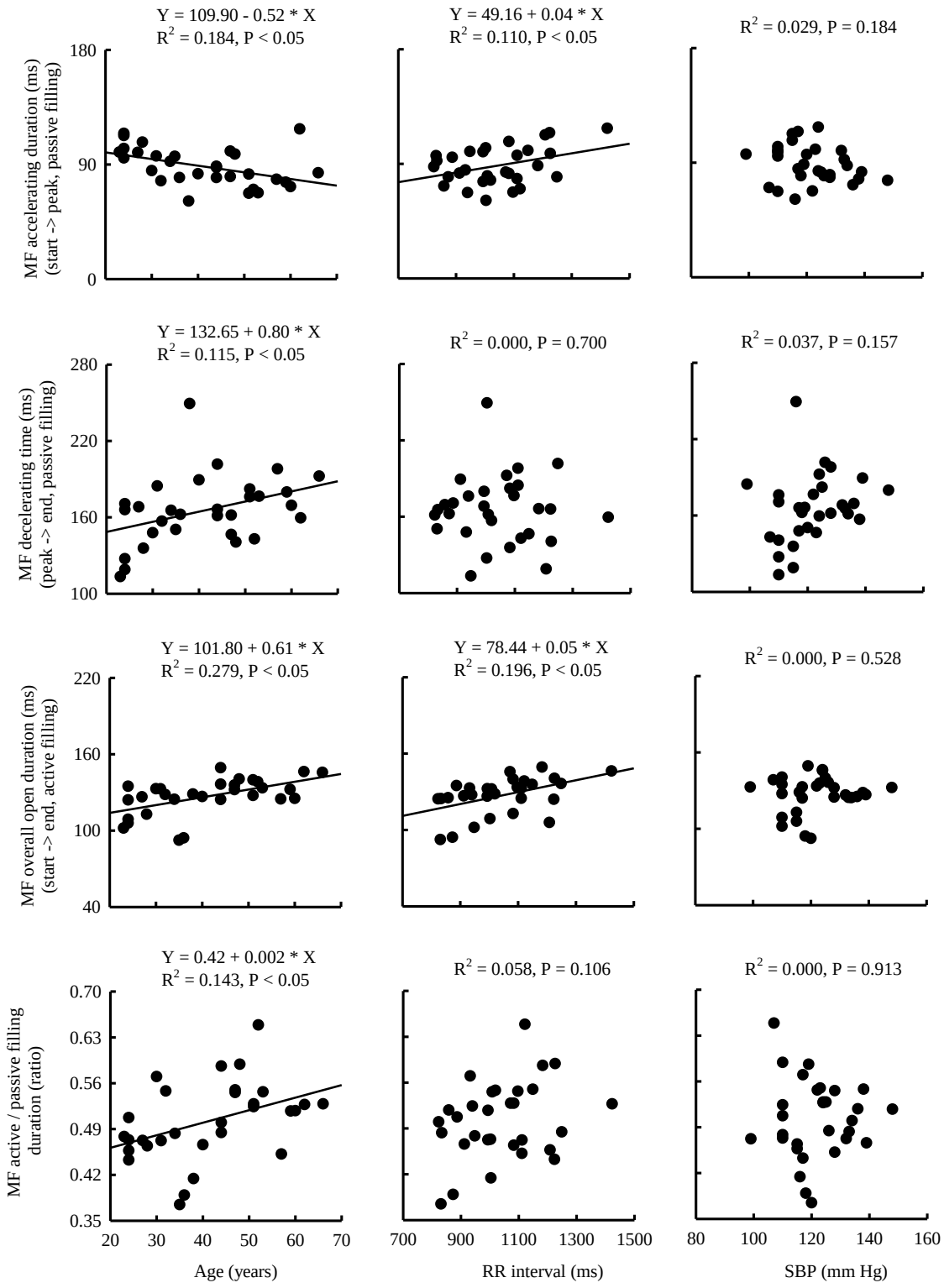

Figure 9-5. Relationships of mitral flow with age, RR interval and blood pressure.

Table 9-5. Summary of multiple linear regression results for the relationsips of age, RR interval and systolic blood pressure with mitral flow durations.

		Mitral flow time intervals (Outcomes)			
Demographic data (Variables)	**Measure**	**Accelerating duration (passive filling) start -> peak (ms)**	**Decelerating duration (passive filling) peak -> end (ms)**	**Open duration (passive filling) start -> end (ms)**	**Active / passive filling durations (ratio)**
Overall	**Adj. R^2**	0.398	0.073	0.368	0.144
	P	< 0.001	0.180	< 0.001	0.071
Age (years)	**β**	-0.702	0.742	0.498	0.002
	P	< 0.001	0.094	< 0.05	< 0.05
RR interval (ms)	**β**	0.054	-0.014	0.038	0.000
	P	< 0.05	0.699	< 0.05	0.366
SBP (mm Hg)	**β**	0.138	0.283	0.056	-0.000
	P	0.534	0.576	0.801	0.489

9.4 Effects of age, heart rate and blood pressure on impedance measurements

9.4.1 Effects of age on the shape of impedance waveforms

One of the most evident influences of age on the impedance waveform was the diastolic wave. Figure 9-6 demonstrates how the diastolic wave on the impedance Z and the derivative impedance -dZ/dt waveforms gradually disappeared with advancing age. The left impedance waveforms were recorded from a subject with an age of 23 years. The amplitude of the diastolic wave was around one third of the systolic wave amplitude, which was easily seen on the both Z and -dZ/dt waveforms. The middle waveforms were from a subject with an age of 44 years. The diastolic wave was still visible, but much smaller than the systolic wave. The last impedance waveforms were from a subject of 64 years. The diastolic waves on the impedance waveforms had completely disappeared.

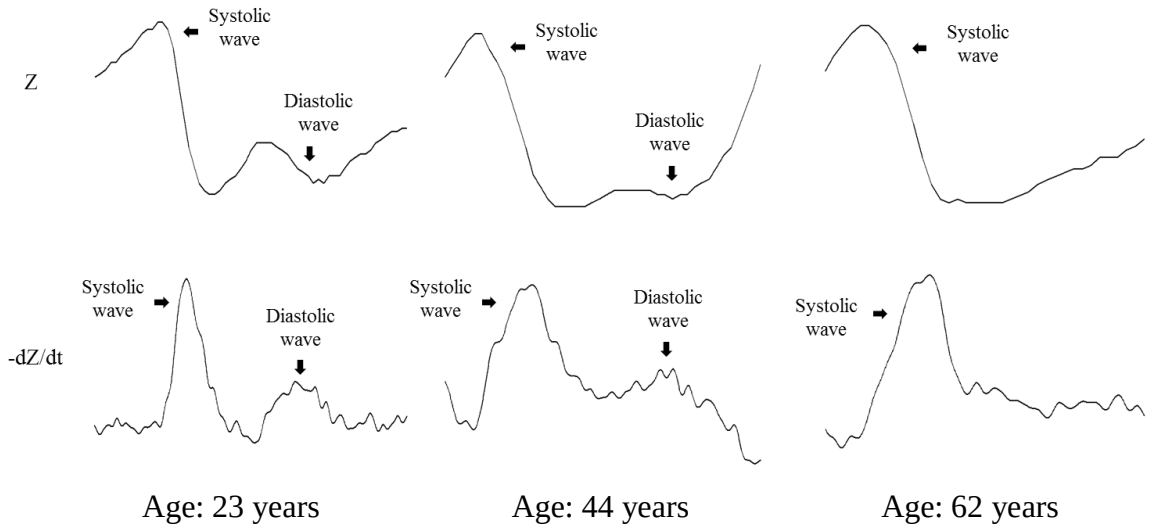

Figure 9-6. Demonstration of aging influence on the shape of impedance waveforms.

As a consequence of the gradual disappearance of the diastolic wave on the impedance waveforms with aging, the diastolic wave features were not always measurable. The most vulnerable features were the diastolic minimum point (2^{nd} min.) on the Z waveform, and the diastolic peak (2^{nd} peak) on the -dZ/dt waveform. There were only 23 subjects out of all the 30 subjects studied with measurable 2^{nd} minimum point on the Z, and 21 subjects with measureable 2^{nd} peak on the -dZ/dt. The comparison of age between the subject group with the measurable features and the group without the features is summarized in Table 9-6. According to the Mann-Whitney test results, the subjects without the 2^{nd} minimum point (age: 53 ± 9 years, Mean ± SDs) were significantly older than those with the minimum point (age: 37 ± 12 years, Mean ± SDs, $P < 0.05$). The subjects without the 2^{nd} peak point (age: 54 ± 9 years, Mean ± SDs) were also significantly older than those with the point (age: 36 ± 10 years, Mean ± SDs, $P < 0.001$).

Table 9-6. Age influence on diastolic features identified on the impedance waveforms.

Groups	Subject numbers	Age (mean ± SD years)	Significance (Difference)
Subjects with 2nd min. on Z	23	37 ± 12	P < 0.05
Subjects without 2nd min. on Z	7	53 ± 9	
Subjects with 2nd peak on -dZ/dt	21	36 ± 10	P < 0.001
Subjects without 2nd peak on -dZ/dt	9	54 ± 9	

9.4.2 Effects of age, RR interval and systolic blood pressure on impedance Z

From the systolic wave of the impedance Z waveform, the duration from the aortic valve opening to the onset of impedance falling, the impedance falling duration (from start to the minimum point), the impedance rising duration (from the minimum point to the end) and the overall systolic wave duration were measured. The relationships of these impedance time durations with age, RR interval and systolic blood pressure are shown in Figure 9-7. The impedance overall systolic duration showed a strongly positive correlation with the RR interval ($R^2 = 0.477$, $P < 0.001$) and weakly positive correlation with age ($R^2 = 0.129$, $P < 0.05$). These significant correlations were mainly associated with the rising part because the falling duration was independent of the RR interval and age.

Furthermore, according to the multiple linear regression results summarized in Table 9-7, only the regression models for the combination effects of age, RR interval and systolic blood pressure on the impedance rising duration and the overall systolic wave duration were significant ($R^2 \geq 0.468$, $P < 0.001$). The RR interval was the only significant factor in the two models ($P < 0.001$).

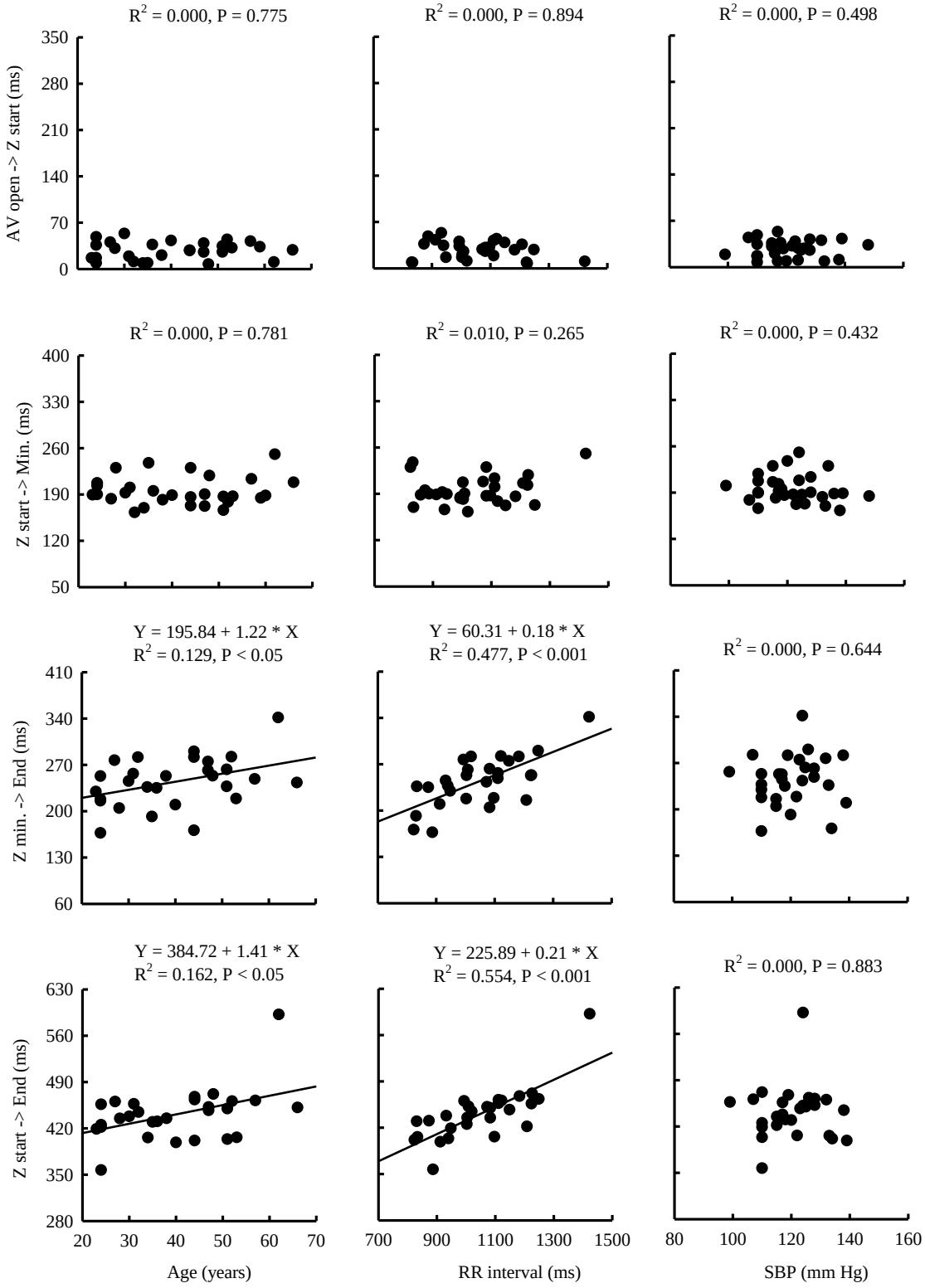

Figure 9-7. Relationships of age, RR interval and blood pressure with impedance systolic durations.

Table 9-7. Summary of multiple linear regression results for the relationships of age, RR interval and systolic blood pressure with impedance Z systolic durations.

		Impedance Z systolic time intervals (Outcomes)			
Demographic data (Variables)	**Measure**	**AV open -> Z start (ms)**	**Falling duration Z start -> Min. (ms)**	**Rising duration Z min. -> End (ms)**	**Systolic duration Z start -> End (ms)**
Overall	**Adj. R^2**	0.000	0.000	0.468	0.572
	P	0.931	0.662	< 0.001	< 0.001
Age (years)	**β**	-0.001	0.110	0.400	0.535
	P	0.974	0.763	0.409	0.248
RR interval (ms)	**β**	-0.000	0.024	0.172	0.195
	P	0.991	0.438	< 0.001	< 0.001
SBP (mm Hg)	**β**	-0.169	-0.262	0.681	0.471
	P	0.576	0.541	0.246	0.394

The relationships of the Z diastolic wave durations, including the diastolic falling duration (from systolic end to the 2nd minimum point) and the time difference between the systolic minimum point to the diastolic 2nd minimum point, with age, RR interval and blood pressure were displayed in Figure 9-8. The impedance diastolic falling duration was independent of age, RR interval and blood pressure, while the time difference between the two minimum points showed a strongly positive linear relationship with RR interval (R^2 = 0.495, P < 0.001).

The multiple linear regression analysis results summarized in Table 9-8 also showed that only the time difference between the two minimum points can be modelled by the combination of age, RR interval and systolic blood pressure (R^2 = 0.451, P < 0.001), but only the RR interval was the significant predictor in the model.

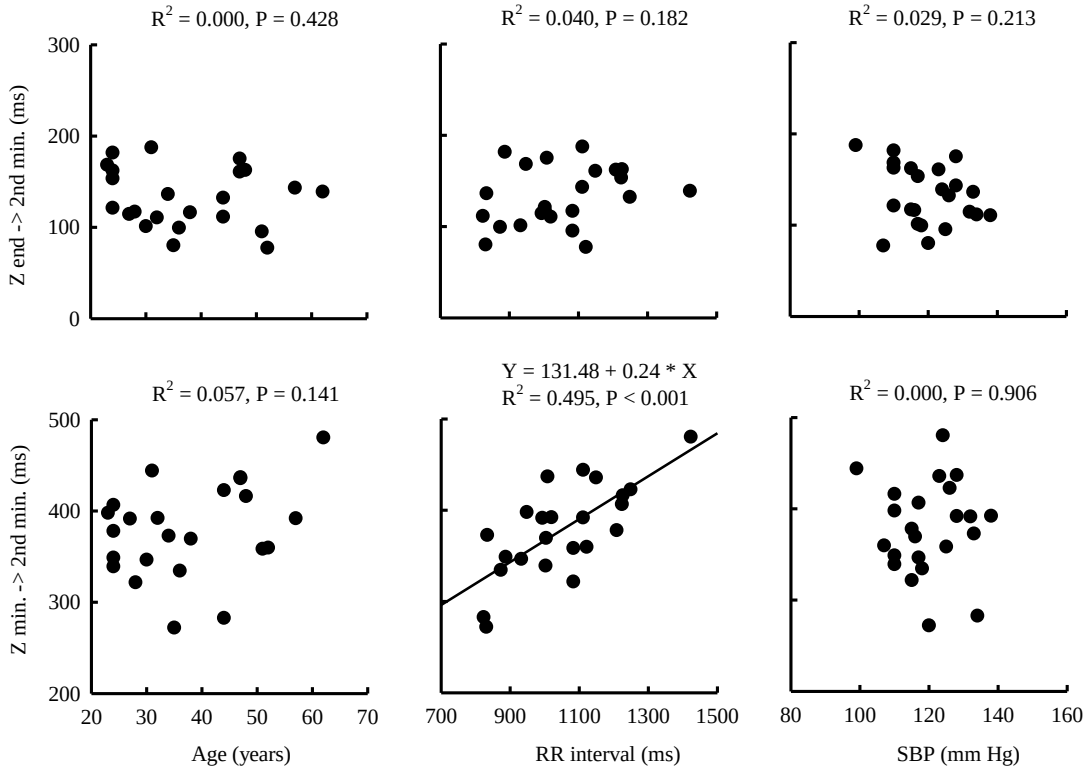

Figure 9-8. Relationships of age, RR interval and blood pressure with impedance Z diastolic durations.

Table 9-8. Summary of multiple linear regression results for the relationships of age, RR interval and systolic blood pressure with impedance Z diastolic durations.

Demographic data (Variables)	**Measure**	**Impedance Z diastolic time intervals (Outcomes)**	
		Falling duration Z end -> 2nd min. (ms)	**Valley-to-valley duration Z min. -> 2nd min. (ms)**
Overall	**Adj. R^2**	0.059	0.451
	P	0.257	< 0.001
Age (years)	**β**	-0.748	-0.053
	P	0.281	0.949
RR interval (ms)	**β**	0.079	0.242
	P	0.129	< 0.001
SBP (mm Hg)	**β**	-0.433	0.489
	P	0.566	0.589

9.4.3 Effects of age, heart rate and blood pressure on derivative impedance -dZ/dt

From the derivative impedance -dZ/dt systolic wave, the duration from the aortic valve initial opening to the -dZ/dt foot, the impedance accelerating duration (from -dZ/dt foot to peak), the impedance decelerating duration (from -dZ/dt peak to end) and the overall systolic duration (from -dZ/dt foot to end) were measured. The linear relationships of these impedance time durations with age, RR interval and systolic blood pressure were shown in Figure 9-9. The duration from the aortic valve opening to the -dZ/dt foot and the impedance accelerating duration were not independent of age, RR interval and systolic blood pressure. The impedance decelerating duration showed positive relationships with both age (R^2 = 0.309, $P < 0.001$) and RR interval (R^2 = 0.335, $P < 0.001$). Although the association was not significant ($P = 0.092$) the decelerating duration showed an increasing trend with elevating systolic blood pressure. The overall -dZ/dt systolic duration increased with only prolonged RR interval (R^2 = 0.330, $P < 0.001$).

The multiple linear regression results for the combination effects of age, RR interval and systolic blood pressure are summarized in Table 9-9. The -dZ/dt decelerating duration was well predicted by the combination of age, RR interval and systolic blood pressure (R^2 = 0.611, $P < 0.001$). All the three variables were significant factors in the model ($P < 0.05$). The model for the -dZ/dt overall systolic wave duration was significant but only the RR interval was a significant factor ($P < 0.001$).

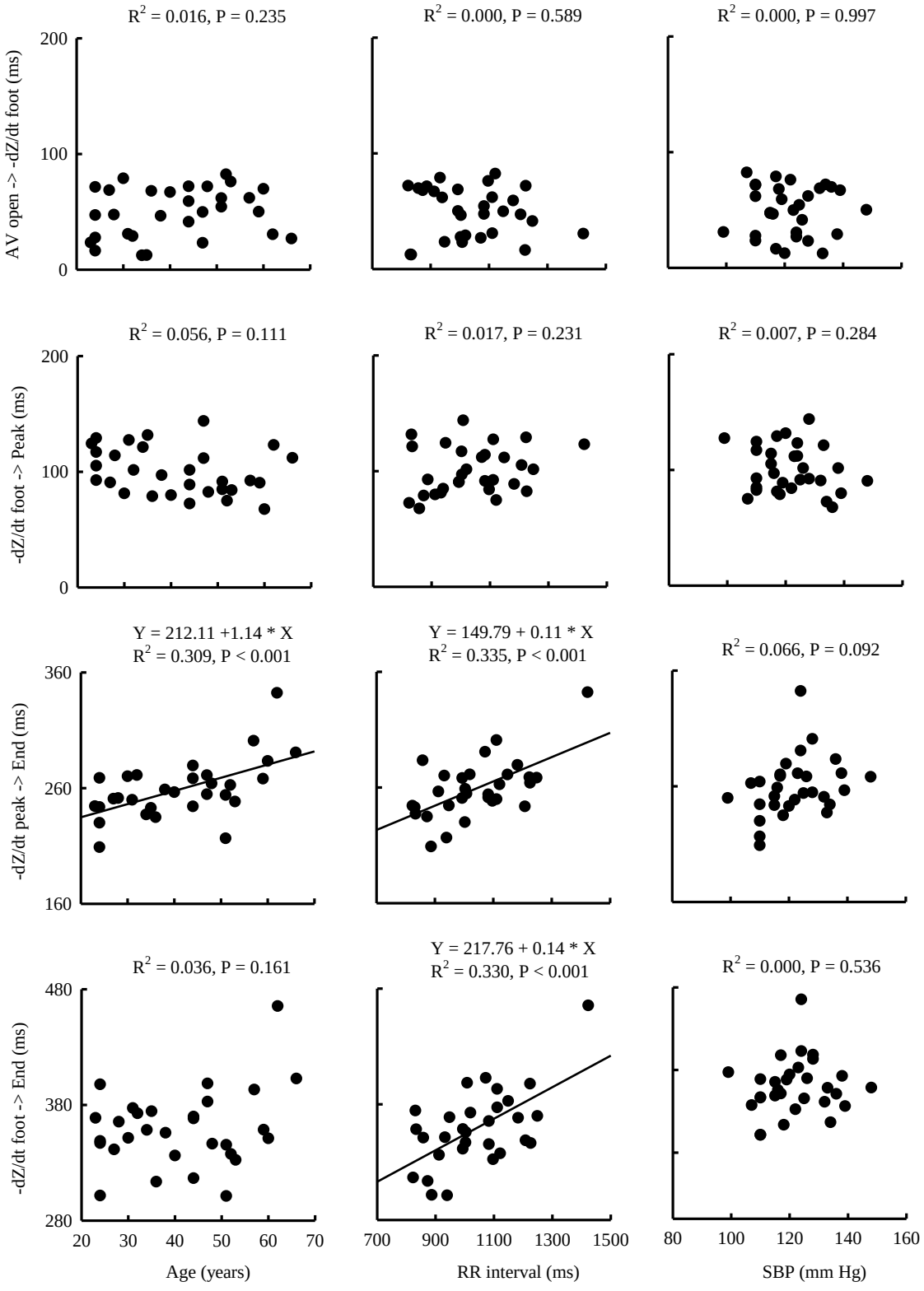

Figure 9-9. Relationships of age, RR interval and blood pressure with impedance -dZ/dt systolic durations.

Table 9-9. Summary of multiple linear regression results for the relationships of age, RR interval and systolic blood pressure with derivative impedance -dZ/dt systolic durations.

		Derivative impedance -dZ/dt systolic time intervals (Outcomes)			
Demographic data (Variables)	**Measure**	**AV open -> -dZ/dt foot (ms)**	**Accelerating duration -dZ/dt foot -> Peak (ms)**	**Decelerating duration -dZ/dt peak -> End (ms)**	**Systolic duration -dZ/dt foot -> End (ms)**
Overall	**Adj. R^2**	0.000	0.083	0.611	0.357
	P	0.435	0.159	< 0.001	< 0.001
Age (years)	**β**	0.559	-0.572	0.625	0.052
	P	0.126	0.082	< 0.05	0.906
RR interval (ms)	**β**	-0.032	0.043	0.106	0.149
	P	0.292	0.124	< 0.001	< 0.001
SBP (mm Hg)	**β**	-0.339	0.011	0.777	0.787
	P	0.421	0.977	< 0.05	0.138

The relationships of the -dZ/dt diastolic wave time durations, including the diastolic accelerating duration (from end to the 2nd peak) and the time difference between the systolic peak and the diastolic 2nd peak, with age, RR interval and blood pressure are displayed in Figure 9-10. The impedance accelerating duration of the diastolic wave was independent of age, RR interval or systolic blood pressure, while the time difference between the two peaks showed a significantly positive linear relationships with age (R^2 = 0.158, $P < 0.05$) and RR interval (R^2 = 0.400, $P < 0.001$).

The multiple linear regression analysis results for the combination effects of age, RR interval and systolic blood pressure are summarized in Table 9-10. Only the time difference of the impedance systolic peak and diastolic peak was well predicted by the combination of the three variables (R^2 = 0.402, $P < 0.05$), but only the RR interval was the significant predictor in the model.

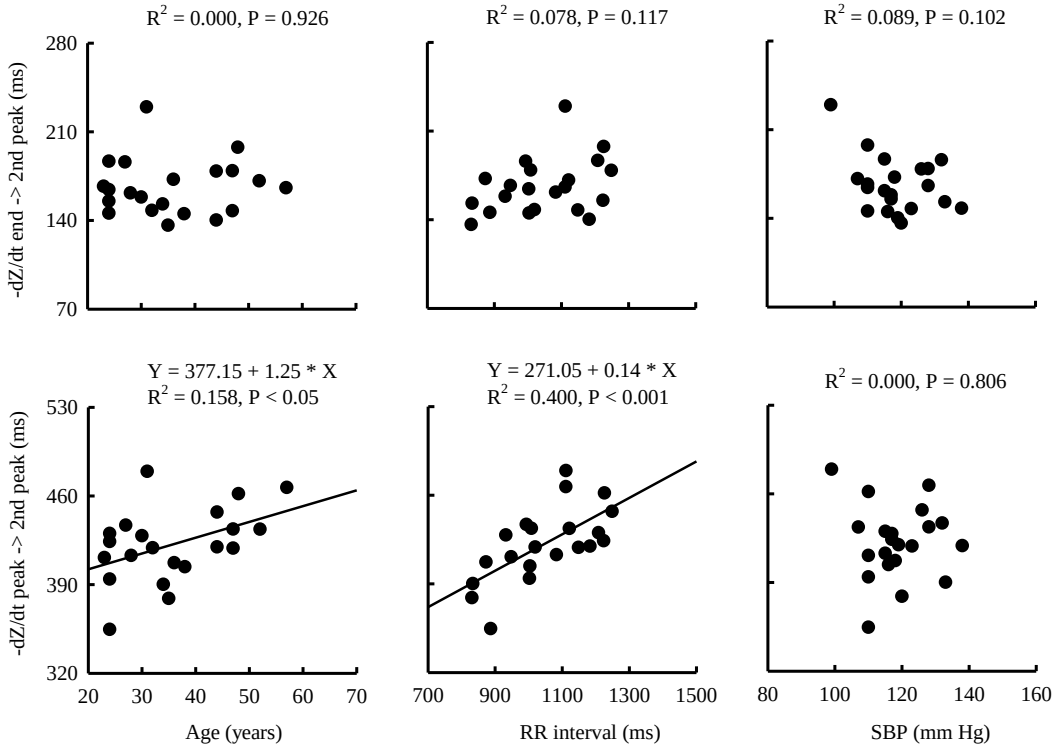

Figure 9-10. Relationships of age, RR interval and blood pressure with derivative impedance diastolic durations.

Table 9-10. Summary of multiple linear regression results for the relation of age, RR interval and systolic blood pressure with derivative impedance -dZ/dt diastolic durations.

Demographic data (Variables)	Measure	Derivative impedance -dZ/dt diastolic time intervals (Outcomes)	
		Accelerating duration	**Peak-to-peak duration**
		End -> 2nd peak (ms)	**Peak -> 2nd peak (ms)**
Overall	**Adj. R^2**	0.087	0.402
	P	0.219	< 0.05
Age (years)	**β**	-0.030	0.750
	P	0.952	0.175
RR interval (ms)	**β**	0.051	0.124
	P	0.204	< 0.05
SBP (mm Hg)	**β**	-0.720	-0.067
	P	0.178	0.904

9.5 Effects of age, heart rate and blood pressure on pulse measurements

From the finger pulse systolic wave, four indices, including the pulse foot transit time (PPT_f, from ECG R wave to the pulse foot), the pulse peak transit time (PPT_p, from ECG R wave to the pulse systolic peak), the pulse rising time (from pulse foot to the systolic peak), the large arterial stiffness index (SI, ratio of height to the pulse peak-to-peak duration), were calculated. The relationships of these pulse indices with age, RR interval and systolic blood pressure are shown in Figure 9-11. The PPT_f showed a significant relationship with all the three variables. It decreased slightly with age ($R^2 = 0.103$, $P < 0.05$) and increased with RR interval ($R^2 = 0.140$, $P < 0.05$). The transit time was significantly shortened driven by elevated systolic blood pressure ($R^2 = 0.367$, $P < 0.001$). By contrast, the PPT_p showed a strongly positive relationship with age ($R^2 = 0.390$, $P < 0.001$) but no significant relationship with blood pressure. The rising time showed a strongly positive relationship with age ($R^2 = 0.542$, $P < 0.001$) and RR interval. The SI showed a strongly positive relationship only with age ($R^2 = 0.628$, $P < 0.001$) but was independent of RR interval or blood pressure, which indicated SI was a good index reflecting the change in vascular stiffness caused by age.

According to the multiple linear regression analysis results summarized in Table 9-11, all the models for the combination effects of age, RR interval and systolic pressure on the 4 indices were significant ($R^2 \geq 0.475$, $P < 0.001$). In the model for PPT_f ($R^2 = 0.475$, $P < 0.001$), both RR interval and systolic blood pressure were the significant predictor ($P < 0.05$). In the models for PPT_p ($R^2 = 0.666$, $P < 0.001$) and rising time ($R^2 = 0.652$, $P < 0.001$), age was the major significant predictor ($P < 0.001$). With every 1 year increase in age, the PPT_p increased by 3.18 ms and the rising time increased by 3.60 ms. In the model for SI ($R^2 = 0.619$, $P < 0.001$), age was the only significant predictor ($P < 0.001$). Every 1 year increase in age caused 0.175 m/s increase in the stiffness index.

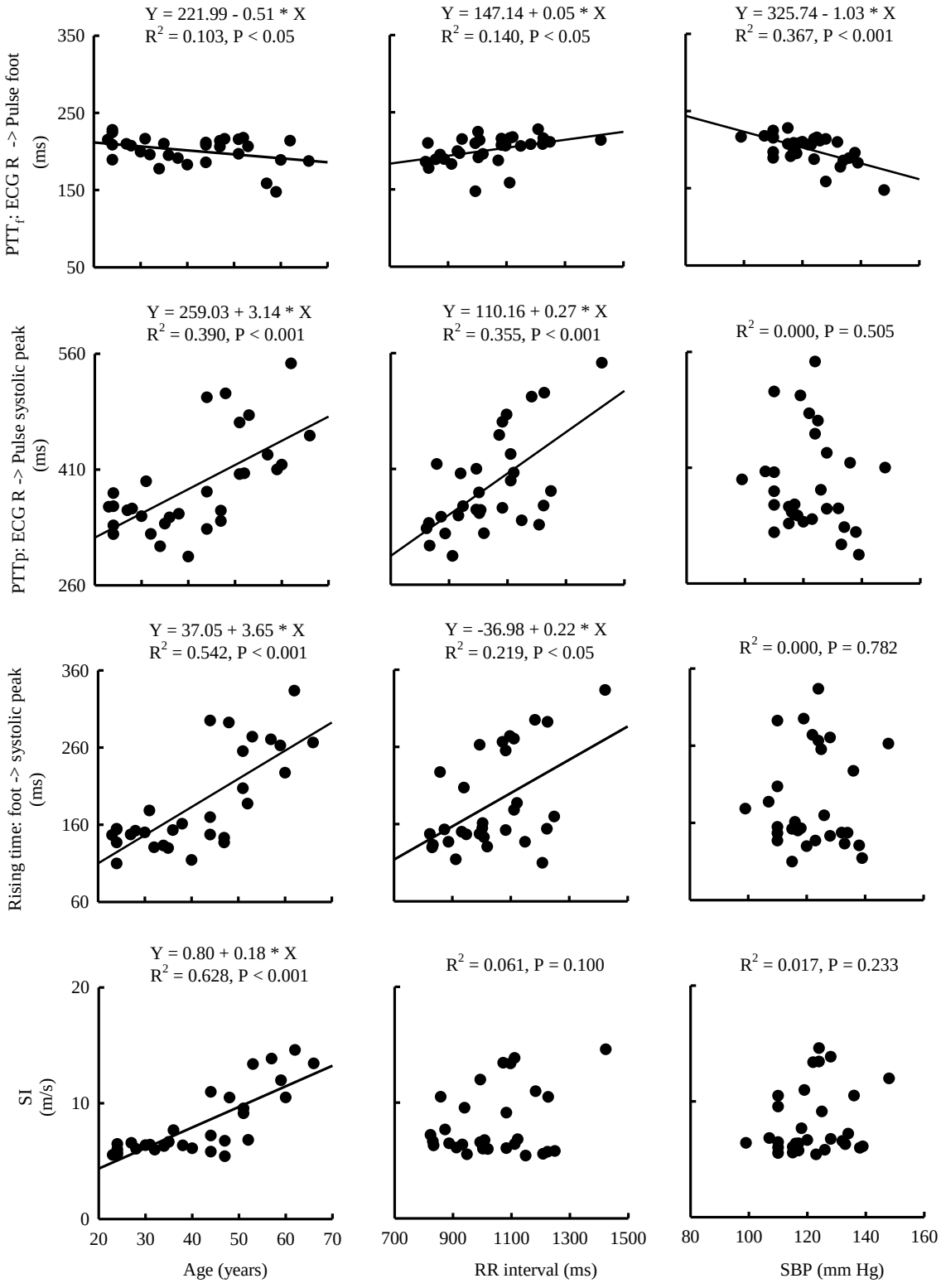

Figure 9-11. Relationships of age, RR interval and blood pressure with indices from finger pulse.

Table 9-11. Summary of multiple linear regression results for the relationships of age, RR interval and systolic blood pressure with indices from finger pulse.

		Finger pulse systolic time intervals (Outcomes)			
Demographic data (Variables)	**Measure**	**PTT_f ECG R -> Pulse foot (ms)**	**PTT_p ECG R -> systolic peak (ms)**	**Rising time Pulse foot -> systolic peak (ms)**	**SI Height / peak-to-peak duration (m/s)**
Overall	**Adj. R^2**	0.475	0.666	0.652	0.619
	P	< 0.001	< 0.001	< 0.001	< 0.001
Age (years)	**β**	-0.411	3.183	3.595	0.175
	P	0.069	< 0.001	< 0.001	< 0.001
RR interval (ms)	**β**	0.047	0.176	0.129	0.002
	P	< 0.05	< 0.05	< 0.05	0.343
SBP (mm Hg)	**β**	-0.704	-1.558	-0.854	-0.010
	P	< 0.05	< 0.05	0.245	0.778

The relationships of finger pulse diastolic durations, including the pulse diastolic rising time (from pulse notch to the diastolic peak) and the time difference between the systolic peak and diastolic peak, with age, RR interval and systolic blood pressure are shown in Figure 9-12. Age, RR interval and systolic blood pressure had a significant influence on the pulse rising time of the diastolic wave. The rising time slightly decreased with advancing age ($R^2 = 0.111$, $P < 0.05$) and increased with RR interval lengthening ($R^2 = 0.100$, $P < 0.05$). The most significant influence on the pulse diastolic rising time was from the systolic blood pressure ($R^2 = 0.380$, $P < 0.001$). The rising time decreased quickly with the systolic blood pressure increase. The time difference between the systolic peak and diastolic peak was strongly correlated with age ($R^2 = 0.590$, $P < 0.001$), which decreased with the age.

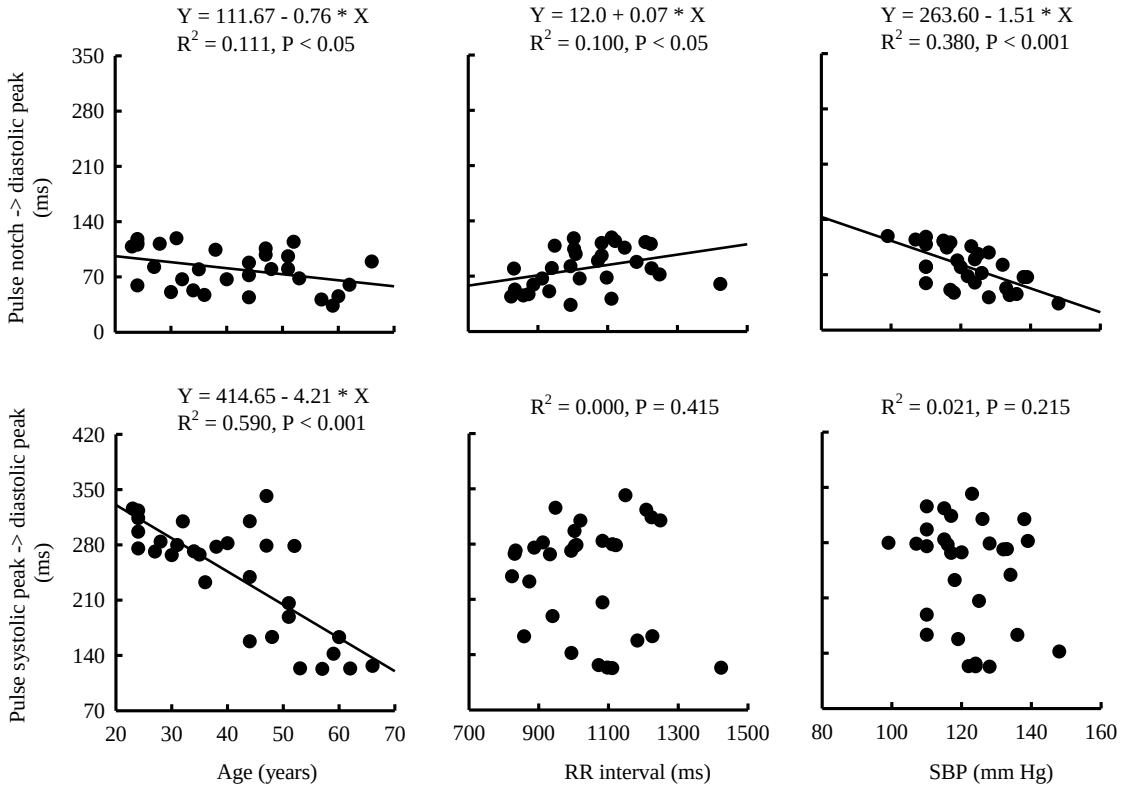

Figure 9-12. Relationships of age, RR interval and blood pressure with finger pulse diastolic durations.

According to the multiple linear regression analysis results summarized in the Table 9-12, both pulse diastolic durations can be well modelled by the combination of age, RR interval and systolic blood pressure ($R^2 \geq 0.453$, $P < 0.001$). In the model for the rising time, RR interval and systolic blood pressure were the two significant predictors. With 1 mm Hg increase in the systolic blood pressure, the rising time shortened by 1 ms. Age was the dominant predictor in the model for the time difference between the systolic peak and diastolic peak ($R^2 = 0.565$, $P < 0.001$). With 1 year increasing in age, the distance shortens by around 4 ms ($P < 0.001$).

Table 9-12. Summary of multiple linear regression results for the relationships of age, RR interval and systolic blood pressure with finger pulse diastolic wave durations.

Demographic data (Variables)	Measure	Finger pulse time intervals (Outcomes)	
		Notch -> Systolic peak (ms)	Systolic peak -> Diastolic peak (ms)
Overall	**Adj. R^2**	0.453	0.565
	P	< 0.001	< 0.001
Age (years)	**β**	-0.567	-4.423
	P	0.088	< 0.001
RR interval (ms)	**β**	0.058	0.023
	P	< 0.05	0.730
SBP (mm Hg)	**β**	-1.085	0.502
	P	< 0.05	0.578

9.6 Discussion and conclusion

In this chapter, the effects of age, heart rate and blood pressure on the imaging and physiological time features were investigated. The key findings include:

- The ECG PQ interval (from P start to Q wave) was positively correlated with age ($R^2 = 0.225$, $P < 0.05$);
- The pre-ejection duration (from ECG Q to aortic valve opening) was negatively correlated with age ($R^2 = 0.175$, $P < 0.05$), while the effect of age on the left ventricular ejection duration was weak (no significant association with any aortic flow duration);
- The mitral valve movement and flow were significantly influenced by age; both the mitral valve closing duration (from valve maximum opening to closing) and the mitral flow decelerating duration (from flow peak to end) during the ventricular passive filling phase were positively correlated with aging ($R^2 = 0.291$ for the valve closing duration, $R^2 = 0.115$ for flow decelerating duration, both $P < 0.05$), but independent of RR interval; both the mitral valve open duration during the rapid

filling phase and the active filling phase were positively correlated with age (R^2 = 0.261 for the rapid filling duration, R^2 = 0.296 for active filling duration, both $P < 0.05$); The ratio of the mitral flow duration (from flow start to end) during the active filling phase to that during the rapid filling phase was positively correlated with age ($R^2 = 0.143$, $P < 0.05$), but independent of RR interval;

- The diastolic wave on the impedance Z and the derivative impedance -dZ/dt gradually disappeared with aging. Both the falling durations during systole and diastole were independent to age and heart rate, while the impedance rising duration during systole (from the systolic minimum to the end) were positively correlated with age ($R^2 = 0.129$, $P < 0.05$) and RR interval ($R^2 = 0.477$, $P < 0.001$). The decreasing duration of the derivative impedance -dZ/dt systolic wave was positively related to age ($R^2 = 0.309$, $P < 0.001$) and heart rate ($R^2 = 0.335$, $P < 0.001$);
- The finger pulse foot transit time (PTT_f) was negatively correlated with age (R^2 = 0.103, $P < 0.05$) and systolic blood pressure ($R^2 = 0.376$, $P < 0.001$). The pulse peak transit time (PTT_p) and the rising time of the finger pulse systolic wave were positively correlated with age ($P < 0.001$) and the RR interval ($P < 0.05$). Stiffness index (SI) showed significantly positive relationship only with age ($R^2 = 0.628$, $P < 0.001$). The rising time of the diastolic wave (from notch to diastolic peak) was negatively correlated with age ($R^2 = 0.111$, $P < 0.05$) and systolic blood pressure ($R^2 = 0.380$, $P < 0.001$) but positively correlated with RR interval ($R^2 = 0.100$, $P < 0.05$). The peak-to-peak distance (from systolic peak to diastolic peak) was significantly reduced with aging advance ($R^2 = 0.590$, $P < 0.001$).

The aging influences on the cardiovascular structure and function have been extensively reported in the literature (Wei 1992, Lakatta 2002, Ferrari et al. 2003). The cardiac systolic function was not largely changed by age. The ECG PR interval, represented the overall time for the action potential transmitted from the atria to the ventricles, was positively correlated with age. The age-associated prolongation of the PR interval was attributed to the change in the atrioventricular node (Fleg et al. 1990). Systolic pre-ejection duration was considered as a measure of myocardial contractility (Ahmed et al. 1972). In this study, the pre-ejection duration was found to decrease with aging.

The effects of age on the diastolic function of resting heart are more significant than that on the systolic function (Wei et al. 1992, Ferrari et al. 2003). Spirito and Maron (1988)

investigated the influence of aging on Doppler echocardiographic indices of the left ventricular diastolic function on healthy subjects. It was found that the peak velocity of mitral flow during the passive filling phase was negatively related with age, while that of the flow during active filling phase was positively related with age, which resulted in the ratio between the maximum rapid filling and active filling velocities significantly decreasing with age. This observation indicates that the reduction in the rapid filling with age is compensated for by an increase in the active filling. By the work of Schirmer et al. (2000), the decelerating duration of the rapid filling flow was also significantly influenced by age. The decelerating duration was prolonged with aging due to the stiffness of left ventricle retarding the relaxation. Based on the imaging recordings in this study, both the mitral flow decelerating duration of the rapid filling flow derived from Doppler images and the mitral valve closing duration during the rapid filling flow derived from M-mode images were found positively related to age. Additionally, the ratio of mitral active filling duration to the rapid filling duration was also significantly related to age.

The aging influences also reflect on impedance and pulse waveforms. The most evident influence of age on impedance waveforms was from the diastolic wave, which gradually disappeared with advancing age. This observation emphasized the association between the impedance diastolic wave and the ventricular rapid filling. Both the rising time of the impedance systolic wave and that of the finger pulse systolic wave were positively related to age. The prolonged rising time of the pulse was attributed to the changes in the properties of arteries with advancing age (Allen and Murray 2003). There was no explanation provided in the literature about the relationship between the rising time of the impedance waveform and age. As discussed in the previous chapter, however, if the impedance recovery was caused by the transportation of blood from the central aorta to the peripheral smaller arteries, it is as expected that the impedance recovering duration varies with the rising time of the peripheral pulse. It is well known that the arteries become stiffer when age increases, which in sequence results in the acceleration of pulse wave transmission (O'Rourke et al. 1992). That was why the pulse foot transit time decreased with age. On the other hand, the pulse systolic wave was more likely to be dominated by the late systolic component in older subjects, which leads to a significant increase in the pulse peak transit time measurement and a decrease in the peak-to-peak distance

measurement with aging. This was why the PPT_p was positively correlated with age, while SI was negatively correlated with age.

Most time intervals from images and physiological measurements were significantly related to heart rate. The intervals were prolonged with heart rate slowing down. The effects of systolic blood pressure were evident on pulse foot transit time and pulse diastolic rising time. Driven by higher systolic blood pressure, both the transit time and rising time were decreased significantly.

Chapter 10 Discussion, conclusions and suggestions for further work

In this chapter, the key findings for the project are reviewed and conclusions are drawn. The limitations of the current studies are discussed. Some suggestions for further work are provided.

10.1 Discussion and conclusions

This project was carried out to investigate the relationship between echocardiography and physiological measurement techniques with the main aims of obtaining a better understanding of the pulsatile thoracic impedance change and peripheral volume pulse, and validating the possibility of cardiovascular function assessment from the impedance cardiogram and PPG techniques by referring them to well-established echocardiographic techniques. The complete thesis was composed of five main parts: 1) literature reviews on the previous studies of cardiac imaging and physiological measurement (Chapter 1); 2) measurement system and protocol development (Chapter 2 to 4); 3) study repeatability assessment (Chapter 5); 4) relationships between echocardiography and physiological measurements (Chapter 6 to 8); 5) effects of age, heart rate and blood pressure on echocardiography and physiological measurements (Chapter 9).

From the literature review part in Chapter 1, both the impedance cardiography and PPG techniques were identified as non-invasive physiological measurements of clinical importance with potential to provide simple and easy assess to cardiovascular function, which are beneficial to patients need continuous monitoring. The history of studying these two techniques can be dated from several decades ago. However, their applications are limited because the origins of the pulsatile impedance change and peripheral volume pulse are poorly understood and the features from the waveforms are lacking cross-validation with gold standards, such as cardiac images. These observations were the basis on which the rationale of this project was established.

The four measurement devices (an echocardiographic device, an ECG device, an impedance device and a pulse device), which were introduced in Chapter 2, were employed in this project for data acquisition. Ideally, all the signals should be recorded from these devices simultaneously. However, in the experimental setting this was not practical. Data were recorded in sequence from different combinations of the devices on each subject in three sessions. Considerations were given for the simultaneous recording of echocardiograms and physiological measurements. The measurement protocol development and data pre-processing procedures, including the multiple signal synchronization, were introduced in Chapter 3. The recorded signals were processed and then features were identified with MATLAB (MathWorks Co., USA) software with graphic user interfaces (Chapter 4). The further studies were based on the times of these identified features and the main contributions of each study are summarized and discussed in the following sections.

10.1.1 Study repeatability

Cardiac images and physiological signals were recorded on each subject in the three sequential sessions within one hour. For each single recording, a repeat recording was taken in the same session. Features were identified separately from the repeated recordings. The majority of the features from the image and physiological signals showed good repeatability within the same session (within-session repeatability). The within-session RR interval variation was less than 20 ms, and the variation of the other features was less than 5 ms. Therefore, in order to improve the reliability of the subsequent analysis, the average values from the two recordings within the same session were used.

The limb lead ECGs were recorded in all three sessions, while the impedance and finger pulse were recorded in session 2 and 3. The between-session repeatability was assessed based on the data from these recordings. The heart rate slowed down slightly across the three sequential sessions ($P > 0.05$). Some ECG features (P wave start and peak, Q wave, T wave peak and end) and finger pulse features (foot and notch) showed small but significant between-session differences. Therefore, the values of the identified features from different sessions were analysed separately in the following analysis.

10.1.2 Timing sequence of cardiovascular events in a cardiac cycle

Based on the features identified from simultaneously recorded echocardiograms and physiological signals, the first important contribution of the project was the reconstructed timing sequence of cardiovascular events in a cardiac cycle.

An example of the overall timing sequence obtained from one subject was provided in Chapter 5. The different parts of the timing sequence obtained across all the subjects were provided at the beginning of Chapter 6 to 8 to give an overview of the timing information of cardiovascular events. The overall timing sequence across all the subjects from the data recorded in the three sessions has been brought together and is shown in Figure 10-1. As was expected, the left ventricular active filling (caused by the left atrial contraction) was seen following the ECG P wave (atrial depolarization). Following the ECG QRS complex (ventricular depolarization), the left ventricular ejection started. After the aortic valve opening, the thoracic impedance started to fall, and then the volume pulse was transmitted to the ear and finger sequentially. With the ventricular relaxation (ECG T wave), the aortic valve closed. After a short isovolumetric phase, the mitral valve opened driven by the transmitral pressure gradient, and thus the ventricular passive, or rapid, filling phase started. The systolic components of the impedance and peripheral pulse ended during this phase, and diastolic components were observed.

The ECG features represented the cardiac electrical activities. The valve movement and blood flow conditions resulted from the cardiac mechanical function, while the thoracic impedance change and pulse resulted from the volumetric change in the ventricles, central great vessels and the peripheral micro vessels. The timing sequence quantitatively described how the cardiac electrical activities initiated the cardiac mechanical function and consequently induced the vascular function in each cardiac cycle. To the author's best knowledge, this is the first study linking ECG, echocardiograms, thoracic impedance and peripheral pulse together, which was helpful to obtain a better understanding of the overall cardiovascular function.

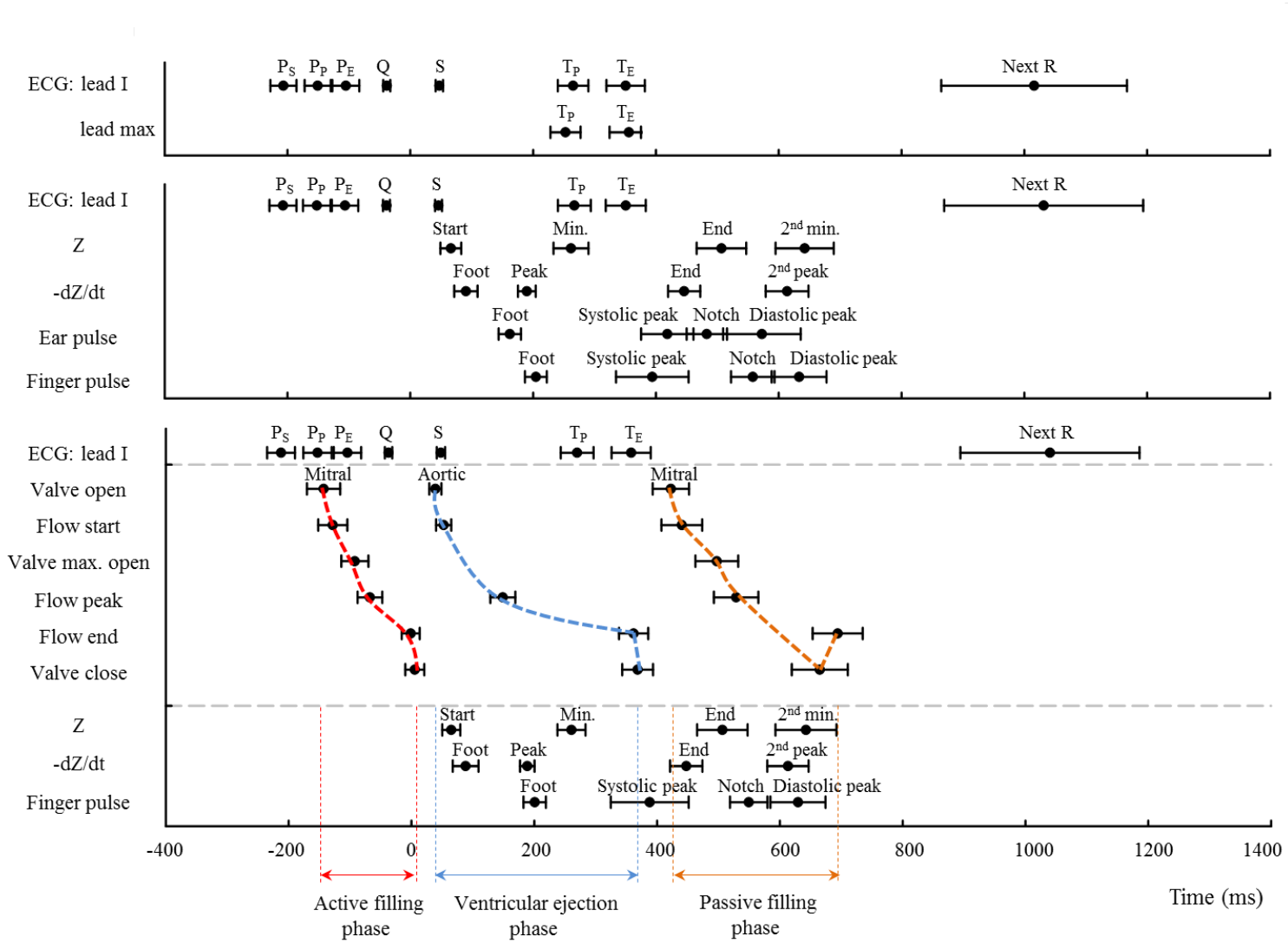

Figure 10-1. The timing sequence of cardiovascular events in the cardiac cycles. The plots from the top to the bottom show the data from sessions 1 to 3. All times were measured from the ECG R wave. The circle denotes the mean and error bar denotes SD of the values across all the subjects. On the bottom panel, the valve movements and the corresponding blood flow conditions during the active filling, left ventricular ejection and passive filling phases were connected by the red, blue and brown lines in sequence.

10.1.3 Dynamic relations of valve movement and blood flow conditions

The investigation on the relations of valve movement and corresponding flow conditions is critical for understanding the mechanism behind the valve movement. The relevant studies were started several decades ago (Landiado et al. 1975, 1978, Higashidate et al. 1995, Howard et al. 2003). The relations of the aortic valve movement times (open and close) and mitral valve movement times (open, maximum opening and close) with the corresponding flow conditions (start, peak and end) were also investigated in this project based on the recorded M-mode echocardiograms and Doppler images (Chapter 6).

Higashidata et al. (1995) and Howard et al. (2003) showed that the aortic valve opens before the onset of aortic flow and elevation of aortic pressure based on the animal experiments on anesthetized dogs and computer simulation. Therefore, they attributed the opening mechanism of the aortic valve to the expansion of the aortic root during the early left ventricular systole. In this study both the mitral valve and aortic valve were found to open just before (less than 20 ms) the onset of the flow detection.

It was reported that the valves were always fully opened before the peak flows, which means that valve leaflets start to close before the flow reaches its peak velocity (Landiado et al. 1975, 1978, Higashidate et al. 1995). This phenomenon was also observed in this study, where the mitral valve maximum opening preceded the mitral flow peak by 25 ms during the ventricular active filling phase and 32 ms during the passive filling phase respectively. Higashidate et al. (1995) explained that this phenomenon as being caused by the combination of the internal forces stored by the displacement of the cusps and the vortexes in the sinuses.

There were few studies reporting the relations of the valve closing and flow ending. According to this project, the valves always closed after the offset of the flows detected. However, it was noted that the mitral flow was still seen a short time after (29 ms) the mitral valve had apparently closed at the end of the left ventricular passive filling. This would be because the valve had not closed completely, allowing blood flow to still be observed after the valve leaflets were apparently closed.

10.1.4 Relations of thoracic impedance change with cardiac mechanical function and peripheral pulse

There are numerous studies which had been performed to investigate the relationship between blood volumetric change in the thorax and the amplitude of the pulsatile impedance Z waveform since 1960s (Patterson 1964, 1966, 1989, Kubicek et al. 1970, 1978). However, the timing information of the Z waveform was usually ignored. The investigation on the relations of the impedance Z feature times with valve movement times and blood flow conditions was able to provide additional information on the origins of the pulsatile impedance waveform in a cardiac cycle.

Several important findings were obtained in this study based on the simultaneously recorded impedance and images (Chapter 7). Firstly, a decrease in the impedance was observed during both the ventricular ejection and ventricular passive filling phase, which confirmed that the volume change in the ventricles would not be the only contributor to the impedance change. Secondly, the impedance falling during systole was found soon after the start of ventricular ejection, but stopped during the late ejection phase (after the aortic peak flow). During the late ejection phase, the blood volume from the left ventricle into the aorta was reduced and slowed down. The volume change in the thorax was dominated by the drainage of volume from the central aorta to the periphery, which resulted in a reduction of the blood volume in the thorax, and thus causing the impedance to restore. This observation suggested that the volume change in the aorta rather than that in the ventricle would be the main generator of the impedance falling during systole. Lastly, the strong relationship between the onset of the impedance Z falling during diastole and the mitral valve movement during the ventricular passive filling phase might indicate that the venous return in this phase would be the main generator of the Z diastolic fall.

The investigation on the relationships between thoracic impedance change and peripheral pulse provided further evidence about the generation of pulse and impedance waveforms. This investigation was firstly implemented in this study based on the simultaneously recorded impedance and ear and finger pulses (Chapter 8). The pulse rising phase followed the impedance falling phase during systole, and the impedance started to recover before the peripheral pulse achieved peaks. This observation can be explained by the blood distribution process in the arterial system. During the early systole, a large

amount of blood entered into the aorta. The impedance dropped rapidly, and achieved the minimum when the aorta was fully filled. However, with the ejection slowing down, the dominance of incoming blood volume to the aorta was gradually replaced by the draining of the volume to peripheral sites. This is why the impedance started to recover when the pulse was rising. During the next stage, the blood volume in the peripheral sites was maintained at a relatively high level, while the impedance recovered slowly.

One of the most important potential clinical applications of the impedance cardiography technique is to provide an easy way to estimate the ventricular systolic time intervals. The time features of the derivative impedance -dZ/dt and the blood flow conditions from Doppler echocardiograms were compared in this study (Chapter 7). The PEP (pre-ejection time) and EMD (electromechanical delay) were significantly longer than those from the images and also longer than those reported in the literature. However, for the LVET measurement, although the value from impedance was still significantly longer than those from images, the difference between the impedance and images in this study (Mean difference ± SD: 30 ± 27 ms) was close to that reported by Fellahi et al. (2009) (Mean difference ± SD: 32 ± 37 ms) and that reported by Carvalho et al. (2011) (Mean difference ± SD: 35 ± 38 ms). This suggests that the measurement of time intervals, such as LVET, from impedance would be less influenced by variation between devices than the measurement of time based features, including PEP and EMD. According to the further analysis, the difference of LVET measurements from impedance and Doppler images was mainly contributed by the difference between the decelerating parts of the impedance and the aortic flow (Mean difference: 46 ms). This observation supported Carvalho et al.'s point (Carvalho et al. 2011) that the current definition of the systolic end of the derivative impedance (the minimum point between the systolic wave and diastolic wave) would probably not be the best for LVET measurement.

10.1.5 Relationship between peripheral pulse and cardiac mechanical function

Pulse is initiated by the ejection of blood from the left ventricle to the aorta, which is then transmitted to peripheral sites along the arterial system. Although the cardiac mechanical function is an important source of the origins of the peripheral pulse, the relationship between them was rarely investigated in the published studies. Based on the

data recorded in session 3 in this project, the relations of finger pulse features with aortic valve movement and aortic flow conditions were investigated (Chapter 8). The pulse foot was observed 162 ms on average after the aortic valve initial opening and significantly correlated with valve open ($R^2 = 0.361$, $P < 0.05$). A more interesting result was from the strong linear relationship between the pulse notch point and the aortic valve close ($R^2 = 0.579$, $P < 0.001$). It was well known that the closing of the aortic valve generated a characteristic notch point on the pressure pulse (O'Rourke et al. 1992, Levick 2010). However, the origin of the notch point on the volume pulse has not been well explained. The observation in this study suggests that the occurrence of the notch point on the volume pulse would also be caused by the aortic valve closing. This explanation is acceptable because the report by Millasseau et al. (2000) showed that the peripheral volume pulse and the peripheral pressure pulse would be determined by a similar mechanism.

It was shown in Chapter 8 that the duration from the pulse foot to notch was close to the LVET from M-mode images with strong correlation (Mean ± SD: 19 ± 16 ms, $R^2 = 0.534$, $P < 0.001$). This means that the PPG technique is able to provide a simple way to estimate LVET at least in healthy subjects, which is based on the observation of the strong association between the pulse and aortic valve movement times.

Clinical indices from the peripheral pulse waveforms, which reflected the cardiovascular function, were proposed in the previous studies. The commonly used indices included the pulse foot transit time (PTT_f, from ECG R wave to the pulse foot), pulse peak transit time (PTT_p, from ECG R wave to the pulse systolic peak), pulse rise time (from the pulse foot to systolic peak) and the stiffness index (SI, the subject height divided by pulse peak-to-peak time). While the pulse transit time was considered as a measure of the pulse wave velocity (Allen and Murray 2000, Allen et al. 2008), the stiffness index was considered as a measure of the stiffness of large arteries (Millasseau et al. 2002, 2003). The normal ranges of these four indices were obtained from both ear and finger pulses recorded in session 2: the mean PTT_f from ear pulse and finger pulse were 162 ms and 205 ms respectively; the mean PTT_p from ear pulse and finger pulse were 419 ms and 394 ms; the mean rise time from ear pulse and finger pulse were 256 ms and 190 ms; the mean SI from ear pulse and finger pulse were 13.1 m/s and 8.0 m/s.

10.1.6 Effect of age, heart rate and blood pressure on cardiac imaging and physiological measurements

The influences of age, heart rate and blood pressure on cardiovascular functions attracted extensive interests of clinical research (Wei et al. 1992, Lakatta 2002, Ferrari et al. 2003). The variation of images, impedance and peripheral pulse with age, heart rate and blood pressure on normal subjects were investigated in this project (Chapter 9).

It was reported that the effects of age on the ventricular diastolic function of the resting heart were more significant than those on the systolic function (Wei et al. 1992, Ferrari et al. 2003). This point was supported by the results provided in Chapter 9. For the systolic function, pre-ejection period was the only time feature which was significantly correlated with age. It showed a decreasing tendency with advancing age. The other systolic time intervals (left ventricular ejection time and eletromechanical delay) were more likely determined by heart rate. Aging influenced the ventricular filling in both passive and active filling phases. The overall mitral valve open durations, the mitral valve closing durations and the mitral flow decelerating durations showed significantly positive correlation with age. The prolonged ventricular filling durations were attributed to the stiffness of left ventricle which retarded the relaxation (Schirmer et al. 2000). It was reported in the past that the ratio of the peak velocity of the mitral flow during the passive filling phase to that during the active filling phase was decreasing with age, which indicated that the decrease of the ventricular passive filling with age would be compensated by an increase in the active filling (Spirito and Maron 1998). A similar situation was found for the flow durations. According to Chapter 9, the ratio of the duration of the mitral flow during these two filling phases was negatively correlated with age. This observation added new information to the way that aging influenced the left ventricular diastolic function on healthy subjects.

The aging influences on the impedance and pulse waveforms were also shown in Chapter 9. The most evident effect of age on the impedance waveforms was that the diastolic component of the impedance waveform gradually disappeared with advancing age. This striking observation emphasized the association between the impedance change during the diastolic wave and the ventricular passive filling. Another interesting observation was that both the impedance systolic recovery time and the pulse rising time were positively related to age. The prolonged rising time of pulse with age was also reported by Allen and

Murray (2003). However, there was no explicit explanation provided. The association between the impedance rising time and age was a new finding in this study although the underlying principle was not clear yet. As discussed in Chapter 8, however, because the impedance recovery was caused by the movement of blood volume from the central aorta to the peripheral arteries, it was expected that the impedance recovery time varies with the rising time of peripheral pulse.

Heart rate was a significant factor influencing many imaging and physiological time features. With heart rate slowing down, the time durations of the cardiovascular activities were prolonged. In contrast, systolic blood pressure was not a significant factor for most difference in imaging or physiological time features. Its effects on pulse transit time and diastolic rising time were evident. Driven by higher systolic blood pressure, both the pulse transit time and rising time were decreased significantly.

10.2 Limitations of the study

The first limitation in this project is that all data were recorded on subjects at rest. The use of multiple echocardiography and physiological measurement devices made it difficult to study the subject in certain conditions, such as breathing following controlled patterns or exercise. Change in respiration and body movement can cause interference with the acquisition of imaging and physiological signals. Therefore, there were practical difficulties in studying the normal subjects with a wide range of variation in cardiovascular function. In this thesis, subjects within a wide range of age were selected to provide cardiovascular mechanical variation.

The second limitation is that only male subjects were studied. It has been well-acknowledged in literature that a marked gender difference exists in cardiovascular function (Martin et al. 1991, Sader and Celermajer 2002, Leinwand 2003). Therefore, the findings from this project could not be generalized to the females directly.

Another limitation is that only the relationships between timing features of images and physiological measurement were investigated in this thesis. It would be also of clinical interest to investigate the associations of the cardiac structures and blood volumetric profile with the amplitude of the change in thoracic impedance and peripheral pulse.

Finally, although automatic signal processing and feature identification were employed for the analysis of the physiological signals, the echocardiograms were analysed beat-by-beat manually, which was very time-consuming.

10.3 Suggestion for further work

Promising results have been shown in this thesis based on the simultaneously recorded echocardiograms and physiological signals. All these are able to provide better understandings on the origins of the pulsatile impedance and peripheral volume pulse and promote the clinical applications of the impedance cardiography and PPG techniques. However, there is still further research and development work that could continue.

1. Greater subject numbers are needed to generalize the results found in this thesis. In order to provide a more wide range of variation in cardiovascular functions, patients with different conditions, such as hypertension or heart failure, would be necessary. In addition, female subjects would also be suggested for the further work.
2. Further repeatability study for the measurement protocol can be done. In this thesis, all the repeated recordings were taken in the same experiment within one hour. A follow-up study over a longer time, such as one week or one month, could provide additional repeatability assessment.
3. The relations of the cardiac structures (such as ventricular dimensions) and blood volumetric profile (such as stroke volume) with the amplitude of the change in thoracic impedance and peripheral pulse could be also investigated.
4. Automatic methods to analyse the images and physiological signals should be further developed. These automatic methods are not only able to improve the efficiency but also reduce measurement variability. Additionally, more indices of cardiac function, such as stroke volume, can be obtained with the assistance of automatic analysis.

References

1. Ahmadpour, H., Shah, A. A., Allen, J. W., Edmiston, W. A., Kim, S. J., Haywood, L. J. (1983). Mitral E point septal separation: a reliable index of left ventricular performance in coronary artery disease. American heart journal, 106(1), 21-28

2. Ahmed, S. S., Levinson, G. E., Schwartz, C. J., Ettinger, P. O. (1972). Systolic time intervals as measures of the contractile state of the left ventricular myocardium in man. Circulation, 46(3), 559-571

3. Alam, M., Wardell, J., Andersson, E., Samad, B. A., Nordlander, R. (2000). Effects of first myocardial infarction on left ventricular systolic and diastolic function with the use of mitral annular velocity determined by pulsed wave Doppler tissue imaging. Journal of the American Society of Echocardiography, 13(5), 343-352

4. Allen, J., Murray, A. (1993). Development of a neural network screening aid for diagnosing lower limb peripheral vascular disease from photoelectric plethysmography pulse waveforms. Physiological Measurement, 14(1), 13-22

5. Allen, J., Murray, A. (2000). Similarity in bilateral photoplethysmographic peripheral pulse wave characteristics at the ears, thumbs and toes. Physiological measurement, 21(3), 369-377

6. Allen, J., Frame, J. R., Murray, A. (2002). Microvascular blood flow and skin temperature changes in the fingers following a deep inspiratory gasp. Physiological measurement, 23(2), 365-373

7. Allen, J., Murray, A. (2003). Age-related changes in the characteristics of the photoplethysmographic pulse shape at various body sites. Physiological measurement, 24(2), 297-307

8. Allen, J., Oates, C. P., Lees, T. A., Murray, A. (2005). Photoplethysmography detection of lower limb peripheral arterial occlusive disease: a comparison of pulse timing, amplitude and shape characteristics. Physiological measurement, 26(5), 811-821

9. Allen, J. (2007). Photoplethysmography and its application in clinical physiological measurement. Physiological measurement, 28(3), R1-39

10. Allen, J., Overbeck, K., Nath, A. F., Murray, A., Stansby, G. (2008). A prospective comparison of bilateral photoplethysmography versus the ankle-brachial pressure index for detecting and quantifying lower limb peripheral arterial disease. Journal of Vascular Surgery, 47(4), 794-802

11. Altman, D. G., Bland, J. M. (2003). Statistics Notes: Interaction revisited: the difference between two estimates. BMJ: British Medical Journal, 326, 219

12. Ambrose, J. A., Teichholz, L. E., Meller, J., Weintraub, W., Pichard, A. D., Smith, H., Herman, M. V. (1979). The influence of left ventricular late diastolic filling on the A wave of the left ventricular pressure trace. Circulation, 60(3), 510-519

13. Aoyagi, T., Kishi, M., Yamaguchi, K., Watanabe, S. (1974). Improvement of the earpiece oximeter. Japanese Society of Medical Electronics and Biological Engineering, 974, 90-91

14. Appleton, C. P., Hatle, L. K., Popp, R. L. (1988a). Relation of transmitral flow velocity patterns to left ventricular diastolic function: new insights from a combined hemodynamic and Doppler echocardiographic study. Journal of the American College of Cardiology, 12(2), 426-440

15. Appleton, C. P., Hatle, L. K., Popp, R. L. (1988b). Demonstration of restrictive ventricular physiology by Doppler echocardiography. Journal of the American College of Cardiology, 11(4), 757-768

16. Balasubramanian, V., Mathew, O. P., Behl, A. R. U. N., Tewari, S. C., Hoon, R. S. (1978). Electrical impedance cardiogram in derivation of systolic time intervals. British heart journal, 40(3), 268-275

17. Baumgartner, H., Hung, J., Bermejo, J., Chambers, J. B., Evangelista, A., Griffin, B. P., Quiñones, M. (2009). Echocardiographic assessment of valve stenosis: EAE/ASE recommendations for clinical practice. European Journal of Echocardiography, 10(1), 1-25

18. Bortolotto, L. A., et al. (2000). Assessment of vascular aging and atherosclerosis in hypertensive subjects: second derivative of photoplethysmogram versus pulse wave velocity. American Journal of Hypertension 13(2): 165-171

19. Brumfield, A. M., Andrew, M. E. (2005). Digital pulse contour analysis: investigating age-dependent indices of arterial compliance. Physiological measurement, 26(5), 599

20. Callaghan, F. J., Geddes, L. A., Babbs, C. F., Bourland, J. D. (1986). Relationship between pulse-wave velocity and arterial elasticity. Medical and Biological Engineering and Computing, 24(3), 248-254

21. Carvalho, P., Paiva, R. P., Henriques, J., Antunes, M., Quintal, I., Muehlsteff, J. (2011). Robust Characteristic Points for ICG-Definition and Comparative Analysis. In Biosignals, 161-168

22. Challoner, A. V. J. (1979). Photoelectric plethysmography for estimating cutaneous blood flow. Non-invasive physiological measurements, 1, 125-51

23. Chan, G. S., Middleton, P. M., Celler, B. G., Wang, L., Lovell, N. H. (2007). Automatic detection of left ventricular ejection time from a finger photoplethysmographic pulse oximetry waveform: comparison with Doppler aortic measurement. Physiological measurement, 28(4), 439-452

24. Chowienczyk, P. J., Kelly, R. P., MacCallum, H., Millasseau, S. C., Andersson, T. L., Gosling, R. G., Änggård, E. E. (1999). Photoplethysmographic assessment of pulse wave reflectionblunted response to endothelium-dependent beta2-adrenergic vasodilation in type II diabetes mellitus. Journal of the American College of Cardiology, 34(7), 2007-2014

25. Cybulski, G., Michalak, E., Koźluk, E., Piątkowska, A., Niewiadomski, W. (2004). Stroke volume and systolic time intervals: beat-to-beat comparison between echocardiography and ambulatory impedance cardiography in supine and tilted positions. Medical and Biological Engineering and Computing, 42(5), 707-711

26. Dawber, T. R., Thomas, H. E., McNamara, P. M. (1973). Characteristics of the dicrotic notch of the arterial pulse wave in coronary heart disease. Angiology, 24(4), 244-255

27. Devereux, R. B., Wachtell, K., Gerdts, E., Boman, K., Nieminen, M. S., Papademetriou, V., Dahlöf, B. (2004). Prognostic significance of left ventricular mass change during treatment of hypertension. JAMA: the journal of the American Medical Association, 292(19), 2350-2356

28. Dillon, J. B., Hertzman, A. B. (1941). The form of the volume pulse in the finger pad in health, arteriosclerosis, and hypertension. American Heart Journal, 21(2), 172-190

29. Douglas, P. S., Hendel, R. C., Cummings, J. E., Dent, J. M., Hodgson, J. M., Hoffmann, U., Weigold, W. G. (2009). ACCF/ACR/AHA/ASE/ASNC/HRS/

NASCI/RSNA/SAIP/SCAI/SCCT/SCMR 2008 Health Policy Statement on Structured Reporting in Cardiovascular Imaging. Journal of the American College of Cardiology, 53(1), 76-90

30. Edvardsen, T., Urheim, S., Skulstad, H., Steine, K., Ihlen, H., Smiseth, O. A. (2002). Quantification of left ventricular systolic function by tissue Doppler echocardiography added value of measuring pre-and postejection velocities in ischemic myocardium. Circulation, 105(17), 2071-2077

31. Einthoven, W. (1903). The string galvanometer and the human electrocardiogram. KNAW, Proceedings, Vol. 6, 1903-1904

32. Fauci, A. S., Braunwald, E., Kasper, D. L., Hauser, S. L., Longo, D. L., Jameson, J. L., Loscalzo, J. (2008). Harrison's principles of Internal Medicine, 18th edition. McGraw-Hill

33. Feigenbaum, H. (2010). Role of M-mode Technique in Today's Echocardiography. Journal of the American Society of Echocardiography **23**(3): 240-257

34. Fellahi, J. L., Caille, V., Charron, C., Deschamps-Berger, P. H., Vieillard-Baron, A. (2009). Noninvasive assessment of cardiac index in healthy volunteers: a comparison between thoracic impedance cardiography and Doppler echocardiography. Anesthesia Analgesia, 108(5), 1553-1559

35. Ferrari, A. U., Radaelli, A., Centola, M. (2003). Invited review: aging and the cardiovascular system. Journal of Applied Physiology, 95(6), 2591-2597

36. Fleg, J. L., Das, D. N., Wright, J., Lakatta, E. G. (1990). Age-associated changes in the components of atrioventricular conduction in apparently healthy volunteers. Journal of gerontology, 45(3), M95-100

37. Giannuzzi, P., Temporelli, P. L., Bosimini, E., Silva, P., Imparato, A., Corrà, U., Giordano, A. (1996). Independent and incremental prognostic value of Doppler-derived mitral deceleration time of early filling in both symptomatic and asymptomatic patients with left ventricular dysfunction. Journal of the American College of Cardiology, 28(2), 383-390

38. Gottdiener, J. S., Bednarz, J., Devereux, R., Gardin, J., Klein, A., Manning, W. J., Weissman, N. J. (2004). American Society of Echocardiography recommendations for use of echocardiography in clinical trials: A report from the american society of echocardiography's guidelines and standards committee and the task force on

echocardiography in clinical trials. Journal of the American Society of Echocardiography, 17(10), 1086-1119

39. Hanzlik, P. J., DEEDS, F., Terada, B. (1936). A simple method of demonstrating changes in blood supply of the ear and effects of some measures. Journal of Pharmacology and Experimental Therapeutics, 56(2), 194-204

40. Hashimoto, J., Chonan, K., Aoki, Y., Nishimura, T., Ohkubo, T., Hozawa, A., Imai, Y. (2002). Pulse wave velocity and the second derivative of the finger photoplethysmogram in treated hypertensive patients: their relationship and associating factors. Journal of Hypertension, 20(12): 2415-2422

41. Hertzman, A. B. (1937). Photoelectric plethysmography of the fingers and toes in man. In Proceedings of the Society for Experimental Biology and Medicine. Society for Experimental Biology and Medicine (New York, NY), 37(3), 529-534

42. Hertzman, A. B. (1938). The blood supply of various skin areas as estimated by the photoelectric plethysmograph. American Journal of Physiology--Legacy Content, 124(2), 328-340

43. Higashidate, M., Tamiya, K., Beppu, T., Imai, Y. (1995). Regulation of the aortic valve opening: in vivo dynamic measurement of aortic valve orifice area. The Journal of thoracic and cardiovascular surgery, 110(2), 496-503

44. Hirschfeld, S., Meyer, R., Schwartz, D. C., Kofhagen, J., Kaplan, S. (1975). The echocardiographic assessment of pulmonary artery pressure and pulmonary vascular resistance. Circulation, 52(4), 642-650

45. Howard, I. C., Patterson, E. A., Yoxall, A. (2003). On the opening mechanism of the aortic valve: some observations from simulations. Journal of medical engineering technology, 27(6), 259-266

46. Jago, J. R., Murray, A. (1988). Repeatability of peripheral pulse measurements on ears, fingers and toes using photoelectric plethysmography. Clinical Physics and Physiological Measurement, 9(4), 319-329

47. Jones, D. P. (1987). Medical electro-optics: measurements in the human microcirculation. Physics in Technology, 18(2), 79-85

48. Karnegis, J. N., Kubicek, W. G. (1970). Physiological correlates of the cardiac thoracic impedance waveform. American heart journal, 79(4), 519-523

49. Kinnen, E., Kubicek, W., Hill, P., Turton, G. (1964). Thoracic cage impedance measurements. Tissue Resistivity in Vivo and Transthoracic Impedance at 100 kc. Minnesota Univ Minneapolis

50. Kizakevich, P. N., Teague, S. M., Nissman, D. B., Jochem, W. J., Niclou, R., Sharma, M. K. (1993). Comparative measures of systolic ejection during treadmill exercise by impedance cardiography and Doppler echocardiography. Biological psychology, 36(1), 51-61

51. Klabunde, R. E. (2005). Cardiovascular physiology concepts, 1st edition. Wolters Kluwer Health

52. Klein, A. L., Burstow, D. J., Tajik, A. J., Zachariah, P. K., Bailey, K. R., Seward, J. B. (1994). Effects of age on left ventricular dimensions and filling dynamics in 117 normal persons. In Mayo Clinic Proceedings, 69(3), 212-224

53. Klemsdal, T. O., Andersson, T. L., Matz, J., Ferns, G. A., Gjesdal, K., Änggård, E. E. (1994). Vitamin E restores endothelium dependent vasodilatation in cholesterol fed rabbits: in vivo measurements by photoplethysmography. Cardiovascular research, 28(9), 1397-1402

54. Konecke, L. L., Feigenbaum, H., Chang, S., Corya, B. C., Fischer, J. C. (1973). Abnormal mitral valve motion in patients with elevated left ventricular diastolic pressures. Circulation, 47(5), 989-996

55. Kubicek, W. G., Karnegis, J. N., Patterson, R. P., Witsoe, D. A., Mattson, R. H. (1966). Development and evaluation of an impedance cardiac output system. Aerospace medicine, 37(12), 1208-1212

56. Kubicek, W. G., Witsoe, D.A., Patterson, R.P., Mosharrala, M.A., Karnegis, J.N., From, A.H.L. (1967). Development and evaluation of an impedance cardiographic system to measure cardiac output and development of an oxygen consumption rate computing system utilizing a quadrapole mass spectrometer. (NASA-CR-92220) Houston: National Aeronautics and Space Adminstration

57. Kubicek, W. G., Patterson, R. P., Witsoe, D. A. (1970). Impedance cardiography as a noninvasive method of monitoring cardiac function and other parameters of the cardiovascular system*. Annals of the New York Academy of Sciences, 170(2), 724-732

58. Kubicek, W. G. (1989). On the source of peak first time derivative (dZ/dt) during impedance cardiography. Annals of biomedical engineering, 17, 459-462

59. Lababidi, Z., Ehmke, D. A., Durnin, R. E., Leaverton, P. E., Lauer, R. M. (1970). The first derivative thoracic impedance cardiogram. Circulation, 41(4), 651-658

60. Lakatta, E. G. (2002). Age-associated cardiovascular changes in health: impact on cardiovascular disease in older persons. Heart failure reviews, 7(1), 29-49.

61. Lamberts, R., Visser, K. R., Zijlsira, W. G. (1984). Impedance cardiography. Assen, Tbc Netherlands: Van Gorcum

62. Lang, R. M., Bierig, M., Devereux, R. B., Flachskampf, F. A., Foster, E., Pellikka, P. A., Stewart, W. J. (2005). Recommendations for chamber quantification: a report from the American Society of Echocardiography's Guidelines and Standards Committee and the Chamber Quantification Writing Group, developed in conjunction with the European Association of Echocardiography, a branch of the European Society of Cardiology. Journal of the American Society of Echocardiography, 18(12), 1440-1463

63. Laniado, S., Yellin, E., Kotler, M., Levy, L., Stadler, J., Terdiman, R. (1975). A study of the dynamic relations between the mitral valve echogram and phasic mitral flow. Circulation, 51(1), 104-113

64. Leinwand, L. A. (2003). Sex is a potent modifier of the cardiovascular system. Journal of Clinical Investigation, 112(3), 302-307

65. Levick, J. R. (2010). An Introduction to Cardiovascular Physiology, 5th edition. Arnold. London

66. Lewis, R. P., Rittogers, S. E., Froester, W. F., Boudoulas, H. (1977). A critical review of the systolic time intervals. Circulation, 56(2), 146-158

67. Lewis, J. R., Parker, J. O., Burggraf, G. W. (1978). Mitral valve motion and changes in left ventricular end-diastolic pressure: a correlative study of the PR-AC interval. The American Journal of Cardiology, 42(3), 383-387

68. Martin Bland, J., Altman, D. (1986). Statistical methods for assessing agreement between two methods of clinical measurement. The lancet, 327(8476), 307-310

69. Martin, W. 3., Ogawa, T., Kohrt, W. M., Malley, M. T., Korte, E., Kieffer, P. S., & Schechtman, K. B. (1991). Effects of aging, gender, and physical training on peripheral vascular function. Circulation, 84(2), 654-664

70. Massie, B. M., Schiller, N. B., Ratshin, R. A., Parmley, W. W. (1977). Mitral-septal separation: new echocardiographic index of left ventricular function. The American journal of cardiology, 39(7), 1008-1016

71. Michael F. O'Rourke, Raymond P. Kelly, Alberto P. Avolio (1992). The arterial pulse. Philadelphia: Lea Febiger

72. Millasseau, S. C., Guigui, F. G., Kelly, R. P., Prasad, K., Cockcroft, J. R., Ritter, J. M., Chowienczyk, P. J. (2000). Noninvasive assessment of the digital volume pulse comparison with the peripheral pressure pulse. Hypertension, 36(6), 952-956

73. Millasseau, S. C., Kelly, R. P., Ritter, J. M., Chowienczyk, P. J. (2002). Determination of age-related increases in large artery stiffness by digital pulse contour analysis. Clinical science, 103(4), 371-378

74. Millasseau, S. C., Kelly, R. P., Ritter, J. M., Chowienczyk, P. J. (2003a). The vascular impact of aging andvasoactive drugs: comparison of twodigital volume pulse measurements. American journal of hypertension, 16(6), 467-472

75. Millasseau, S. C., Patel, S. J., Redwood, S. R., Ritter, J. M., Chowienczyk, P. J. (2003b). Pressure wave reflection assessed from the peripheral pulse is a transfer function necessary?. Hypertension, 41(5), 1016-1020

76. Millasseau, S. C., Ritter, J. M., Takazawa, K., Chowienczyk, P. J. (2006). Contour analysis of the photoplethysmographic pulse measured at the finger. Journal of hypertension, 24(8), 1449-1456

77. Miller, J. C., Horvath, S. M. (1978). Impedance cardiography. Psychophysiology, 15(1), 80-91

78. Mohapatra, S. N. (1981). Non-invasive cardiovascular monitoring by electrical impedance technique. Pitman Medical

79. Molitor, H., Kniazuk, M. (1936). A new bloodless method for continuous recording of peripheral circulatory changes. Journal of Pharmacology and Experimental Therapeutics, 57(1), 6-18.

80. Mor-Avi, V., Lang, R. M., Badano, L. P., Belohlavek, M., Cardim, N. M., Derumeaux, G., Zamorano, J. L. (2011). Current and evolving echocardiographic techniques for the quantitative evaluation of cardiac mechanics: ASE/EAE consensus statement on methodology and indications: endorsed by the Japanese

Society of Echocardiography. Journal of the American Society of Echocardiography, 24(3), 277-313

81. Morikawa, Y., Muraki, K., Ikoma, Y., Honda, T., Takamatsu, H. (1967). Organic nitrate poisoning at an explosives factory: plethysmographic study. Archives of Environmental Health: An International Journal, 14(4), 614-621

82. Morikawa, Y., Matsuzaka, J., Kukatsune, M., Tsukamoto, S., Makisumi, S. (1968). Plethysmographic study of effects of alcohol. Nature, 220, 186-187

83. Nagueh, S. F., Appleton, C. P., Gillebert, T. C., Marino, P. N., Oh, J. K., Smiseth, O. A., Evangelisa, A. (2009). Recommendations for the evaluation of left ventricular diastolic function by echocardiography. European Journal of Echocardiography, 10(2), 165-193

84. Nagueh, S. F., Middleton, K. J., Kopelen, H. A., Zoghbi, W. A., Quiñones, M. A. (1997). Doppler tissue imaging: a noninvasive technique for evaluation of left ventricular relaxation and estimation of filling pressures. Journal of the American College of Cardiology, 30(6), 1527-1533

85. Nichols, W. W., O'Rourke, M. F. (1990). Blood flow in arteries. Philadelphia: Lea Febiger

86. Nosir, Y. F., Fioretti, P. M., Vletter, W. B., Boersma, E., Salustri, A., Postma, J. T., Roelandt, J. R. (1996). Accurate Measurement of Left Ventricular Ejection Fraction by Three-dimensional Echocardiography: A Comparison With Radionuclide Angiography. Circulation 94(3): 460-466

87. Ommen, S. R., Nishimura, R. A., Appleton, C. P., Miller, F. A., Oh, J. K., Redfield, M. M., Tajik, A. J. (2000). Clinical utility of Doppler echocardiography and tissue Doppler imaging in the estimation of left ventricular filling pressures a comparative simultaneous Doppler-catheterization study. Circulation, 102(15), 1788-1794

88. Patterson, R. P. (1989). Fundamentals of impedance cardiography. Engineering in Medicine and Biology Magazine, IEEE, 8(1), 35-38

89. Patterson, R. P., Kubicek, W. G., Kinnen, E., Witsoe, D. A., Noren, G. (1964). Development of an electrical impedance plethysmography system to monitor cardiac output. In Proc of the First Ann Rocky Mountain Bioengineering Symposium , 56-71

90. Patterson, R. P., Kubicek, W. G., Witsoe, D. A., From, A. H. L. (1978). Studies on the effect of controlled volume change on the thoracic electrical impedance. Medical and Biological Engineering and Computing, 16(5), 531-536

91. Patterson, R. P. (1965). Cardiac output determinations using impedance plethysmography. MSEE Thesis, University of Minnesota, Minneapolis, Minnesot

92. Penney, B. C., Patwardhan, N. A., Wheeler, H. B. (1985). Simplified electrode array for impedance cardiography. Medical and Biological Engineering and Computing, 23(1), 1-7.

93. Petrovick, M. L., Kizakevich, P. N., Stacy, R. W., Haak Jr, E. D. (1980). A comprehensive cardiac exercise stress processor for environmental health effects studies. Journal of medical systems, 4(2), 137-150

94. Pickett, B. R., Buell, J. C. (1993). Usefulness of the impedance cardiogram to reflect left ventricular diastolic function. The American journal of cardiology, 71(12), 1099-1103

95. Quiñones, M. A., Otto, C. M., Stoddard, M., Waggoner, A., Zoghbi, W. A. (2002). Recommendations for quantification of Doppler echocardiography: a report from the Doppler Quantification Task Force of the Nomenclature and Standards Committee of the American Society of Echocardiography. Journal of the American Society of Echocardiography, 15(2), 167-184

96. Sader, M. A., Celermajer, D. S. (2002). Endothelial function, vascular reactivity and gender differences in the cardiovascular system. Cardiovascular research, 53(3), 597-604

97. Sakamoto, K., Kanai, H. (1979). Electrical characteristics of flowing blood. Biomedical Engineering, IEEE Transactions on, (12), 686-695

98. Schieken, R. M., Patel, M. R., Falsetti, H. L., Barnes, R. W., Lauer, R. M. (1978). Effect of aortic valvular regurgitation upon the impedance cardiogram. British heart journal, 40(9), 958-963

99. Schirmer, H., Lunde, P., Rasmussen, K. (2000). Mitral flow derived Doppler indices of left ventricular diastolic function in a general population. The Tromsø study. European heart journal, 21(16), 1376-1386

100. Sherwood, A., Allen, M. T., Fahrenberg, J., Kelsey, R. M., Lovallo, W. R., Doornen, L. J. (1990). Methodological guidelines for impedance cardiography. Psychophysiology, 27(1), 1-23

101. Sohn, D. W., Song, J. M., Zo, J. H., Chai, I. H., Kim, H. S., Chun, H. G., Kim, H. C. (1999). Mitral annulus velocity in the evaluation of left ventricular diastolic function in atrial fibrillation. Journal of the American Society of Echocardiography, 12(11), 927-931

102. Solomon, S. D., Bulwer, B. E. (Eds.). (2007). Essential echocardiography: a practical handbook with DVD. Springer

103. Spirito, P. A. O. L. O., Maron, B. J. (1988). Influence of aging on Doppler echocardiographic indices of left ventricular diastolic function. British heart journal, 59(6), 672-679

104. Stern, H. C., Wolf, G. K., Belz, G. G. (1985). Comparative measurements of left ventricular ejection time by mechano-, echo-and electrical impedance cardiography. Arzneimittel-Forschung, 35(10), 1582-1586

105. Surawicz, B. (1998). U Wave: Facts, Hypotheses, Misconceptions, and Misnomers. Journal of Cardiovascular Electrophysiology 9(10): 1117-1128

106. Takazawa, K., et al. (1998). Assessment of Vasoactive Agents and Vascular Aging by the Second Derivative of Photoplethysmogram Waveform. Hypertension 32(2): 365-370

107. Teng, X. F., Zhang, Y. T. (2006). The effect of applied sensor contact force on pulse transit time. Physiological measurement, 27(8), 675-684

108. Thakor, N. V., Webster, J. G., Tompkins, W. J. (1984). Estimation of QRS complex power spectra for design of a QRS filter. Biomedical Engineering, IEEE Transactions on, (11), 702-706

109. Thubrikar, M., Harry, R., Nolan, S. P. (1977). Normal aortic valve function in dogs. The American journal of cardiology, 40(4), 563-568

110. Tseng, K. H., Walfish, P. G., Persaud, J. A., Gilbert, B. W. (1989). Concurrent aortic and mitral valve echocardiography permits measurement of systolic time intervals as an index of peripheral tissue thyroid functional status. Journal of Clinical Endocrinology Metabolism, 69(3), 633-638

111. Ulbrich, M., Mühlsteff, J., Zink, M., Leonhardt, S., Walter, M. (2013). Feasibility of Impedance Cardiography to Assess Hemodynamic Changes and Fluid Loss Related to Pleural Drainage. Computing in Cardiology 2013. 40:663-666

112. Wei, J. Y. (1992). Age and the cardiovascular system. New England Journal of Medicine, 327(24), 1735-1739.

113. Wexler, L., Bergel, D. H., Gabe, I. T., MAKIN, G. S., MILLS, C. J. (1968). Velocity of blood flow in normal human venae cavae. Circulation research, 23(3), 349-359

114. Yeo, T. C., Malouf, J. F., Oh, J. K., Seward, J. B. (1998). Clinical profile and outcome in 52 patients with cardiac pseudoaneurysm. Annals of internal medicine, 128(4), 299-305

115. Zhang, X. Y., Zhang, Y. T. (2006). The effect of local mild cold exposure on pulse transit time. Physiological measurement, 27(7), 649-660

NHS
Regional Medical Physics Department

Freeman Hospital
High Heaton
Newcastle upon Tyne
NE7 7DN

Tel: 0191 233 6161
Fax: 0191 213 0290
www.rmpd.org.uk

Research Participant Information Sheet

23rd July 2012 (Version 4)

Dynamic Cardiac Imaging and Relationship to Physiological Measurements

You are being invited to take part in a research study. Before you decide it is important for you to understand why the research is being done and what it will involve. Please take time to read the following information carefully and discuss it with others if you wish. Ask us if there is anything that is not clear or if you would like more information. Take time to decide whether or not you wish to take part. Your participation is entirely voluntary and you may withdraw your consent at any time and do not have to justify your decision.

What is the purpose of the study?

Cardiovascular disease is the leading cause of death in the UK. Heart disease can cause abnormalities in the way the heart contracts and ejects blood to the circulation. The purpose of this project is to find relationships between different measurements of heart function. Images of the heart will be obtained using echocardiography and these will be related to measurements of the electrical activity of the heart and pulse measurements.

Why have I been chosen?

Anyone over 18 years old is eligible to take part in this study. We would like to undertake research in a group of healthy people without heart disease or high blood pressure.

Do I have to take part?

No. Your participation in this study is completely voluntary. If you do decide to take part you will be given this information sheet to keep together with a copy of the signed consent form. You are under no obligation to participate in this study, and you may withdraw at any time without it affecting your normal care in any way.

What will be involved if I agree to take part in the study?

If you agree to take part in the study, we will ask you to sign a consent form after reading this information sheet. The following measurements will be made:

- The electrical activity of your heart will be recorded by placing ECG electrodes on your chest.
- Your pulse will be recorded by placing a probe on your finger.
- Your blood pressure will be recorded by placing a cuff on your arm.
- An ultrasound scan of your heart will be recorded.
- Sensors will be placed on your chest and neck to record impedance.

In addition, we will ask some basic information, such as age, sex, weight and height. The whole session should take about 45 minutes of your time. The data will be recorded to a computer and analysed. No measurement is invasive or involves needles. All measurements are in regular clinical use and are safe.

What are the benefits?

There are no benefits to you personally by taking part in this study, but the results should eventually benefit others, giving information for clinical diagnosis, therapy assessment and detecting cardiovascular disease early.

What are the risks?

There are no risks in taking part in this study.

What if some unknown clinical condition is discovered?

A consultant relevant to the finding will be contacted, and if an abnormal condition is confirmed we will contact you and your GP will be informed, and if appropriate you will also be contacted by the hospital consultant.

Will my taking part in this study be kept confidential?

Your data will be anonymised and identified by a code. All information will be kept strictly confidential. The combined results from all subjects will be analysed and may be published in scientific journals.

What happens if something goes wrong?

If you are harmed as a result of taking part in this study, then compensation can be sought from the study sponsor under the NHS Indemnity arrangements. A copy of the guidelines is available on request. However, the sponsor will not compensate you where harm results from any procedure that is not in accordance with the study protocol. Under these circumstances, your right at law to claim compensation for harm where you can prove negligence is not affected.

What will happen to the results of this study?

The results will be published in a PhD thesis. They might also be published in science, medical and medical engineering journals and at conferences. No personal data is published. We will publish the references to any papers on our website http://research.ncl.ac.uk/cardio_phys_eng. Alternatively, if you not have access to the internet, you can contact us. We will be happy to provide you with copies.

Who is organising and funding the research?

This is a PhD research study undertaken by Wenfeng Duan. It is being supervised by Dr Philip Langley and Professor Alan Murray. It is funded by The Newcastle upon Tyne Hospitals NHS Foundation Trust and Wenfeng Duan.

Will I be reimbursed for participating in this study?

The only cost to you for participating in this study will be travel to the Freeman Hospital for the measurement. Unfortunately we are unable to reimburse these costs.

Who has reviewed the research?

All research in the NHS is looked at by an independent group of people, called a Research Ethics Committee to protect your safety, rights, wellbeing and dignity. This study has been reviewed and given favourable opinion by a local Research Ethics Committee.

If you have any questions or would like further information contact:

Wenfeng Duan, PhD student, Medical Physics Department, Freeman Hospital,
Telephone: 0191 2336161 ext 26727. Email: w.duan@ncl.ac.uk
or
Dr Philip Langley, PhD student's supervisor, Medical Physics Department, Freeman Hospital, Telephone: 0191 2231664, Email: philip.langley@ncl.ac.uk

Appendix 1

If you would like to seek independent advice:

Patient Advice and Liaison Service (PALS) provides confidential advice and support, helping you to sort out any concerns that you may have about any aspect of NHS care.

Telephone: 08000 320202 Email: northoftynepals@nhct.nhs.uk